Near Infrared Variability of Active Galactic Nuclei

Keigo Enya

Doctor of Philosophy

Department of Astronomical Science
School of Mathematical and Physical Science
The Graduate University for Advanced Studies

1999

abstract

Results of near infrared(J,H,K' band) variability observations of 226 AGN are shown in this thesis. Samples are mainly QSO and Seyfert 1 AGN, and are radio quiet samples and radio quiet samples. Redshift(z) of the samples are from 0 to 1, and absolute magnitudes at V band(Mv) are from -30mag to -20mag. Each objects were broad line observed 2 times and the variabilities were measured by differential photometry.

Differential photometry reduction system specialized to this work feature where near infrared images are treated and the objects are not always point source was developed. As factor which is not canceled even by differential photometry, effect by that the AGN are not always point source and for the samples of this word, the effect was about 0.01mag for variability. Because the effect was estimated, 3 arcsec aperture which is comparable to seeing size could be used and better signal noise ratio was realized. Another systematic error mainly made by flat fielding was negligible for most often case, but it was more than 0.1mag for some cases, and its average was 0.03mag at J,H,K' band image pairs. Comparing these systematic errors, statistic error was sometimes dominant and total error of each variability data at J,H,K' bands were 0.05mag by average.

Variability of the all sample or of subsamples of observed AGN were estimated by calculating ensemble for at least 5 samples. In all subsamples, significant difference of ensemble variability was found between the ensemble variability of J,H,K' bands. The ensemble variability of all sample was 0.22mag, and ensemble variabilities of long interval samples had tendency to be larger than short interval samples. Ensemble variabilities of all radio loud samples in this work were 0.26mag and this was larger than these of all radio quiet samples which was 0.18mag, and the difference was couldn't explained by difference of rest frame interval of twice observations. In raw data of radio quiet ensemble variabilities, significant dependence to Mv was found. By J-H and H-K' color analysis by standard star photometry, it was understood that bright sources at V band were less effected by host galaxies than dark sources. So real ensemble variability of radio quiet sample was thought that had negative dependence on those Mv at V band. On the other hand, in radio loud samples, significant positive dependence between Mv or z and ensemble variability of raw data.

More than 2(or 3)σ probability, the variability detected objects were 58%(44%) of all and significant difference between the observed band were not existed. The probability of variability detection became higher with accuracies of the data became higher together and saturation of the probability of variability detection was not seen. In subsamples whose σ were smaller than 0.03mag, probability of variability detection was 80%(64%). As the simplest interpretation, maybe most of AGN are variable in infrared was concluded.

In the all sample and subsamples, positive correlations between different bands variability were

found and their correlation coefficients $r_{JH}, r_{HK'}, r_{JK'}$ was in from about 0.6 to 0.9. For radio quiet samples, $r_{HK'}$ at $0.1 < z < 0.3$ was significantly higher than $r_{JH}, r_{JK'}$ and z dependence of $r_{JH}, r_{HK'}, r_{JK'}$ was consistent with emission and variability by dust reverberation. On the other hand, $r_{JH}, r_{HK'}, r_{JK'}$ of far object in this work($0.6 < z < 1.0$) were high(about 0.95) were characteristic. The $r_{JH}, r_{HK'}, r_{JK'}$ of radio quiet samples were low accuracy at now z objects but those of radio loud samples were high accuracy at high z objects. So significant difference of $r_{JH}, r_{HK'}, r_{JK'}$ between radio quiet samples and radio loud samples were not detected.

Time development of ensemble variability of the subsamples were fitted by $A_0[1/(1+z)]^p$ and $B_0[1-\exp(-t/\tau(1+z))]$ and estimated. In radio quiet,radio loud samples and their subsamples by Mv,z, difference of time scale of variability by observed band were not found. Both p and τ was seem to be faster in radio loud samples than radio quiet samples but because those errors were large, difference of the time scale of the variability between radio loud samples and radio quiet samples were not concluded enough.

The features of the variability of the radio quiet samples were consistent dust reverberation model. But for radio loud samples, simple dust reverberation model couldn't explain the features which was Mv dependence difference from radio quiet samples and larger, faster variability than radio quiet samples.

In radio loud source, variability of sample whose spectrum is flat at radio wavelength were larger than variability of sample whose spectrum is steep at radio wavelength. OVV, high polarized QSO, BL lac effected the ensemble of flat samples is reasonable. On the other hand, steep spectrum sources variability was significantly smaller than flat spectrum sources variability but larger than radio quiet samples. And, positive correlation between variability and luminosity was found like flat samples. So, in the steep samples, nonthermal component effected radiation and variability and it is different from radio quiet's radiation and variability. Another probability which explain the steep samplers variability features is contamination of flat sources by error of splitting flat source or steep source. This effect bring flat source like weak features to steep sources.

Contents

Chapter 1

introduction

Active galactic nuclei(hereafter AGN) emit very large energy and those emitting regions are far smaller than scale of host galaxies. Some interesting models which is ,for example, spermassive blackhole and accretion disc or model based on supernovae have been discussed to understand the mechanism of the emission. To check these hypothesis and understand the emission mechanism is one of the important aim of studies of AGN.

AGN are used as cosmological probes because they are extremely bright and therefore can be observed even at cosmological distance. Observing more far AGN brings informations of earlier universe and cosmological geometry. to understand physics of AGN is also important to use them as cosmological probes.

It is well established fact that at least some fraction of AGN vary their luminosity for lifetime of a human. The variability is strong evidence which means that size of emitting regions of those objects are limited in few light-years scale. If such object is at distance of z=1, the optical or infrared largest telescope, best interferrometer and space telescope of now can't resolve such small region. However, observation of variability of AGN has potential to understand the central region of AGN. Scale of the emitting region could be limited in $\sim c\Delta t$ detection of the variability with time scale Δt. Correlation or time lag between the variability of different wavelength, relation between the variability and characters of AGN could be important informations.

AGN emit substantial fraction of their bolometric luminosity in infrared and relation between optical or UV variability from the central region and infrared variability from surrounding dust torus is suggested. However, quality and quantity of infrared data of AGN variability which have been reported are very (less) than optical data. Though observation of AGN variability need some span(typically a few years), infrared array appearance was later than CCD. data stock by Shumit telescope and photographic plates at optical wavelength exist but such infrared data stock not. These differences of conditions between infrared and optical observations are thought to be the reason of the lac of infrared data of AGN variability.

In this thesis, result of near infrared observation of the variability of many AGN are shown. The sample was more than 200 which is larger than previous work in infrared wavelength. In this

chapter, studies of AGN's optical long term variability are (shown) first. Next, previous studies about infrared SED of AGN and optical infrared multicolor monitors are (shown). Suggested the relation between optical,UV and infrared emission are shown there. Furthermore, MAGNUM project (which means multi-color active galactic nuclei and author's group is now preparing) is (shown) simply. MAGNUM project is study where AGN is used as the cosmological probes to estimate cosmological parameters. At last, thesis outline is shown.

1.1 optical long term variability of AGN

The mechanism of the variability of AGN is not understand, but there is possibility to distinguish whether the variability is originated by multiple component from relation between the variability and Mv etc. of AGN(Pica & Smith 1983). So many efforts to observe the variability of many AGN were done. Statistic studies of dependence of the variability on Mv or z for many samples has been done at optical wavelength. Super novae model is one of the multiple source model(for example, Terlvich et al.1992), while super massive black hole and accretion disk model is single source mechanism (for example, Rees et al.1984).

Negative correlation between the variability and absolute luminosity of quasar is important expectation of the multiple unit model. Such negative correlation is seen in some studies like early work by Uomoto et al.1976, Pica & Smith 1983. After them, there were the works of Cristiani et al.1990 for SA94, Tervese et al.1994 for SA57 and Hook et al.1994 for South Galactic Pole(SGP). Criatiani et al.1996 compiled those data and discussed about the correlation. However, obtained correlation between the variability and absolute magnitude tended to be weaker than expectation of the Poisson model (inclination of -0.5 at log scale). Resemble result was obtained by Paltani & courvoisier(1997) for Seyfert 1, radio quiet QSO, small polarized radio loud QSO from the UV continuum of IUE database.

On the other hand, Cid Fernandes, Aretxage & Terlvich 1996 obtained the inclination of -0.5 as the result of analysis of SGP data. Aretxage,Cid Fernandes & Terlvich 1997 explained the data as compilation of random event.

However, the anti correlation was not always found. The negative correlation was found in Lloyd et al.1984, Netzer et al.1996.

Recently high accuracy monitor campaign with CCD detector became to be executed. Borgeest & Schramm 1994, Netzer et al.1996, Giveon et al.1999 are the example. Flux limited observation usually has problem that is redshift dependence of the absolute magnitude of the observable sample. The sample was divided by redshift and absolute magnitude independently in Cristiani et al.1996, and significant positive correlation between the variability and the redshift. Similar tendency was found in Giallongo et al.1991, where the result was interpreted as the wavelength

dependence of the variability. Cid Fernandes et al.1996 supported those interpretation.

Observations of wavelength dependence of the variability of AGN have been done too. For example, there are Cutir et al.1985, Edelson et al.1990, Paltani & Walter 1998, Cristiani et al.1997, Paltani et al.1998 and so on. Edelson et al.1996 includes multi wavelength monitoring of NGC4151. The studies of the relation between the variability of AGN and wavelength is continued now since to clarify the dependence has possibility to limit the emission and variability of AGN.

1.2 relation between optical and infrared emission and variability of AGN

The relation between optical and infrared emission and variability of AGN was suggested by studies of AGN of spctral energy distribution(hireafter SED). Sanders et al.(1989) presented the SED of 109 PG quasars from 0.3 - 6cm. The SED of the objects in the work were resembled each other except flat spectrum radio loud source like 3C 273. Thermal emission from dust was reasonable as the origin of infrared bump which was seen from 2μm to 1mm in usual sample's SED. In this work, feature of nonthermal emission was'nt found at the SED of radio quiet and steep spectrum radio loud source from 3mm to 300μm.

Near infrared detail SED of 14 quasars were studied using 16 channel prism spectrometer by Kobayashi et al.(1993). Power law component and blackbody radiation component was used to fit the data, and the best fit temperature of black body component was generally about 1500K. This result was (interpreted) that hot dust surrounded nucleus and was in equilibrium to evaporation because the temperature is almost equal to evaporation temperature of dust. Ratio of power law component and blackbody component was different each other, but the ratio of IRAS selected samples were higher than other samples.

Some of nearby AGN are monitored in both optical and infrared wavelength and light curve of both wavelength were compared. Clavel,Wamsteker & Glass(1989) showed result of monitor observation of Fairall 9 at infrared J,H,K,L band. Barvanis(1992) explained the data with dust reverberation model. In this model, dust torus surround central source and is heated by UV radiation from central source and emit infrared flux. Therefore time delay of infrared from optical variability was explained naturally.

More than 50 AGN were monitored at V and K band in Nelson(1996a,his thesis). Correlations between optical and infrared light curves were found in 13 objects and detail modeling was done from the point of view of dust reverberation. Mark 744 was object where outburst was observed and its light curves were well explained by reverberation model in the work(Nelson 1996b). On the other hand, the variability of Fairall 9 was not explained well by the dust reverberation model(Nelson 1996a). So infrared emission mechanism of AGN were different for each other and mixture of thermal and nonthermal component concluded to be plausible.

As above, link between UV-optical emission and variability and infrared emission and variability is also suggested from multicolor light curves. Observation of the time delay of the optical and infrared light curves and to test the model application is good method to check whether the emission and variability mechanism is dust reverberation. However, it is usually hard to monitor in both optical and infrared wavelength with different instruments for long term. So the variability data whose accuracy, span and interval are enough to determine time delay between optical and infrared is only obtained for small number of objects. The light curves that couldn't be explained by the dust reverberation model such as Fairall 9 in Nelson 1996a was also reported. In such situation, it is unclear how general is the dust reverberation as the mechanism of emission and variability of AGN.

1.3 near infrared long term variability of AGN

However, infrared variability data of AGN observed up to now are far less than optical. Neugebauer et al.(1989) is statistic study of infrared variability of many AGN though it doesn't include optical observation. Optically selected PG quasars had been monitored at J,H,K,L and 10μm band for more than 20 years. Reliability of variability at K band was estimated for each objects. Some fraction of the samples were concluded to have varied certainly and some were not significant variability. This result at infrared wavelength was in contrast with optical result most of whose variability was significant(Usher 1978). As the reason why variability was harder to detected at infrared than at optical, probability that the source emitting infrared was dust region and central variability was dulled because of large scale of emitting region was suggested. Radio loud samples tended to show higher reliability of variability than radio quiet samples, and higher bolometric luminosity samples tended to show lower reliability of variability than lower bolometric luminosity samples. And variability at 10μm wavelength of 3C 273 was detected. If the emission of 3C 273 at 10μm was simple thermal emission from dust, time scale of variability was estimated to be about a few hundreds of years. So the emission of 3C 273 at 10μm was interpreted by nonthermal component naturally or by thermal component from very complicated system.

There is a short comment about rate of objects with highly certain reliably variability. 51 objects were observed at V and K band, and 4 objects were not variable at both band, 12 objects were detected the variability at only one band. The variability of 35 objects were detected at both V and K band. It was concluded that the variability of optical and infrared continue was common property of quasars and Seyfert 1 AGN.

Neugebauer & Matthews(1999) discussed variability of AGN at 10μm wavelength. The samples contained 20 radio quiet and 5 radio loud and their monitored data at 1.25-10μm wavelength were shown there. The variability at 10μm wavelength that was thought to mean existence of nonthermal emission component was detected for some radio loud samples and one radio quiet sample PG 1535+547. Median variability was determined for each objects and similarity between

those of radio quiet and radio loud, those of near infrared and 10μm wavelength. They were also compared with optical data(Netzer et al.1996) and concluded that some fraction of emission of both radio quiet and radio loud were caused by nonthermal component from their similarity. Periodic variability component of PG 1226+023(3C 273) at near infrared wavelength was also concluded.

The samples of Neugebauer et al.(1989) was largest, but the data was obtained with single detector and therefore photometric accuracy was limited. 2D infrared array was used in Nelson(1996a), but its aim was rather dust reverberation than to show basic features of variability. So the object was limited in near($z<0.3$, most of them were <0.1) and most of their Mv was darker than -24mag. fig(1.1) shows the samples of statistic previous study at optical and infrared wavelength. It is clear that infrared data is much less than optical.

1.4 MAGNUM project

In this section, MAGNUM project is introduced simply and relation between the project and this work is written. MAGNUM project that is under preparation by us is new study to determine cosmological parameters using AGN as the probes. This work is not only independent study of AGN but also pre-observation of MAGNUM project.

The primary aim of the project is to determine the cosmological parameters Ω_0, λ_0. Fig(1.2) support explanation of the principle to measure cosmological parameter. The principle is as following: It is thought that there are hot dust that is equilibrium to evaporation surround central nucleus and emission and variability mechanism is dust reverberation at least for some fraction of AGN. Absolute magnitude at UV-optical wavelength is determined by time delay between optical and infrared time curve using that distance between central source and dust torus is determined by absolute luminosity of central source. Luminosity distance is estimated by comparing the absolute luminosity and apparent luminosity. Filally, cosmological parameters are determined by comparing the luminosity distance and redshift of AGN.

2m special telescope is set at (Hale...) for MAGNUM project. Automatic observation and data analysis is very effective and indispensable in fact to monitor about 100 AGN for at least some years. Observation under normal condition will be done without manual operation except maintenance time that is 1 or 2 times per a year. Now we are preparing multicolor imaging photometer, automatic observation scheduler,cloud monitor,vacuum and cooling system and automatic data analysis system. This work relates to MAGNUM project especially following.

- to obtain basic properties of emission and variability of AGN and consider generality and limit of the dust reverberation mechanism.
- to measure variabilities of many AGN by imaging. Obtained properties of each object(magnitude,inf

color, variable or not, whether good reference stars exist or not etc.) is used to select target object of MAGNUM monitoring and to decide concrete observation mode (exposure time, dithering pattern) of each object.

- to establish differential photometry for infrared imaging of AGN , check error origin and estimate their properties.
- to extend atomization of data analysis as far as possible ,list up problems against the full atomization and think about the way to realize full atomization in MAGNUM project.

1.5 aim of this work

As described above, the observation of the variability is powerful method to clarify the mechanism of central compact region of AGN. The optical monitoring of AGN has been done for many samples and statistic studies of general properties of the variability. The link between optical and infrared emission is suggested from studies of SED of AGN. Feature of the dust reverberation in the light curves are reported what support the link between UV,optical and infrared variability though the sample is limited in some nearby AGN. However, infrared variability data of AGN observed up to now are far less than optical.

In such situation, it is important to extend the data of infrared variability of AGN and to clarify basic property of the variability of AGN, what is the primary motivation of this work. The aims of this work are following.

- to obtain variability data of AGN systematically for larger sample than up to now and to clarify basic property of the variability of AGN.
- to consider rather general mechanism of emission and variability of AGN than character of each object.
- to establish the differential photometry infrared imaging
- feedback to MAGNUM project written in previous section.

1.6 thesis outline

In chapter 2, sample selection concerning MAGNUM project and observation are written. Date reduction is written in chapter 3. Image reduction and differential photometry method is explained. Error origin,scale and

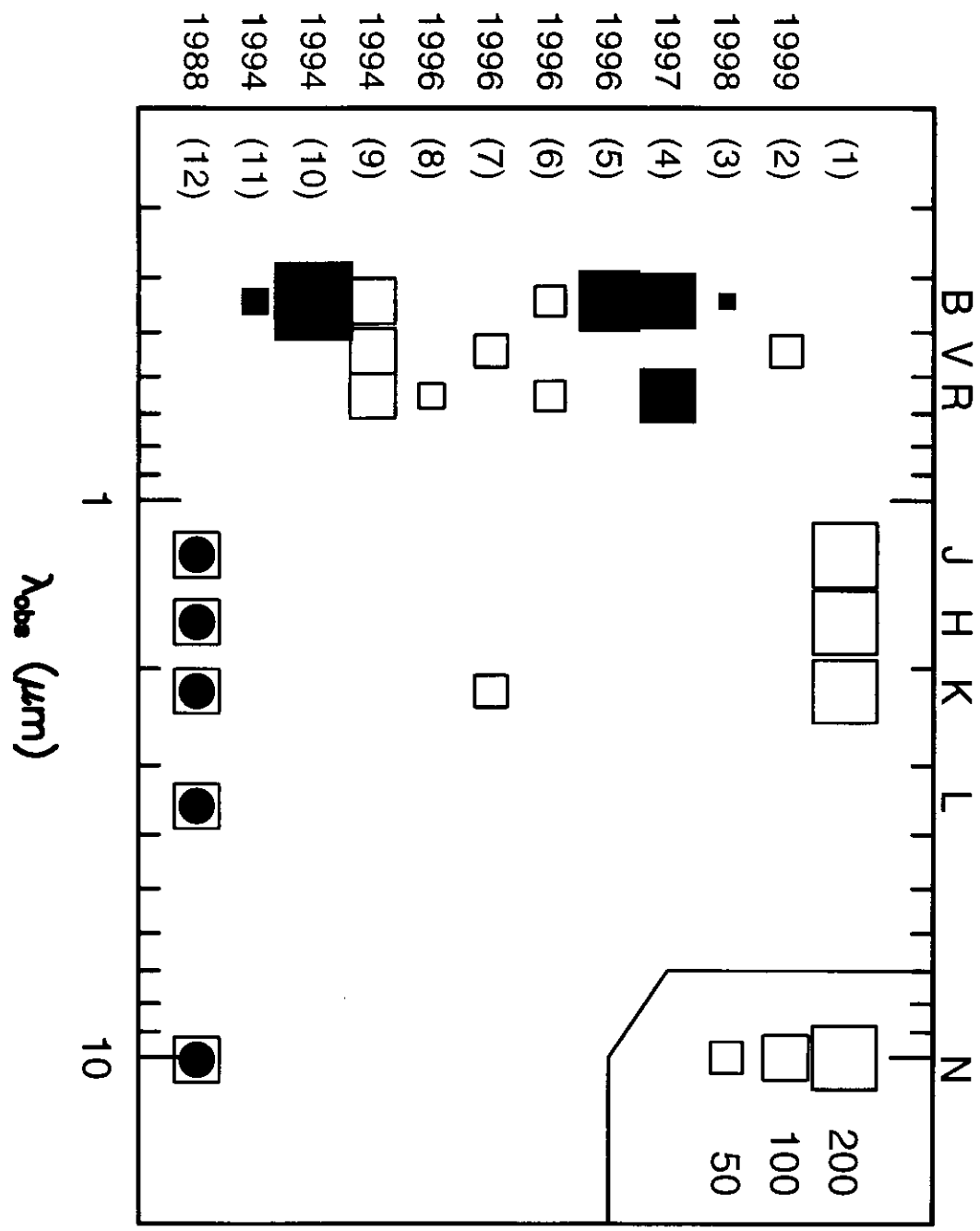

Figure 1.1: The distributions of observing wavelicgth and sample number in the studies of the variabiity of many AGN. The area of each square represents the sample number. Filled and open square represents the study with plate and with 2D device like CCD or infared array, respectively. Filled circle in open square means the observation with single IR device. (1) coresponds to this work, and reference of others are shown in folowing table.

Table 1.1: The references of previous figure

(1)	this work
(2)	Aurea A. et al, 1999
(3)	Bershady et al, 1998
(4)	Cristiani et al, 1997
(5)	Cristiani et al, 1996
(6)	Netzer et al ,1996
(7)	Nelson 1996
(8)	Clemente et al, 1996
(9)	Borgeest & Schramm 1994
(10)	Hook et al, 1994
(11)	Trevese et al, 1994
(12)	Neugebauer et al, 1989

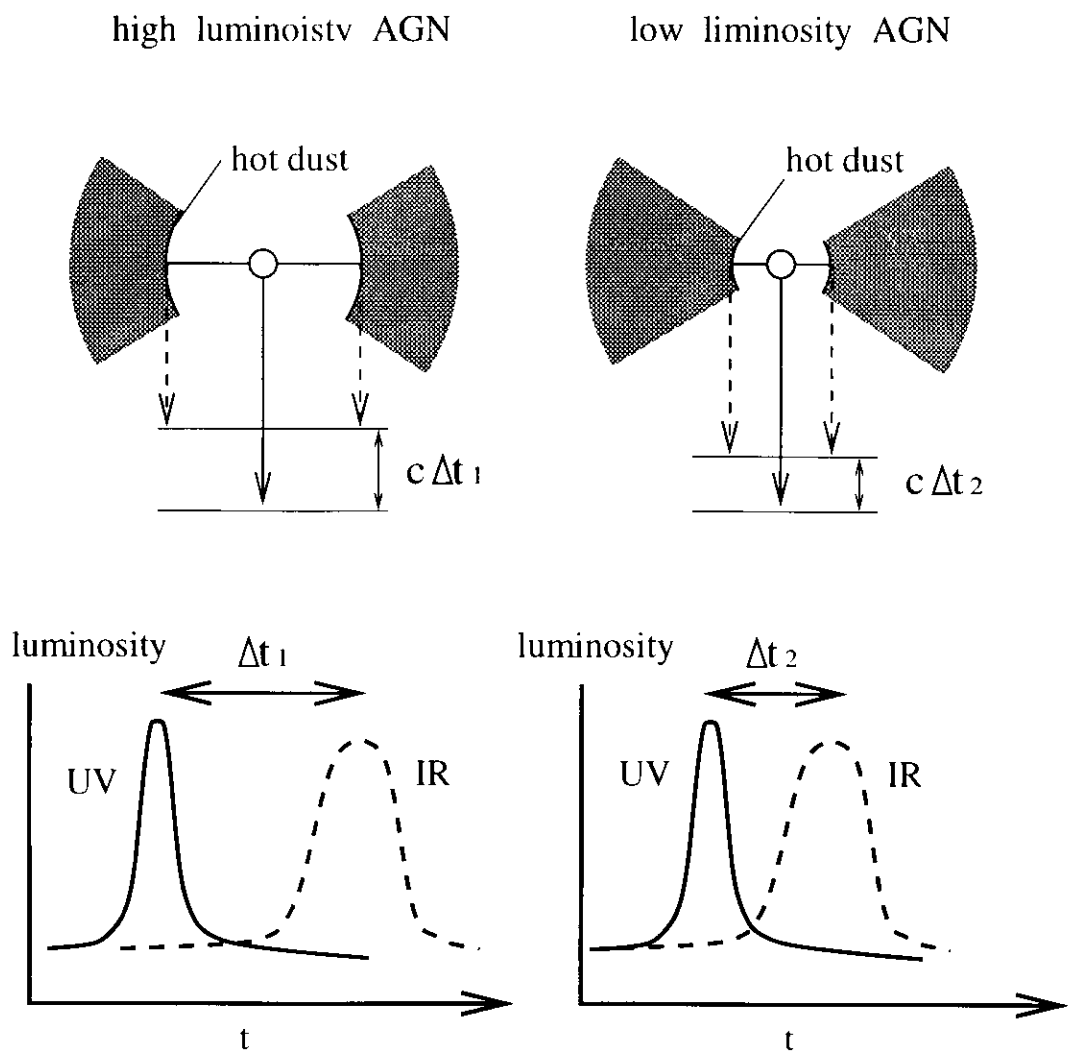

Figure 1.2: The principle to determine the absolute luminosity of AGN. There is the hot dust further from the central source at the brighter source. The variation of UV- from the central source arrives at the dust torus with the delay of dt and causes the variation of infrared radiation from the hot dust. cdt represents the scale of the region with no dust and therefore the absolute luminosity of the central source. The central luminosity is estimated to determine the time delay of the infrared variabiity from the UV-optical variability by the monitoring observation.

Chapter 2

observation

2.1 sample selection

The sample was selected from Quasars and Active Galactic Nuclei catalog (Veron-Cetty M.P., Veron P, hearafter 'VV') by following condition at beginning of the observation. Later the newest version of the catalog VV7,VV8 was used. The sample selection related to MAGNUM project since the objects of this work were also candidates of monitoring objects of MAGNUM project.

- to let R.A. wide spread
- to let absolute luminosity(Mv) and redshift(z) wide spread
- to be selected mainly Seyfert 1 AGN and quasars
- to avoid BL lac object
- to select AGN with nearby stars good for differential photometry

Aim of wide spread R.A. of objects was to realize effective observation at MAGNUM project where exclusive telescope would be used and observation would be done all through the year.

The primary aim of wide spread Mv and z was to study relation between these parameters and variability in this work. However, this condition was also important for MAGNUM project. Luminosity distance is determined by the time delay between UV, optical light curve and infrared light curve at MAGNUM project. Therefore using wide spread Mv sample at MAGNUM have not only significance to determine luminosity distance but also to check the mechanism of determining luminosity distance.

Furthermore, wide spread Mv and z would realize both early result and final high accuracy result of monitoring at MAGNUM monitoring. Low luminosity object would have short time delay of the light curves, but only nearby objects can be observed. On the other hand, monitoring far objects is important to determine cosmological parameters with high accuracy though time delay of such objects would be long because of not only their high luminosity but also cosmological time expansion.

The redshift of the sample was limited at $0 < z < 1$ in principle because to detect infrared radiation from hot dust of $1 < z$ objects would be hard. Good wavelength to detect the radiation from hot dust goes to comparable or longer than L band wavelength. L band observation is harder than K band or shorter wavelength at MAGNUM.

The sample consisted of mainly Seyfert 1 AGN and quasars to observe better candidates of monitoring by MAGNUM. As was pointed out in the unified model of AGN, dust torus of Seyfert 2 AGN might be seen from edge on. Therefore infrared radiation from inside of hot dust or UV radiation from more inner region would be absorbed by the dust on line of sight and detection of variability and measure the luminosity would become difficult. The infrared variability would become dull more strongly because of effect of geometry of dust torus if the torus was seen from edge on. At BL lac object, nonthermal emission would be dominant and therefore BL lac object was not selected. To select Seyfert 1 AGN and quasars, table.1 and table.3 of the VV catalog were used.

The condition that nearby stars for differential photometry were near the AGN didn't relate the properties of AGN themselves. But it turned out indispensable since this work.

This problem was not considered in the first season of this observation. But error of airmass correction and determining astronomical magnitude from instrumental magnitude was too large to detect small variability of AGN. The differential photometry was adopted since the second season of the observation and variability of the airmass correction, point spread function and influences of thin cloud were canceled. The differential photometry needed some reference stars in same image of AGN. Degitized sky survey(DSS) images they were degitalized Palomar chart were used to select sample of the observation of the second season. First the sample was selected using data of position, Mv and z, and then whether good nearby stars existed or not using was checked and unsuitable sample was rejected. DSS image because to get a image need time and human operations for database didn't accept batch request at that time. Number of the reference stars was better when it was more many, in principle. If DSS images of all candidate were checked before sample selection, objects with more nearby reference stars could be selected.

Later, batch request to get DSS images became possible at NAOJ database. This function could be used for data analysis of this work.

Figure(2.1) shows distributions of the R.A. and declination of the observed object at J,H and K' band. Filled circle represents the object that was observed 2 times and open circle represents the object that was observed only once. The objects are few at region around R.A.=20h since observation of the region is hard in Japanese winter season. The sample is limited at $dec. < +50$ to observe from the Maui inland that latitude is 20 degree. It is also limited at $-10 < dec.$ because observable term of the object in a year from the Northern hemisphere tend to be shorter if the latitude become smaller and therefore become unsuitable for MAGNUM monitoring.

Figure(2.2) shows distributions of Mv and z of the sample. Filled circle represents the object that was observed 2 times and open circle represents the object that was observed only once. z of the sample is spread from 0 to 1. There is negative correlation between Mv and z. This feature

comes from that far and dark objects cannot be observed and near luminous objects are few.

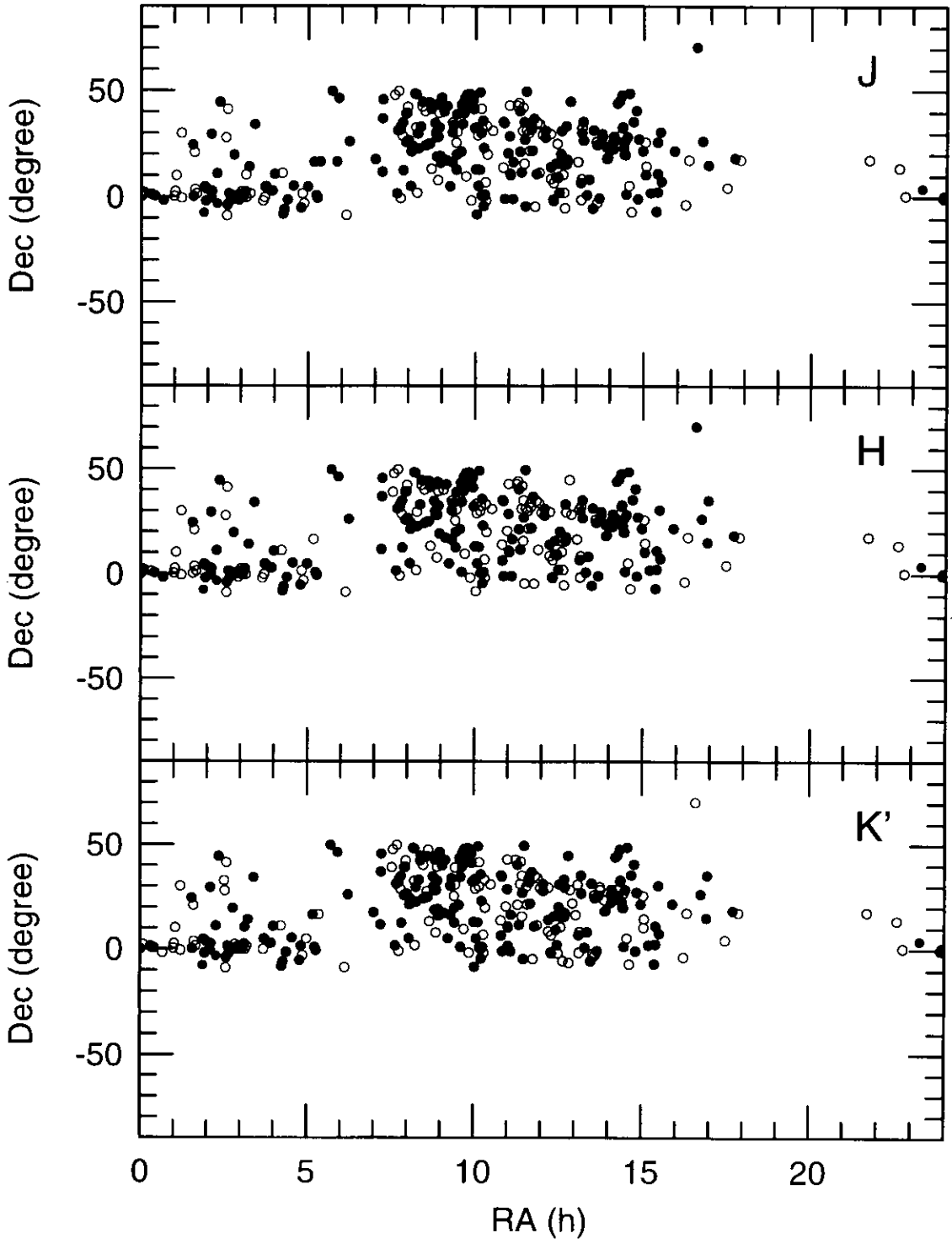

Figure 2.1: The distributions of right ascension and decilnation of observed objects. Filled circle represents the object to be apllied the differential photometry at least in one band, while open circle represents the object only at once.

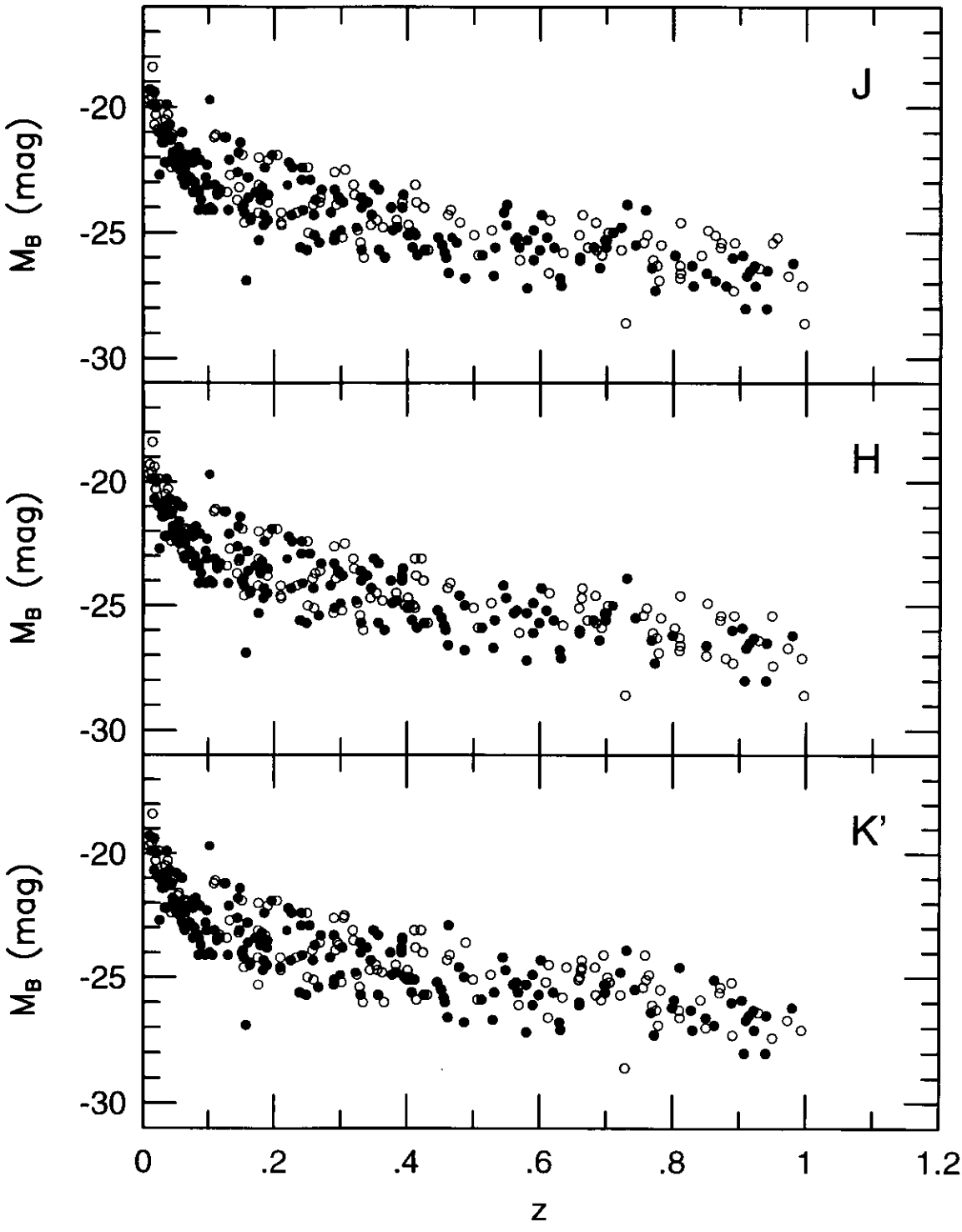

Figure 2.2: The distributions of redshift and absolute magnitude in V band of observed objects. Filled circle represents the object to be apllied the differential photometry at least in one band, while open circle represents the object only at once.

2.2 observation

All observations of this work were done by 1.3m telescope at ISAS(institute of space and astronomical science) and near infrared camera PICNIC (prism spectrometer polalimeter infrared camera with NICMOS). Broad band imaging photometry in near infrared J,H and K' was done for the many sample explained at previous section. The observation consists of 3 terms. The 1st term is from January 1996 to April 1996, the 2nd is from November 1996 to February 1997 and the 3rd is from December 1997 to April 1998. More than 300 objects were observed in the 1st and 2nd term and more than 200 objects that had been observed before were again observed to determine their variability. Exposure time of the 2nd term observation was determined using relation between V band magnitude in catalog and observed infrared magnitude at the 1st term observation. Exposure time of the 3rd term observation was determined using result of photometry of the 1st and the 2nd term observation.

Photometric standard stars were observed 3 times in one night, i.e. at beginning of observation, midnight and ending of observation using about 15 minutes for each times. Other time was spent to observe AGN. If above schedule was impossible because of bad weather etc., photometric standard stars were observed before and after observation of AGN as possible.

18 frames were taken for a standard star using dithering method with high altitude at J,H and K' band, and then same observation was done for but for a star with low altitude. This process was done 3 times in one night. Exposure time of standard star imaging was usually 0.3-2 second since they were bright source. AGN were observed also with dithering. Typical exposure time for AGN imaging was 35,17 and 8 second at J,H and K' band. Frame numbers of AGN at J H and K' band were 4,4 and 9 for the smallest case and 50,200 and 200 for largest case.

The 4nd quodorant of detector was in bad condition and observation was done using other regions on detector. AGN and photometric standard stars were observed in the 2nd quodorant. Reference stars for differential photometry were observed in the 1st,2nd and 3rd quodorant.

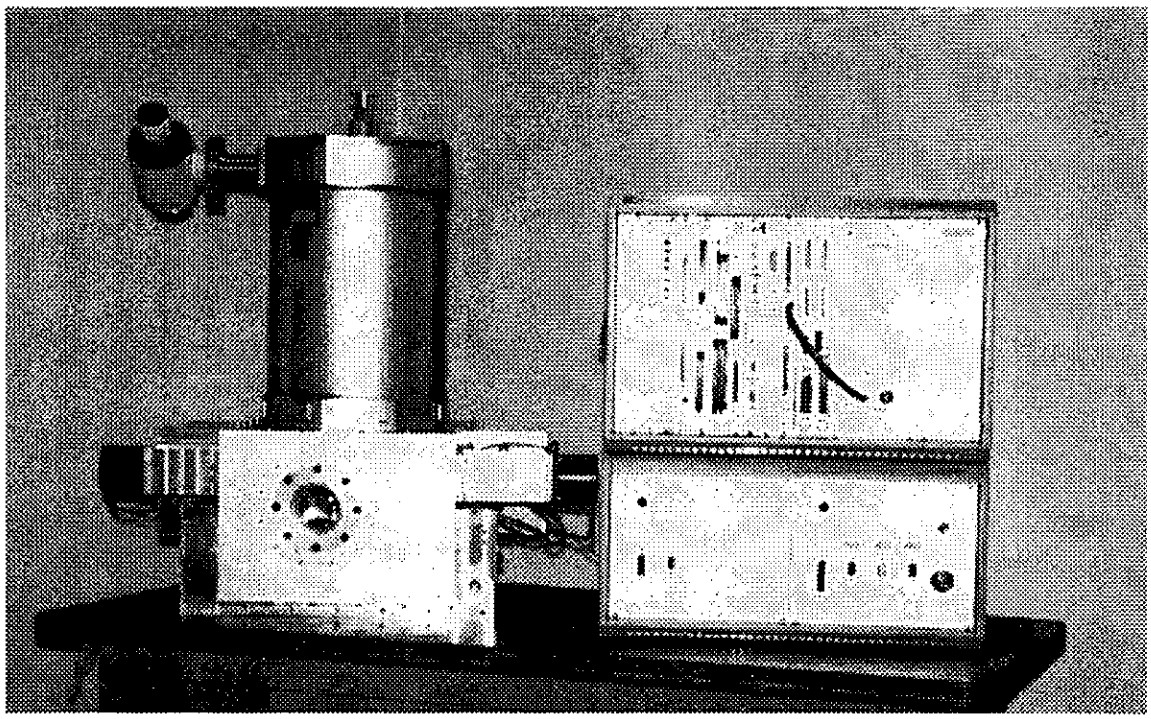

Figure 2.3: PICNIC(Prism spectrometer Polalimeter Infrared Camera with NICmos)

Table 2.1: observation

observation type	broadband imaging differential photometry
wavelength	J(1.25μm),H(1.65μm),Kd(2.2μm)
instrument	ISAS 1.3m telescope and near infrared camera PICNIC
actual term	1995/01/24-1996/04/05(the 1st term)
	1996/11/25-1997/02/24(the 2nd term)
	1997/12/18-1998/04/03(the 3rd term)

Table 2.2: telescope

site	ISAS,3-1-1 Yoshinodai, Sagamihara, Kanagawa 229, JAPAN
aparture	1.3m
primary mirror	Al coated
secondary mirror	Al at the 1st and 2nd term,Au at the 3rd term.
	optimized size for infrared.
third mirror	Au on glass. infrared transmissive beamsplitter.

Table 2.3: PICNIC

detector	NICMOS3(HgCdTe,256X256pixels)
wavelength	1.0-2.5μm
field	1.07"/pixel, 4.'6X4.'6
observation mode	broad or narrow band imaging,polalization,prism spectroscopy
polalizaion	1/2 wavelength plate spining
spectroscopy	direct view method, slitless low resolution spectroscopy(R-50)

Chapter 3

data reduction

In this chapter, process of data reduction is shown. This chapter consists of three section. The process from many raw frames of AGN and photometric standard stars to final images is shown in the section3.1. Most of process of the reduction was atomized, this has significance not only to realize more efficient analysis in this work but also to examine test of full automated reduction system that is planed for the MAGNUM project. The atomization of the reduction of this work and the MAGNUM project is shown at appendix.E.

In section 3.2, comparing instrumental magnitude of AGN to photometric standard stars the magnitude of AGN at J,H and K' band and their errors are determined. Variability of atmosphere transmissivity in one night is also estimated and shown that the variability is larger in order of at J,H and K' band. Furthermore, it is shown that dispersion of the instrumental magnitude of the photometric standard is different when dithering pattern is different, and discussion of flat fielding error is done.

Process to obtain the variability of AGN using differential photometry is written in section3.3. The variability of AGN is the most important output of this chapter. Even if the differential photometry is applied, effect of variability of PSF is not canceled completely because all AGN is not point source. Error caused by this feature is estimated and include to the result. At the end of the section, reliability of error estimation of this work is tested to apply the differential photometry process to the reference stars. As the result, it is shown that the given error of AGN is reasonable in the region of 0.01-0.10mag.

3.1 image reduction

The process from making the object frames to combining these frames is regarded as the image reduction in this work. The process of the image reduction is described in this section. All of the frames of AGN and photometric standards in this work was obtianed with short integration time with dithering, what made number of frames to be large. The aim of the short integration time is to avoid saturation of the dynemic range of measurement by sky background. The aim

of the dithering is to reduce the affection of bad pixel and the objects and to make high quality sky flat image. The raw frames obtained by the observation of this work are affected by various component as below.

- Sky background very larger then that of optical wavelength. It can be regarded as homogenious in the field of PICNIC for the acuracy required in this work. The background is variable in observation.
- The thermal emission from the object except sky, for example, telescope. It is remarkable at K' band and is not homogenious and variable in observation.
- The thermal emission and absorption by the dust on the optics, that is also remarkable at K' band. The number of the dust tends to increase in ling time scale, and the concerning position on detector slightly move with the change of the instrument direction.
- The inhomogenity of sensitivity of the infrared array larger than CCD.
- Bad pixel.
- 50Hz noise.

The software system specialized to analyze the data obtained by PICNIC(hereafter PICRED) was used to execute the reduction where the above components were reduced or cariburated and the obtained objects frame were conbined(Minezaki 1995,master thesis). The flow of the image reduction of this work is shown in fig.3.1. PICRED is semi-automized system, however, manual operations and human's decisions are also necessary to the reduction by PICRED. The manual operations ans human's decisions made it possible to deal various data like from Jupitar to quasars.

Further aoutomization of the reduction is executed through this work based on PICRED. It is the feartuers of this work that the amount of the data is large and the reduction is repeating of resemble process. The first aim of the further automization is to execute such reduction more efficiently. On the other hand, it is one of the important aim of this work as the pre observation of the MAGNUM project to extablish the automatic data reduction.

As the result, most of the process of the reduction was automized in this work. It was concluded and that to realize the full automatic reduction system was possible at the MAGNUM. For it should make the automization of the process not automized in this work possble to design not only the soutware but also the hardware and the AGN selection suitable to automization. Fuethermore the benchmark test of the automized reduction was done and it was concluded that to complete the reduction of one night data in less than 24 hours was possible at the MAGNUM proect. The automization of the reduntion and the relation to the MAGNUM is described in appendix E more deatily.

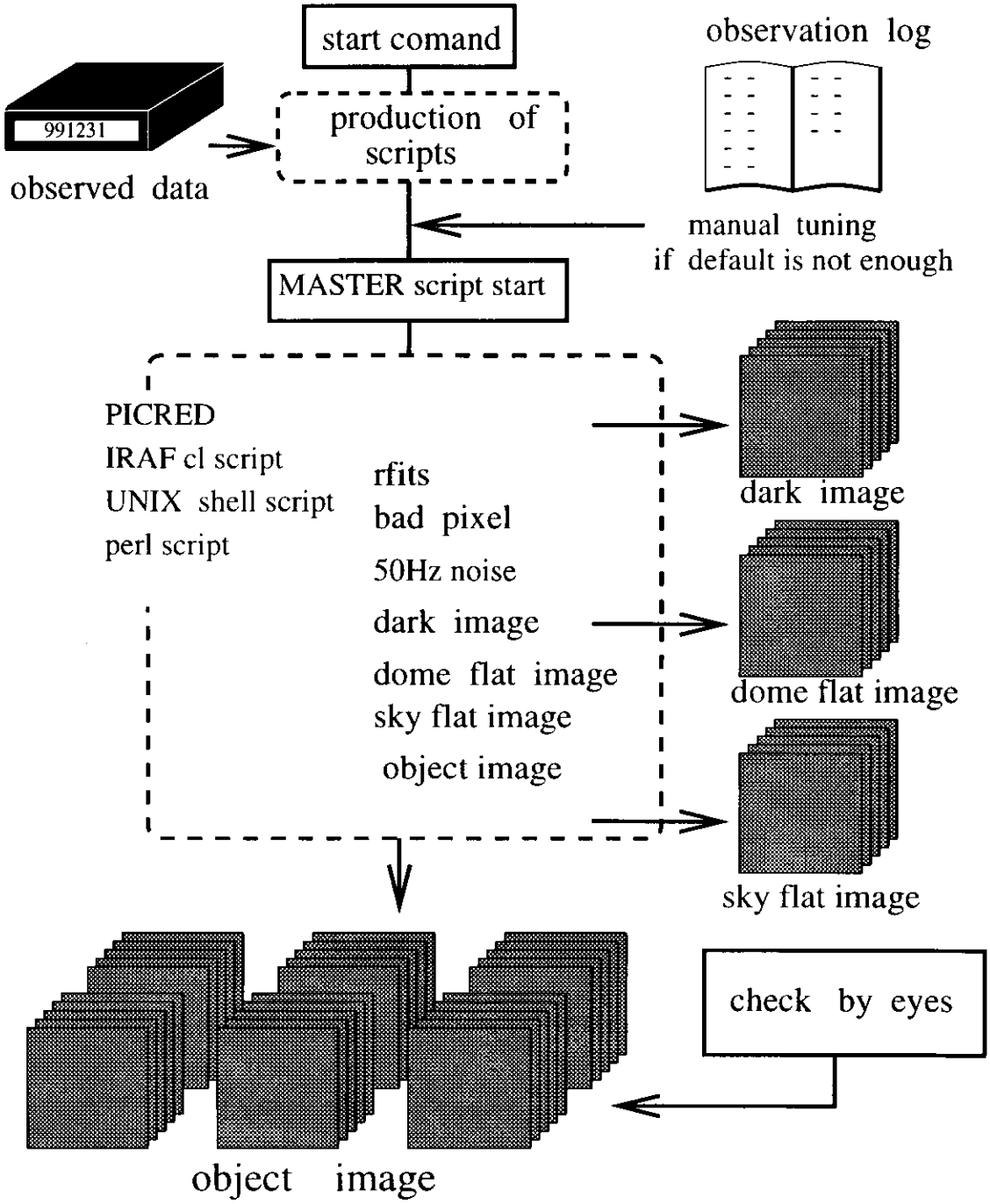

Figure 3.1: Flow of the image reduction(the former half). The process in the dashed line is executed automatically.

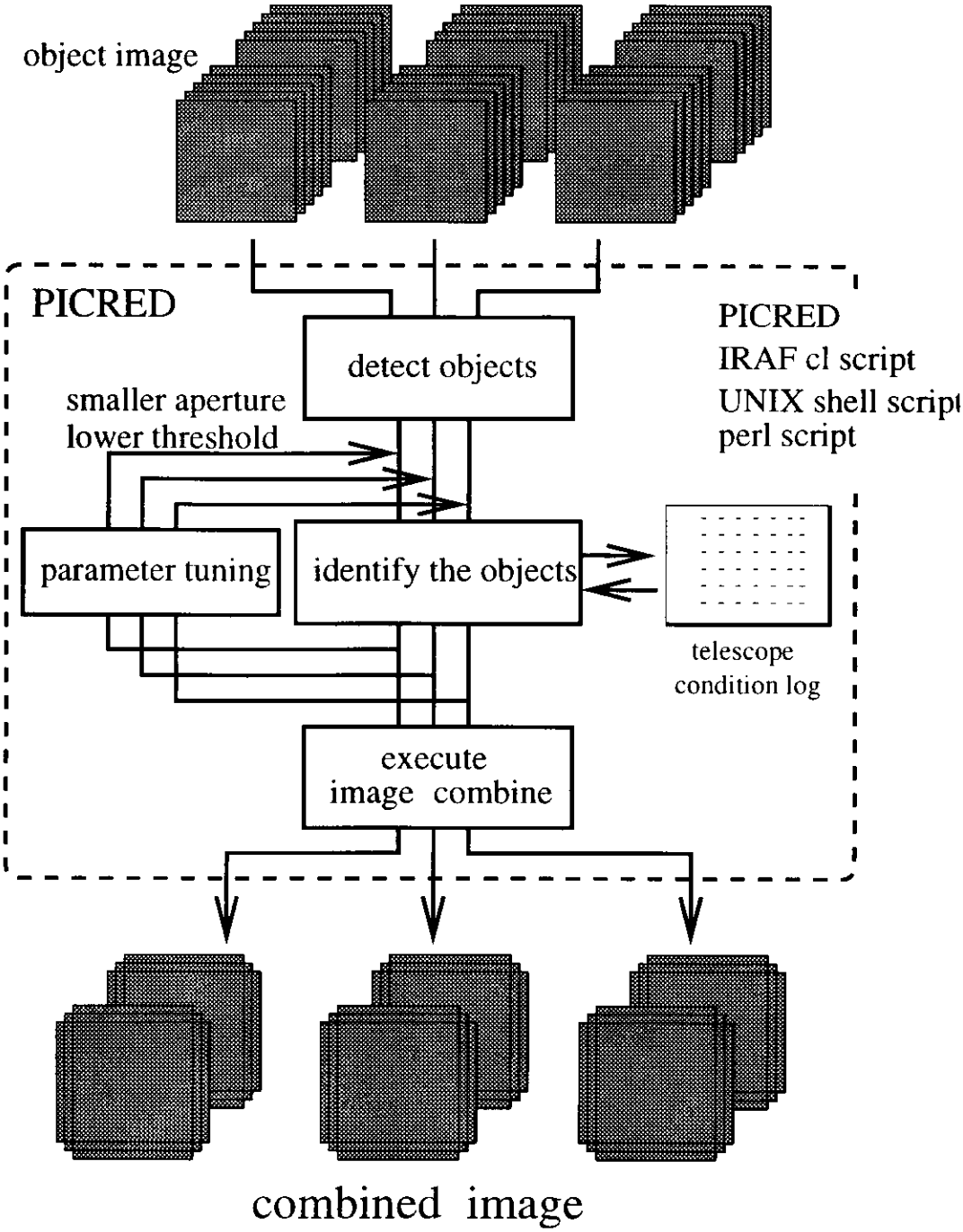

Figure 3.2: Flow of the image reduction(the later half). The process in the dashed line is executed automatically.

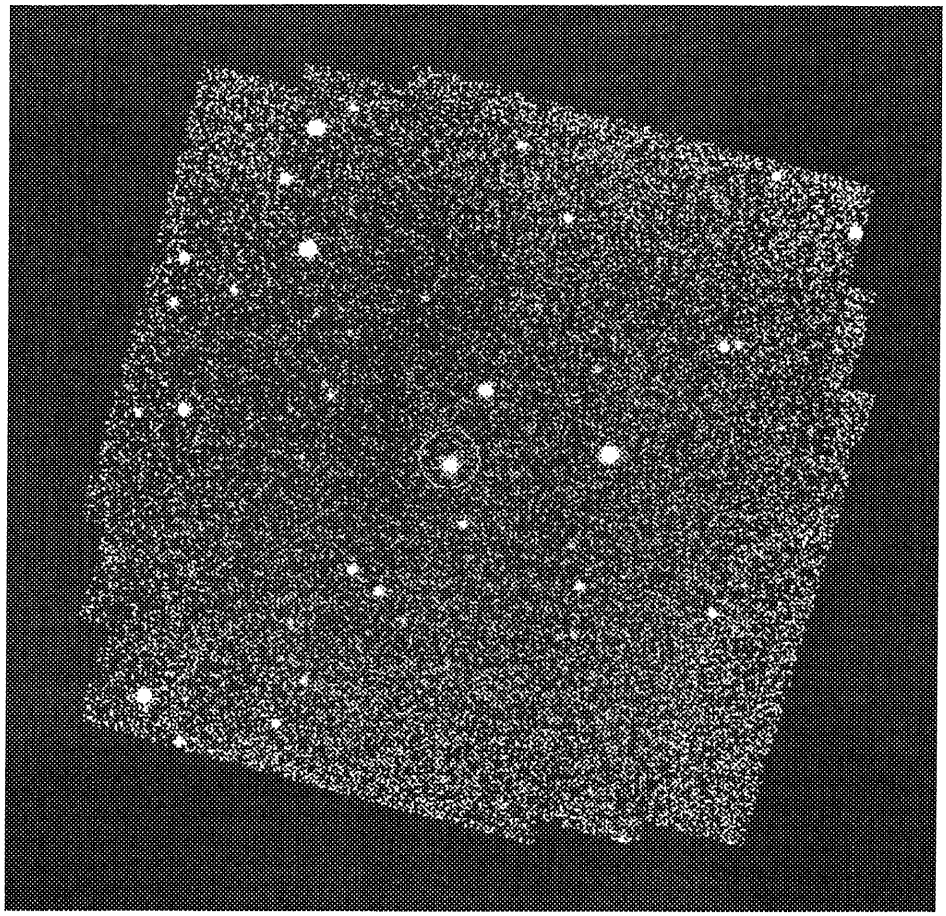

Figure 3.3: A sample of the combined image that the reduction is completed. Central object marked with a circle is target object(B2 0321+33). 9 frames observed at K' band with 8sec. integration time were combined. The observation was done on February 5,1996.

3.2 standard star photometry

3.2.1 estimation of magnitude of AGN

Photometric standard stars were observed 3 times in one night, i.e. at beginning of observation, midnight and ending of observation using about 15 minutes for each times. 18 frames were taken for a standard star using dithering method with high altitude at J,H and K' band, and then same observation was done for but for a star with low altitude. This process was done 3 times in one night.

At the first of the process, frame that bad condition like weather changing worse or else might affect was rejected. Median of instrumental magnitude of the photometric standard of the 18 continuous frame was determined and difference between obtained value and known value was estimated. Cariburation equation and its error σ_a to transform the instrumental magnitude to astronomical magnitude were obtained by linear fitting for airmass dependence of the medians. The data that was rarely seen and remarkably different from other was also rejected. The origin of such abnormal data would be influence of cloud that were not detected on observation, effect of bad pixel and identification error of the target star. Astronomical magnitude of AGN at J,H and K' band were determined using the obtained equation. Total error of the magnitude was defined as $\sqrt{\sigma_i^2 + \sigma_a^2}$ where σ_i was statistic error of the instrumental magnitude. The AGN magnitudes of J,H and K' band were obtained for 7,10,12 and 15 pixel aperture.

3.2.2 error related to atmosphere variation

Variation of seeing or atmosphere transmissivity would be cause of variation of the instrumental magnitude of the photometric standard star in one night.

Fig.3.5 is histogram of σ_a which is the standard deviation of the airmass cariburation. Abscissa and vertical arises represent σ_a and their frequency. The data determined with large 15 pixel aperture were used here. Therefore it is guessed that the origin of σ_a is rather variation of atmosphere transmissivity than of PSF. It is understand that distribution of σ_a of H band is closer to 0 than that of J band, and σ_a of K' band is further closer to 0 than that of H band. This property means that the variation of atmosphere transmissivity is more sensitive to detected photon counts at more shorter wavelength in comparison of J,H and K' band.

Parameters that characterize these features are shown in table.3.1. Only the values of σ_a that is smaller than 0.3mag were used to estimate the parameters. Both average and median of those parameters are largest at J band and smallest at K' band.

3.2.3 error related to dithering

The instrumental magnitudes of 18 continuous frames of the photometric standard tend to disperse larger than amount expected by their signal noise ratio($\leq$ 0.01mag). Influence of the variation of the atmosphere transmissivity or difference of airmass because the frames was obtained for single star continuously for a few minutes. Therefore error of flat fielding and bad pixel are reasonable candidate of the dispersion.

Fig.3.6 shows distributions of σ_d, where σ_d is standard deviation of the instrumental magnitudes of 18 frames of the photometric standard continuously obtained. Abscissa and vertical axis represent σ_d and their frequency. Solid line shows the distributions of σ_d of the 1st and the 3rd term of observation and dashed line shows those of the 2nd term. The histogram of J,H and K' band are resembled each other, especially difference of peak positions between the 1st,3rd term and the 2nd term are common feature. Observation of the 2nd term was done with only the 2nd quodorant of the detector to avoid the 4th quodorant that was under trouble. Therefore shift of the dithering in the 2nd term observation was about 30 arcsec that was a half of normal observation of the photometric standards. The fact that the difference of the dithering pattern cause the difference of the σ_d suggests that flat field error with more than a few 10 arcsec scale contributes to σ_d.

Parameters that characterize these features are shown in table.3.2. Only the values of σ_d that is smaller than 0.3mag were used to estimate the parameters. σ_d of the 1st and 3rd term of J,H and K' band are comparable and average and median are $\sim$0.033mag and $\sim$ 0.027mag respectively. σ_d of the 2nd term are smaller than those of the 1st and 3rd term, however, those of J,H and K' band are also comparable. The independence of σ_d from wavelength is contrast to the wavelength dependence of σ_a. As the result, σ_a is larger than σ_d at J band but smaller at K' band.

As described above, the dispersion of the 18 continuously observed frame tends to be larger than that expected from SN. If observation of 18 frame was done with 0.034mag statistic error (that is the value of σ_d of the 1st and 3rd term), error of the average of the frame is $0.034/\sqrt{18} = 0.008$mag. However, this value is smaller than both typical statistic error of AGN and σ_a in this work. Furthermore, affection of σ_d to the magnitude determination with photometric standard would be somewhat canceled because the dithering of AGN and photometric standard are done with almost same central position and shift step. Because of such reason, σ_a was considered as error but σ_d was not at the determination of magnitude of AGN using photometric standard.

On the other hand, affection of the variation of the atmosphere transmissivity is canceled in principle at differential photometry of point source as described in nest section. However, the error of flat fielding can not be neglected at differential photometry because AGN and reference stars with different position are compared. Therefore method using photometric standard and differential photometry are in contrast for the influence of kind of errors.

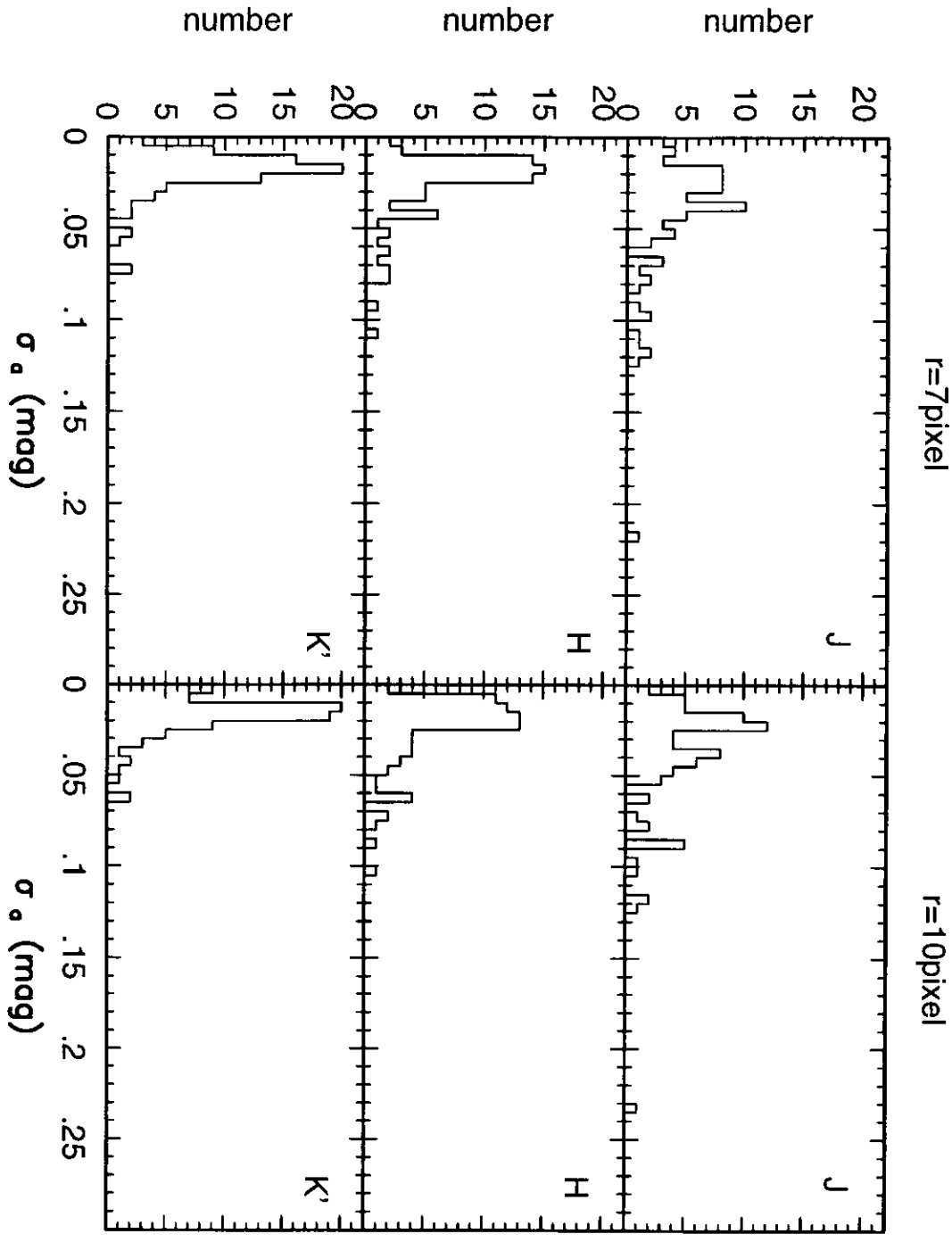

Figure 3.4: Frequency distributions of σ_a that reflects mainly the variation of the atmosphere transmissivity in one night. Top, middle and bottom figure represents the σ_a at J,H and K' band, respectively.

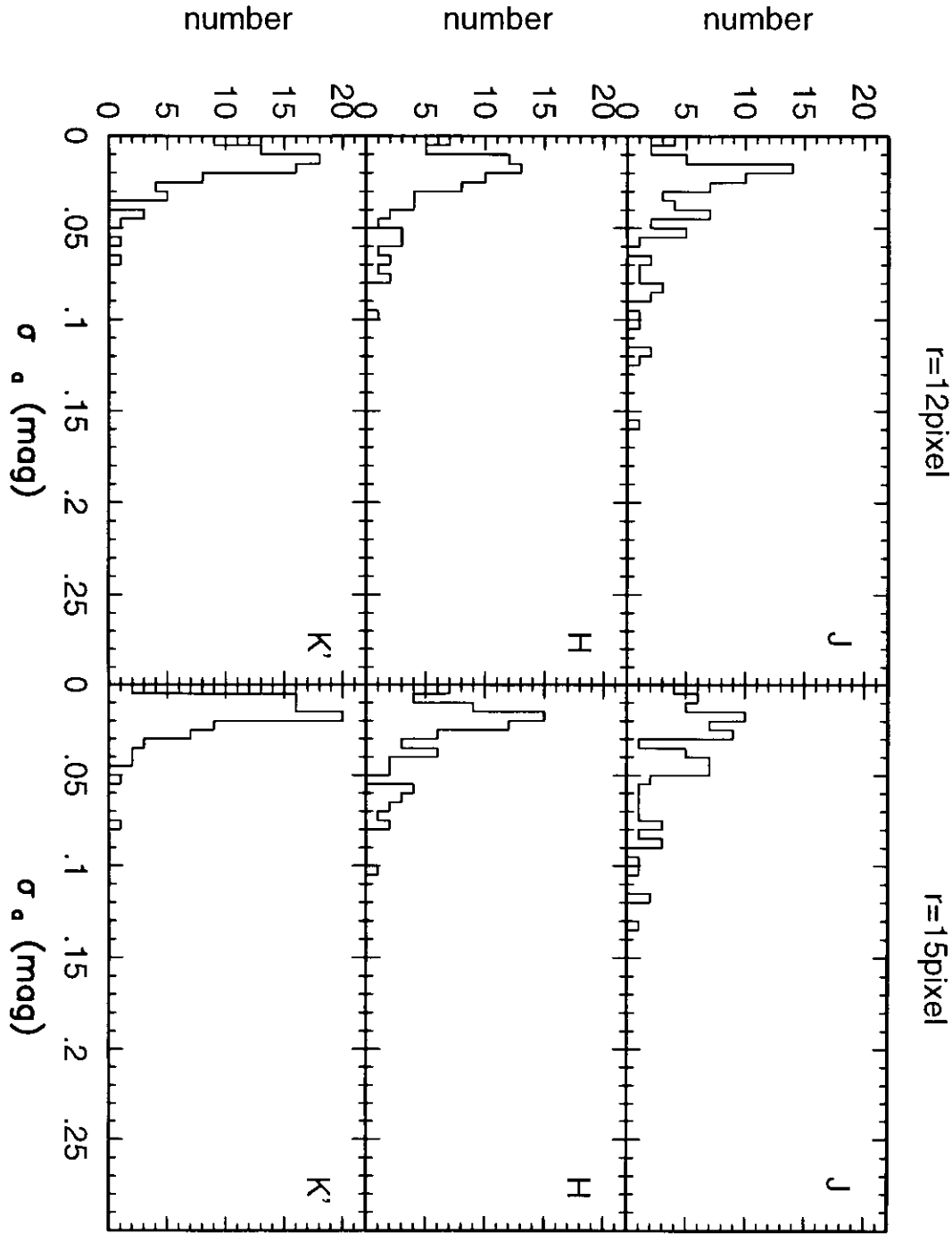

Figure 3.5: Frequency distributions of σ_a that reflects mainly the variation of the atmosphere transmissivity in one night. Top, middle and bottom figure represents the σ_a at J,H and K' band, respectively.

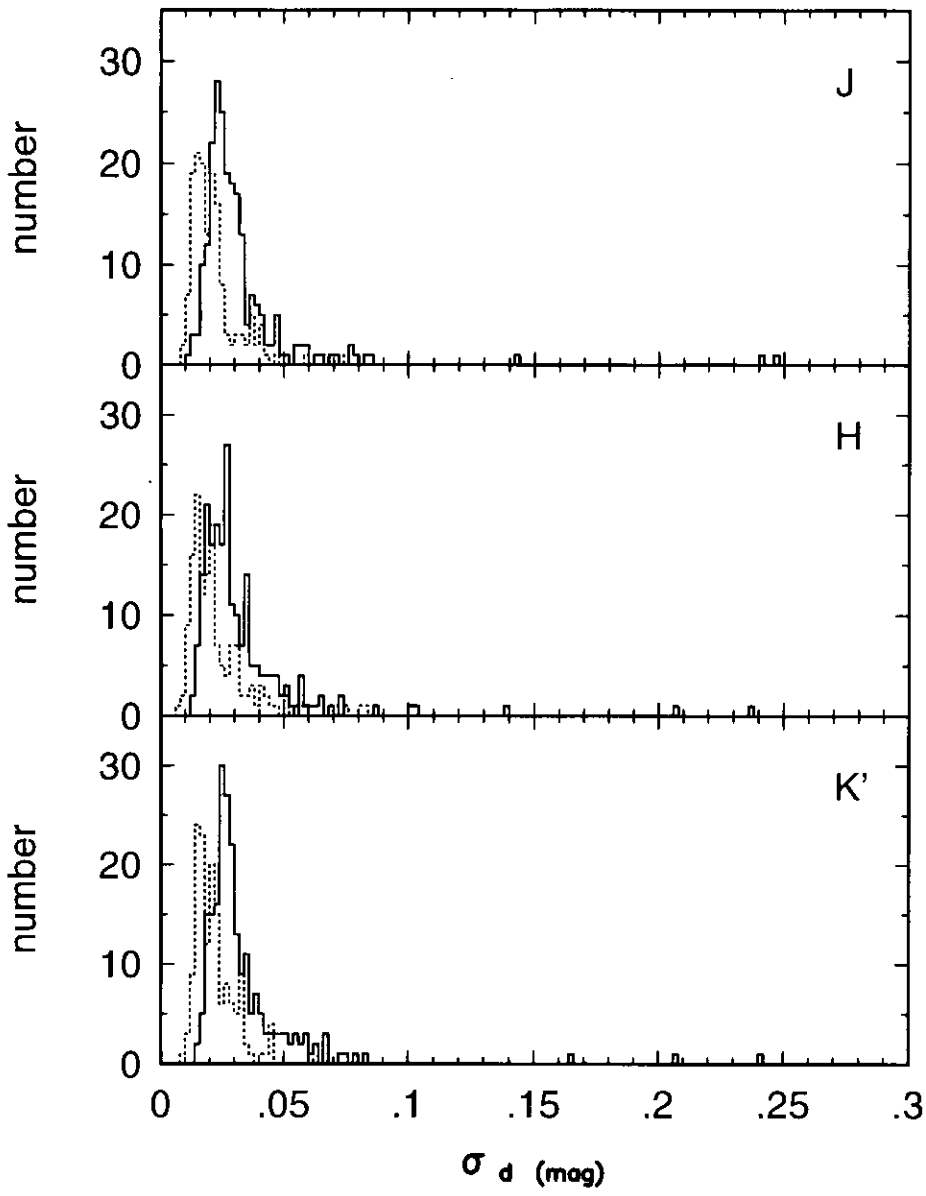

Figure 3.6: Frequency distributions of σ_d that accompanied the continuous dithering of photometric standards. Solid line represents the data of the 1st and 3rd term of the observation respectively. Dashed line represents the data of the 2nd term.

Table 3.1: Characteristic parameters of the distribution of σ_a.

	J	H	K'
data num	79	79	79
average	0.039	0.028	0.018
median	0.029	0.021	0.016

Table 3.2: characteristic parameters of the distribution of σ_d

	the 1st,3rd term			the 2nd term		
	J	H	K'	J	H	K'
data num	222	216	220	154	149	151
average	0.032	0.033	0.034	0.022	0.024	0.022
median	0.027	0.027	0.028	0.020	0.019	0.020

3.3 differential photometry

3.3.1 introduction

<problems of photometry with photometric standards>

As described before, magnitude determination of AGN with photometric standards were done in this work. However, there are some problems in variability determination where difference of the magnitudes of AGN is regarded as the variability.

One of the problems is affection of difference of PSF between AGN frames and photometric standard frames, especially in the case with small aperture. The cause of the PSF difference would be variation of seeing and/or condition of tracking of telescope.

Another problem is affection of difference of atmosphere transmissivity between AGN observed time and photometric standard observed time. The atmosphere transmissivity and seeing condition should be understand always to be varying. Total throughput of the observation vary largely when cloud comes on line of sight of the telescope. The observation was done with great care to find and avoid cloud. However, undetectable very thin cloud that could be identified after daybreak existed and therefore the detection of the cloud was limited. Observing time must be threw away even if such thin cloud is found completely. Loss of observation efficiency because the observation is limited only at photometric night is also problem of the photometry with the photometric standard.

The influence of the variation of the PSF can be avoided by to adopt large aperture. But SN of the object becomes worse when large aperture is used. The affection of the variation of atmosphere transmissivity can be somewhat avoid by to observe the photometric standards frequently. However, it isn't in principle solution, and too frequent observation of the photometric standard makes the total efficiency of the observation low.

SN of AGN caused by the photon statistic can become better and better if very long integration time is adopted. However, systematic error caused by the variation of PSF or throughput affects on the result of photometry regardless of SN of the object. So accuracy of the photometry with photometric standard is usually limited by these effect. Too long integration time isn't good because it makes the total efficiency of the observation low too.

In principle, the problems described above originate in comparison of images which were taken on different time and line of sight and instrument condition like tracking of telescope. In this work, differential photometry was adopted to detect the variability of AGN with high accuracy and reliability.

<principle and features of differential photometry>

The problems of the variation of PSF and throughput are avoided by differential photometry in principle. The principle and features of differential photometry is described bellow. At first time simple condition where target object and nearby reference objects are point sources and flat fielding error doesn't exist is thought.

- Aperture photometry is done to obtain instrumental magnitude of target object and reference objects in image of the 1st and 2nd observations.
- PSF of the objects in each frames can be regard as almost same in accuracy needed by this work.
- The variation of throughput affects equally on all object in a image.
- Therefore difference of the instrumental magnitudes between the target object and reference objects reflect real difference of their flax regardless of variation of PSF or throughput.
- The variability of the target object is determined regardless of above error effect by estimating the variation of the difference of the instrumental magnitudes between the target object and reference objects.
- As the result of canceling the systematic errors such as the variations of PSF or throughput, smaller aperture could be used for differential photometry than at analysis of photometric standards. Therefore statistic error can be smaller.
- Observation time efficiency can be higher at differential photometry than at analysis of photometric standard because observation through thin cloud is possible.

There are some kind of errors that were not canceled even by differential photometry. Error of flat fielding affects to the difference of the instrumental magnitudes between the target object and reference objects. The affection of the variation of PSF is not canceled completely if profiles of the target object and reference objects are not same. Furthermore, variability of the reference objects of course affect to the result of differential photometry.

However, as describe following, these errors that were canceled in differential photometry were not fatal defect in this work where the target AGN were not very extended samples and the most reference objects would be stars.

3.3.2 process of the differential photometry

<DSS image as position reference>

Identification of objects in the 1st and 2nd observations is important for the differential photometry. DSS images were used as reference of the identification of the AGN and reference objects. DSS(digitized sky survey) images are digitized Palomar chart. Therefore they are only useful as the position reference though their photometric accuracy couldn't expected. The reasons of adopting not infrared images obtained in this work but DSS images as the identification reference are following.

- DSS images turned to be superior to distinguish object and noise than infrared images.
- Reliability of identification with 3 image(DSS image,the 1st and 2nd images) was higher than with only the 1st and 2nd infrared images.
- Lack of photometric accuracy that is defect of the DSS image is no problem for usage of identification of the objects.
- By larger DSS image than the infrared images, objects near edge of the observed image can be detected. Such objects is not useful for the differential photometry, but the information would be useful for sample selection of the MAGNUM project.
- By larger DSS image than the infrared images, identification of AGN and nearby objects is possible even in the image of AGN that was observed only once. The result would be useful for sample selection of the MAGNUM project.

Flowchart of the differential photometry in this work is shown in fig.3.7.

DSS images were prepared for each AGN observed in this work. Size of images were 12X12 $arcmin^2$, that was larger than infrared images obtained with dithering. The DSS images used for the analysis were obtained automatically from database of Data Analysis Center of NAOJ with batch script. DSS2 images that resolution was better than DSS1 image were used as possible as could, but DSS1 images were used for the region where DSS2 didn't cover.

Obtained DSS images were done fits and objects in the images were detected by IRAF cl script that consisted of DAO find task and perl script automatically. After some try and error of tuning of detection threshold, DSS images turned out to be more useful to distinguish the objects and noise than the infrared images of this work.

Marking the target AGN on each DSS images were done by manual operation comparing the images and finding charts since the most central object was usually the target AGN, but sometimes not because of error of position data. The finding charts were prepared based on information in

VV catalog. To mark more easily on many images, cl script was prepared and used where the nearest object from mouse clicked point was searched and found object was regarded as the target AGN if it was enough near, or regarded as not found and error message was uttered. The result of the detection of AGN and nearby objects were written into text file with other information automatically.

<detection of objects in infrared images>

Detection of objects in infrared images were done with cl script that was resembled to the script for DSS images automatically. Luminosity of observed AGN distributed wide range. Large numbers of noises were detected if the threshold was set enough low to detect faint AGN of this work. However, the threshold of the detections were set somewhat lower than that for DSS images because AGN had to be detected. There were very much miss detection at edge of the obtained infrared images. Level of the images were estimated and the edges were smoothed with IRAF task for image replace automatically. After those operations, the miss detections fairly reduced but were not exterminated.

Most of AGN were detected in the automatic detection process together with nearby objects, however, some of the faint AGN were not. Manual try and error with tuning of parameters of detection were done. Invisible AGN in the infrared image or very faint AGN that were not detected in any try were regarded as non detected.

The most central object were not always the target AGN in obtained infrared images partly because tuning of telescope pointing were omitted for some interval. Furthermore, offcenter region of detector was used to detect AGN for the 2nd term of the observation because of the trouble of the 4th quodorant of the detector. Therefore it was necessary to identify and mark target AGN in infrared images by manual operations with the finding charts. The process which was similar to those for DSS images were used to mark on more than 1500 images more easily.

<identification of reference objects>

It was necessary to identify detected reference objects in the 1st and 2nd infrared images of AGN for the differential photometry of AGN. The process of identification of the objects was automated since number of the reference objects was larger than that of AGN for one order.

Top of the DSS images and the infrared images corresponded to north and dispersion of the direction was smaller than a few degree. Coordinates of the detected objects in the DSS images and the infrared images were transformed to new coordinates that the origin was AGN and unit was arcsec. The objects in each infrared images closer than 10 arcsec from the position in DSS image were regarded as candidate of same objects. If two or more objects were found in the aperture, each or all of them were not adopted to avoid error of identification. Comparing the

DSS images and infrared images, least square fitting was executed where the direction of the images and expansion factor were free parameters. The fitting were iterated with smaller aperture and new starting parameters which were obtained as the result of the last fitting. The final value of rotation parameter was smaller than a few degree and expansion parameter was in 100± a few % for most case. The processes were almost always successful and script produced from the result of last iteration automatically was useful except some cased where only very faint objects were detected in the images. The most typical cause of the case where the parameters didn't converge well were that only very faint objects were detected in the images. The parameters were tuned with manual operation. Data sets where the identification processes were not successful were neglected in following analysis.

The aperture was reduced toward 2 arcsec and only the objects which were survived those process were regarded as same objects. The size of the aperture(2 arcsec) was comparable with FWHM of typical point source in infrared images. Correction of distortion was not necessary in above processes.

<estimation of the variability of AGN>

At the first step of the estimation of the variability of AGN, origin of the variability of AGN were determined, and then the variability of the AGN were estimated as following. Variations of the instrumental magnitudes $\Delta m_i = m_{2i} - m_{1i}$ of each reference objects(i=1,2,3,..) and their statistic error σ_i were calculated.

$$\Delta m_i = m_{2i} - m_{1i} \tag{3.1}$$

$$\sigma_i = \sqrt{\sigma_{2i}^2 + \sigma_{1i}^2} \tag{3.2}$$

where $m_{1i}, m_{2i}, \sigma_{2i}, \sigma_{1i}$ are the instrumental magnitudes and their statistic errors of the i-th object of the 1st and 2nd observations. Difference of the instrumental magnitudes Δm_i sometimes dispersed larger than amount of expected by its statistic error σ_i. Error of flat fielding is reasonable as the candidate of the origin of the dispersion. The flat fielding error would affect on all reference objects equally regardless of their luminosity. And then σ_f was determined to fill next equation(3.3) to take account of the effect of the dispersion. This means that σ_f was added to errors to make left hand of (3.3) expectation of the χ^2 distribution with N freedom. The value of σ_f was obtained by numerical solution. If the solution of real value didn't exist, σ_f was determined as 0 because no addition of σ_f was necessary to explain the dispersion.

$$\sum_i \frac{(\Delta m_i - \Delta m_{ave})^2}{\sigma_i^2 + \sigma_f^2} = N \tag{3.3}$$

Next, weighted average Δm_{ave} of the variations of the instrumental magnitudes of the reference objects and their errors $\sigma_{\Delta m_{ave}}$ were calculated. These values were used as the origins and their errors to determine the variabilities of AGN.

$$\Delta m_{ave} = \sum_i \frac{\Delta m_i}{\sigma_i^2 + \sigma_f^2} / \sum_i \frac{1}{\sigma_i^2 + \sigma_f^2} \tag{3.4}$$

$$\sigma_{\Delta m_{ave}} = \sqrt{\frac{1}{(n-1)} \sum \frac{(\Delta m_i - \Delta m_{ave})^2}{\sigma_i^2 + \sigma_f^2} / \sum \frac{1}{\sigma_i^2 + \sigma_f^2}} \tag{3.5}$$

The variability of AGN Δm_{agn} was obtained after estimating the difference between variation of instrumental magnitudes of AGN and the origin of the variability. The error was estimated using the instrumental magnitudes errors of AGN in the 1st and 2nd observations $\sigma_{\Delta m_{1agn}}$, $\sigma_{\Delta m_{2agn}}$, the error of the origin $\sigma_{\Delta m_{ave}}$ and σ_f as below.

$$\Delta m_{agn} = m_{2,agn} - m_{1,agn} - \Delta m_{ave} \tag{3.6}$$

$$\sigma_{\Delta m_{agn}} = \sqrt{\sigma^2_{\Delta m_{2,agn}} + \sigma^2_{\Delta m_{1,agn}} + \sigma_f^2 + \sigma^2_{\Delta m_{ave}}} \tag{3.7}$$

Those processes were also applied to determine the reference objects. Abnormal data were found by 5 σ rejection, and the process to determine the variability of AGN was iterated. After 3 times iterations, no more object was found as the abnormal data. Most of the objects detected by the 5 σ rejections would be originated by error of identifications or effect of positioning edge of the frame, however, some of them could be variable stars. 3 σ rejection was done once after 5σ rejections.

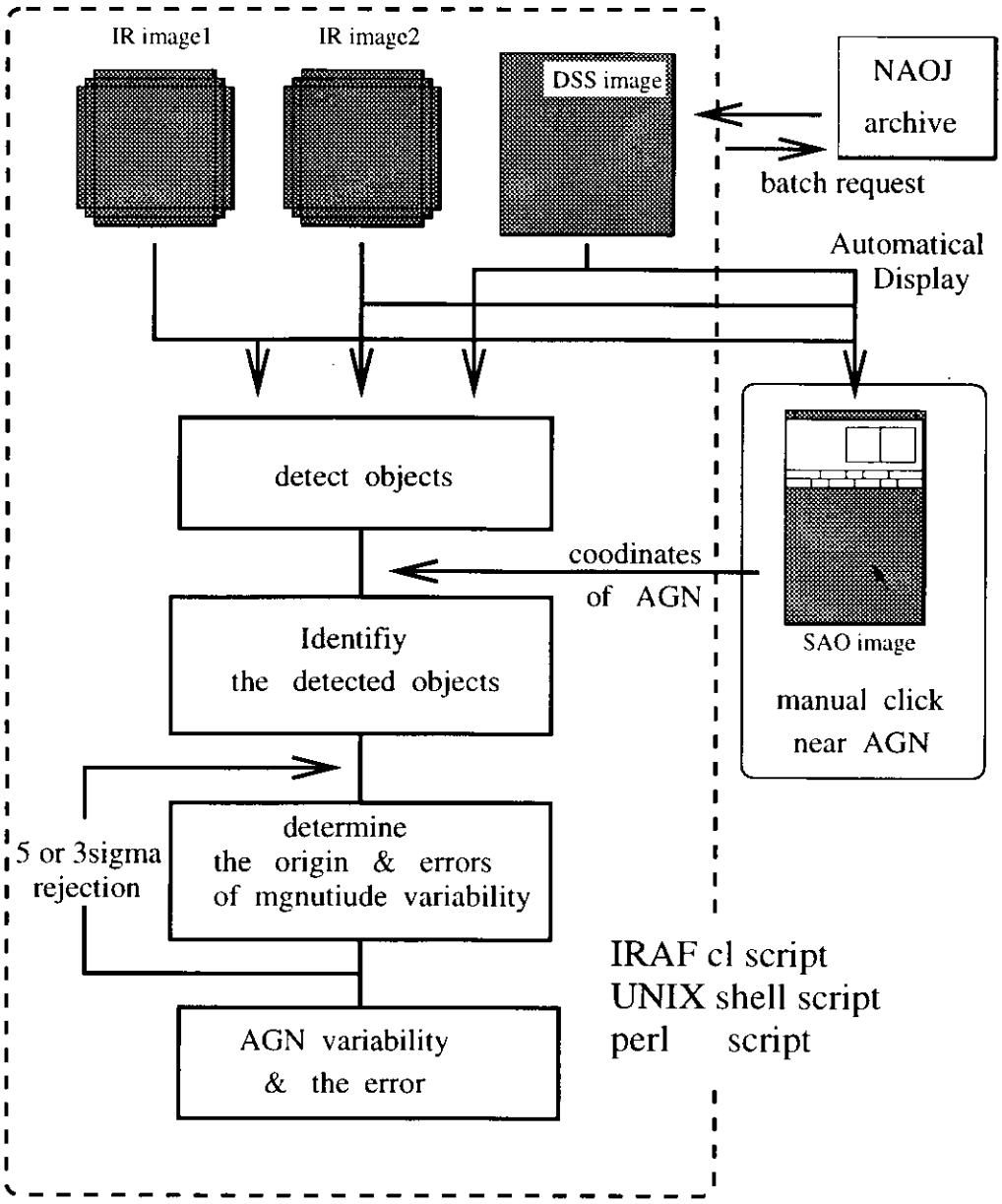

Figure 3.7: Flow of the differential photometry. The processed in the dashed line are atomized and each of them are completed without manual operation but start commands. The identifications of the target AGN on the images need human's judgment. To make the manual process of ~2000 images, the system is developed where the identification of one image needs only once mouse click.

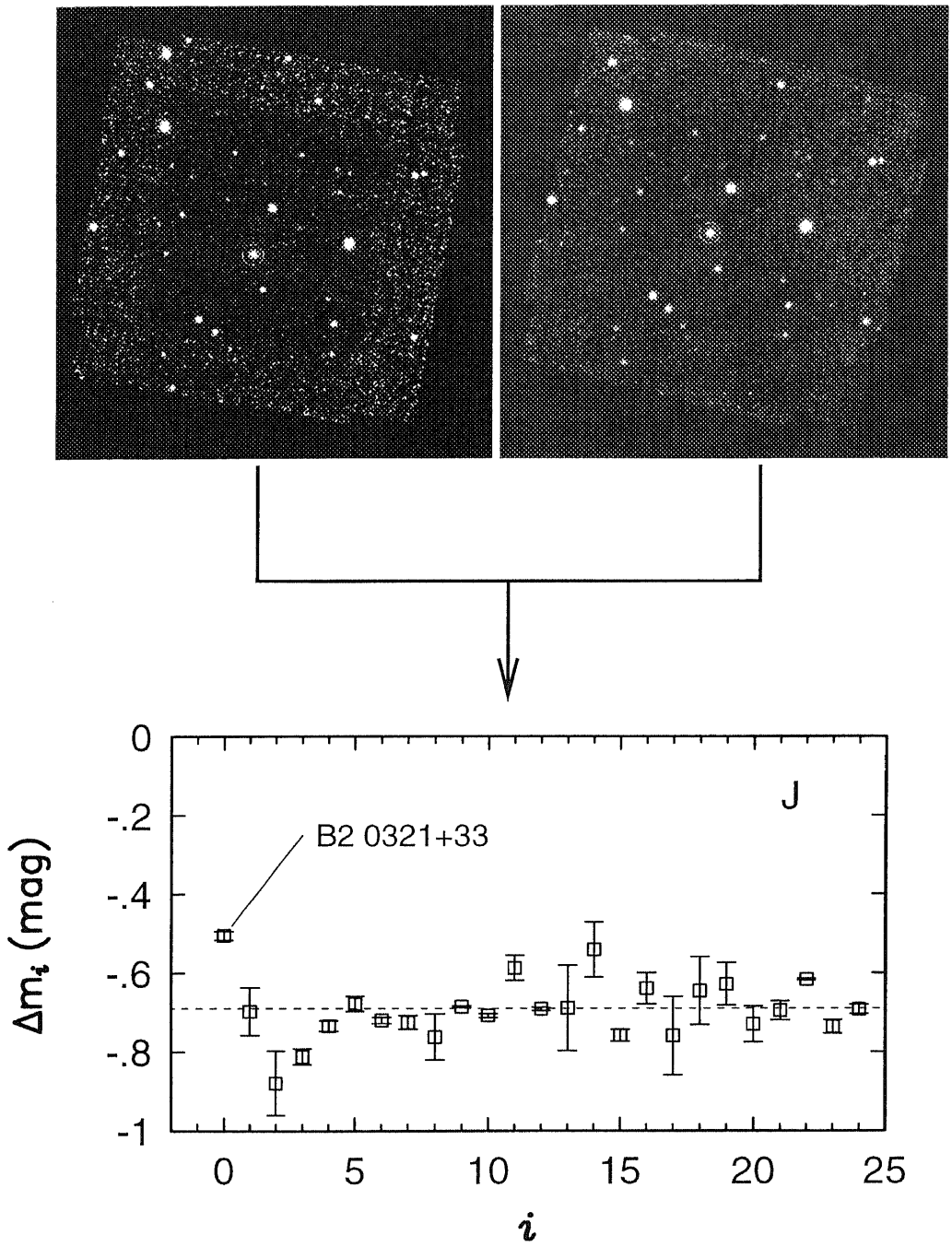

Figure 3.8: Figures for principle of the differential photometry. The left is the 1st image of B2 0321+33 at J band with 136sec integration time. The target object is shown by the circle. The right is similar but the 2nd image. The 1st and 2nd observations were done on 1996 February 5 and 1998 January 5. The lower figure shows the variations of the instrumental magnitude of the identified objects in those images. The abscissas axis represents merely number of identification. For the objects except the AGN, the instrumental magnitudes turned smaller in average by $\sim$0.7mag, while the variation of AGN is smaller, what means that the AGN turned to be dark. It is the main reasons why the instrumental magnitudes of all objects turned smaller to restore the Al coating of the primary mirror, to change coating of the secondary mirror from Al to gold, to restore the coating of the beamsplitter and to differ the seeing of conservations.

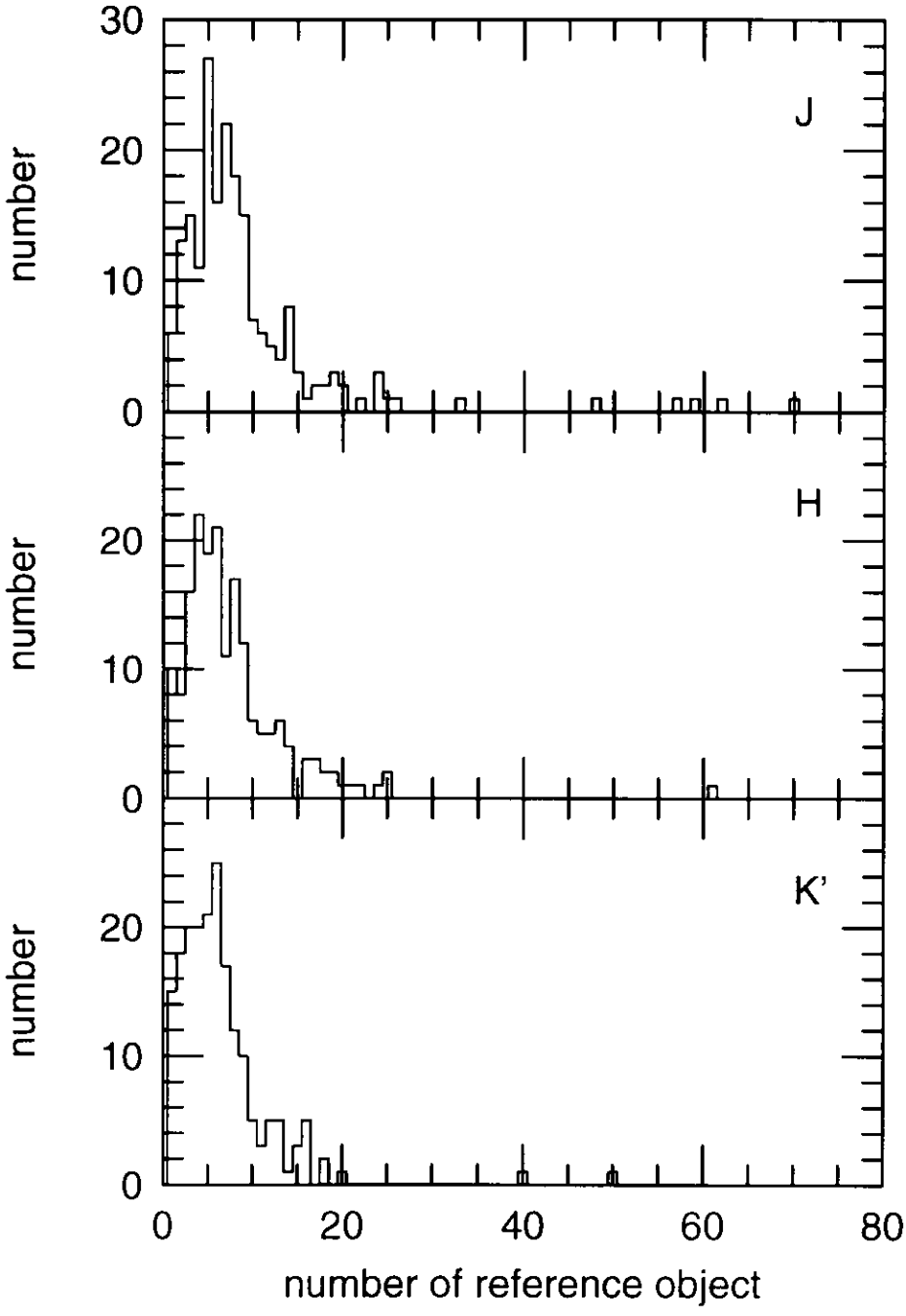

Figure 3.9: Frquency ditributions of the reference objects used for each differential photometry.

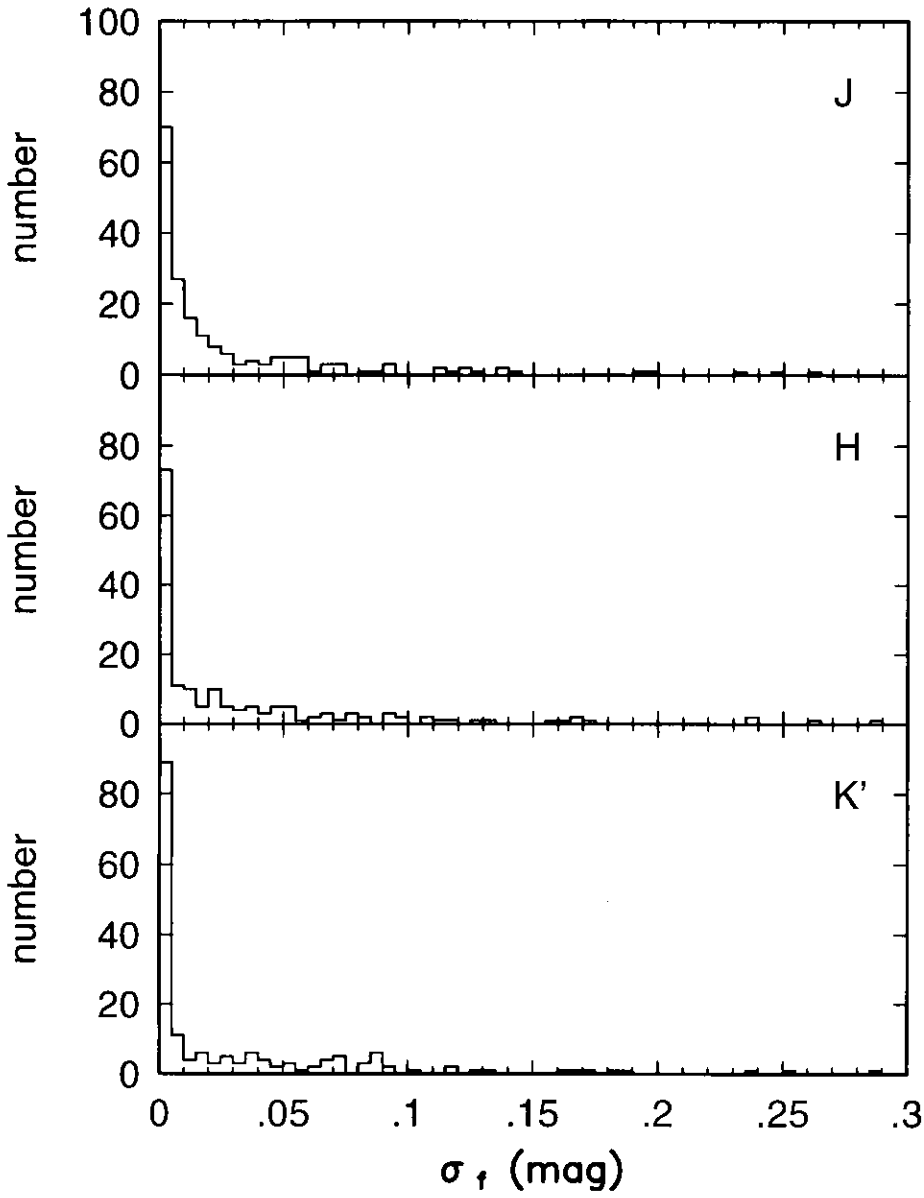

Figure 3.10: Frequency distributions of σ_f.

Table 3.3: characteristic parameters of the distribution of σ_f

	J	H	K'
sample	189	168	172
average(mag)	0.028	0.033	0.030
median(mag)	0.009	0.009	0.000
standard deviation(mag)	0.046	0.053	0.051

3.3.3 effect of PSF variability

It is important advantage of the differential photometry that the result is less sensitive to variation of PSF than in photometry with photometric standard. In principle, effect of the variation of PSF should be canceled completely if PSF of the reference objects and target object were same shape (3.11a). However, most of the reference objects were stars in this work while the target object was AGN, therefore there was probability that the result of the differential photometry was affected by the variation of PSF. As shown in fig.3.11b, it is expected that seeing of growing better(or worse) bring to add fake brightening(or darkening) to the result of the differential photometry when the PSF of the target object is more extended than the PSF of the reference objects. In this section, difference of FWHM of the 1st and 2nd infrared images, and then the affection of the PSF variation to the result of the differential photometry is estimated.

Estimation of the FWHM in the 1st and 2nd infrared images was done with cl script that including IRAF imexamine task. The FWHM as output of the imexamine task tended to be larger for more dark objects. To avoid this effect, variation of the FWHM of each reference objects were estimated in the first step of determining the difference of FWHM between the 1st and 2nd infrared images. Only reference objects that peak count of the instrumental magnitude was more than 50 were used in the process. Next, median of the variations of FWHM of each objects were estimated that was regarded as the variation of FWHM between the 1st and 2nd infrared images.

Fig.3.12 shows distributions of the difference of FWHM between the 1st and 2nd infrared images for J,H and K' band. The shape of the distribution is like Gaussian at each band. Center of the distribution is shifted toward positive side, what means that the case that PSF was turned worse was more frequent than turned better. Change of light axis of the telescope is plausible as the cause of this feature because the primary mirror was removed once to repair coating in off season between the 2nd term and the 3rd term of the observation. However, it is impossible to deny that bad seeing night was significantly more at the 3rd term by only above data.

Average,median,mode and standard deviation of the distributions are shown at fig.3.4 for J,H and K band. The distribution is extended more widely at the band corresponding to shorter wavelength. The mode of the distribution of each band tends to be large at each bands, however, significance of the differences are unclear.

Next, the influence of the variation of PSF to the result of differential photometry way considered. Analysis was done using IRAF gaus task where the infrared image with smaller FWHM of the two was convolved and differential photometry for the image was done.

Fig.3.13 shows the process as a flow chart. The convolution with σ=0.5, 1.0, 1.5 ... 4.0 was executed and then the differential photometry was done for each times. Region including the point where the difference became 0 was determined and corrected variability of AGN was obtained by interpolation of the result of differential photometry at both end of the region. cl script to be con-

sisted of IRAF gaus, DAO phot, imexamine task, perl and UNIX shell script was developed and used to make the analysis efficient. All operation for all images were completed after automated process for about 3 days.

Fig.3.14 shows the dependence of the correction of the AGN variability on the variation of the FWHM between the 1st and 2nd infrared images. The error of the correction was estimated as following.

$$\frac{\Delta m_l - \Delta m_r}{FWHM_l - FWHM_r}\sigma_{\Delta FWHM} \tag{3.8}$$

where $FWHM_l - FWHM_r$, $\Delta m_l - \Delta m_r$ was difference of the FWHM and variability of AGN at the both side of region including the best convolution. $\sigma_{\Delta FWHM}$ was error of estimation of FWHM difference. To avoid other errors, only the data of which accuracy of the instrumental magnitude of AGN was better than 0.02mag and the error of the correction was smaller than 0.05mag were used in the analysis. Data of J,H and K' band were mixed and used here because the sample of each band became too small under the limit of above condition.

The results of the analysis tend to plotted on increasing sequence toward right direction from the origin in fig.3.14. This feature is consistent with the fake variability commented above. When those process were applied to the data with less SN, the plot was extended widely and significant result was not obtained. Distribution of frequency of the corrections is shown at fig.3.14. σ of this distribution is 0.01mag.

In the analysis of this section, AGN of which determined the apparent variability caused by the variation of the PSF were limited in the bright and nearby objects. Therefore it was impossible to correct the effect for all AGN in this work. Fortunately, extension of host galaxy of dark and further AGN tend to be small, so the influence of the PSF variation for those objects tend to be small too (fig.3.11a). The correction of the fake variability would be smaller for such case. The value of 0.01mag is smaller than scale of other errors in this work and is not dominant error. For these reasons, the affection of the PSF variation was treated as below.

- The Correction of the variability data of AGN was done.
- The error of 0.01mag was added to the total error by (3.11a)

There is possibility that the correction of the variability data of AGN is necessary to the MAGNUM project where observation with 0.01mag accuracy is planed. Figure shown in fig.3.11 will be able to make for each AGN since each AGN will be observed for many times at the project. In such case, the sequence of dependence of the correction for the apparent variability on the variation of seeing will be able to determined for each objects. Therefore the correction of the variability data of each AGN is expected to be done without convolution of obtained images.

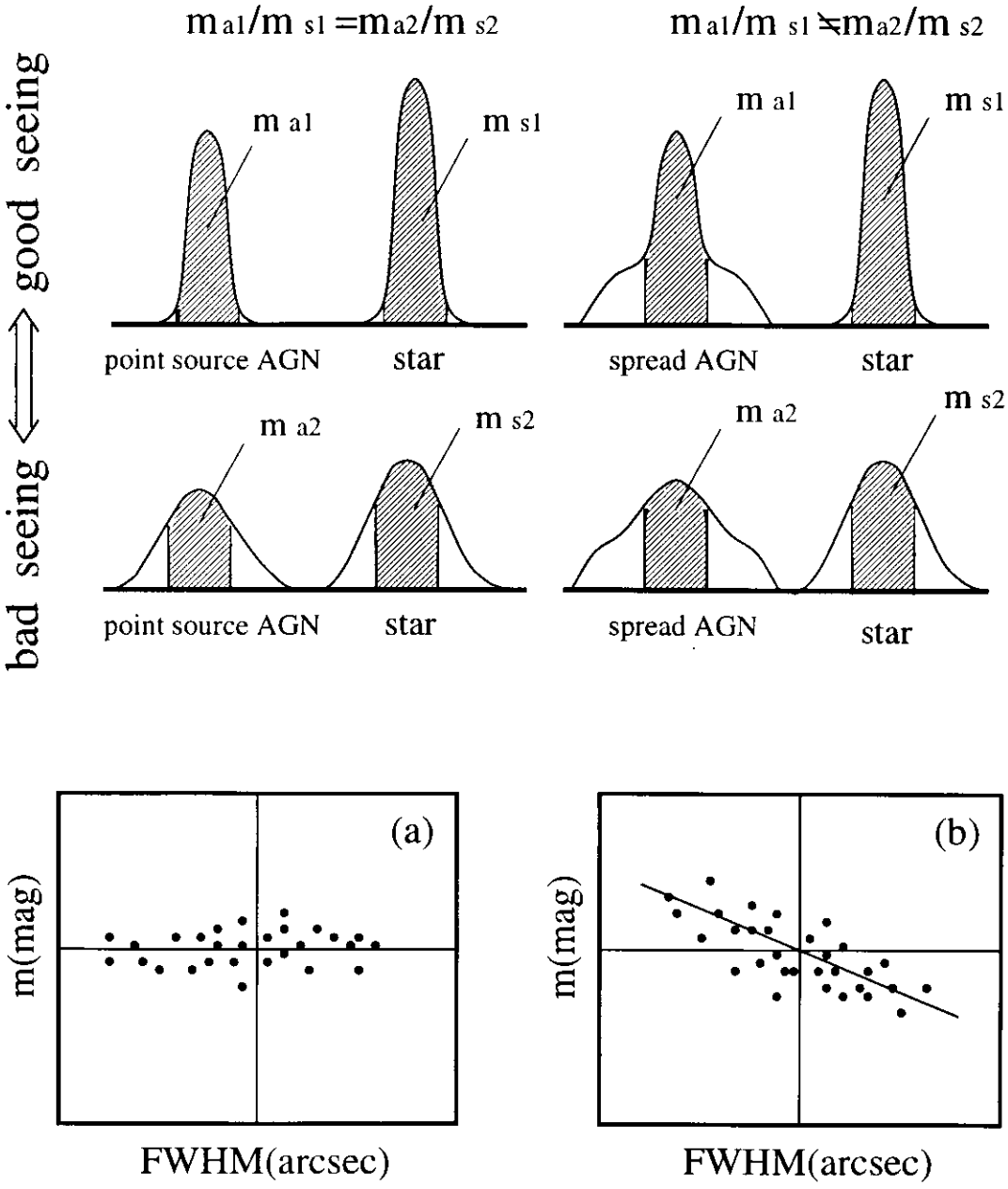

Figure 3.11: Figure to show the influence of the PSF variation to the differential photometry. m_{a1},$s_{s1}$$m_{a2}$,$s_{s2}$ represents the instrumental magnitude of the AGN and the reference star obtained in the 1st and 2nd observations. The left side(a) represents the case to regard the AGN as a point source. The ratio of the flux in the aperture isn't changed with the broadening of the PSF and the variability obtained by the differential photometry is not affected. This is the important feature of the differential photometry. Th right side(b) represents the case when the profile of AGN is extended. AGN's flux in the aperture isn't decrease as much as that of the reference star with the broadening of the PSF. Therefore apparent brightening of the AGN can be detected.

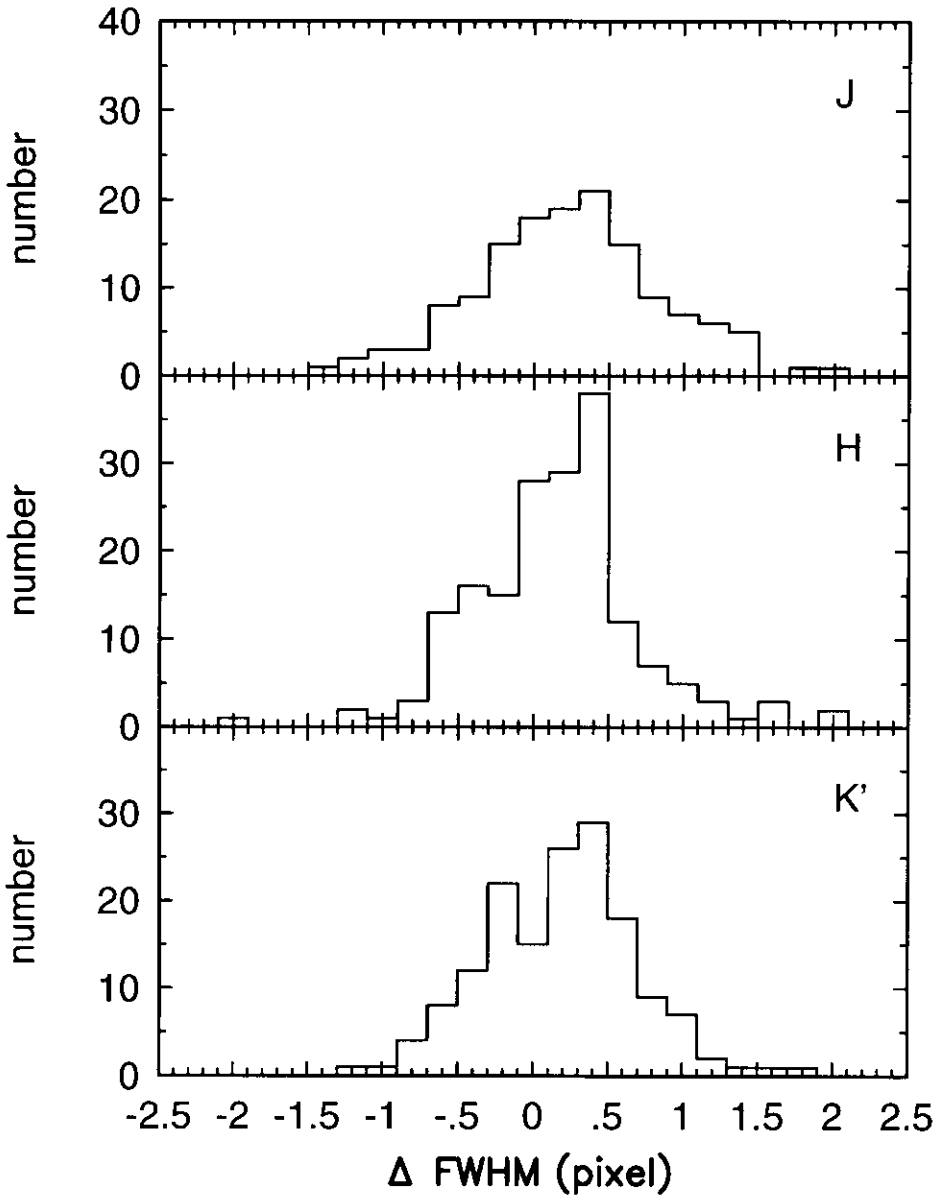

Figure 3.12: Frequency distributions of the variations of the FWHM. Top, middle and bottom represents the result of J, H and K' band respectively. The cases with increased FWHM are more frequent than decreased case, what is probably caused by the change of the light axis of the telescope accompanied with the coating of the primary mirror.

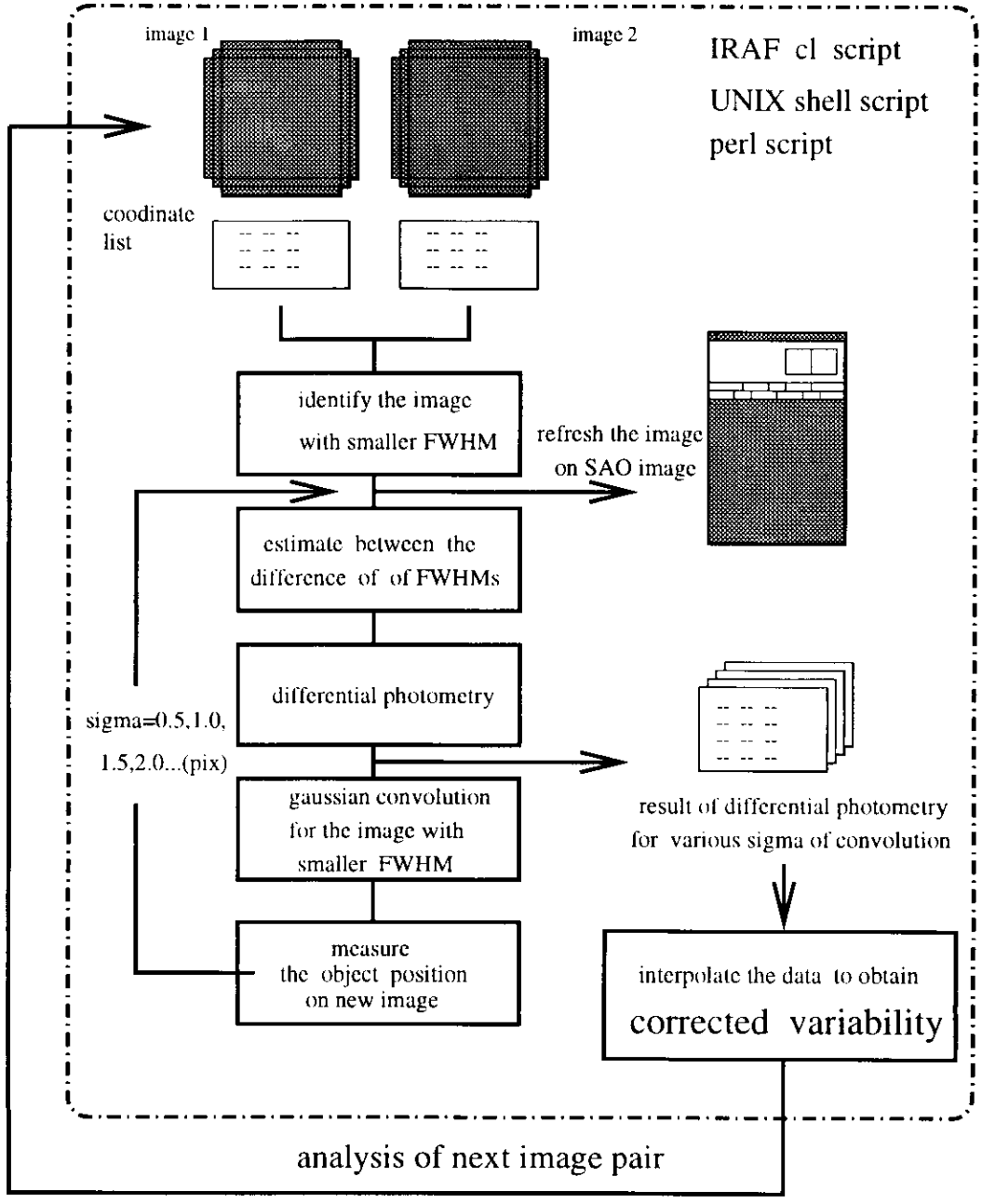

Figure 3.13: Flow of the processes to estimate the influence of the difference of the PSF between the 1st and 2nd observations.

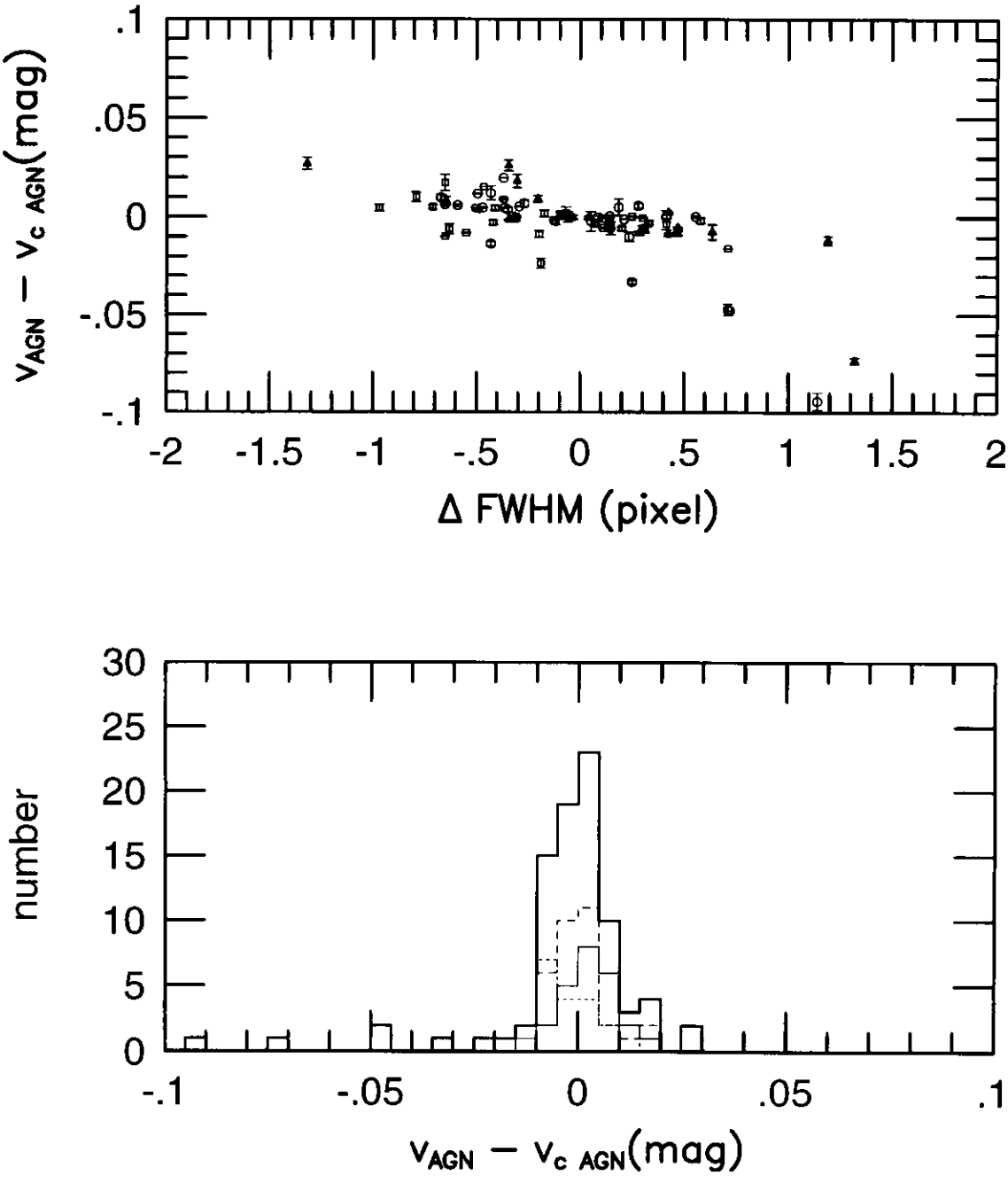

Figure 3.14: Top figure shows the relation between the variation of FWHM of point sources and the apparent variabilities of AGN obtained by the analysis of this section. Bottom figure shows the distribution of the apparent variability of AGN.

	J	H	K'
sample	144	180	157
average	0.14	0.06	0.09
median	0.13	0.06	0.14
standard deviation	0.64	0.58	0.50
mode	0.4	0.4	0.4

Table 3.4: Characteristic parameters of the distributions of the difference of FWHM between the 1st and 2nd observations.

sample	84
average	-0.017
median	-0.000
σ	0.010

Table 3.5: Characteristic parameters of the distribution of the apparent variabilities of AGN obtained by the analysis of this section.

3.3.4 test of the error estimation

The error estimation of the variability data is very important. If the error is estimated too small, fake variability is concluded from dispersion of data that is originated by not intrinsic variability but only statistic dispersion. If the error is estimated too large, the variability cannot be concluded with certain significance even when the variability was detected.

The variability of the reference objects was fairly smaller than those of AGN because most of the reference objects consisted of stars. In this section, the variability of the reference objects was determined by differential photometry, and then the the error estimation of the differential photometry in this work was tested in comparing the calculated errors and dispersions of the result of the photometry.

The variability of the reference objects was calculated using the origin $\Delta m_{ave}, \sigma_{\Delta m_{ave}}$ that was obtained in the analysis of AGN variability. The reference objects were divided into subsamples that the calculated error was $0 \leq \sigma < 0.01$,$0.01 \leq \sigma < 0.02$,...$0.09 \leq \sigma < 0.1$. Table3.6 shows the sample number of each subsamples. Fig3.15 shows relation between the calculated error and the standard deviations of the value of the variability in each subsamples. The plot of J,H and K' band are similar to each other, and it is shown that the calculated errors are nearly equal to the result of the differential photometry. Most of the plots are below the line of $y = x$ slightly, what is in rather desirable sense that is over estimation of the error in the differential photometry of this work. Some plots are above the line of $y = x$ at the region of calculated error < 0.03mag, however, what is not serious problem because excess is small and explained by inclination of the objects toward the side of large value in the subsamples.

It is reasonable that averages of the result of the differential photometry are almost equal to 0 at the region of calculated error < 0.07mag for J,H and K' band. However, the averages tend to be plotted above 0 at the region of calculated error > 0.07mag, what corresponds to the sense becoming more dark. This feature is explained by improvement of throughput of the telescope that primary mirror coating was repaired.

As above, it was confirmed that the error given in the process of the differential photometry was the best value or slightly larger. Therefore, it is concluded that the error estimation of the differential photometry of this work is reliable quantitatively in the region of the error 0.01$\sim$0.1 for J,H and K' band.

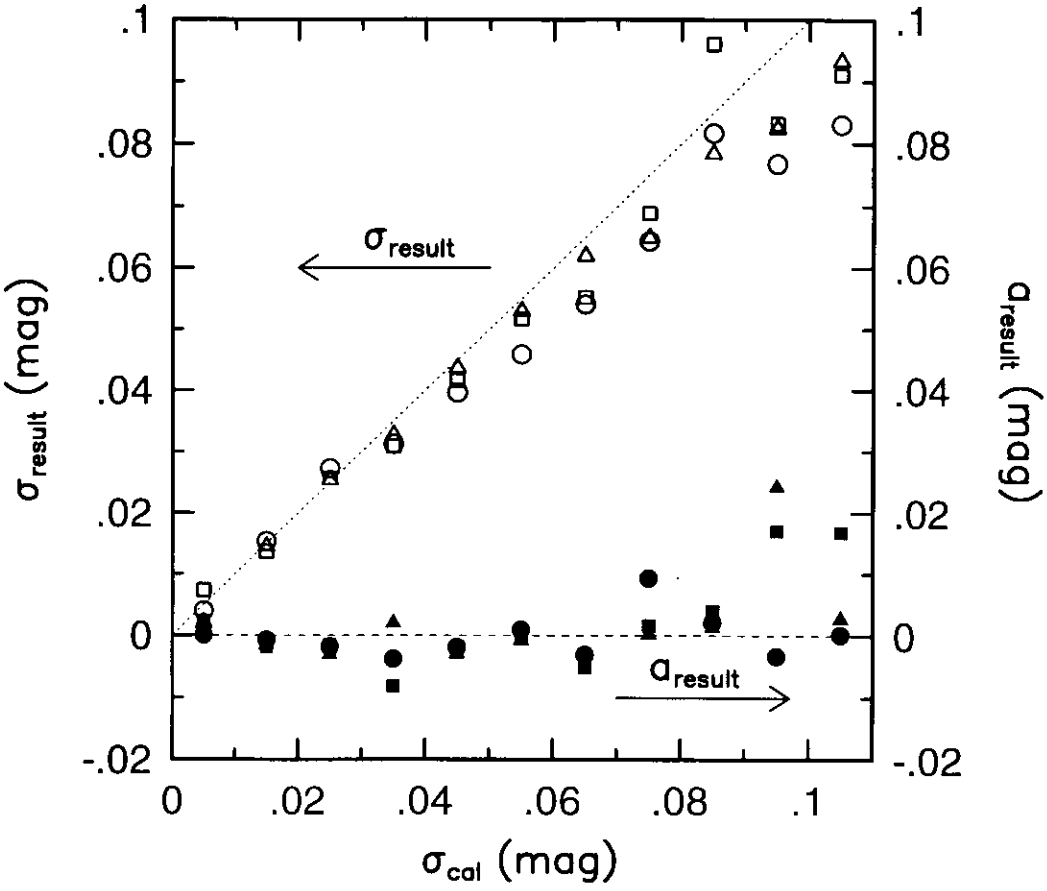

Figure 3.15: The relation between calculated errors and standard deviations of obtained variability of the reference objects which are the result of the differential photometry for the reference objects. The abscissas axis means the errors of the reference objects given by the differential photometry. Open triangle, square and circle represents the standard deviation of obtained variability at J,H and K' band respectively. Filled triangle, square and circle represents the average of obtained variability rat J,H and K' band respectively.

	J	H	K'
0.00-0.01	5	6	9
0.01-0.02	65	41	33
0.02-0.03	117	70	54
0.03-0.04	165	88	77
0.04-0.05	176	102	72
0.05-0.06	178	130	103
0.06-0.07	212	150	114
0.07-0.08	144	106	89
0.08-0.09	150	75	83
0.09-0.10	103	86	57
0.10-0.11	57	60	55

Table 3.6: the reference objects used the test of this section

3.4 accuracy comparison between the two photometry methods

In this work, the differential photometory specialized to detect AGN variability in near infrared wavelength were developed. On the other hand, the variability can be calculated from two times photometory by photometric standard star not for all but for many objects of this work. In this section, to estimate the accuracy realized by the differential photometory, the accuracy is compared to accuracy by the photometory by photometric standard stars. It is merit of this estimation to use same images to calculate the accuracy of two different method and can discuss the influence of the difference of photometory method avoiding the influence of the difference of observation and image reduction.

First, for the objects obtained the magnitude and the error $(m_1, \sigma_{m_1}), (m_2, \sigma_{m_2})$ by both two observations, the variability determined by standard star Δm and $\sigma_{stand} = \sqrt{\sigma_{m_2}^2 + \sigma_{m_2}^2}$ (mag) were calculated. These values were obtained for J, H and K' band and for $r = 7, 10, 12, 15$ pixel apertuers. The variability and the error by the differential photometory were for J, H and K' band and for $r = 3$ pixel apertuers obtained in previous section.

Fig ?? is for to compare the errors of those tow method to determine the variability. Only the data by the differential photometory using more than 2 reference stars were used here. Fig ?? is about the case of J band and for $r = 7, 10, 12, 15$ pixel apertuers standard star photometory. The figures about H, K' band were shown at B.2, B.3.

The first feature of the fig.?? is that many data are plotted around one sequence. The second feature is that the sequence becomes closer to x axis when the aperture for standard star photometory becomes larger. Those tendencies are also seen at the figure about H and K' bands. Because the signal noise ratio of the aperture photometory becomes lower when the aperture becomes larger if the other conditions are same, those features are reasonable. The sequence concentrated by the plot can be seen roughly as linear. The slope of the sequence regarded as the linear is smaller than 1 even for the case of 7 pixel aperture for the standard star photometory, where the slope is largest in fig.??. Therefore the typical accuracy of the variability measurement by the differential photometory is higher than the value by standard star photometory. These feature are also seen at the figure about H and K' bands.

However, there are some data distributed not around the sequence and above the sequence. It is thought that one cause to born the feature is that the sequence is closed to x axis and therefore the dispersion along the x axis direction is not seen remarkable. But more essential cause of the feature is thought to be the error of the origin of the variability determined in the differential photometory because in such case total error of the differential photometory becomes larger even if the signal noise ratio of the AGN in image is higher. The cause of the error of the origin in the differential photometory thought to be the error of flat fielding, variability of the reference objects and the effect of the edge of frames. What the accuracy of the variability determined by differential photometory is high and the small amount of them are lower accuracy is consistent to

the distribution of σ_f shown in fig. 3.10.

Next, the result of accuracy of the variability to be compared between those tow method is estimated by using $c = \sigma_{stand}/\sigma_{diff}$. Here larger c means that the variability by the differential photometory is higher than by photometory by standard star. The ratio filling $c > c_0$ is determined as $R(\%)$. Here $c_0 = 1/3, 1/2, 1, 2, 3$ are considered.

Fig.3.18 shows that the relations between the apertuers used by the standard star photometory and R for each c_0 for J, H and K' band. Here the data plotted in ??, B.2 and B.3 are used. These figures show that the plot of J, H and K' band are resemble for each other. The curves in the figures are increasing to right side as the result of that the sequence of the plotted data becomes closer to x axis when the photometric aperture becomes larger. The objects of $c_0 = 1$ are more than 80% for the most case of J, H and K' band and apertuers. This result shows that the accuracy of the variability by the differential photometory is higher than by the photometory by the photometric standard for most case.

For usual photometory using photometric standard, 3-4 times larger aperture than FWHM is used to avoid the influence of the variation of the PSF. In this work, the case consistent to this condition is the case of 10 or 12 pixel aperture because the seeing size of this work is about 3 pixel. For such aperture size, $c_0 = 2-3$ is the border line if R becomes larger than 50% in fig.3.18. Therefore the accuracy of the variability determined by the differential photometory is concluded to be $2-3$ times higher than by the photometory using the photometric standard in this work. The method to express the mean of ??, B.2 and B.3 by value is not one way, however, above result is at least one of the guide.

It is effective to reduce the frequency of the case with large error in the origin of differential photometory to realize more higher accuracy of differential photometory than that of this work. Such cases were small fraction, but certainly existed in the differential photometory of this work. On the other hand, because the slope of the sequence made by most data points are limited by the signal noise ratio of the AGN, it is thought to be hard to realize more higher σ_{diff} there by the improvement of the analysis.

It is hoped that there are many good bright reference stars around the AGN to reduce the frequency of the case with large error in the origin of differential photometory. And the reference objects are hoped to be more closer in the region not cause the confusion. In such situation, the influence of the edge of the frames and the large scale flat fielding error shown in section 3.2.3 can be reduced. If enough many reference objects are near the AGN, differential photometory can be possible only using the union area of all dithering frames. This is in contrast with the differential photometory of this work using all area of conbined image and is necessary to realize more higher accuracy differential photometory in the MAGNUM project.

The objects monitored in the MAGNUM project are less than the objects of this work and it is possible to prepare the objects filling above conditions. We are planning that differential photometory with more closer to the limit of the signal noise ration by not only the reduction

method but also to consider the sample selection, exposing time and dithering pattern.

The relation between the J band variability of AGN determined by the differential photometory and the photometory using the photometric standards ΔJ_{diff}, ΔJ_{stand} in fig.3.17. The case of other bands are shown in fig.B.5 and fig.B.6. In the case of 7 pixel aperture is used for the photometory using photometric standard, the plotted data distribute from left and bottom side to right and top side, what is reasonable. For the more larger aperture case, the error of ΔJ_{stand} becomes larger and the shape of the distribution also becomes unclear.

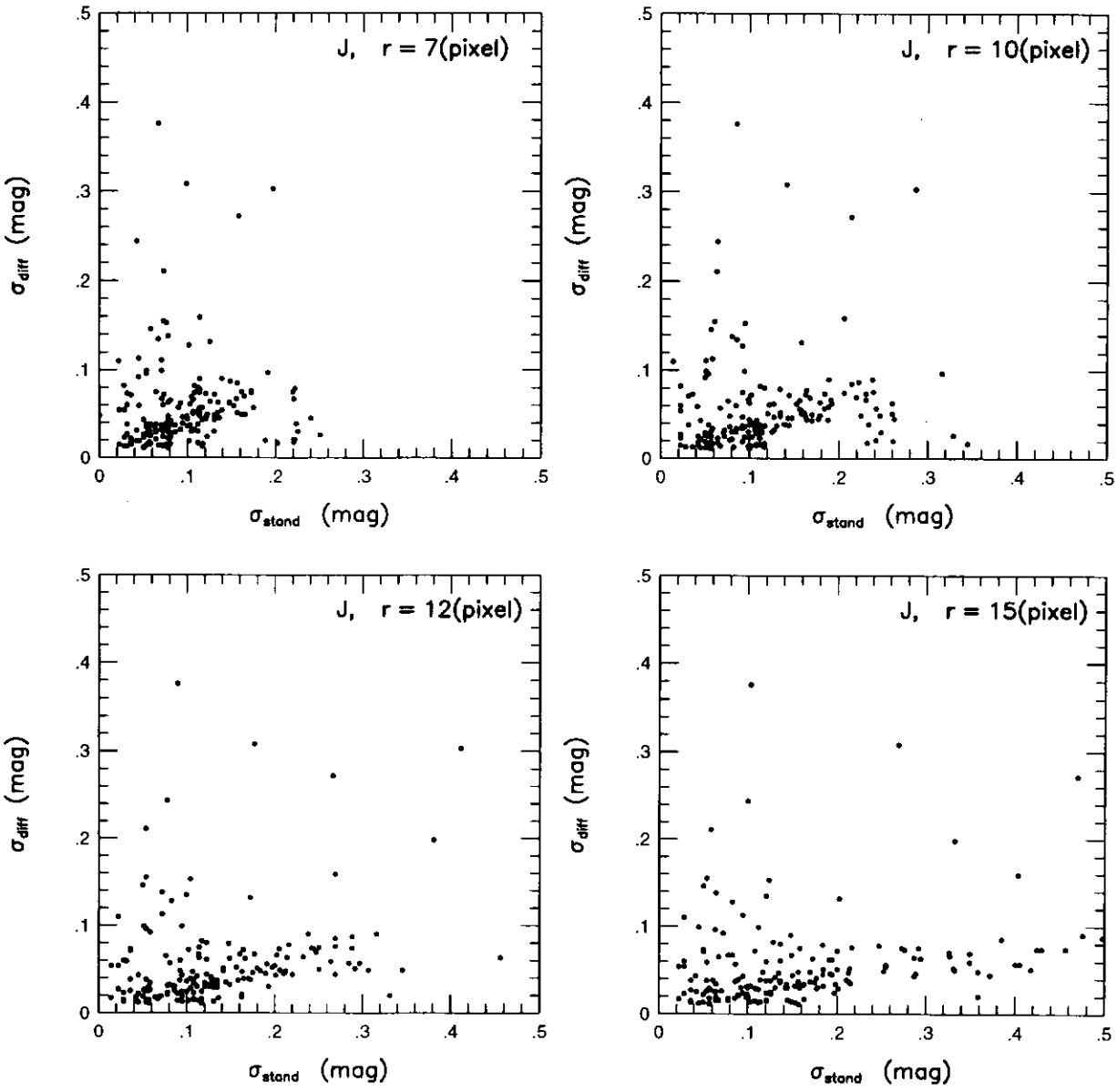

Figure 3.16: The relation between the error of the AGN variability in J band determined by the differential photometory σ_{diff} and by the photometory using phtometoric standard σ_{stand}. r shows the aperture used in the later method.

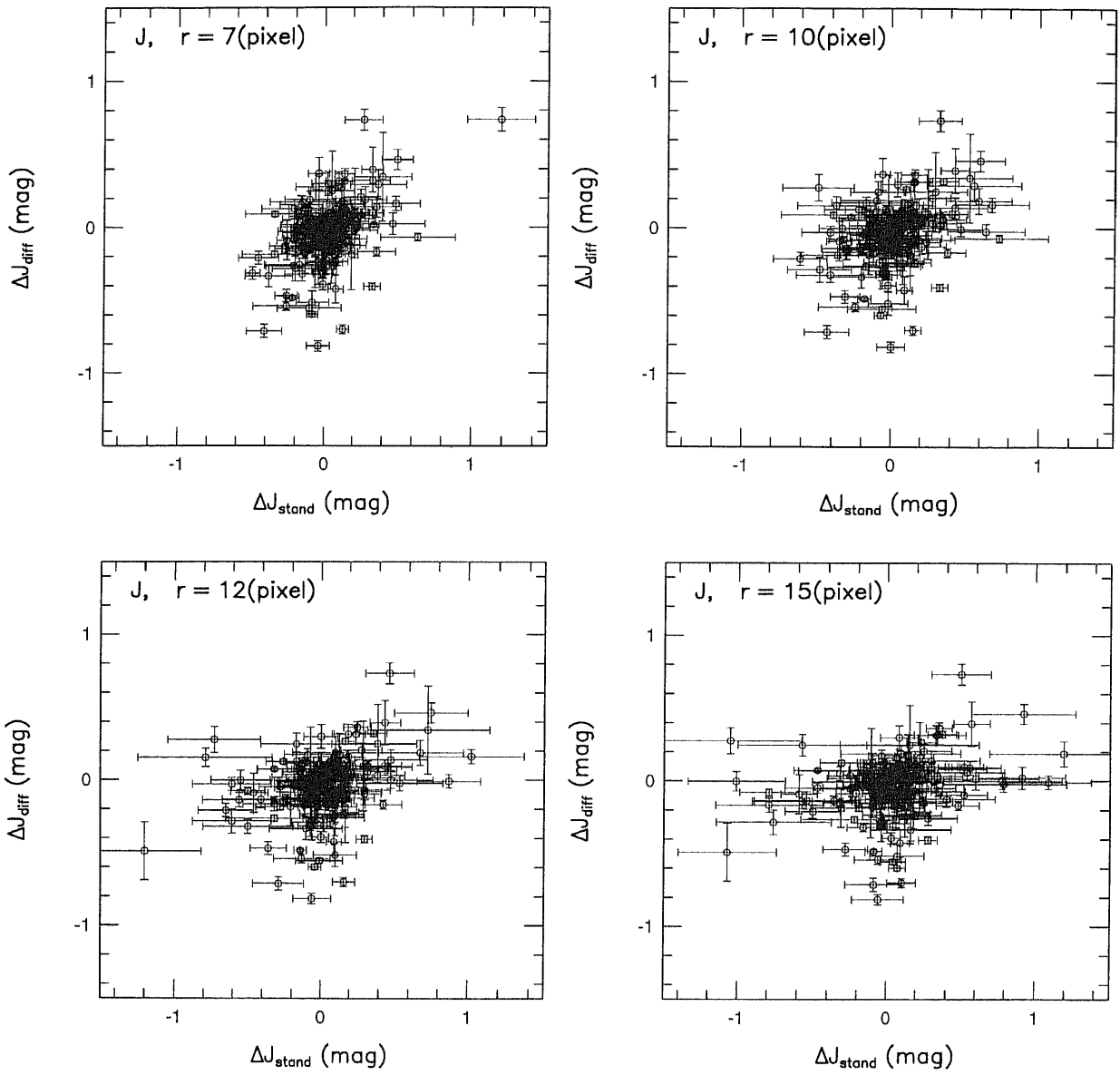

Figure 3.17: The relation between the AGN variability in J band determined by the differential photometory Δ_{diff} and by the photometory using phtometoric standard Δ_{stand}. r shows the aperture used in the later method.

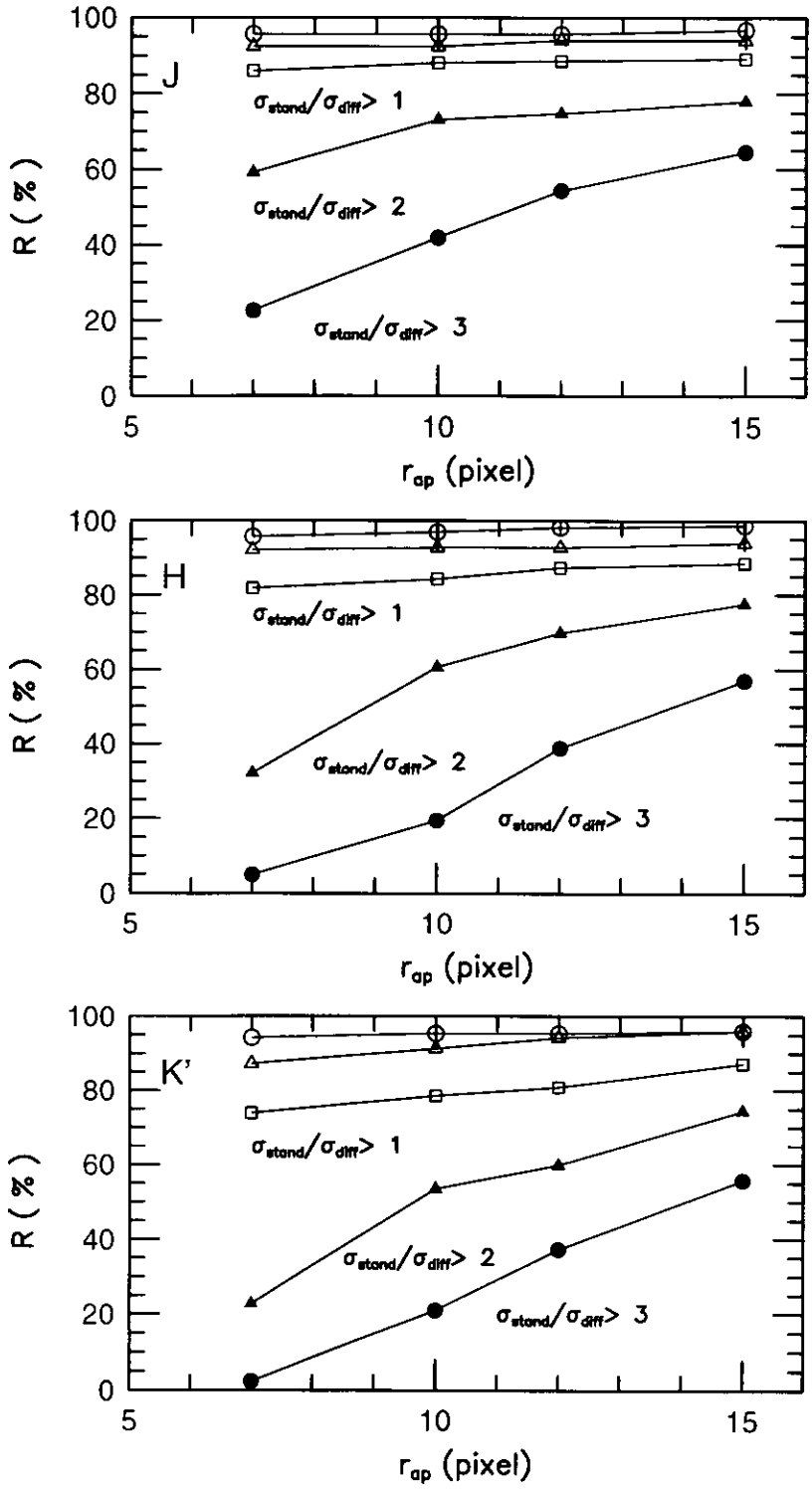

Figure 3.18: The ratio of the object number that fill the condition of $c > 0.33, c > 0.5, c > 1, c > 2, c > 3$ from top to bottom respectively. Here c is the ratio of the accuracy of the AGN variability determined by two method in J band, determined by the differential photometory σ_{diff} and by the photometory using phtometoric standard σ_{stand}.

Chapter 4

result

In this chapter, objects list, table of the variabilities and magnitude at J,H and K' band as the result of the data analysis of this work. Next, overview was done with figure that showed certain detection of AGN variability etc. before detail analysis of magnitude of variabilities, wavelength or other characters dependence of AGN variabilities.

4.1 result of the data reduction

As the result of the observation of this work, objects with any result were listed in table.A.1. There are 331 objects in the table. The objects in the table are sorted by R.A., and the first column is serial number. Later columns are name,R.A. and dec., z and Mv by VV catalog. The last column shows radio activity of the objects defined using 6cm wavelength flux. L means radio loud, Q means radio quiet and A,U correspond to ambiguous and unknown. The distributions of R.A. and dec, z and Mv were shown at fig.2.1 and fig.2.2.

The variabilities of the objects are shown at table.A.10 that is main result of the data analysis of this work. The first column is the number given in table.A.1. Missing of the serial number in table.A.1 correspond to objects that variability was not determined but magnitude at any band was obtained. Next column of (A.10) means name same as A.1. From the third columns show the variability of J band magnitude, its error and number of reference object to be used for the differential photometry. Following columns are H and K' band data. The last 2 columns are date of the first and the second observation.

Magnitude of the objects estimated by the photometric standard stars are shown at table.A.15 for J,H and K' band. The first and second columns show the serial number given at table.A.1,object name. J,H and K' band magnitude and its error by 7 pixel aperture are following. Same data but by 10 pix aperture are shown following. The last column means date of the observation. Many of the objects that was observed 2 times to detect the variability were also succeeded to determine

their magnitude 2 times. Both of result of the two observations are shown in table.A.15. Table.A.3 shows the magnitude determined by 12 and 15 pix aperture as same way.

4.2 overview

In this section, the overview of the results are done before detail analysis of the variability of AGN. Top and bottom at fig.4.1 are the first and the second images of B2 0827+24 at J band. The AGN is marked by circle on each images. The first observation was done on December 1996 and the second was done on January 1998. z and Mv of this object are z=0.941 and Mv=-26.5 that means the object is fairly far and bright in the sample. It is understood that the AGN became brighter for the interval of the observations from the images. As the result of the analysis with differential photometry, the variability of the object is -0.71±0.05(mag) and the variability can be concluded enough significant. The value of 0.71mag is one of the largest variability in the sample of this work. The variabilities of some fractions of sample is smaller than 0.1mag. It is impossible to find variability by comparing the first and second image of such object. However, it will be possible to conclude the variability of most AGN and discuss about relations between characters of AGN and their variability by statistic analysis discussed in following chapter.

Other fig.4.3 shows that the estimated variabilities are certainly real. Number of object that variability is as large as B2 0827+24 is small, but histogram of total data of the variability shows that many AGN are variable objects. Solid line of fig.4.3 means distribution of variability at J,H and K' band of AGN that was estimated with more than 2 reference stars and its error is smaller than 0.1 mag. The distribution seems to spread wider than its typical error of the variability of AGN that is 0.05mag. Dashed line means resemble but for the reference stars used to estimate the variability of AGN. Scale of number for the AGN and the reference stars are different because the number of the reference stars is larger than that of AGN. The distribution of AGN is wider extended than the reference stars, this is also the significance of the variability of AGN.

J,H and K' band magnitudes of AGN obtained by this work by photometric standard star photometry by 7 pixel aperture are shown in fig.4.6. Here the data with error smaller than 0.2mag was plotted. For the objects that magnitude was obtained for twice observations, both data of the 1st and 2nd observation are shown.

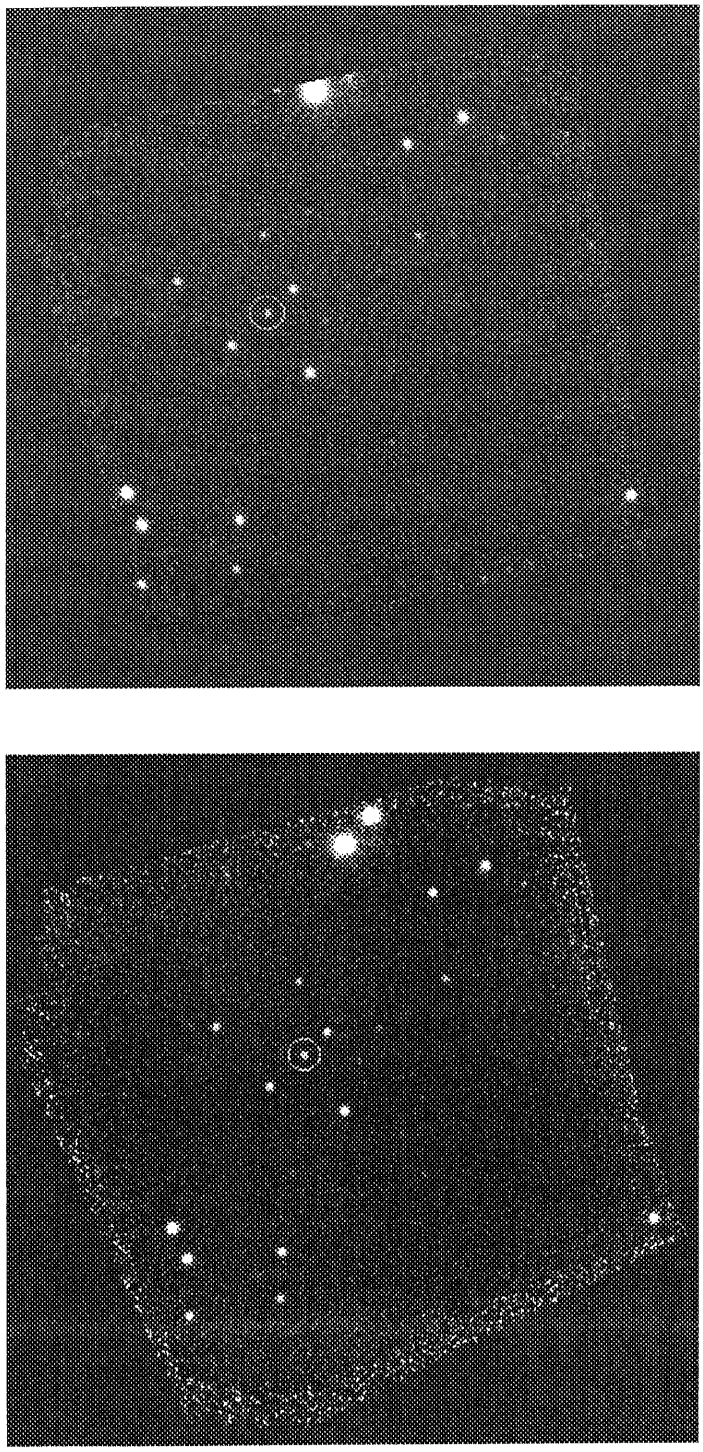

Figure 4.1: Top is the 1st image of B2 0827+24 at J band observed on 1996 December 7. The target AGN is marked with circle. Bottom is same but the 2nd image observed on 1998 January 16. The object of the 2nd observation seems to be somewhat brighter than the 1st. The difference of luminosity between the objects in these images is -0.712±0.046mag that is one of the largest variation in the data of this work.

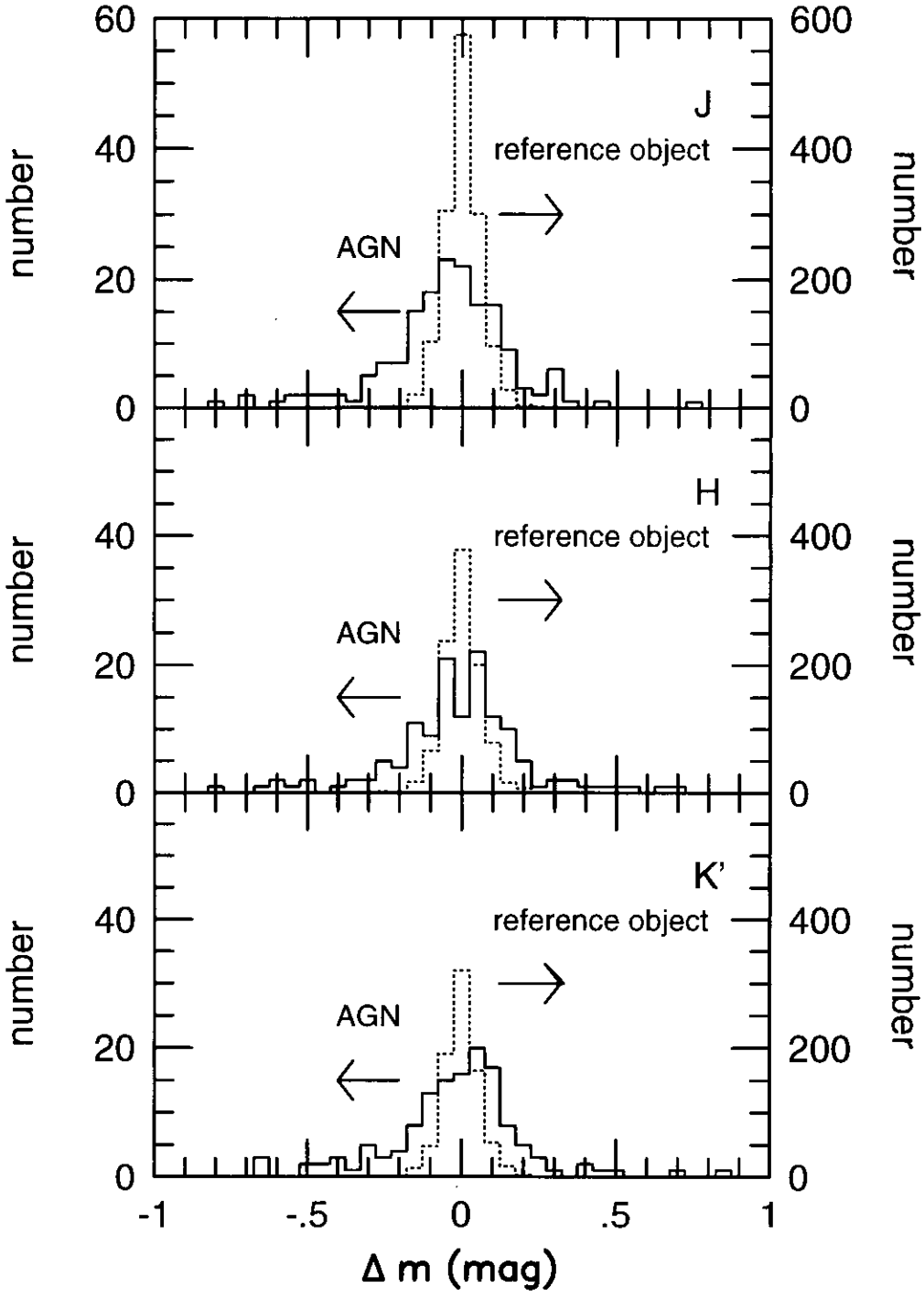

Figure 4.2: Frequency distributions of the variabilities of AGN and the reference objects obtained by the differential photometry in this work. Solid line and dashed line represents the distributions of AGN and the reference objects respectively. For both AGN and the reference objects, only the data with accuracy higher than 0.1mag is used here. It is seen that the distributions of AGN are more extended than the those of the reference objects.

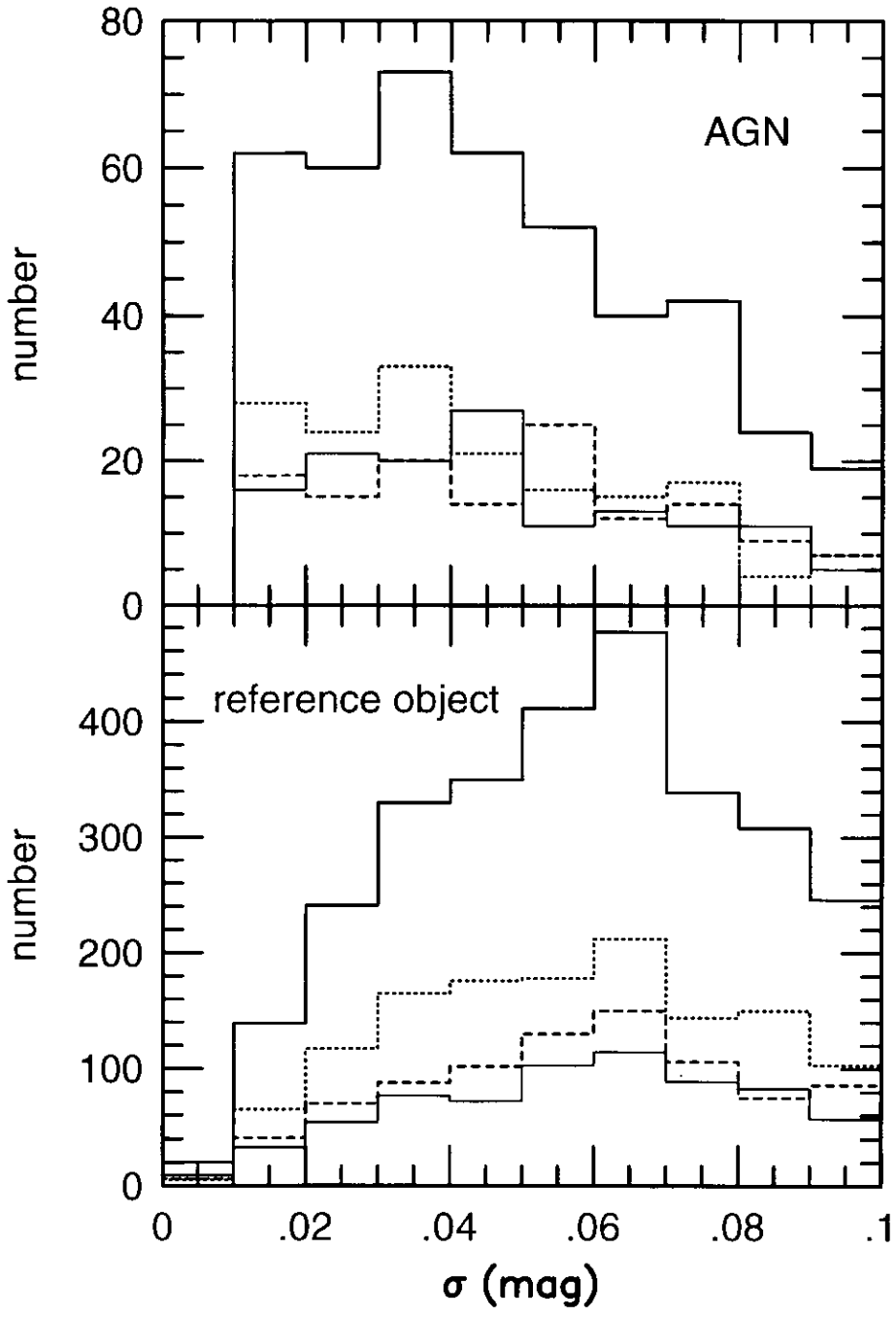

Figure 4.3: Frequency distributions of errors of the variabilities of AGN and the reference objects obtained by the differential photometry in this work. Dotted line, dashed line and narrow solid line represents the distributions at J,H and K' band respectively. Wide solid line represents total of those distributions.

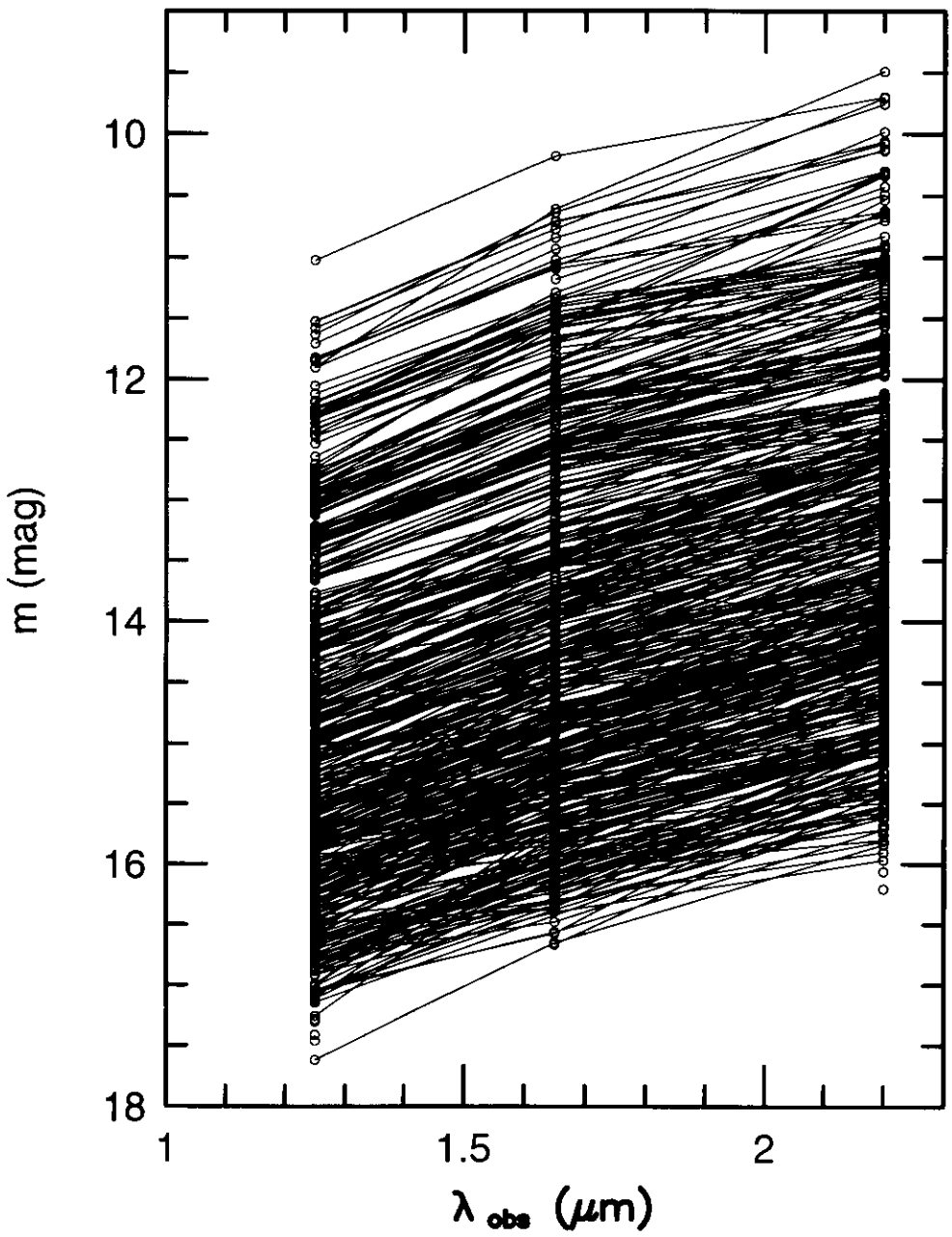

Figure 4.4: The magnitude of AGN obtained by this work with 7pix aperture. Only the data with accuracy higher than 0.2mag is used here. For the object that was observed twice, both of the results are plotted.

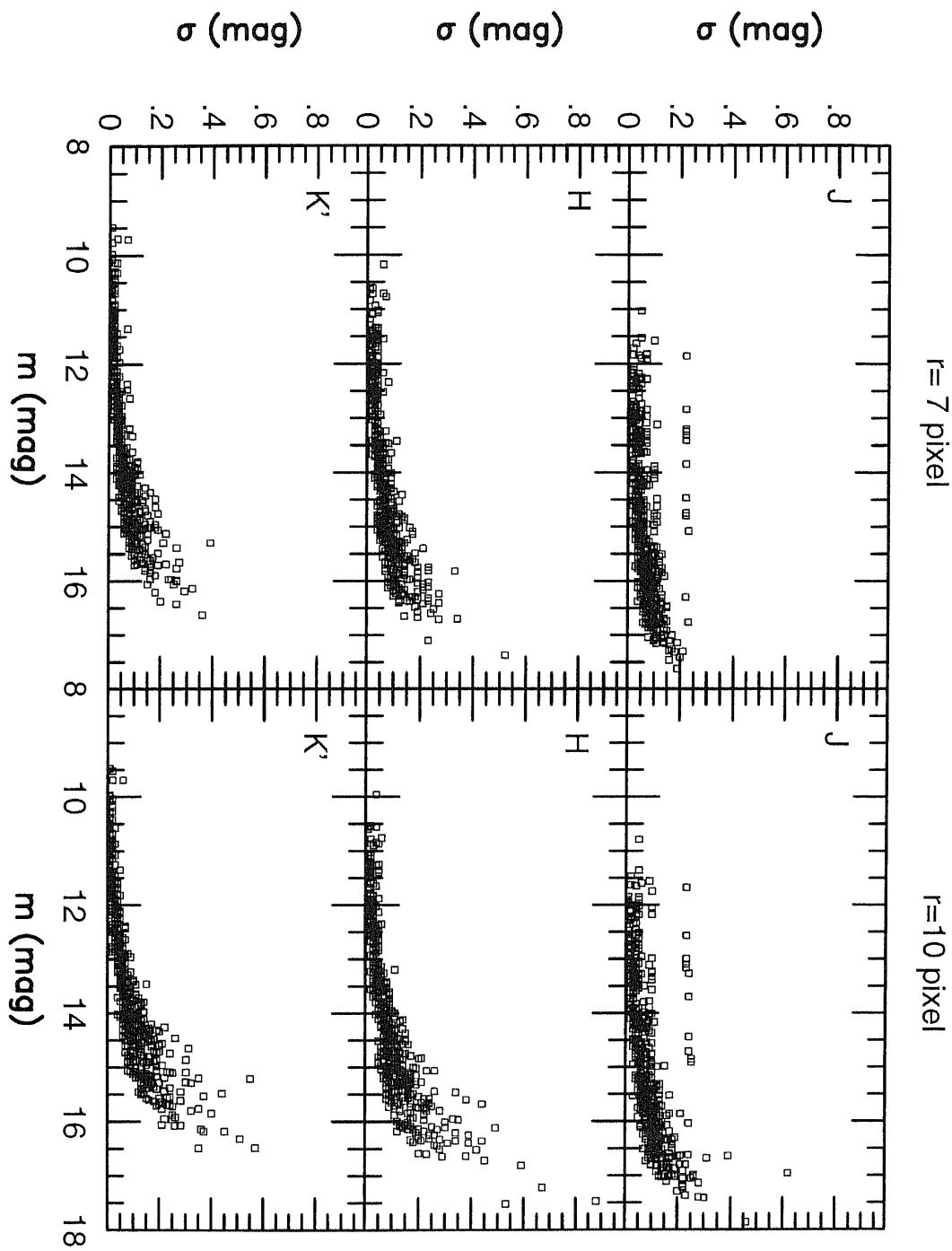

Figure 4.5: Relations between the magnitudes obtained with photometric standard with 7pixel and 10pixel apertuer and their errors. For the case of the object were observed twice and the magnitude was obtained, both of them are plotted.

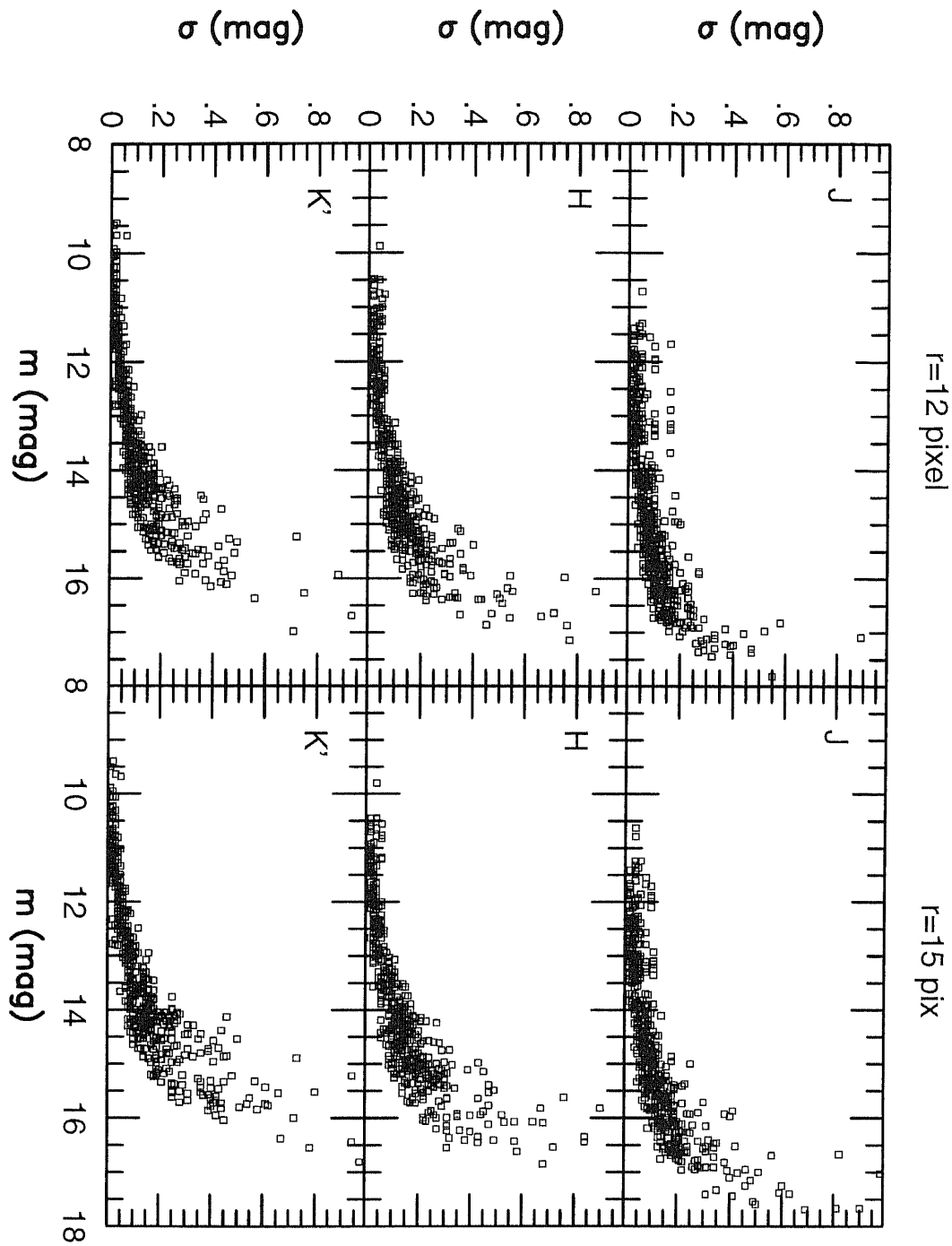

Figure 4.6: Relations between the magnitudes obtained with photometric standard with 12pixel and 15pixel apertuer and their errors. For the case of the object were observed twice and the magnitude was obtained, both of them are plotted.

Chapter 5

discussion

Discussion using the result of the variability and photometry data is done in this chapter. In section.5.1, the photometric data was discussed with JHK' 2 color diagram. Relations between the JHK' color and V band absolute magnitude(M_B), Seyfert type or radio activity are estimated for sample of $z << 1$ where SEDs of many AGN were obtained with high signal noise ratio. Difference of JHK' color between AGN and host galaxies were discussed by comparing the color analyzed with various size of aperture.

In section.5.2.3, discussion of the variability of AGN are done. Ensemble variability is introduced to estimate the typical value from data set of AGN variability subtracted contribution of error. The sample is divided by parameter like observed wavelength, radio activity, rest frame observational interval, M_B , z and the ensemble variabilities are obtained for each subsamples. It is the important aim of the section to obtain the value of variability and to research correlations between the variability and characteristic parameters. Next, ratio of sample that was concluded as certainly varied is estimated and universality of variability of AGN is discussed in section.5.2.3 Correlation of the variability of different band is considered in section.5.2.4. Time scale of the variability of some subsamples is estimated in section.5.2.5.

Using the result of those discussion and data of other papers, mechanism of the emission and variability is discussed in section.5.3 for radio quiet and radio loud sample.

5.1 JHK' 2 color diagram

Fig.B.35 is the 2 color diagram for $z < 0.3$ sample divided by M_B. Only data of which errors at 12 pixel aperture are smaller than 0.2mag are plotted. Open square,triangle represents M_B<-26,-26<M_B<-24 sample, and filled triangle, square represents -24<M_B<-22,-22<M_B sample respectively. The data of M_B were obtained from VV catalog.

Fig.B.36is the 2 color diagram for $z < 0.3$ sample divided by Seyfert type. Only data of which errors at 12 pixel aperture are smaller than 0.2mag are plotted. Open square,triangle and circle represents Seyfert 1, 1.2, 1.5 sample, and filled circle, triangle and square represents Seyfert 1.8,

1.9, 2.0 sample respectively. The data of the Seyfert type were obtained from VV catalog.

Fig.B.37 shows is the 2 color diagram for $z < 0.3$ sample divided by radio activity. The radio activity was determined as $f_{\nu 6cm}/f_{\nu V}$ using the data of flux at 6cm wavelength and V band magnitude. Open and filled triangle represents $f_{\nu 6cm}/f_{\nu V} < 10, 100 < f_{\nu 6cm}/f_{\nu V}$ sample respectively.

The magnitude of the sample for each 7,10,12 and 15 pixel aperture was determined by the same size aperture between AGN and photometric standards. However, when the aperture was small like the 3 or 5 pixel, influence of scintillation by atmosphere wavering became strong. Therefore it was hard to compare directly the result of photometry of photometric standards by 3 or 5 pixel aperture to AGN. So the correction equation for 7 pixel aperture was applied to estimate the color of AGN of 3 or 5 pixel aperture. In general, the magnitude of the object is systematically estimated to be darker by this method because flux inside the aperture depends the size of the aperture. However, the affect of different aperture size is canceled in principle if ratio of flux f_{3pix}/f_{7pix}, f_{5pix}/f_{7pix} are equal in J,H and K' band. It is to use the correction equation for 7 pixel aperture to estimate the color by 3 or 5 pixel aperture in those case. However, if $f_{r=3pix}/f_{r=7pix}$ has wavelength dependence, the dependence can be cause of systematic error of color for 3 or 5 pixel aperture.

Plotted objects is distributed from about (H-K',J-H)=(0.3, 0.7) to about (H-K',J-H)=(1, 0.8) in figB.35, figB.36 and figB.37. These place of (H-K',J-H)=(0.3, 0.7) or (H-K',J-H)=(1, 0.8) are correspond to normal galaxies and QSO on the near infrared 2 color diagram. In figB.35, it is seen that bright sample at absolute magnitude tends to be plotted near the QSO position and dark sample tends to be plotted near the normal galaxy position. And it is also seen that the plotted position in figB.36 tend to localized near the normal galaxy position when Seyfert type become closer to 2. Averages of the colors in the diagram and the errors were determined to discuss those tendency quantitatively and the results were shown in fig5.4. (a) and (d) of the figure show the dependency of J-H, H-K' on M_B. The sample was divided into M_B<-26, -26<M_B<-24, -24<M_B<-22 and -22<M_B as above, and average of M_B for each subsamples were used as the value of abscissas axis. The estimation of the average was done with the data with no weighted. Open square, triangle and circle represents the data estimated with 3, 5, 7 pixel aperture and filled circle, triangle and square represents the result with 10, 12, 15 pixel aperture respectively. The errorbars mean the standard deviations of the color by 7pixel aperture on the diagram.

H-K' has the tendency to become bluer when plotted sample become darker at M_B for all apertuers at fig5.4(d). H-K' is about 1.1 for sample of M_B<-26 that is comparable to the value of QSO, while H-K' is about 0.5 that is closer to the color of normal galaxy for -22<M_B sample. On the other hand, J-H is kept to be about 0.8 and the M_B dependence of J-H is weaker than H-K' (fig5.4(a)). And it is seen that the colors determined with larger aperture are more galaxy like for each subsamples divided by M_B. This feature cannot be explained by only the error caused by wavelength dependence of f_{3pix}/f_{7pix}, f_{5pix}/f_{7pix} describe above because the feature is also seen

in the data estimated with the aperture larger than 7 pix. So it is reasonable that this feature is originated by the color gradient from central region of AGN to host galaxy. In fig??(d), the difference of H-K' by the difference of the aperture size is more remarkable for the darker sample in M_B than blight sample. This feature can be explain to think that ratio of component of the host galaxy to AGN is larger at darker sample in M_B than brighter sample.

Fig5.4(b),(e) show relation between Seyfert type and J-H, H-K', and unknown sample was not used here. Fig5.4(c),(f) show relation between radio activity and J-H, H-K'. Condition of dividing sample by Seyfert type or radio activity into subsamples was same to figB.36, and unknown sample was not used here. Meaning of the symbol and errorbar are same to (a),(b).

In fig5.4(e), when the Seyfert type is closer to 2, the H-K' become closer to the value of normal galaxy while J-H is almost constant. These feature is resemble to the case seen in the relation between M_B and JHK' color. The Seyfert from 1.8 to 2.0 sample tend to be dark in M_B and their number is small. Therefore it is difficult to estimate the dependence of JHK' color on M_B and Seyfert type independently.

On the other hand, the difference of JHK' color between radio quiet and radio loud sample isn't found in 5.4(c),(f). This is in contrast to the feature seen in the M_B dependence of JHK' color for z<0.3 sample.

For high redshift sample of 0.3<z, there are less sample with good SNR compared with z<0.3 sample. In fig5.5 or fig5.6, the color estimated by small aperture is not always more AGN like than estimated by large aperture. It is reasonable that the reversal isn't caused by real property of AGN but lac of SNR of the color. High z sample in the figure tends to be blight AGN and radio loud AGN. Therefore it is hard to discuss the relation between their character and JHK' color for high z sample in this work.

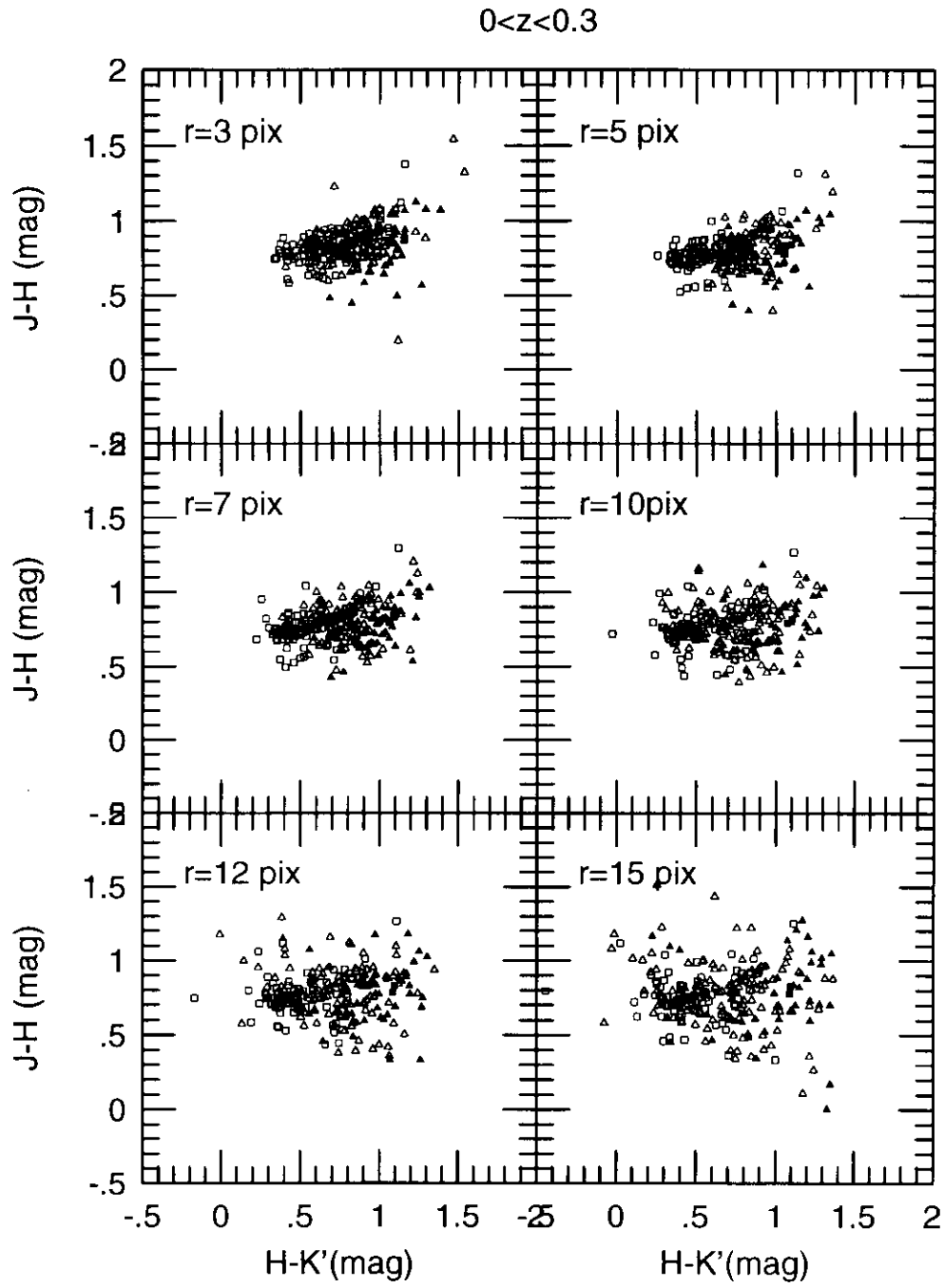

Figure 5.1: JHK' tow color diagram of the objects in z<0.3 classified by their M_B. Only the data of which the accuracy is more than 0.2mag at 12 pixel apertuers are plotted. Open square and triangle represents M_B<-26 and -26<M_B<-24 objects, and filled triangle and square represents -24<M_B<-22 and -22<M_B, respectively.

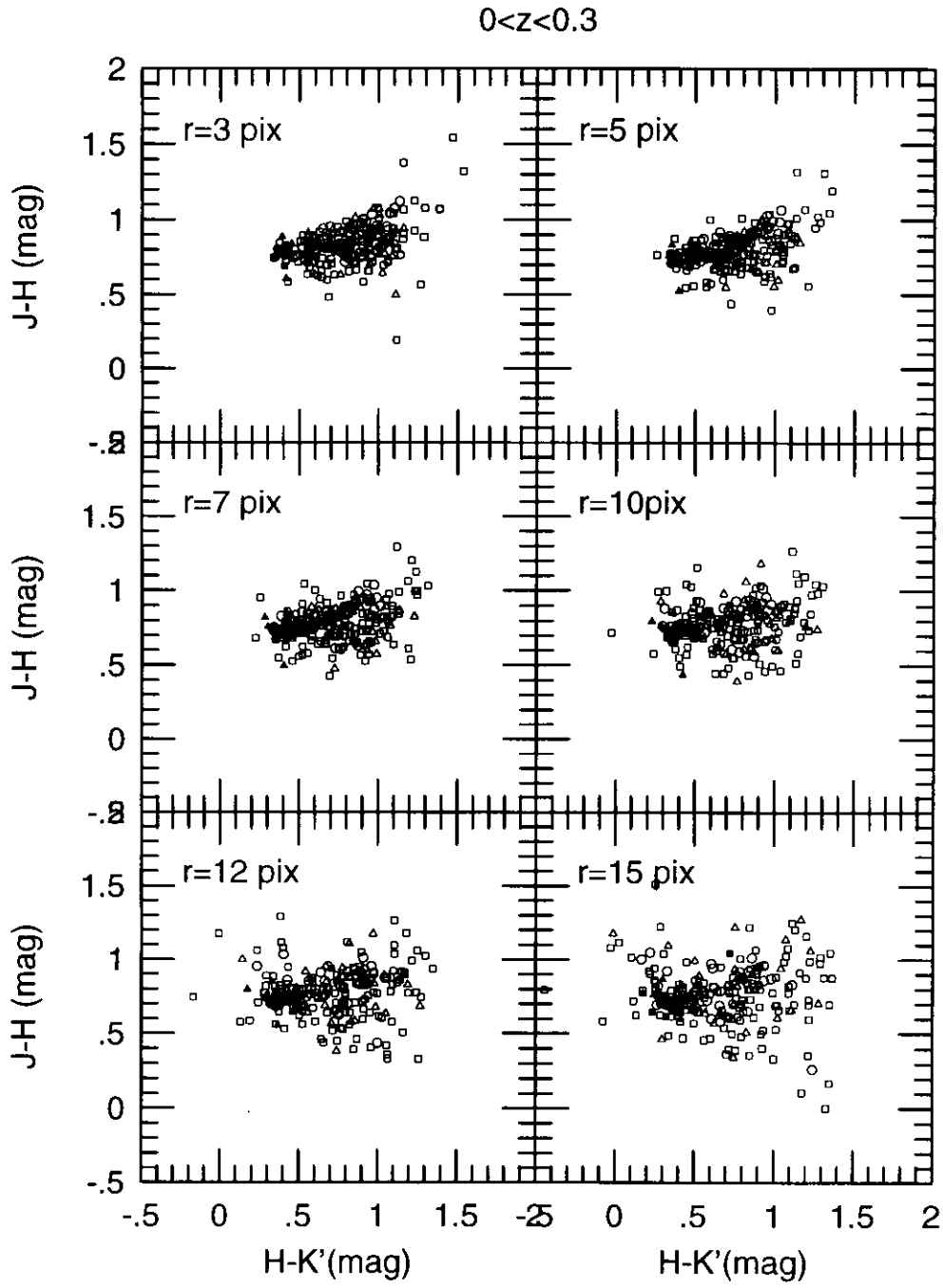

Figure 5.2: JHK' tow color diagram of the objects in z<0.3 classified by their Seyfert type. Only the data of which the accuracy is more than 0.2mag at 12 pixel aperture are plotted. Open square, triangle and circle represents Seyfert 1, 1.2 and 1.5 objects, and filled circle, triangle and square represents Seyfert 1.8, 1.9 and 2, respectively.

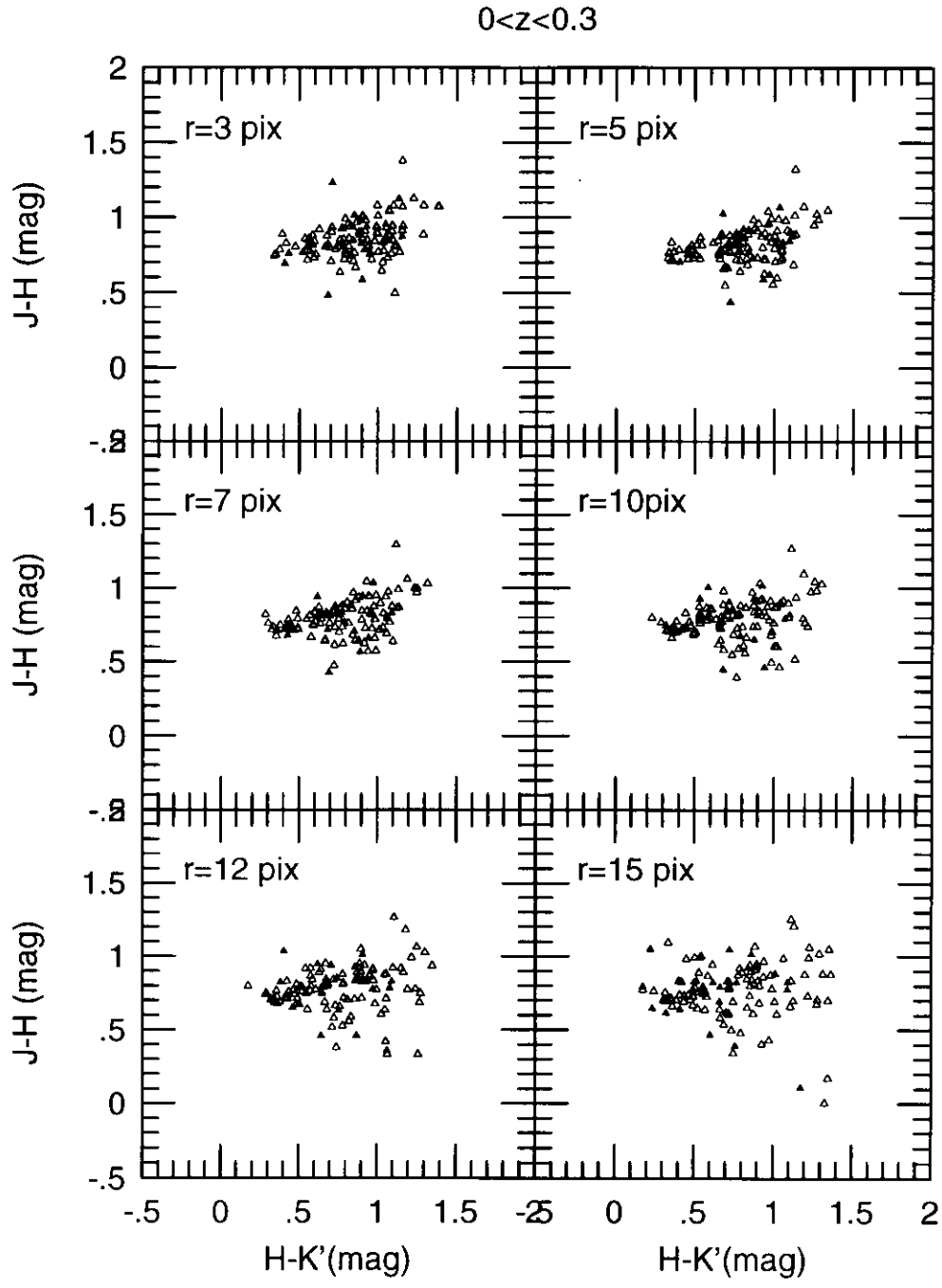

Figure 5.3: JHK' tow color diagram of the objects in z<0.3 classified by their radio activity. Only the data of which the accuracy is more than 0.2mag at 12 pixel aperture are plotted. Open triangle represents objects with $f_{\nu 6cm}/f_{\nu V} < 10$, and filled triangle represents objects with $f_{\nu 6cm}/f_{\nu V} > 100$.

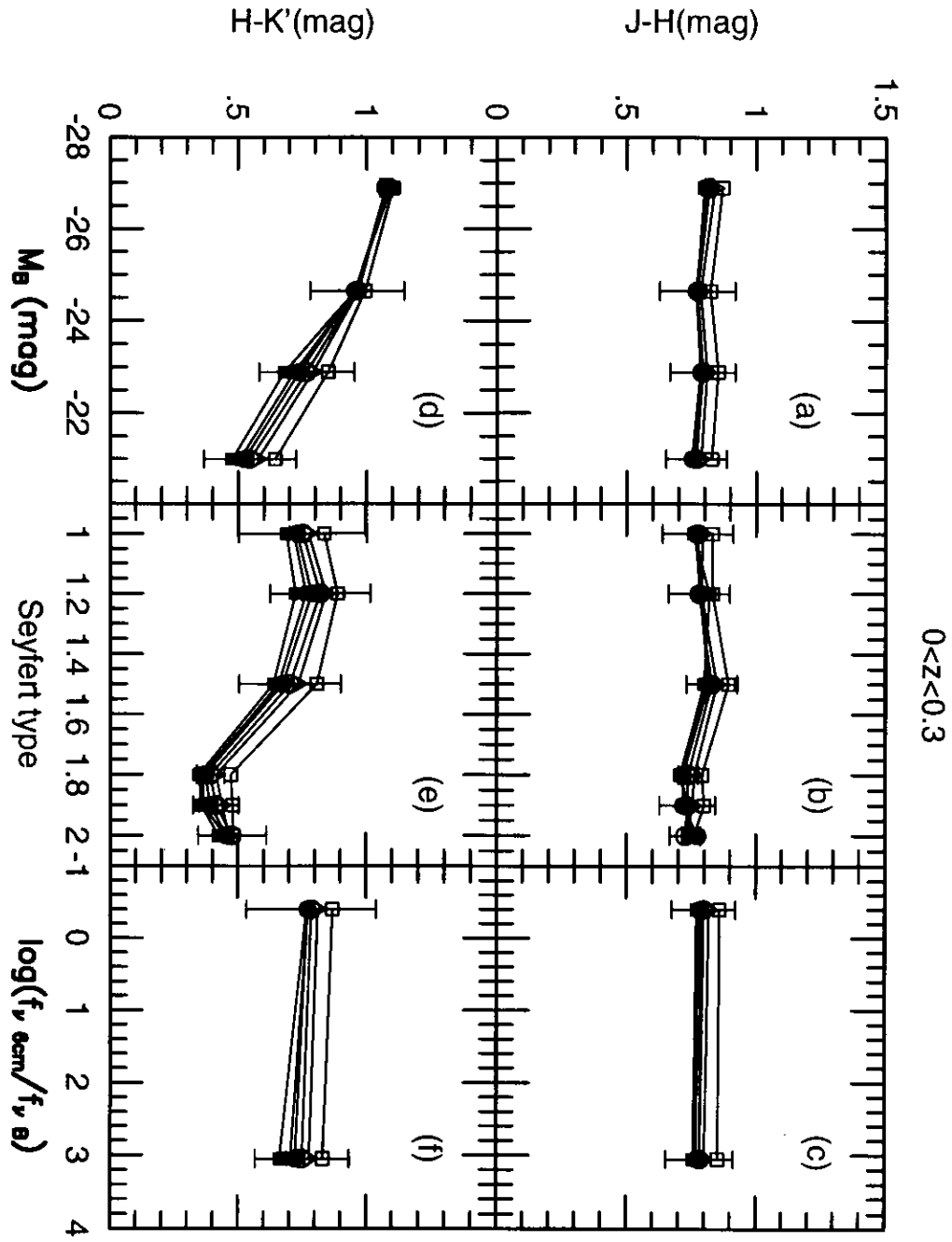

Figure 5.4: Relations between the J-H,H-K' colors and MV, Seyfert type, radio activity of the objects with $0 < z < 0.3$. Open square, triangle, circle and filled circle, triangle, square represents the result obtained with 3,5,7,10,12,15 pixel aperture.

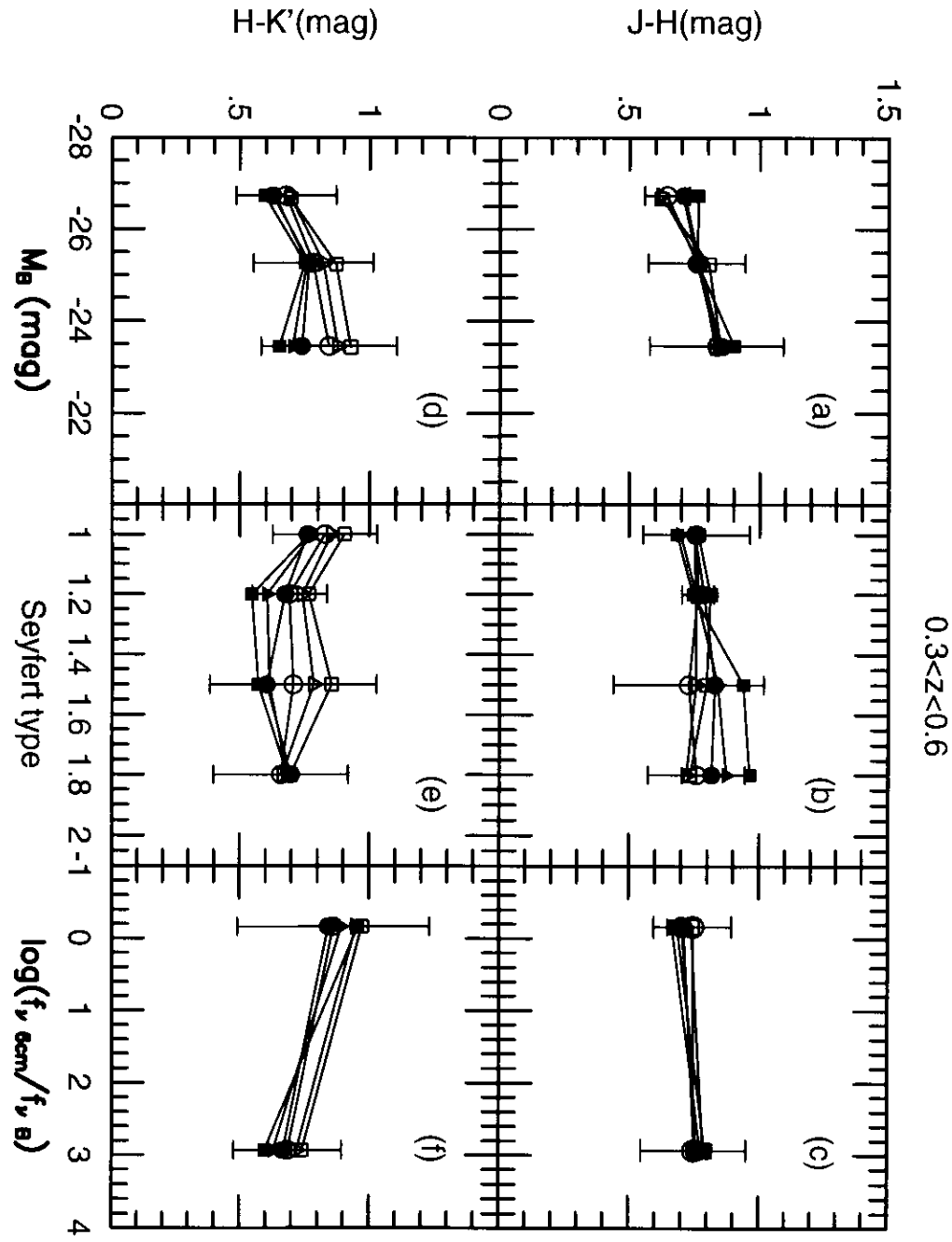

Figure 5.5: Relations between the J-H,H-K' colors and MV, Seyfert type, radio activity of the objects with $0.3 < z < 0.6$. Open square, triangle, circle and filled circle, triangle, square represents the result obtained with 3,5,7,10,12,15 pixel aperture.

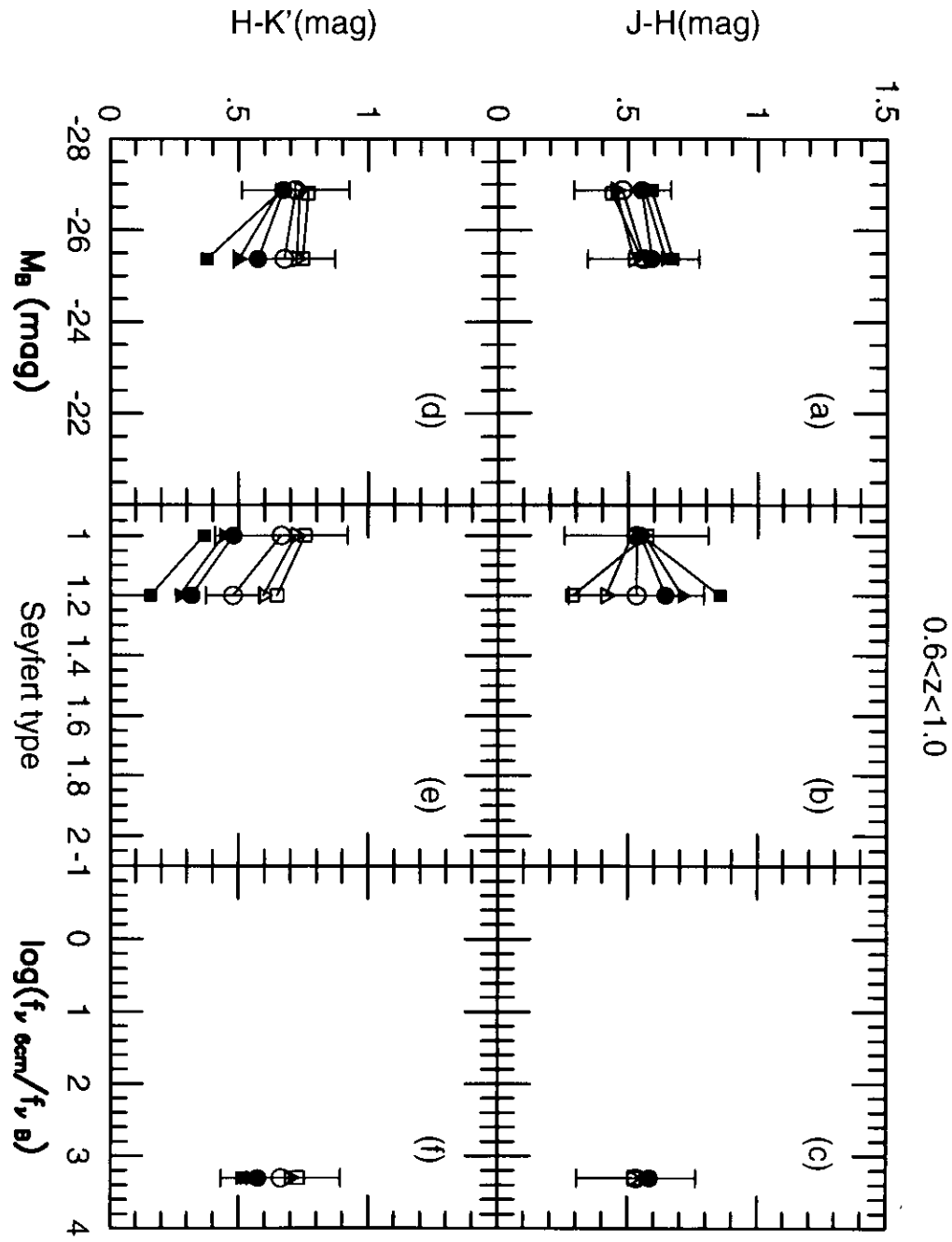

Figure 5.6: Relations between the J-H,H-K' colors and MV, Seyfert type, radio activity of the objects with $0.6 < z < 1$. Open square, triangle, circle and filled circle, triangle, square represents the result obtained with 3,5,7,10,12,15 pixel aperture.

5.2 the variability of AGN

5.2.1 introduction of ensemble variability

Because each object was observed only two times in this work, each variability data don't always reflect the characteristic amplitude of the variability of the AGN. Therefore , the variability of AGN is discussed with the ensemble variability that reflects the dispersion of variabilities in the ensemble of many objects. It was overviewed at fig.4.3 that the variability data of AGN is extended broader than reference objects around AGN. However, the usual standard deviation is not best parameter to estimate the variability of AGN from the observed data, because not only the intrinsic variability of AGN but also the measurement error contribute the broadening of fig.4.3. So the ensemble variability described as following is introduced to reduce the contribution of measurement error and to get representative value of the variability of the ensemble.

$$V = \sqrt{\frac{\sum_i^N \Delta m_i^2 - \sum_i^N \sigma_i^2}{N}} \tag{5.1}$$

$$\sigma_v = \frac{1}{2V}\sqrt{\frac{\left(\sum_i^N \Delta m_i^2 - \sum \sigma_i^2\right)^2}{N^3} + \frac{\sum_i^N (4\Delta m_i^2\sigma_i^2 - 2\sigma_i^4)}{N^2}} \tag{5.2}$$

Here σ_v is the error of V. The first term of right hand of eq.(5.1) represents the dispersion of the observed variability data. The second term represents the dispersion caused by the error of each data. eq.(5.2) show the error of V, however, the derivation of those form isn't shown here but in appendixC.

In following, the ensemble variability and its error is estimated for the subsamples made by dividing the sample with various criterion and the property of AGN variability.

5.2.2 relation between the variability and character of AGN

< research of the way to divide the sample >

It is one of the best method to adopt multivariate analysis for the data extended widely in the parameter spade to discuss the correlation between the variability of AGN and their absolute magnitude M_B, redshift z, interval of the observations and so on. However, the distribution of the sample in this work is not uniform and not always extended enough in the parameter space. Furthermore, making ensemble is necessary in this work to estimate the variability because each AGN was observed only two times. So number of sample isn't enough even in this work in the case

of the number of free parameter increases at multivariate analysis. As a first step to estimate the dependence of the variability on the characteristic parameters, it was adopted that the sample was divided into two subsamples by each parameters and the ensemble variabilities of the subsamples were compared. The way to divide the sample into various subsamples are determined in this section. This is the preparation to analyze the correlation between the variability of AGN and their characteristic parameter in next.

It is the primary aim of the method where the all sample is divided into two and their ensemble variabilities are compared to estimate whether there is the main parameter that dominate the variability of AGN. There is the possibility that the influence of focused parameter to the ensemble variability isn't detected when the variability depends not simply on the parameter even if strong dependence is exists. However, such remarkable feature isn't seen in from fig.B.7 to figB.13 that show the relation between various parameters and the ensemble variability. The frequency distributions of some parameters like radio activity or observation interval at rest frame are roughly separated into two regions. The method to divide the sample into two subsamples at first is suitable to this feature. Only the data estimated with more than two reference objects and with accuracy higher than 0.1mag are used in the analysis of this section.

The radio activity was focused first. There seems from fig.B.11 that the ratio of f_{6cm} on f_v is extended for some decades, however, they are localized two places around 1 and 1000. It is thought that this feature is originated by the fact that the sample include radio quiet AGN and radio loud AGN. The sample with the ratio $f_{\nu 6cm}/f_{\nu V} > 100$ was regarded as radio loud here, while the sample with the ratio $f_{\nu 6cm}/f_{\nu V} < 10$ was regarded as radio quiet. The sample that wasn't detected in radio flux were classified to radio quiet. The radio loud and the radio quiet sample was regarded as the a and b group at the two dividing test and the ensemble variability of each groups were calculated with eq.(5.1). The result is shown in table5.1. The number in bracket in the table represents the sample number.

Next, observation interval at rest frame was focused. There seems from fig.B.9 that the interval $\Delta t/(1+z)$ is localized two places around 300days and 600 days. It is thought that this feature is originated by limit of the season of the observation in this work, and the former includes mainly the sample observed at the 2nd and 3rd term of the observation and the later includes mainly the sample observed at the 1nd and 3rd term. The sample with the observation interval at rest frame $400(days)\Delta t/(1+z) < 800(days)$ was classified into a group, while The sample with the observation interval at rest frame $100(days)\Delta t/(1+z) < 400(days)$ was classified into b group.

M_B was obtained from VV catalog. The sample with $M_B < 23.5$ was classified into a group, while The sample with $M_B > 23.5$ was classified into b group. z was also obtained from VV catalog. The sample with $0.3 < z$ and $0.3 > z$ was regarded as a and b group. Concerning the near infrared color, the sample with $J-H < 0.8$ and $H-K' < 0.8$ was classified into a group, while the sample with $J-H > 0.8$ and $H-K' > 0.8$ was classified into a group.

Table5.2.2 shows the ratio of the ensemble variabilities of the a and b group made by dividing by each parameter for J,H, and K' band. The last column represents average of the ensemble variabilities of J,H,K' band. The ratio is 1.46 and the largest value when the sample was divided by the ratio activity. The ratio for the observation interval 1.24 at rest frame and for M_B 1.20 is following. On the other hand, the ratio for z, Seyfert type, near infrared color J-H,H-K' are more closer to 1.

Based on those result, the sample is divided by the ratio activity into the radio quiet and the radio loud sample at first later than here. The criterion of division is same to above, sample with the ratio $f_{\nu 6cm}/f_{\nu V} > 100$ was regarded as radio loud here, while the sample with the ratio $f_{\nu 6cm}/f_{\nu V} < 10$ was regarded as radio quiet. The sample that wasn't detected in radio flux were classified to radio quiet.

Next, each radio quiet and the radio loud sample was divided by the observation interval at rest frame into the short interval sample and the long interval sample. The frequency of the radio activity and the observation interval at rest frame distribute localized around two place. And it is preferable that the subsamples in this stage include as many samples as possible to divide by M_B or z at next step. Therefore the number of bin of dividing by the radio activity and the observation interval at rest frame was limited as two.

The case where significant ensemble variability cannot obtain because of the lack of the sample when further dividing is executed. But the four subsamples that is the radio quiet with long observation interval at rest frame and with short interval, the radio loud with long interval and with short interval were divided by M_B into $-18 < M_B < -22$, $-22 < M_B < -24$, $-24 < M_B < -26$, $-26 < M_B < -32$. If those subsamples were divided further, the lack of the sample number were fatal. Therefore the division by z was done from above four subsample into $0 < z < 0.1$, $0.1 < z < 0.3$, $0.3 < z < 0.6$, $0.6 < z < 1$.

Fig.5.7 left shows the ensemble variabilities estimated for the all sample and plotted as abscissas axis is wavelength. The value of the ensemble variability is about 0.2mag at J,H and K' band, and at least remarkable wavelength dependence of the ensemble variability aren't found there.

Fig.5.7 right shows the ensemble variabilities of the radio quiet and the radio loud sample. Two features are seen in this figure, one is that the ensemble variabilities of radio quiet sample are smaller then those of the radio loud sample at all of J,H and K' band. Another is that the ensemble variabilities at J,H and K' band are similar value at each of the radio quiet and the radio loud sample.

Fig.5.8 show the ensemble variabilities of of the subsamples made by dividing the radio quiet and the radio loud sample. The further division was done by observation interval at rest frame into $100days < \Delta t/(1+z) < 400days$ and $400days < \Delta t/(1+z) < 800days$. The left and right figure represents the radio quiet and the radio loud sample. The ensemble variabilities of the subsamples with linger observation interval are larger than those with shorter interval ant all wavelength. And the ensemble variabilities at J,H and K' band are similar to each other for each

samples here too.

The error of the ensemble variability tends to increase because of the lack of the sample number when further division is executed. And it is possible that the lack is fatal and estimating the ensemble variability is impossible. The ensemble variabilities obtained by dividing subsamples shown above by M_B and z are shown in from fig.5.9 to fig.5.10. For example shown in fig.5.9, the missing of the ensemble variabilities of the short interval radio quiet sample with $M_B < -26$ is happen. Like the case of dividing the long interval radio loud by M_B or z, the subsample of which the ensemble variability was obtained for only one band is also happened. It is impossible to discuss the wavelength dependence of the ensemble variability for such sample. Comparing to the sample before further division, there are some cases where the ensemble variabilities of J,H and K' band tends to be scattered like the short interval radio quiet with $0.1 < z < 0.3$, or where the ensemble variabilities of J,H and K' band are inclined like the short interval radio loud with $-26 < M_B < -24$.

In next section, statistic test and estimation is done to check the significance of the features like found in above in from fig.5.7 to fig.5.10.

< statistic test and estimation of λ dependence of the ensemble variability >

The statistic test and estimation of the wavelength dependence of the ensemble variability was done by to optimize assumed function to data and to apply the χ^2 test to the result.

Only there ensemble variabilities were available at a subsample in this work even when the ensemble variability of J,H,K' band are obtained. Therefore the fitting parameters included in the function form to use for fitting must be less than 3. As above, it is the feature of the overview of the ensemble variabilities that at least remarkable wavelength dependence of the ensemble variability was not found, especially for the sample that had many objects and the accuracy of the ensemble variability was high like fig.5.7 or fig.5.8. So it is reasonable to make working hypothesis that the ensemble variability is constant in spite of observed band. Therefore the function form of

$$V_{(\lambda)} = Ce^{a\lambda} \tag{5.3}$$

was adopted in this work. The reason to use this function is that eq.(5.3) includes $V_{(\lambda)} = const.$, is always positive for all a if C was selected as positive, and is simple form with only two free parameters. Therefore the selection of the form wasn't based on the consideration of the mechanism of the variability or emission of AGN.

The wavelength dependence of the ensemble variabilities of various samples were estimated with eq.(5.3). a of eq.(5.3) was given and varied numerically, and C was calculated with method

of least square for every a. For each C and a,

$$\chi^2 = \sum_i^N \left(\frac{V_i - V(C, a, \lambda_i)}{\sigma_{V_i}} \right)^2 \tag{5.4}$$

was calculated. Here V_i and σ_i represent the ensemble variability of each band and N=3 when the ensemble variability of J,H,K' band are obtained. The 95% and 99% confidence intervals of a were estimated with the χ^2 distribution. Hereafter C_0, a_0 represent the C, a that make χ^2 minimum.

Table 5.3 shows the result of the test and estimation by above way. The first line of the table represents the result for the all sample. The optimized values are $C_0 = 0.21, a_0 = 0.029$, this means that $V(2.2\mu m)/V(1.25mum) = 1.03$ therefore $V(\lambda)$ at J band and K' band are almost equal to each other. The value of $a = 0$ that means no wavelength dependence is in the 95% confidence interval shown in the table. Therefore the hypothesis where the ensemble variability for all sample doesn't depend on wavelength at from J to K' region is accepted. And the value of a at outside of the confidence interval is rejected. The value except from $a = -0.192$ to $a = 0.242$ is rejected if the 95% confidence interval is used, while the value from $a = -0.248$ to $a = 0.295$ is rejected for 99% case. Those value represents $V(2.2\mu m)/V(1.25mum) = 0.83 \sim 1.26$, $V(2.2\mu m)/V(1.25mum) = 0.79 \sim 1.32$.

Nest, the radio quiet sample and the radio loud sample are discussed as same. The optimized value is $a_0 = -0.065$ for the radio quiet sample and $V(2.2\mu m)/V(1.25\mu m)$ when $a_0 = -0.065$ is 0.94. This value is close to 1. The value of $a = 0$ is enough inside of the 95% confidence interval, and the hypothesis where the ensemble variability for radio quiet sample doesn't depend on wavelength at from J to K' region is also accepted. The confidence interval of a of the radio loud sample is extended somewhat wider than radio quiet and then the ability of rejection becomes lower. This feature is caused by that the accuracy of the ensemble variabilities of the radio loud sample are lower that those of the radio quiet sample. The hypothesis of no wavelength dependence is accepted for the radio loud sample too. The result of the test and estimation for the subsample made by dividing by $\Delta t'$ are similar. The confidence intervals of a include $a = 0$ and significant wavelength dependence of the ensemble variabilities aren't detected though the ensemble variability sometimes extended with the decreasing of sample with the further division.

The ability of rejection in the test remarkably decrease when the subsample obtained by above process is furthermore divided by M_B or z. The blank line in table 5.3 represents the case where the test and the estimation were impossible because more than two ensemble variability wasn't obtained. There are some blank shown as (1) in the table meaning that very large or small value was accepted since the ability of rejection was too low (a was surveyed from -10 to 10. This wasn't enough to reach the edge of the confidence interval for those case). All of the confidence intervals of a shown in the table include $a = 0$. This result means that it is impossible for all the sample of table.5.3 to conclude the significant wavelength dependence of the ensemble variability.

As shown above, somewhat significant test and estimation could be executed for the all sample, the radio quiet and the radio loud sample and further divided sample by the observation interval at rest frame. As the result, The wavelength dependence of the ensemble variability of those samples could be limited around "no wavelength dependence".

On the other hand, the significance of accept "no wavelength dependence" was decreased at the subsample more further divided by M_B or z. However, it could be shown that there was no sample where the wavelength dependence of the ensemble variability was significantly concluded in all the sample obtained in the analysis in this section.

< statistic dependence test of the ensemble variability on characteristic parameters >

In this section, the dependence of the ensemble variability on the radio activity, observation interval at rest frame, M_B, z is tested. Based on the results of the previous section, weighted average of the ensemble variabilities of each band $V_J, V_H, V_{K'}$ is determined as $V_{\overline{\lambda}}$ and $V_{\overline{\lambda}}$ is used as the index of the variability. It is the merit of this method that $V_{\overline{\lambda}}$ with more smaller error is obtained and that the data of the sample where the ensemble variabilities aren't obtained at all band are also useful and possible to compare with other data.

However, it is the important problem that the groups consist of completely different samples must be compared when the relation between the parameter except wavelength like the radio activity, observation interval at rest frame, M_B, z are discussed in this work. There is the possibility that the localization of hidden parameter affect to the relation between $V_{\overline{\lambda}}$ and the focusing parameter because observed sample is uniform for all parameters.

It is also the problem which weren't seen in the analysis of the wavelength dependence that to describe the dependence on various parameters with same function form is almost impossible. For example, the radio activity seen in fig.B.11 distribute for some decades in log scale, while z is in the region from 0 to 1. There are unique relation between observation interval and the ensemble variability and the function form of growth of the ensemble variability has proper significance.

Under the background like above, it determined as the aim of this section to test statistically weather $V_{\overline{\lambda}}$ depends on each parameter with single method. The influence of hidden parameter is considered later. The hypothesis to assume that $V_{\overline{\lambda}}$ doesn't depend on focusing parameter was tested with the method of chi-square test with simple function form $V_{\overline{\lambda}} = C$. This function form has only one free parameter and has the feature that same way of test can be executed in spite of the character of focusing parameter. The sample was divided by the radio activity and next the observation interval at rest frame, what was done in previous section and the equivalence of $V_{\overline{\lambda}}$ for obtained samples were tested. Furthermore, produced subsamples were divided by M_B or z into many subsamples with $-32 < M_B < 026, -26 < M_B < -24, -24 < M_B < -18$ or with $0 < z < 0.1, 0.1 < z < 0.3, 0.3 < z < 0.6, 0.6 < z < 1.0$, what was same as shown in from fig.5.9

to fig.5.10.

Table 5.5 shows the results of the test. C_0 is the result of optimization. P represents the reliability to reject the hypothesis that $V_{\overline{\lambda}}$ doesn't depend on the focused parameter. The first line of the table shows the result of the test between the radio quiet and the radio loud samples. The value of χ^2 is large, and the statistic equivalence of $V_{\overline{\lambda}}$ of the radio quiet and the radio loud sample is strongly rejected. The second line shows the result of comparison between divided radio quiet sample with $100 < \Delta t/(1+z) < 400$ and $400 < \Delta t/(1+z) < 800$. The significance of the difference is high here too. On the other hand, the significance of the difference between the radio loud sample divided into $100 < \Delta t/(1+z) < 400$ and $400 < \Delta t/(1+z) < 800$ is 71.1% and this is lower than above value. It is thought that it contributed to cause this feature that the accuracy of $V_{\overline{\lambda}}$ is low at the radio loud sample with $400 < \Delta t/(1+z) < 800$ because of lack of the data(fig.5.10). Therefore it is impossible to conclude that the dependence of $V_{\overline{\lambda}}$ on the observation interval of the radio loud sample is smaller than that of the radio quiet sample.

P is 75% when the M_B dependence was tested for the radio quiet sample with $100 < \Delta t/(1+z) < 400$. Therefore the hypothesis of equivalence cannot be rejected for example the 95% confidence level was adopted. Then it is impossible to conclude the M_B dependence of $V_{\overline{\lambda}}$ is significant at the radio quiet sample with $100 < \Delta t/(1+z) < 400$. On the other hand, the result of the same test but for z is $P = 95.5\%$ and the z dependence is statistically concluded somewhat strongly.

The results for the radio loud sample with $100 < \Delta t/(1+z) < 400$ are remarkably different from those of radio quiet. High significance of z dependence of $V_{\overline{\lambda}}$ is similar to that of the radio quiet sample, however, χ^2 is further higher at the radio loud sample than the radio quiet sample. M_B dependence of $V_{\overline{\lambda}}$ of the radio loud sample is also highly significant, what is in clear contrast with the case of the radio quiet sample. The test for the radio loud sample with $400 < \Delta t/(1+z) < 800$ couldn't be executed because of the lack of the data.

As described above, the test of whether $V_{\overline{\lambda}}$ depended on various characteristic parameters was executed with simple form $V_{\overline{\lambda}} = C$ and the chi-square test in this section. However, the result of this section represents merely statistic feature of the data. The systematic influence between the result obtained here and hidden parameters is considered later.

< discussion of parameter dependence of the ensemble variability >

The all sample was at first divided by the radio activity into the radio quiet and the radio loud at the analysis by dividing the sample and comparing the subsamples done at previous. It was shown that there was statistically significant difference between the value of $V_{\overline{\lambda}}$ of the radio quiet sample and the radio loud sample. At first, it is discussed whether such difference is caused by the difference of the observation interval at rest frame $\Delta t' = \Delta t/(1+z)$.

The average of $\Delta t'$ at J,H and K' band are 491,503 and 492 days for the radio quiet sample while 337,358 and 321 days for the radio loud sample. It is reasonable to think that the ensemble

variability of AGN is statistically increasing function of $\Delta t'$ though the time dependence of the variability of AGN isn't clear. In such case, It is impossible to explain the difference between the radio quiet sample and the radio loud sample by the difference of $\Delta t'$, because $V_{\overline{\chi}}$ of the radio loud sample is larger than that of radio quiet sample though $\Delta t'$ of the radio loud sample is shorter than that of radio quiet sample.

It is sometimes problem that the shift of the rest frame wavelength corresponding to observing wavelength when the variability of AGN of which z distribute widely extended is studied (for example,). However, multi-wavelength observation at J,H and K' band is effective solution of this problem in this work. In fact, it can be concluded that difference of the ensemble variability between the radio quiet and the radio loud sample is not merely apparent caused by the shift of observing wavelength, based on the result of the statistic test in previous section and fig.5.11

The average of z and M_B at J,H,K' band is 0.251, 0.222, 0.236 and -23.5, -23.4, -23.4mag for the radio quiet sample in this work, while 0.526, 0.488, 0.528 and -24.9, -24.8, -24.8mag for the radio loud sample. Therefore the radio loud sample tends to be brighter at M_B and distribute further than the radio quiet sample in this work. However, it is high probability that the dependence of the radio quiet and the radio loud sample on z and M_B is different, as describe below. Therefore it is impossible to explain the difference of the ensemble variability between the radio quiet and the radio loud sample.

Next, the relation between the ensemble variability of the radio quiet sample and $\Delta t'$, M_B, z is discussed. In the test of the previous section, there was the remarkable difference between the ensemble variabilities of the radio quiet sample with long and short $\Delta t'$. And the z dependence of the ensemble variability was found at both subsamples with long and short $\Delta t'$, while the M_B dependence wasn't found.

As the first step to consider those features, the shift of the rest frame wavelength of the observation is focused on. It is understood that z dependence of the ensemble variability for the radio quiet sample isn't merely apparent feature by the effect of the redshift from the result of previous statistic result and fig.5.9.

As the next step, The relation between the ensemble variabilities and M_B, z for the radio quiet sample. Fig.5.13 was plotted to consider localization of the hidden parameters for the radio quiet sample. The left column shows the relations of z, $V_{\overline{\chi}}$, $\Delta t'$ and M_B for the subsample made by dividing the radio quiet sample by z into $0 < z, 0.1$, $0.1 < z < 0.3$, $0.3 < z < 0.6$, $0.6 < z < 1.0$. Here $V_{\overline{\chi}}$ is the weighted average of $V_J, V_H, V_{K'}$, and z,M_B,$\Delta t'$ are the average of used value. Open and filled square represents the sample with short and long observation interval at rest frame. The right column show similar figures but plotted for the subsample made by dividing the radio quiet sample by M_B into $-32 < M_B < -26$, $-26 < M_B < -24$, $-24 < M_B < -22$, $-22 < M_B < -18$.

It can be thought that $V_{\overline{\chi}}$ is roughly decreasing function of z from fig.5.13 top of the left side. On the other hand, it is shown from fig.5.13 middle of the left side that $\Delta t' = \Delta t/(1+z)$ is decreasing with increasing z at both of the sample with long and short interval at rest frame. The main reason why such relation between $\Delta t'$ and z is cosmological time delay. Therefore,

the correlation between $V_{\bar{\chi}}$ and z found in previous statistic test is qualitatively consistent with the effect of $\Delta t'$, where $V_{\bar{\chi}}$ is larger at the sample with longer $\Delta t'$. Fig.5.15 shows the relations between $V_{\bar{\chi}}$ and $\Delta t'$ for various subsamples of the radio quiet sample. Top and bottom of fig.5.15 represents the case of dividing by M_B and z. And fig.5.16 is for the radio loud sample resemble. From these figures, M_B or z dependence of growth curve of $V_{\bar{\chi}}$ of the subsamples of the radio quiet are smaller than those of the radio loud, and are roughly equal to each other regardless of M_B or z.

As shown above, it is impossible in this work to reject the possibility where the z dependence of the ensemble variability of the radio quiet AGN is merely apparent by the difference of $\Delta t'$. Therefore, it is also impossible to conclude the intrinsic z dependence of the ensemble variability of the radio quiet AGN though the difference of the data is statistically significant.

From here the effect of the host galaxy and the variability of pure AGN component is considered. It was shown in above discussion that the intrinsic M_B or z dependence of the ensemble variabilities small for the radio quiet sample of this work. However, it is thought that the data used there is contaminated by the host galaxy component nevertheless the data was obtained with small 3 arcsec aperture. The ensemble variability becomes smaller when the contamination of the host galaxy is larger because the host galaxy component doesn't vary in some years. It is thought that the ratio of host galaxy component on total flux is larger at darker AGN(for example, shown in Kotilainen& ward,1994). On the other hand, because dark sample is limited in nearby region because of the observation limitation, the ratio of the flux overflowing from aperture becomes high at the dark sample. Those effects compete, therefore the influence of the host galaxy to the M_B or z dependence of variability is complex.

Color analysis with multi-aperture photometry shown in fig.5.4 is effective to consider the influence of the host galaxy contamination. It was understood that the contamination of host galaxy is larger at the darker AGN discussed in section5.1. There were little M_B dependence of the ensemble variability of the radio quiet sample in this work, what means that there is negative correlation between the pure variability of the radio quiet AGN and their luminosity. On the other hand, it can be understood from fig.5.13 left side that the sample with small z tends to be dark at M_B. Therefore it is expected that the ensemble variability of the sample with smaller z change more larger at the subtraction of the host galaxy contamination. As the result, the negative correlation between $V_{\bar{\chi}}$ and z seen in fig.5.13 top of the left side is in the sense to become more remarkable. However, the understanding of z dependence of $V_{\bar{\chi}}$ by the difference of $\Delta t'$ becomes impossible when the change by subtraction is too large. Therefore, it is unknown in this work how the pure variability of the radio quiet AGN correlate with z without the apparent difference caused by the difference of $\Delta t'$.

when the dust reverberation model is considered, the hot dust torus of more brighter AGN is more larger, therefore the variability of the central heating source is dulled more strongly at the dust torus. The relation between the variability and luminosity of AGN at UV-optical wavelength is still discussed, however the resulted relations are localized from negative correlation to no correlation. Therefore, if the emiiison and variability mechanism is dust reverberation,

negative correlation between near infrared variability and luminosity is required regardless of the real property of the central source variability. Considering the host galaxy contamination, the result of this work for the radio quiet sample fills this requirement.

Next, the relation between the ensemble variability of the radio loud sample and $\Delta t'$, M_B, z are considered. It was shown in the statistic test of the previous section that the dependence of $V_{\bar{\lambda}}$ on both z and M_B were enough significant for the radio loud sample. Fig.5.10 shows that the sense of detected dependence is that the ensemble variability becomes larger at more far object in z and more brighter in M_B object for the radio loud sample.

Fig.5.14 is drawn to show the hidden parameter of the radio loud sample like fig.5.13. Open and filled square represents the sample with short observation interval at rest frame ($100 < \Delta t' < 400$) and with long interval($400 < \Delta t' < 800$), though plotted data of the later is very few because of the lack of the sample. The middle and left of fig.5.14 shows the $\Delta t'$ of the subsample made by dividing by z for the radio loud sample. In data with short interval shown by open square, it is recognized that $\Delta t'$ decreases with z increasing. This feature is mainly caused by the cosmological time delay. Therefore, it is impossible to explain the z dependence of $V_{\bar{\lambda}}$ for the radio loud sample with the effect of $\Delta t' = \Delta t/(1+z)$ because $V_{\bar{\lambda}}$ increase with increasing z in spite of decreasing $\Delta t'$. The M_B dependence of $V_{\bar{\lambda}}$ for the radio loud sample is in same situation and cannot be explained by the effect of $\Delta t'$.

Furthermore, it is understood from fig.5.10 that the z and M_B dependence of $V_{\bar{\lambda}}$ of the radio loud sample is not merely apparent feature originated by the shift of the rest frame wavelength from the observation wavelength by cosmological redshift.

However, there is the correlation between z and M_B in each of the radio loud sample with long and short rest frame observation interval, what was seen in the radio quiet sample too(fig.5.14 bottom). The subsamples with different $\Delta t'$ should be compared if comparison of the subsamples with similar z but different M_B is executed because the short and long interval sample tends to distribute separately in the z-M_B plane. Therefore it is hard to estimate the z and M_B dependence of $V_{\bar{\lambda}}$ independently at the radio loud sample in this work.

As the result of those consideration, it can be concluded that the ensemble variability of object with brighter M_B and higher z is significantly larger than darker M_B and lower z object for the radio loud sample in this work, and the correlations aren't merely apparent features caused by the effect of $\Delta t'$ or shift of the rest frame wavelength from the observation wavelength by cosmological redshift.

If the contamination of the host galaxy is larger at the darker AGN for the radio loud sample too, the positive correlation between M_B and luminosity found in this work is in the sense to become weak at the subtraction of the host component. However, it is difficult to estimate quantitatively how the correlation becomes weaker, or vanish or turn over. But the difference of M_B dependence of the ensemble variability is clear between the radio quiet and the radio loud sample, so extremely different contribution between the radio quiet and loud AGN is required to explain the difference of M_B dependence of the ensemble variability if the difference is entirely

originated by host galaxy. Therefore it is reasonable to think that not only the variability of observed AGN but also the pure AGN component variability is different between the radio quiet and the radio loud sample.

It is efficient to make the sample distribution widely in both z and M_B to estimate the z and M_B dependence of the ensemble variability more in detail. The z and M_B of the sample were extended as widely as possible, however, there were tendency that $\Delta t'$ of bright apparent magnitude sample was long and dark sample had short interval. So it became somewhat difficult to compare the samples with almost same z, $\Delta t'$ and with different M_B. It is thought that this features is originated that from the brighter apparent magnitude objects were observed in the 1st and 2nd term of the observation. It is one of the reason to observe such process that this work is also the pre observation of the MAGNUM project and necessary to observe many sample at first time of the observation.

It is efficient to avoid such problem to observe in the season from 1999 autumn(the 4th term) the object that was observed at th 2nd and 3rd term and add the result to this work. As the result, the interval between the 3rd and 4th term becomes about 2 years and the interval between the 2nd and 4th term becomes about 3 years. Therefore it becomes possible to compare those results to the sample observed at the 1st and 3rd term with similar observation interval at the rest frame. This way is enough possible with the instrument used in this work without expanding of the region of z and M_B with large telescope.

<comparison with the results in other wavelength >

Fig.5.11 and fig.5.12 show the ensemble variabilities at near infrared wavelength obtained from this work with the result of other work at UV and optical wavelength. Large filled circle, square and triangle in fig.5.11 represents the ensemble variability of the all sample, the radio quiet sample and the radio loud sample. Large open and filled square in fig.5.12 represents the ensemble variability of the radio quiet sample with short observation interval ($100 < \Delta t/(1+z) < 400$) and with long interval($400 < \Delta t/(1+z) < 800$), while open and filled triangle in fig.5.12 represents the ensemble variability of the radio quiet sample with short and long observation interval. Small triangle, circle, square, pentagon and hexagon in both fig.5.11 and fig.5.12 represents the result of De Clemente et al.(1996),Hook et al.(1994) and Cristiani et al.(1990) with 0.3 year interval. The filled symbols represent as same but with 2 years interval. Fig.5.11 and fig.5.12 show that the frequency region where the ensemble variability was obtained was expanded about two times wider in log scale by the result of this work.

The inclination of the plot in fig.5.11 and fig.5.12 is clearly different between the UV· optical region and near infrared region. The ensemble variability tends to be smaller with decreasing of frequency in UV or optical region. Paltani & Courvoisier(1995) explained such intrinsic feature by model by the thermal radiation. If the variability is caused by the temperature change of source, hardening of the spectrum is expected in the high temperature and bright phase of the variability.

In the case, if the temperature of the source is very high and the turn over of the black body radiation is in far shorter region, the ensemble variability is expected to have less dependence on frequency. The study to limit the emission and variability mechanism of AGN from the frequency dependence of the ensemble variability was done like such discussion(De clemente et.al.1996).

On the other hand, similar frequency dependence of the ensemble variability obtained in this work isn't found in near infrared wavelength, what is contrast with the feature in UV or optical region. This feature found in near infrared region is consistent with the dust reverberation model, because SED doesn't change but the flux change if the near infrared emission from AGN is dominated by the thermal radiation from hot dust that is equilibrium to evaporation.

The comparison between the ensemble variabilities at the near infrared and shorter wavelength needs to be careful because the compared ensemble variabilities are the results of different works. The near infrared ensemble variability of the radio quiet sample with long observation interval is comparable to the value at the lowest frequency region of optical data with 2 years rest frame interval in fig.5.12. And the near infrared ensemble variability of the radio quiet sample with short observation interval is between the lowest frequency region of optical data with 2 and 0.3 years rest frame interval in fig.5.12. On the other hand, near infrared ensemble variabilities of the radio loud sample are larger.

The light curve at the near infrared wavelength is thought to be dulled shape from the light curve of the heating source because of the effect of geometry of the dust torus in the dust reverberation model. Therefore it is expected that the ensemble variability at near infrared wavelength is smaller than that of the heating source. As opposed to it, if it is confirmed that the dulling isn't exist, dust reverberation mechanism is able to rejected or limited. However, it is impossible to conclude about the emission and variability mechanism of AGN from the comparison of the ensemble variabilities at UV-optical and near infrared in fig.5.11 and fig.5.11 because the influence to compare the result of the different work of which the sample, analysts method and contribution of the host galaxy is unknown.

Many AGN is monitored at multi-wavelength from UV to infrared in the MAGNUM project. It is expected that the data corresponding to fig.5.11 or fig.5.11 will be obtained for each AGN by single instrument, observation and analysis method.

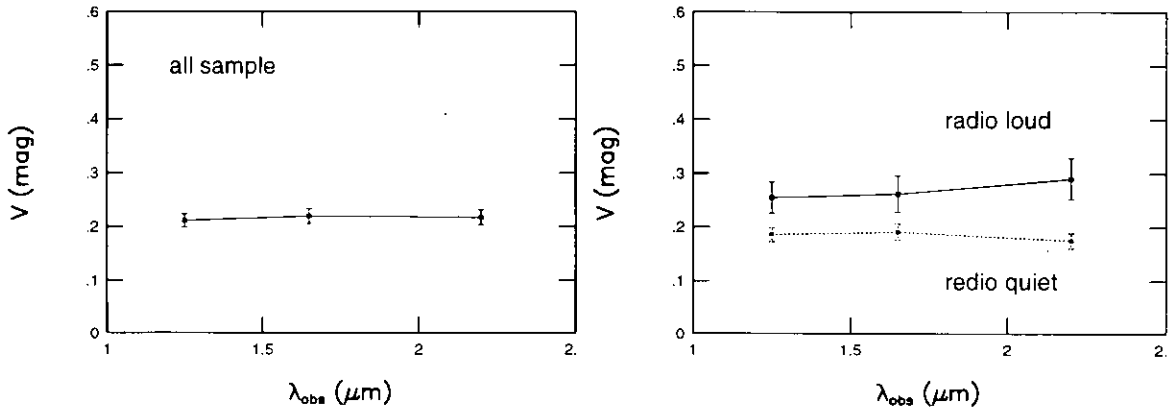

Figure 5.7: Left figure shows the ensemble variability of all sample at j,H and K' band. Right figure shows the ensemble variability of the radio quiet and radio loud sample. Only the data estimated with more than two reference objects and with accuracy higher than 0.1mag are plotted.

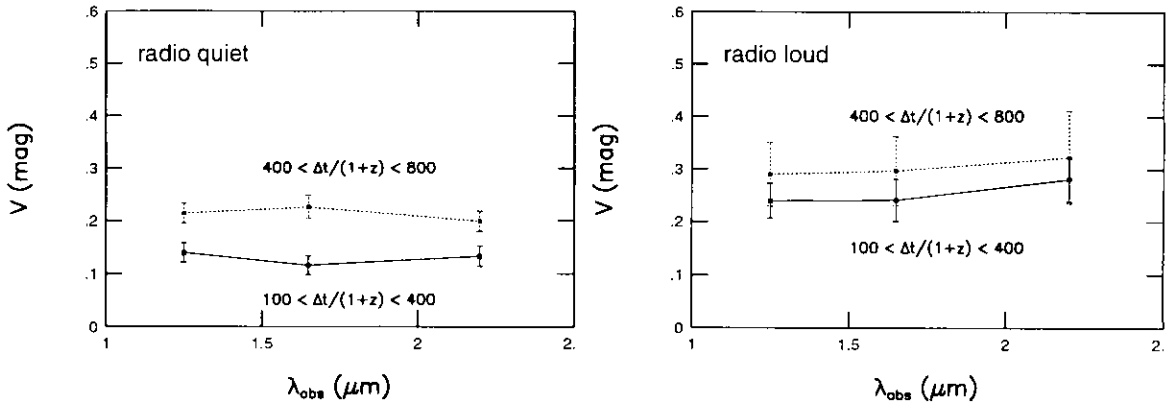

Figure 5.8: Left figure shows the ensemble variability of the radio quiet sample with short interval of the observation (100days $< \Delta t/(1+z) <$400days) and with short interval of the observation (400days $< \Delta t/(1+z) <$800days). Right figure is same but for the radio loud sample. Only the data estimated with more than two reference objects and with accuracy higher than 0.1mag are plotted.

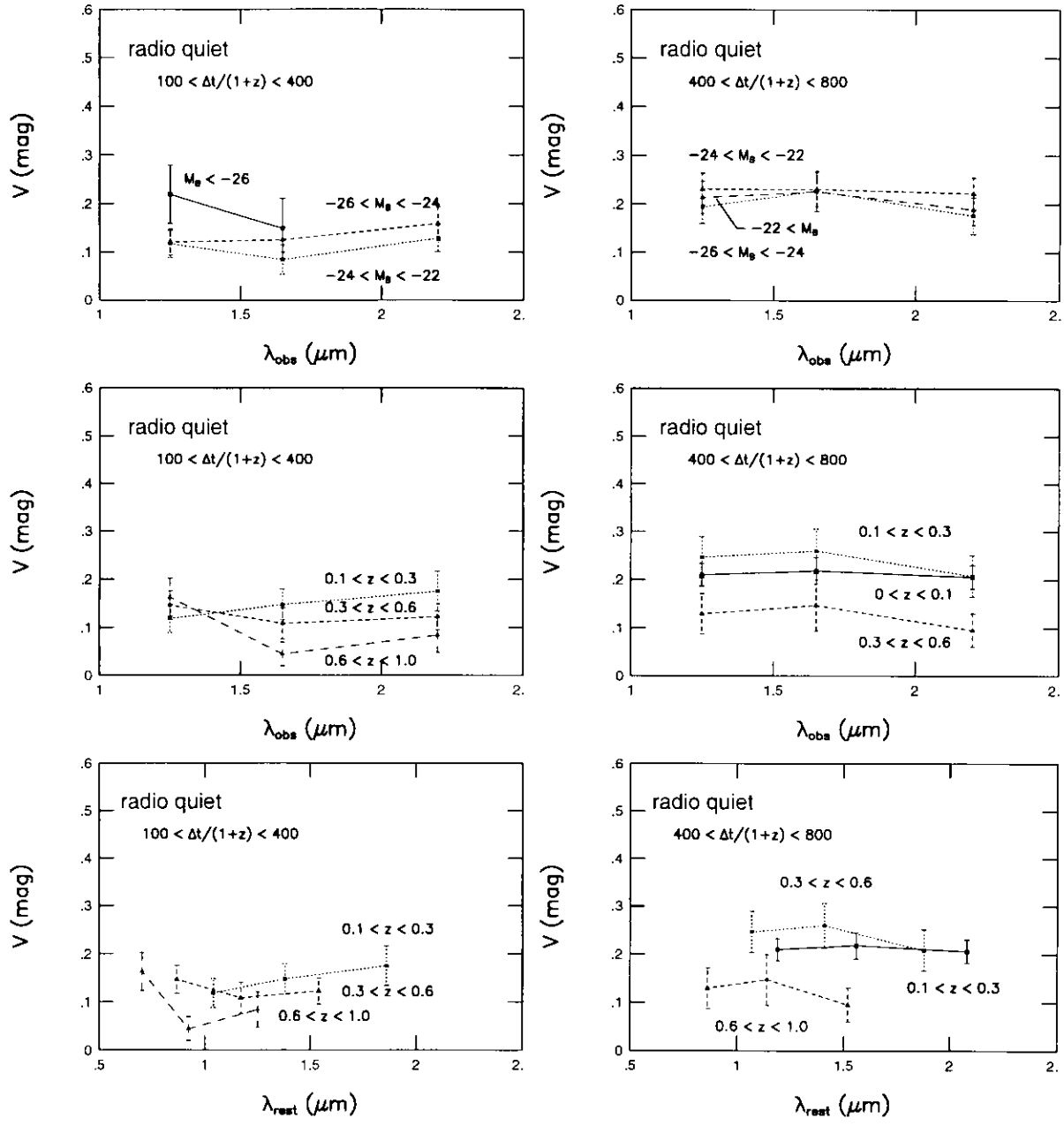

Figure 5.9: Left side figures show the relation between the ensemble variability of the radio quiet sample with short interval of the observation (100days $< \Delta t/(1+z) <$ 400$days$) and M_B, z. Right side figures are same but for sample with long interval of the observation (400$days$ $< \Delta t/(1+z) <$ 800$days$). Only the data estimated with more than two reference objects and with accuracy higher than 0.1mag are plotted.

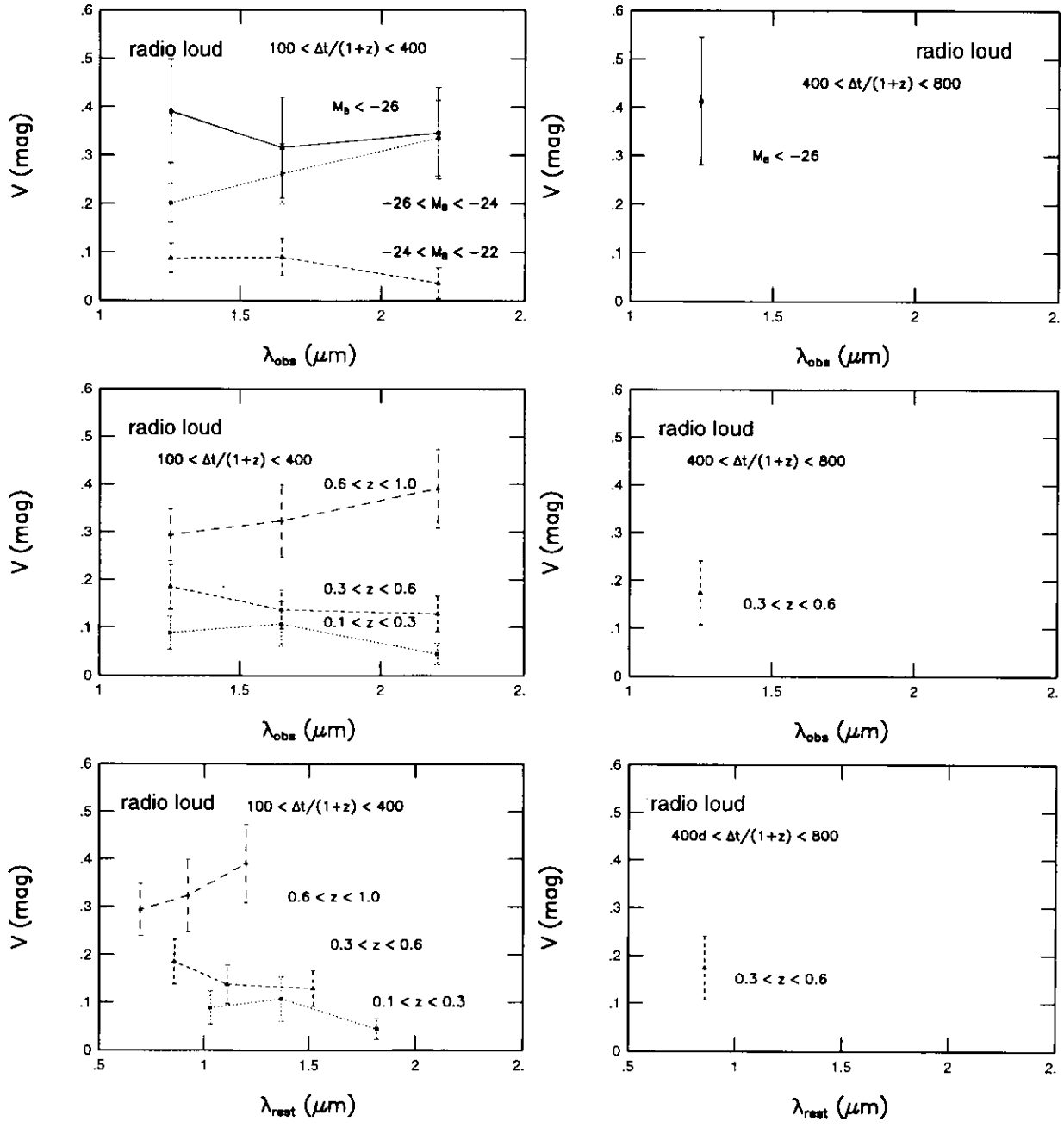

Figure 5.10: Left figures show the relation between the ensemble variability of the radio loud sample with short interval of the observation (100days $< \Delta t/(1+z) <$400days) and M_B, z. Right side figures are same but for sample with long interval of the observation ($400days < \Delta t/(1+z) < 800days$). Only the data estimated with more than two reference objects and with accuracy higher than 0.1mag are plotted.

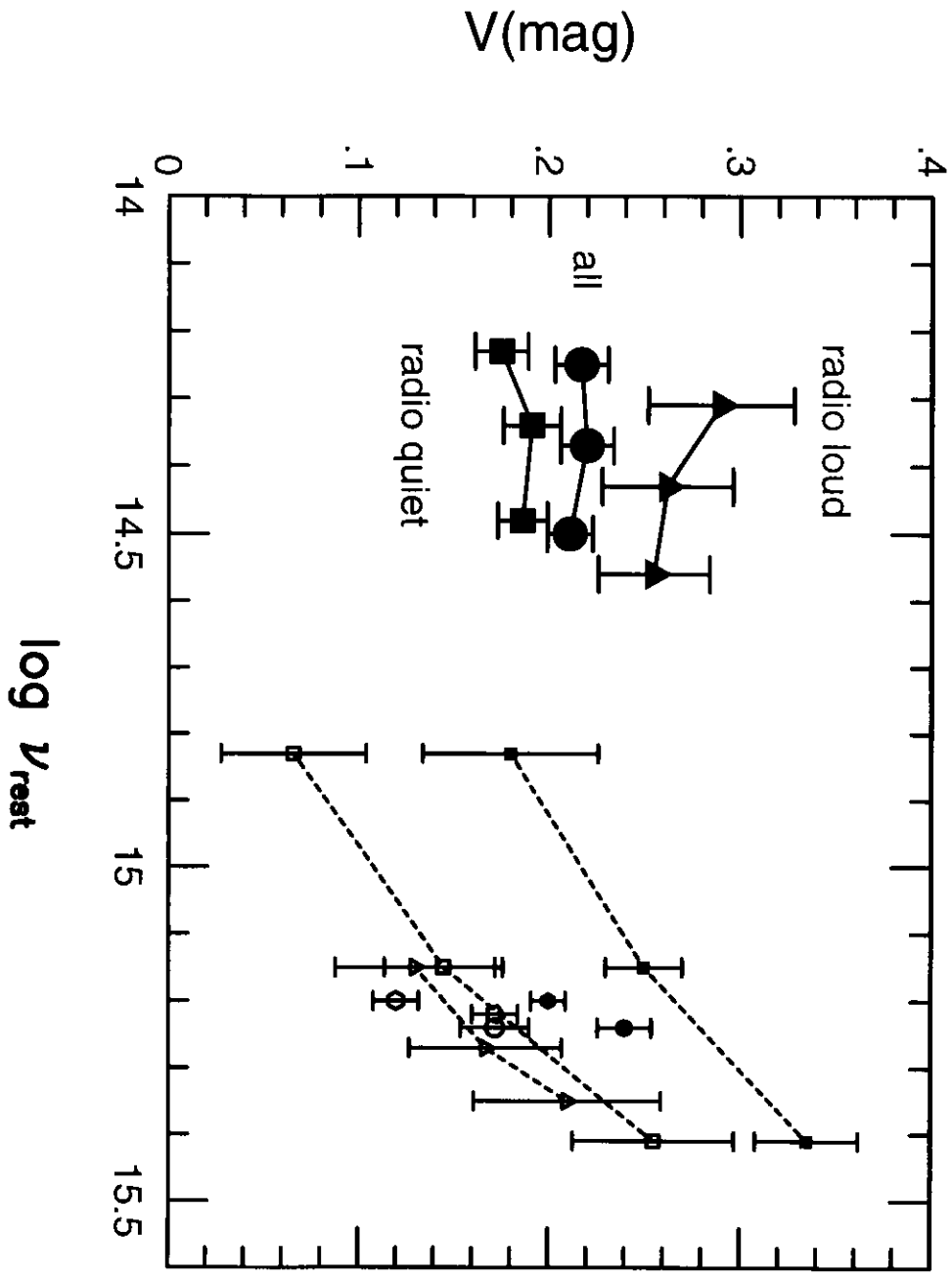

Figure 5.11: Wavelength dependence of the ensemble variabilities obtained by this work and by other works. Large symbols represent the result of this work, where filled circle, square and triangle represent the ensemble variability of the all sample, the radio quiet sample and the radio loud sample,respectively. Filled small triangle, circle, square, pentagon and hexagon represents the result of Cimatti et al.(1993), Trevese et al.(1994), De Clemente et al.(1996), Hook et al.(1994) and Cristiani et al.(1990) with 0.3 year span of the observations, respectively. Open small sample represents same but with 2 year span. De Clemente et al.(1996) was refereed to plot those variabilities.

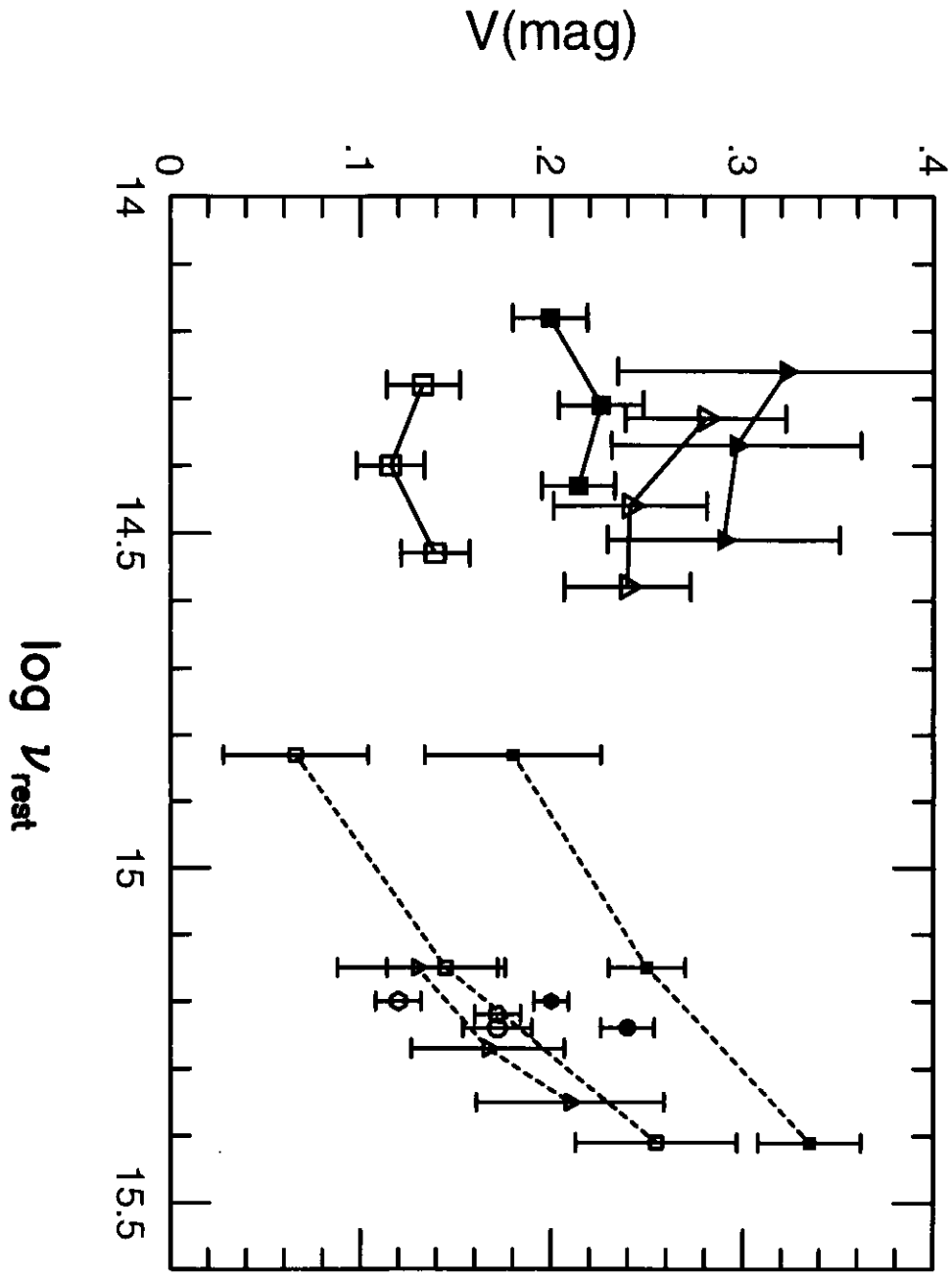

Figure 5.12: Wavelength dependence of the ensemble variabilities obtained by this work and by other works. Large symbols represent the result of this work, where filled square and triangle represents the ensemble variability of the radio quiet and radio loud sample with $400 < \Delta t/(1+z) < 800$. Open symbols represent same but with with $100 < \Delta t/(1+z) < 400$. Filled small triangle, circle, square, pentagon and hexagon represents the result of Cimatti et al.(1993), Trevese et al.(1994), De Clemente et al.(1996), Hook et al.(1994) and Cristiani et al.(1990) with 0.3 year span of the observations, respectively. Open small sample represents same but with 2 year span. De Clemente et al.(1996) was refereed to plot those variabilities.

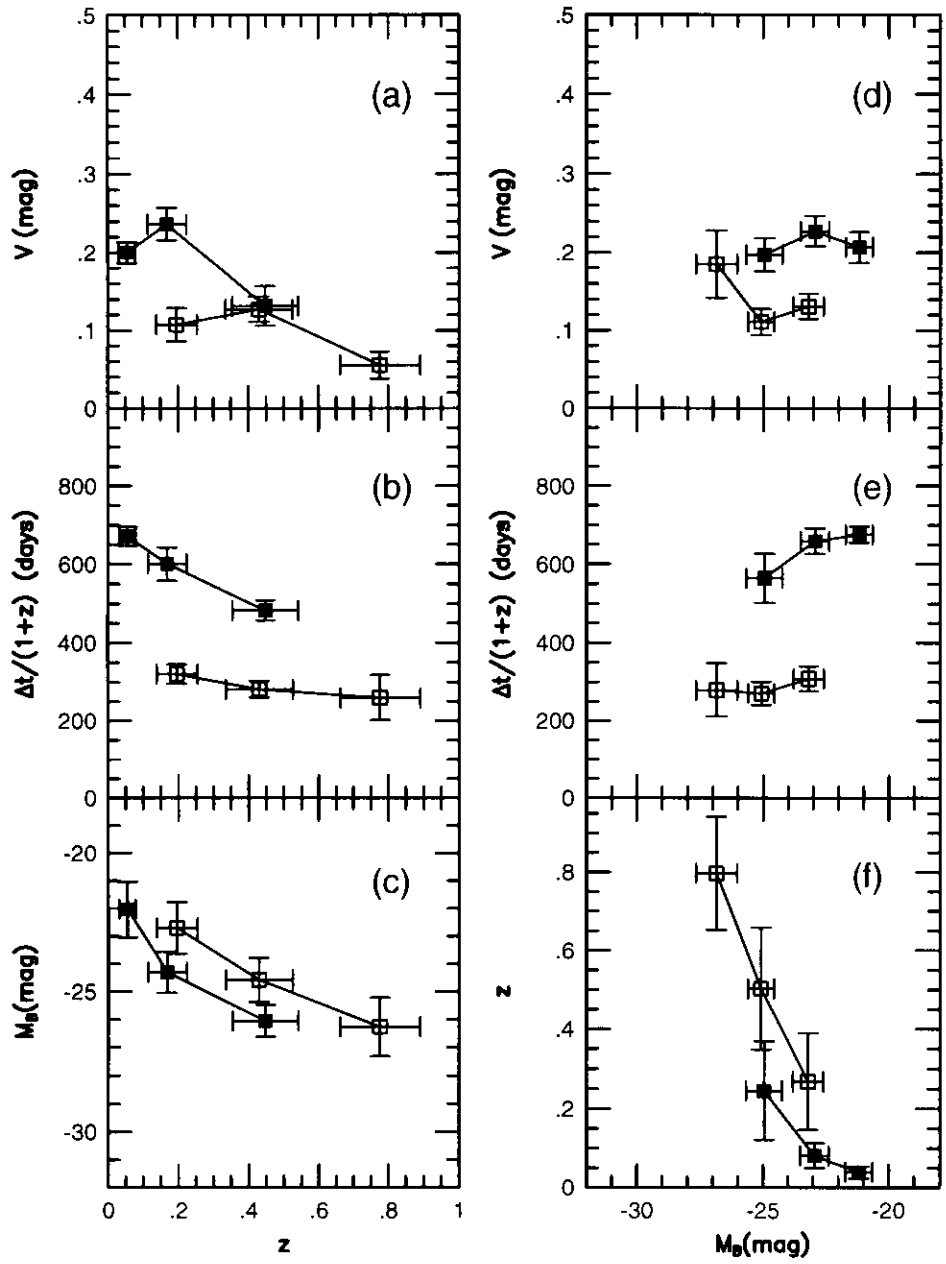

Figure 5.13: Relation of the characteristic parameters each other for the radio quiet sample. Left side figures show the relations between z and $V_{\overline{\chi}}$, $\Delta t'$, M_B where each subsamples are made by dividing by z as $0 < z, 0.1, 0.1 < z < 0.3, 0.3 < z < 0.6, 0.6 < z < 1.0$. Open and filled square represents the sample with $100 < \Delta t' < 400$ and $400 < \Delta t' < 800$, respectively. Right side figures are same but for the subsamples made by dividing by M_B as $-32 < M_B < -26$, $-26 < M_B < -24$, $-24 < M_B < -22$, $-22 < M_B < -18$.

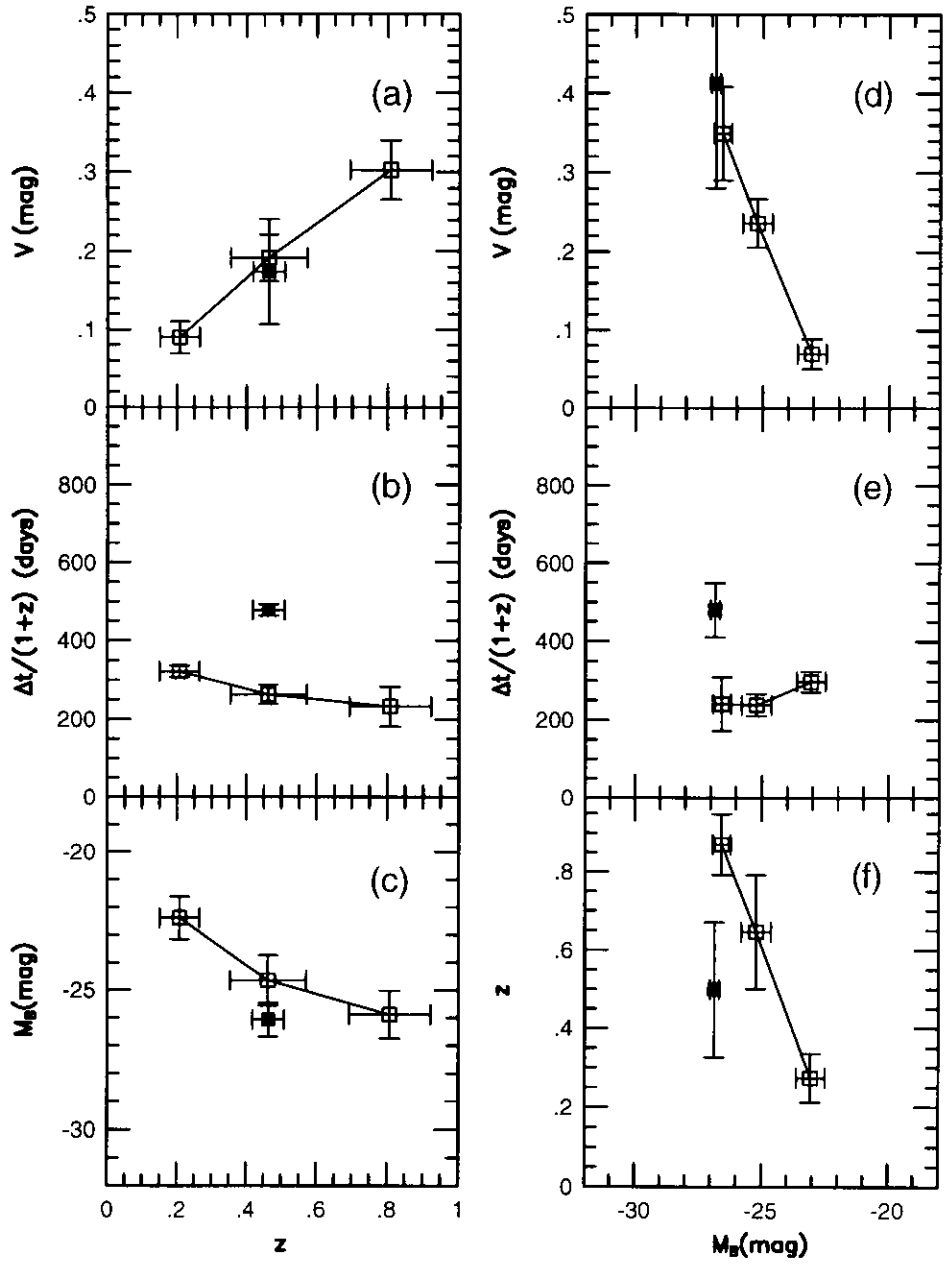

Figure 5.14: Relation of the characteristic parameters each other for the radio loud sample. Left side figures show the relations between z and V_{χ}, $\Delta t'$, M_B where each subsamples are made by dividing by z as $0 < z, 0.1, 0.1 < z < 0.3, 0.3 < z < 0.6, 0.6 < z < 1.0$. Open and filled square represents the sample with $100 < \Delta t' < 400$ and $400 < \Delta t' < 800$, respectively. Right side figures are same but for the subsamples made by dividing by M_B as $-32 < M_B < -26$, $-26 < M_B < -24$, $-24 < M_B < -22$, $-22 < M_B < -18$.

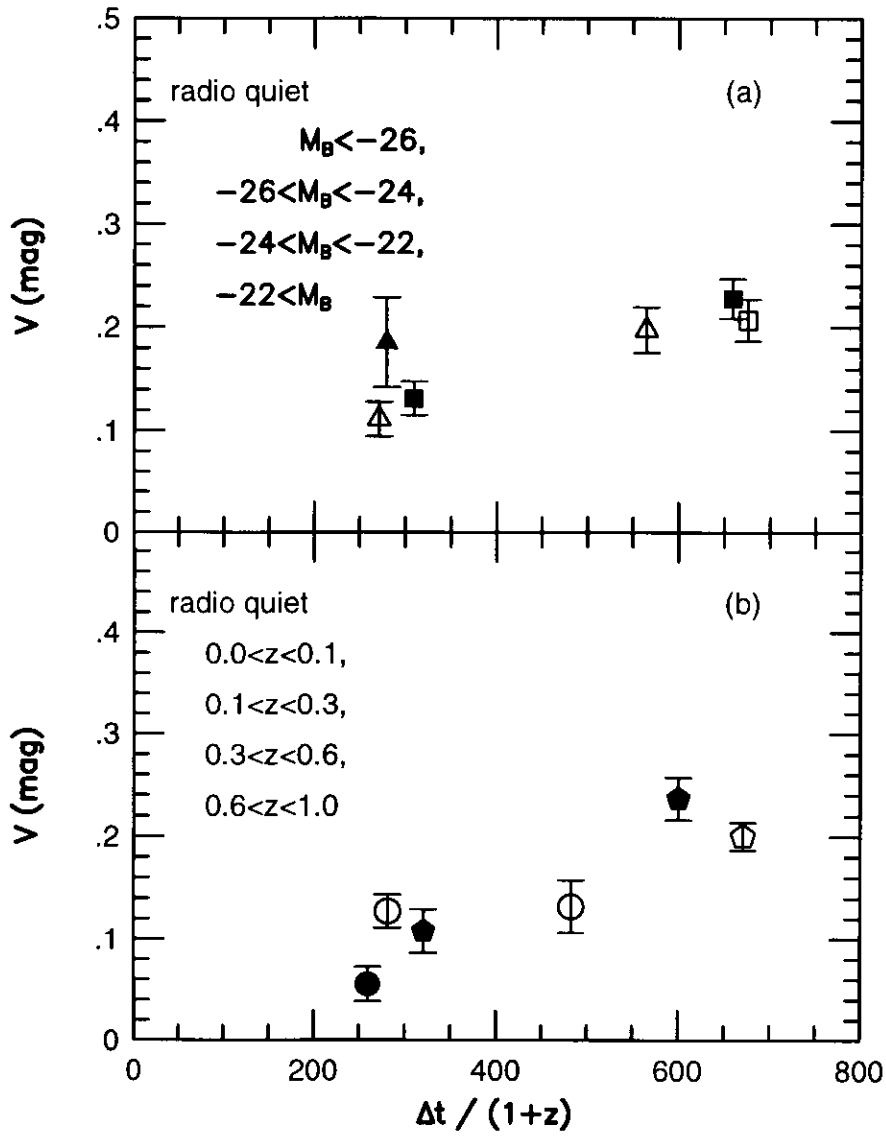

Figure 5.15: Relation between $V_{\bar{\lambda}}$ and rest frame interval of the observation. Top figure shows for the case of the samples divided by M_B. Filled triangle, open triangle, filled square and open square represents $M_B < -26, -26 < M_B < -24, -24 < M_B < -22, -22 < M_B$, respectively. Bottom figure shows for the case of the samples divided by z. Open pentagon, filled pentagon, open circle and filled circle represents $0 < z < 0.1, 0.1 < z < 0.3, 0.3 < z, 0.6, 0.6 < z < 1$, respectively.

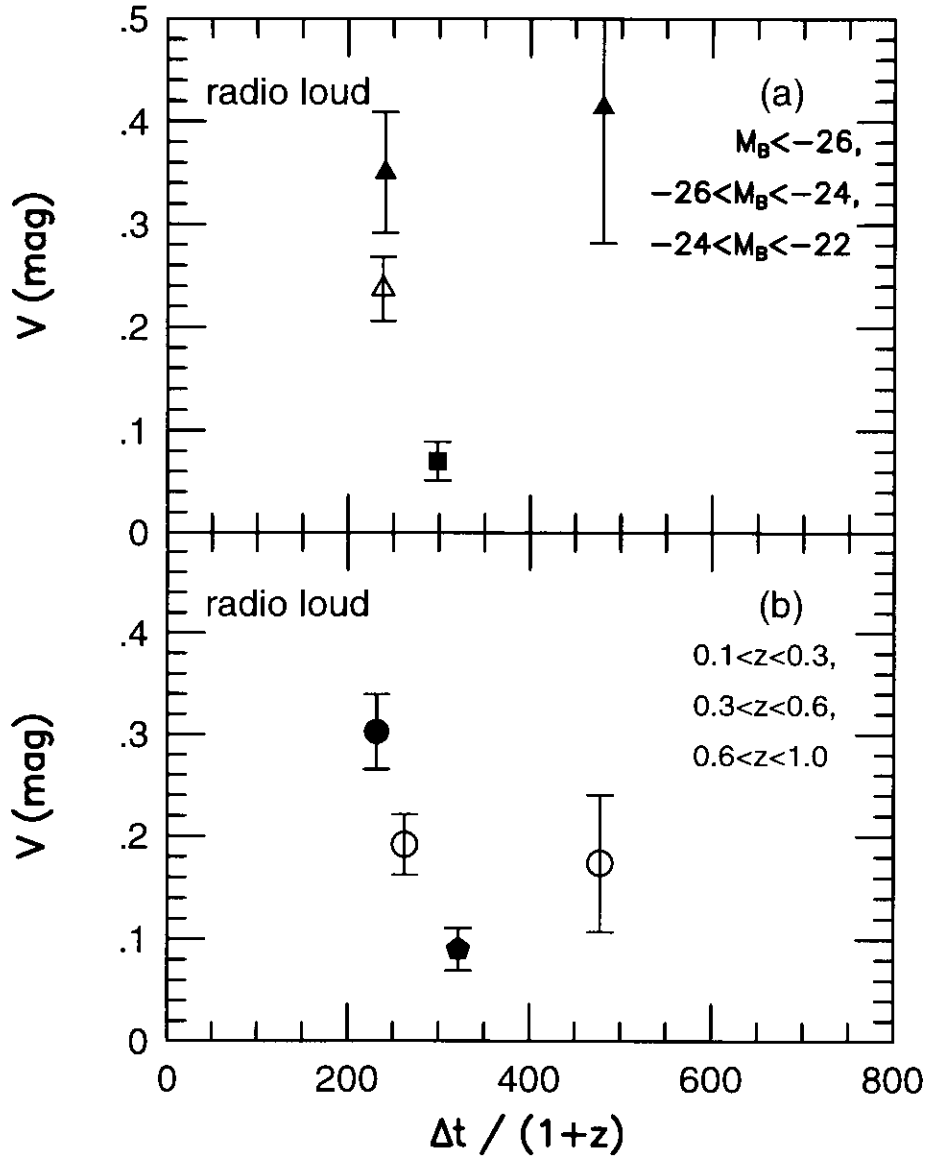

Figure 5.16: Relation loud $V_{\frac{1}{V}}$ and rest frame interval of the observation. Top figure shows for the case of the samples divided by M_B. Filled triangle, open triangle and filled square represents $M_B < -26, -26 < M_B < -24, -24 < M_B < -22$ respectively. Bottom figure shows for the case of the samples divided by z. Filled pentagon, open circle and filled circle represents $0.1 < z < 0.3, 0.3 < z, 0.6, 0.6 < z < 1$, respectively.

	ΔJ_a(mag)	ΔJ_b(mag)	ΔH_a(mag)	ΔH_b(mag)	$\Delta K'_a$(mag)	$\Delta K'_b$(mag)
radio activity	0.255 ± 0.029(42)	0.186 ± 0.013(116)	0.262 ± 0.034(32)	0.191 ± 0.015(97)	0.290 ± 0.038(32)	0.175 ± 0.014(100)
$\Delta t/(1+z)$	0.230 ± 0.018(84)	0.189 ± 0.017(81)	0.250 ± 0.021(74)	0.182 ± 0.019(60)	0.230 ± 0.021(68)	0.201 ± 0.019(67)
M_B	0.233 ± 0.018(90)	0.180 ± 0.015(75)	0.238 ± 0.022(67)	0.201 ± 0.019(67)	0.230 ± 0.021(71)	0.201 ± 0.019(64)
z	0.219 ± 0.020(72)	0.204 ± 0.016(93)	0.213 ± 0.024(49)	0.224 ± 0.018(85)	0.235 ± 0.024(57)	0.202 ± 0.017(78)
Seyfert type	0.213 ± 0.021(57)	0.201 ± 0.023(40)	0.241 ± 0.026(48)	0.231 ± 0.029(35)	0.211 ± 0.023(47)	0.230 ± 0.030(34)
J-H	0.212 ± 0.018(79)	0.208 ± 0.017(75)	0.221 ± 0.022(58)	0.221 ± 0.019(75)	0.207 ± 0.020(64)	0.204 ± 0.018(69)
H-K'	0.234 ± 0.019(80)	0.186 ± 0.016(84)	0.228 ± 0.214(65)	0.213 ± 0.019(69)	0.203 ± 0.019(67)	0.206 ± 0.019(67)

Table 5.1: the ensemble variability of of divided sample into two

	ΔJ_a / ΔJ_b	ΔH_a / ΔH_b	$\Delta K'_a$ / $\Delta K'_b$	average
radio activity	1.37	1.37	1.65	1.46
$\Delta t/(1+z)$	1.22	1.37	1.14	1.24
M_B	1.29	1.18	1.14	1.20
z	1.05	0.95	1.16	1.05
Seyfert type	1.06	1.04	0.92	1.01
J-H	1.02	1.00	1.01	1.01
H-K'	1.25	1.07	0.99	1.10

Table 5.2: the ratio of the ensemble variability of divided sample into two

Table 5.3: the result of λ dependence test of the ensemble variability

	C_0	a_0	confidence interval of a(95%)	confidence interval of a(99%)
all sample	0.205	0.029	-0.192 $\sim$ 0.242	-0.248 $\sim$ 0.295
radio quiet	0.205	-0.065	-0.333 $\sim$ 0.193	-0.403 $\sim$ 0.258
radio loud	0.213	0.136	-0.342 $\sim$ 0.582	-0.470 $\sim$ 0.693
radio quiet,				
$100 < \Delta t' < 400$	0.139	-0.044	-0.575 $\sim$ 0.452	-0.741 $\sim$ 0.593
$400 < \Delta t' < 800$	0.242	-0.079	-0.404 $\sim$ 0.234	-0.494 $\sim$ 0.316
radio loud,				
$100 < \Delta t' < 400$	0.190	0.169	-0.398 $\sim$ 0.703	-0.556 $\sim$ 0.841
$400 < \Delta t' < 800$	0.251	0.111	-0.952 $\sim$ 0.992	-1.313 $\sim$ 1.228
radio quiet ,$100 < \Delta t' < 400$				
$-32 < M_B < -26$	0.729	-0.962	-5.316 $\sim$ 1.468	$-^{(1)} \sim 2.560$
$-26 < M_B < -24$	0.085	0.153	-0.823 $\sim$ 1.132	-1.200 $\sim$ 1.515
$-24 < M_B < -22$	0.081	0.296	-0.622 $\sim$ 1.150	-0.904 $\sim$ 1.390
$-22 < M_B < -18$	-	-	-	-
$0 < z < 0.1$	-	-	-	-
$0.1 < z < 0.3$	0.073	0.404	-0.546 $\sim$ 1.302	-0.842 $\sim$ 1.564
$0.3 < z < 0.6$	0.171	-0.178	-1.091 $\sim$ 0.651	-1.416 $\sim$ 0.910
$0.6 < z < 1.0$	1.610	-1.920	-4.960 $\sim$ -0.136	$-^{(1)} \sim 0.772$
$0 < z < 0.1$(r)	-	-	-	-
$0.1 < z < 0.3$(r)	0.074	0.468	-0.634 $\sim$1.502	-0.980 $\sim$ 1.804
$0.3 < z < 0.6$(r)	0.173	-0.263	-1.538 $\sim$ 0.919	-1.984 $\sim$ 1.290
$0.6 < z < 1.0$(r)	1.685	-3.488	-8.926 $\sim$ -0.252	$-^{(1)} \sim 1.368$
radio quiet,$400 < \Delta t' < 800$				
$-32 < M_B < -26$	-	-	-	-
$-26 < M_B < -24$	0.232	-0.098	-0.783 $\sim$ 0.516	-1.010 $\sim$ 0.693
$-24 < M_B < -22$	0.244	-0.041	-0.592 $\sim$ 0.482	-0.741 $\sim$ 0.616
$-22 < M_B < -18$	0.259	-0.132	-0.738 $\sim$ 0.432	-0.915 $\sim$ 0.583
$0 < z < 0.1$	0.219	-0.023	-0.443 $\sim$ 0.380	-0.554 $\sim$ 0.481
$0.1 < z < 0.3$	0.320	-0.178	-0.890 $\sim$ 0.463	-1.110 $\sim$ 0.635
$0.3 < z < 0.6$	0.206	-0.323	-1.828 $\sim$ 0.937	-2.673 $\sim$ 1.467
$0.6 < z < 1.0$	-	-	-	-
$0 < z < 0.1$(r)	0.219	-0.025	-0.474 $\sim$ 0.404	-0.592 $\sim$ 0.513
$0.1 < z < 0.3$(r)	0.320	-0.209	-1.044 $\sim$ 0.542	-1.302 $\sim$ 0.745
$0.3 < z < 0.6$(r)	0.205	-0.467	-2.642 $\sim$ 1.356	-3.862 $\sim$ 2.122
$0.6 < z < 1.0$(r)	-	-	-	-

Table 5.4: continued

	C_0	a_0	confidence interval of a(95%)	confidence interval of a(99%)
radio loud ,$100 < \Delta t' < 400$				
$-32 < M_B < -26$	0.424	-0.111	-1.372 $\sim$ 1.054	-1.874 $\sim$ 1.471
$-26 < M_B < -24$	0.103	0.540	1.547 $\sim$ 1.328	-0.648 $\sim$ 1.547
$-24 < M_B < -22$	0.238	-0.750	-[1] $\sim$ 0.844	-[1] $\sim$ 1.510
$-22 < M_B < -18$	-	-	-	-
$0 < z < 0.1$	-	-	-	-
$0.1 < z < 0.3$	0.235	-0.711	-2.920 $\sim$ 0.847	-[1] $\sim$ 1.883
$0.3 < z < 0.6$	0.282	-0.379	-1.676 $\sim$ 0.713	-2.194 $\sim$ 1.058
$0.6 < z < 1.0$	0.200	0.301	-0.522 $\sim$ 1.042	-0.780 $\sim$ 1.245
$0 < z < 0.1$(r)	-	-	-	-
$0.1 < z < 0.3$(r)	0.232	-0.850	-3.476 $\sim$ 1.025	-[1] $\sim$ 2.280
$0.3 < z < 0.6$(r)	0.273	-0.528	-2.438 $\sim$ 1.007	-3.238 $\sim$ 1.487
$0.6 < z < 1.0$(r)	0.197	0.563	-0.973 $\sim$ 1.969	-1.449 $\sim$ 2.356
radio loud ,$400 < \Delta t' < 800$				
$-32 < M_B < -26$	-	-	-	-
$-26 < M_B < -24$	-	-	-	-
$-26 < M_B < -22$	-	-	-	-
$-26 < M_B < -18$	-	-	-	-
$0 < z < 0.1$	-	-	-	-
$0.1 < z < 0.3$	-	-	-	-
$0.3 < z < 0.6$	-	-	-	-
$0.6 < z < 1.0$	-	-	-	-
$0 < z < 0.1$(r)	-	-	-	-
$0.1 < z < 0.3$(r)	-	-	-	-
$0.3 < z < 0.6$(r)	-	-	-	-
$0.6 < z < 1.0$(r)	-	-	-	-

Table 5.5: The result of the radio activity, $\Delta t'$, M_B, z, dependence test of $V_{\overline{\lambda}}$

sample	parameter	C0	σ of C0	χ^2	P(%)
all	radio quiet/loud	0.196	0.007	15.767	> 99.9
radio quiet	$\Delta t'$	0.167	0.008	27.797	> 99.9
radio loud	$\Delta t'$	0.262	0.019	1.125	71.1
radio quiet,					
$100 < \Delta t' < 400$	M_B	0.126	0.011	2.757	75.0
	z	0.115	0.010	6.179	95.5
radio quiet,					
$400 < \Delta t' < 800$	M_B	0.212	0.012	1.167	44.0
	z	0.196	0.011	14.692	> 99.9
radio loud,					
$100 < \Delta t' < 400$	M_B	0.131	0.016	35.898	> 99.9
	z	0.117	0.013	39.503	> 99.9
radio loud,					
$400 < \Delta t' < 800$	M_B	-	-	-	-
	z	-	-	-	-

5.2.3 probability of having varied for each objects

In this section, each objects are focused on, and the ratio of the objects that is concluded to have certainly varied in this work. Top of figB.14 shows the distributions of the ratio for all samples of each J,H and K' band. Only variability data of each objects estimated with more than two reference stars and their accuracy was better than 0.1mag was used to determine those ensemble variability. The abscissas axis shows R=Δm(mag)/$\sigma_{\Delta m}$(mag) and the vertical axis shows the frequency. The object included in more right bin is concluded to have varied more certainly. The objects with R>5 is included in the most right bin. Middle and bottom of fig.B.14 shows the same distributions but for the radio quiet and radio loud sample.

The distribution of R of J,H and K' band is similar for each other at top of fig.B.14 and it is the feature of the distribution that the frequency is decreasing from R=0 to R=4. The bin of R>5 include more objects because the objects with R>5 is included. Similar features are seen for the radio quiet sample shown in middle of fig.B.14. For the radio loud sample, it is hard to read some features in the distribution because of lack of the sample number(bottom of fig.B.14).

Fig.B.16 shows the distributions of R for the sample made by dividing the radio quiet and radio loud sample by rest frame observation interval. Comparing to radio quiet with the long interval (400< $\Delta t/(1+z)$ <800), R of radio quiet with the short interval(100< $\Delta t/(1+z)$ <400) is localized more left side of the histogram and the frequency is decreasing with R increasing. And the sample of R>5 is rare in the radio quiet with short interval. On the other hand, R of radio quiet with the long interval isn't localized to the left side as remarkable as that of short interval, and R is almost constant at 0<R<5. And there are 20$\sim$30 samples in the bin of R>5 in the radio quiet with the long interval. Those features mean that the variability of the radio quiet sample was identified in long interval sample for more sample with higher reliability than in short interval sample. And it is shown that the excess at the bin of R>5 found in the histogram of all radio quiet is caused by the long interval sample, and the localization toward the left side of histogram is caused by the short interval sample. Those features are consistent with the result of sec.5.2.2 where it was shown that the ensemble variability of long interval radio quiet is larger than that of short interval. For radio loud sample, it is hard to discuss the distributions of divided radio loud because of lack of the sample number.

Fig.B.19 is the distribution of further divided sample by radio activity, M_B or z like done in sec.5.2.2. It is seen that the shape of distribution of the further divided sample is similar to the distribution of before dividing sample if the sample number is enough and the shape of the distribution is identified. However, radio quiet objects with short interval of z<0.1 or long interval of z>0.1 are rare. There are some case in fig.B.19 like above, where the shape of the distribution cannot identified because of lack of the objects.

R=Δm(mag)/$\sigma_{\Delta m}$(mag) that is focused on in this section depends not only on the intrinsic variability of AGN but also on the error of measurement. If the error is estimated too small, fake variability is concluded from dispersion of data that is originated by not intrinsic variability but only statistic dispersion. If the error is estimated too large, the variability cannot be concluded with certain significance even when the variability was detected. As shown in sec.3.3.4, the error estimation of the differential photometry of this work is reliable quantitatively in the region of the error 0.01$\sim$0.1 for J,H and K' band. Therefore, the sample of each J,H and K' band was divided by their error into high accuracy group with σ <0.03mag, middle accuracy group with 0.03< σ <0.05mag and lowest accuracy group with 0.05< σ <0.1mag and the distributions of R is researched for each groups. Fig.B.21 is plotted for these 3 groups as same as above. It is seen that the R distribution of each groups for J,H and K' band is resemble to each other. On the other hand, the shape of the R distributions of different accuracy group differ remarkably each other. The distributions of R of the lowest accuracy sample are localized to left side of the histogram, while the localization to left side is weaker in middle accuracy sample than the lowest accuracy sample. And the localization to left side is not found in the distributions of the highest accuracy sample, and there are many objects with very certainly having varied in the highest accuracy sample.

The ratio of the object that concluded to have varied with more than 2 or 3σ confidence are shown in table5.7. Those ratio varied more than 2σ(or 3σ) confidence for the highest accuracy sample is 85%(73%), 82%(67%) and 73%(65%) at J,H and K' band and 80%(68%) as the average, those are high value.

If observed sample include some fraction of non-variable objects, it is possible that increasing of the ratio of the objects confirmed to be variable is saturated nevertheless the accuracy of measurement becomes higher. Comparing the three groups that was made by dividing by measurement accuracy, the ratio is increasing with the accuracy and is not saturated. Therefore there is possibility in which the ratio of the variable object approach to 100% when the observation with more higher accuracy is done, though the ratio in the highest accuracy sample of this work is already high.

However, it is impossible to conclude directly that almost all objects observed in this work is variable because not only the accuracy but also other parameters are not uniform in those 3 samples made by dividing the measurement accuracy. AGN observed with high accuracy tend to be nearby bright objects, to be radio quiet, and the accuracy isn't completely independent from other parameters. However, it is possible to conclude that more than 80% objects are variable with 2σ confidence and non-variable objects are few when non-variable objects localize in the low accuracy parameter region of this work even if the sample of this work include non-variable objects. It is also concluded that the ratio of the variable object may approach to 100% with more higher accuracy measurement. The simplest interpretation to explain those results is to conclude that almost all of quasars and Seyfert 1 AGN are variable in near infrared wavelength.

In the result of the monitoring of K band in Neugebauer et al.(1989), the objects having varied with more 99.7% confidence was about 24%. This value is comparable to the value for the sample with $0.05< \sigma <0.1$mag of this work. And K band variable object distribution in Neugebauer et al.(1989) is also resemble to that of the value of the sample with $0.05< \sigma <0.1$mag and clearly different from the sample with with $\sigma <0.03$mag of this work. It was concluded in Neugebauer et al.(1989) that here were both evident variable object and ambiguous object at half ratio each other. In those point of view, the result of detection of variability is most similar to the sample with $0.05< \sigma <0.1$mag of the three groups made by dividing by the measurement accuracy in this work.

The ratio of the certainly varied objects of this work is higher than the value of Neugebauer et al.(1989) where 108 objects were monitored at K band for about 20 years with Hale 5m telescope. High detection ratio of variability of this work is mainly caused to adopt the differential photometry method and using small aperture of 3 arcsec. On the other hand, observation of Neugebauer et al.(1989) was done by single detector with 5-15 arcsec beam. The advantage of the small aperture is not only improvement of SNR but also reducing the contribution of the host galaxy into the aperture, especially for nearby AGN. Furthermore, the policy of this work was thought to be efficient at least to detect the variability of many AGN at infrared wavelength, where the observations of each object was limited only tow times with long interval and increasing the sample as far as possible. However, it is possible that the difference of detection rate of the variability is also caused by the difference of the sample selection between this work and Neugebauer et al.(1989).

It is the important result of this work to have detected the variability of many AGN with high detection ratio and discussed about the generality of the variability of AGN.

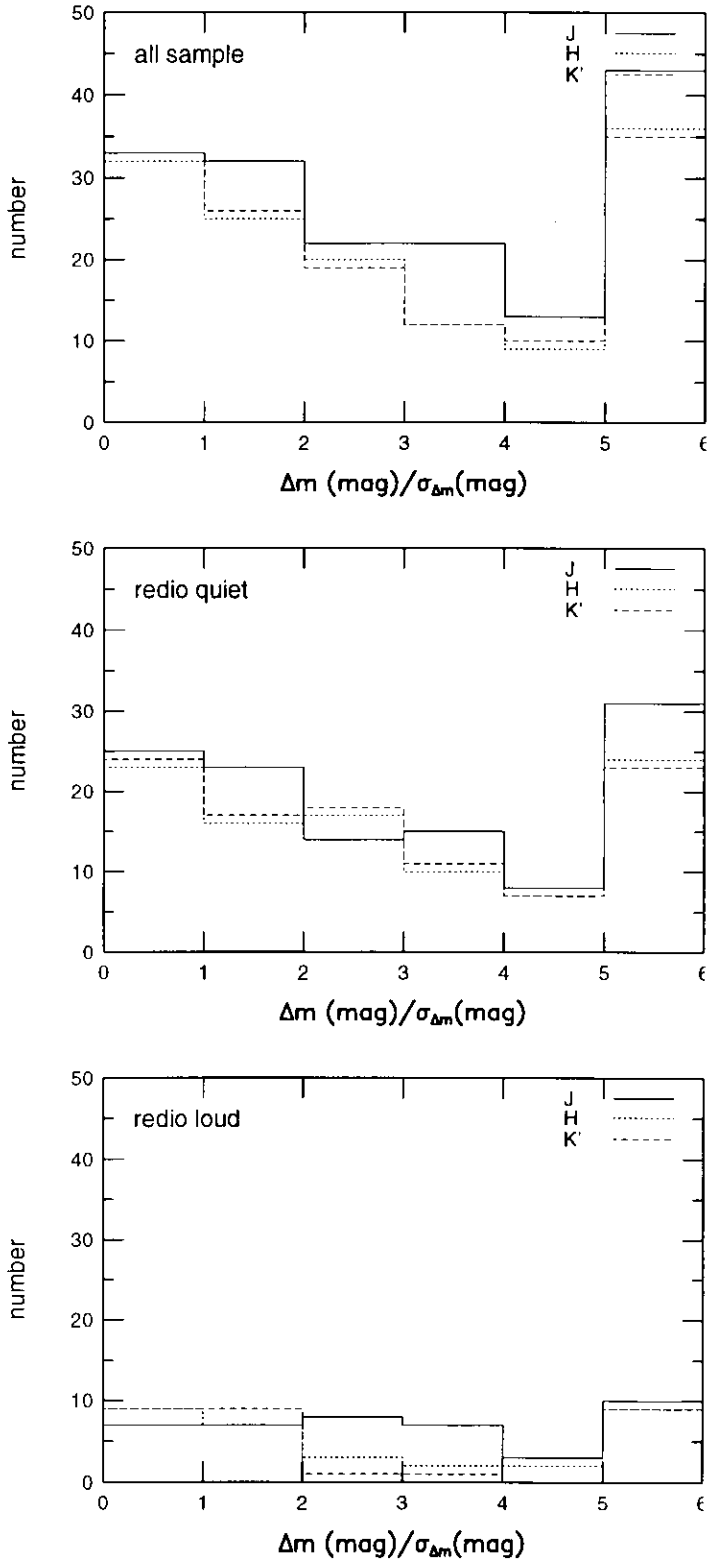

Figure 5.17: Frequency distributions of the probability of having varied Δm(mag)/σ(mag) of each AGN. Δm(mag) is the variation of luminosity and σ(mag) is its error. Top, middle and bottom figure represents the distributions for the all sample, the radio quiet sample and the radio loud sample, respectively.

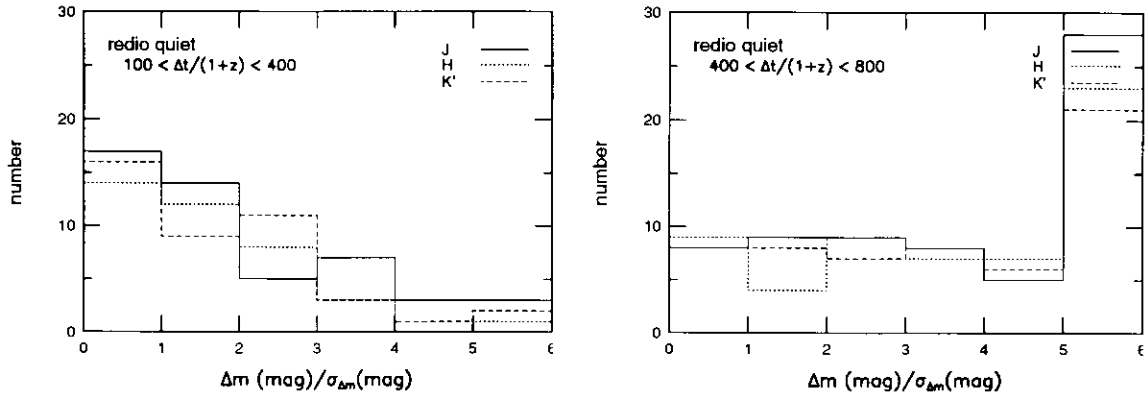

Figure 5.18: Left figure shows frequency distributions of the probability of having varied Δm(mag)/σ(mag) of each AGN in the radio quiet subsamples with short rest frame observation interval of $100days < \Delta t' < 400days$. Right figure is same but for subsample with long rest frame observation interval of $400days < \Delta t' < 800days$.

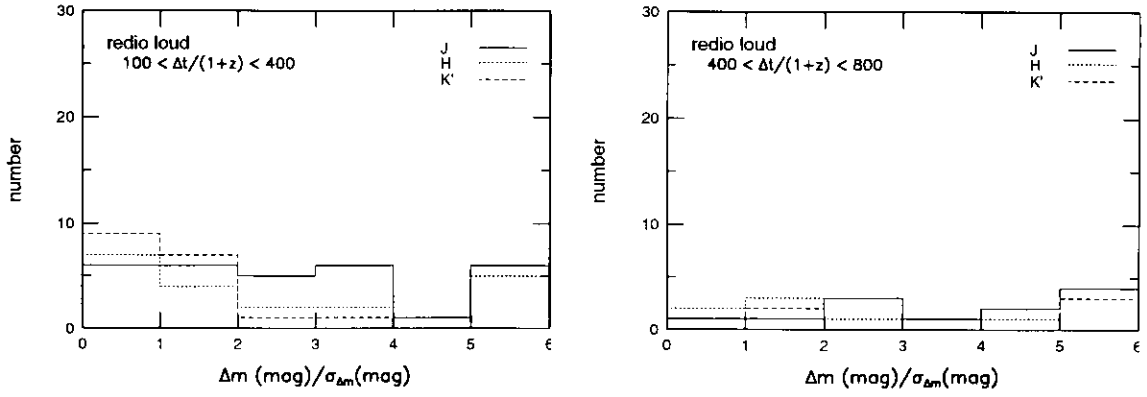

Figure 5.19: Left figure shows frequency distributions of the probability of having varied Δm(mag)/σ(mag) of each AGN in the radio loud subsample with short rest frame observation interval of $100days < \Delta t' < 400days$. Right figure is same but for subsample with long rest frame observation interval of $400days < \Delta t' < 800days$.

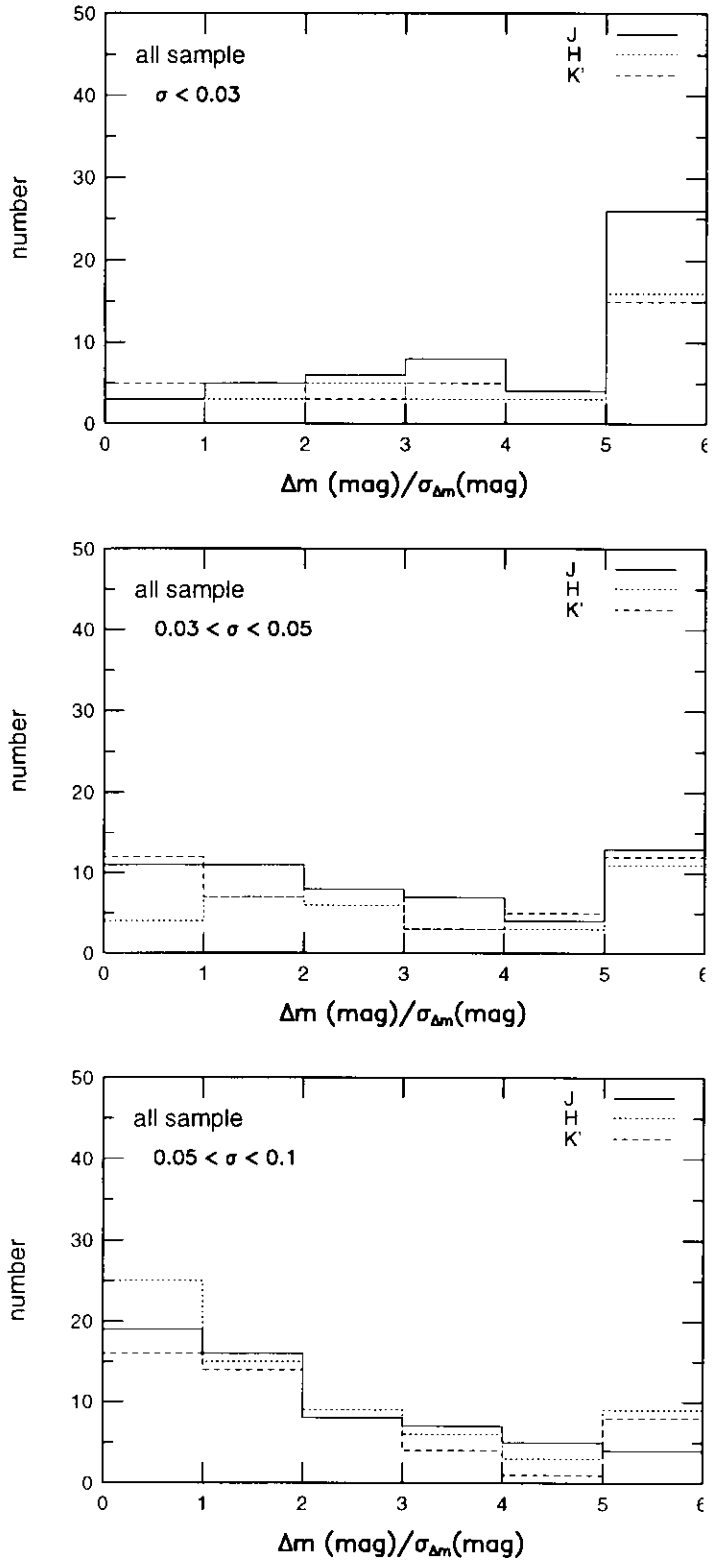

Figure 5.20: Frequency distributions of the probability of having varied Δm(mag)/σ(mag) of each AGN in the subsample made by dividing all sample by the accuracy of variability determination. Top, middle and bottom figure represents the highest accuracy group with σ(mag)< 0.03, intermediate accuracy group with 0.03< σ(mag)<0.05 and the lowest accuracy group with 0.05< σ(mag)<0.1

	J	H	K'	average
all sample	61%,47%(165)	58%,42%(134)	56%,42%(135)	58%,44%
radio quiet	59%,47%(116)	60%,42%(97)	59%,41%(100)	59%,43%
radio quiet,$100 < \Delta t/(1+z) < 400$	38%,27%(49)	32%,11%(38)	41%,14%(42)	37%,17%
radio quiet,$400 < \Delta t/(1+z) < 800$	75%,61%(67)	78%,63%(59)	72%,60%(58)	75%,61%
radio loud	67%,48%(42)	50%,41%(32)	44%,41%(32)	54%,43%
radio loud,$100 < \Delta t/(1+z) < 400$	60%,43%(30)	48%,38%(21)	36%,32%(25)	48%,38%
radio loud,$400 < \Delta t/(1+z) < 800$	83%,58%(12)	55%,46%(11)	71%,71%(7)	70%,58%

Table 5.6: The ratio of the object of which variability was detected with more than 2σ, 3σ reliability in various subsamples. The value in the bracket represents the sample number.

	J	H	K'	average
$\sigma < 0.03$	85%,73%(52)	82%,67%(33)	73%,65%(37)	80%,68%
$0.03 < \sigma < 0.05$	59%,44%(54)	68%,50%(34)	60%,43%(47)	62%,46%
$0.05 < \sigma < 0.10$	41%,27%(59)	40%,27%(67)	41%,26%(51)	41%,27%

Table 5.7: The ratio of the object of which variability was detected with more than 2σ, 3σ reliability in the three subsamples made by dividing all sample by the accuracy of variability determination. The value in the bracket represents the sample number.

5.2.4 correlation of variability of different band

<overview>

In this section, the correlation of variability of other band is discussed. Only variability data estimated with more than two reference stars and their accuracy was better than 0.1mag was used following discussion. Top of fig.B.26 shows the relation of the variabilities between J and H band for radio quiet and radio loud sample. Middle and bottom of those figures correspond same but to J and K', and to H and K' respectively. Fig.B.31 $\sim$ B.34 are for the subsamples made by dividing radio quiet and radio loud sample by z, and fig.B.27 $\sim$ B.30 correspond to same but by M_B.

The data tends to be plotted like a sequence from left and bottom to right and top and almost through origin, what means that the object that became brighter at one band tends to become brighter at other band too. The data also tends to be plotted more frequently at left and bottom of the origin than right and top. However, the tendency doesn't represent the real property of the AGN variability because the objects turned darker tend to be not detected or to be rejected by the accuracy limitation.

<analysis by correlation coefficient>

Next, the relation of the variabilities of J,H and K' band is research by the correlation coefficient. The correlation coefficient of the variability of J and H band is estimated as following,

$$r_{JH} = \frac{\sum_{i=1}^{N}(v_{Ji} - \overline{v_J})(v_{Hi} - \overline{v_H})}{\sqrt{\sum_{i=1}^{N}(v_{Ji} - \overline{v_J})^2 \sum_{i=1}^{N}(v_{Hi} - \overline{v_H})^2}} \tag{5.5}$$

where $v_{J,i}, v_{H,i}$ is the variability data of the i-th object and N means sample number. $\overline{v_J}, \overline{v_H}$ is the average of the variability data of each band. $r_{JK'}, r_{HK'}$ is determined similarly. The data for the discussions of this section were no weighted. About estimation of the confident interval of the correlation coefficient is described in appendixD. The correlation coefficients and their 68.3% confident intervals obtained for all sample, radio quiet and radio loud sample are shown in table 5.8.

The errors of each data affect the correlation coefficient though eq.(5.5) doesn't contain the errors of the data as a explicit parameter. As a expectation, the errors of the data make real correlation to be dulled and shift $|r|$ toward 0. The degree of the affection of the errors depends on not only the errors but also the variability and real correlation coefficient. The sample number affect the confident interval of r. However, because the confident interval depends on the sample

number and r, r and its confident interval are not independent from the errors of the data after all.

As shown in table 5.8, $r_{JH}, r_{HK'}, r_{JK'}$ for the all sample are high value of more than 0.7. The width of 68.3% confident interval is about 0.1 or less. r of the radio quiet sample is > 0.65 and their lower limit is > 0.59, and these value of radio loud sample is more higher. Those features are clearly different from the case of non-correlated($r = 0$). It is concluded that there are the positive correlations in $r_{JH}, r_{HK'}, r_{JK'}$ of all sample, radio quiet and radio loud sample of this work. This conclusion is not changed to consider the effect of the errors of the data, because the errors affect r in the sense of changing toward 0.

In 5.8, the value of $r_{JH}, r_{HK'}, r_{JK'}$ of radio loud sample are larger than of radio quiet sample. However, it is not possible directly from the values to conclude that the difference of real $r_{JH}, r_{HK'}$ and $r_{JK'}$ between the radio quiet and the radio loud sample. The errors of the data make $|r|$ to be smaller, while the data with large variability make $|r|$ to be larger, if the measurement errors is constant. It is hard to judge weather the real correlation of the variability in near infrared different band is stronger at the radio loud sample than at the radio quiet sample.

For correlation efficient of the all sample, $r_{HK'}$ is 0.81 that is a little larger than r_{JH} and $r_{JK'}$ that are 0.74 and 0.71 and similar to each other. For the radio quiet and radio loud sample, $r_{HK'}$ shows larger value than other combinations too. However, those differences are comparable to their confidence intervals and it is impossible to conclude that the differences are significant from only the result in table5.8.

However, by only the research for the all sample, the radio quiet or radio loud sample, feature of the emission depending on rest frame band may be dulled because z of the objects in those sample distribution spread widely. Top of fig.5.23 shows $r_{JH}, r_{HK'}$ and $r_{JK'}$ of the subsample made by dividing the radio quiet sample by z. The criterion of the division was $0 < z < 0.1, 0.1 < z < 0.3, 0.3 < z < 0.6$ and $0.6 < z < 1.0$, same as before. Open square, open triangle and filled circle mean $r_{JH}, r_{HK'}$ and $r_{JK'}$ respectively.

In top of fig.5.23, $r_{JH}, r_{HK'}, r_{JK'}$ of $0 < z < 0.1$ radio quiet sample are high and they seem almost equal to each other. $r_{JH}, r_{HK'}$ is getting smaller but r_{JH} keeps somewhat high value in higher z sample of $0.3 < z < 0.6, 0.6 < z < 1.0$. However, the statistic accuracy of $r_{JH}, r_{HK'}, Hr_{JK'}$ is fairly low at high z region because of lack of the sample. Furthermore, the errors of each variability data of high z sample tend to be larger because those objects tend to be faint while the variabilities tend to be small because those objects tend to have short observation interval. The large error and small variability lead to the underestimate of $|r|$ systematically. Because of those reasons, it seems difficult to conclude significant z dependence of each of $r_{JH}, r_{HK'} and r_{JK'}$.

Therefore $r_{JH}, r_{HK'}, Hr_{JK'}$ of the bin characterized with same z was compared as the next examination. In principle, each AGN of this work is observed by multi color almost simultaneously. So the influence of the difference of the measurement error, sample number or observation interval is rather smaller in comparing $r_{JH}, r_{HK'}, r_{JK'}$ of the sample in the bin with same z than in

comparing each $r_{JH}, r_{HK'}, r_{JK'}$ of different z.

The equivalence of $r_{JH}, r_{HK'}, r_{JK'}$ was tested and the estimation of the real correlation coefficient under the assumption of equality of them were done. The results are shown in table5.9. r_0 means estimated real correlation coefficient. Such test and estimation is described in appendixD. P is the reliability to reject the hypothesis in which $r_{JH}, r_{HK'}, r_{JK'}$ are equivalent. In the results for radio quiet sample, the hypothesis is rejected only in the case with $0.1 < z < 0.3$ significantly, for example with 95% confidence. The hypothesis isn't reject in other z region. However, the interpretation of the test isn't same for the nearby sample with $0 < z < 0.1$ and higher z samples with $0.3 < z < 0.6, 0.6 < z < 1.0$. because the accuracy of $r_{JH}, r_{HK'}, r_{JK'}$ are remarkably different by z. It is significant to be accepted the nearby case with $0 < z < 0.1$ because the accuracy of each $r_{JH}, r_{HK'}, r_{JK'}$ are high. On the other hand, It is impossible to conclude the difference of $r_{JH}, r_{HK'}, r_{JK'}$ is significant for the higher z samples with $0.3 < z < 0.6, 0.6 < z < 1.0$ because the accuracy of $0.3 < z < 0.6, 0.6 < z < 1.0$ are fairly low and rejecting ability of the test is poor.

It is a few significant result that $r_{JH}, r_{HK'}, r_{JK'}$ is almost equal to each other in $0 < z < 0.1$ sample and $r_{HK'}$ is significantly higher than $r_{JH}, r_{JK'}$ in $0.1 < z < 0.3$. As discussed following, those features are consistent with the emission and variability by dust reverberation mechanism. In hot dust reverberation model, it is reasonable that the flux of $z \sim 0$ objects observed at J,H and K' band is mainly emitted from the hot dust in evaporation equilibrium (e.g. Kobayashi et al.1994). The equivalence of $r_{JH}, r_{HK'}, r_{JK'}$ in $0 < z < 0.1$ can be explained by the black body radiation with constant 1500K temperature dominating the near infrared emission. when z becomes $0.1 < z < 0.3$, the 1μm minimum that is seen the SED of AGN and quasars affects to the observed flux at J band. The main variable component at the wavelength shorter than 1μm is thought to be power low component, and its variability is not synchronized with the infrared variability. It can explain the feature that $r_{JH}, r_{JK'}$ is lower than $r_{HK'}$ at $0.1 < z < 0.3$ to think that the correlation between J band variability and more longer wavelength becomes worse by the non-synchronicity, though this explanation is only qualitative. The 1μm minimum at rest frame shifts between H and K' band at observed frame. In such case, r_{JH} is affected by mainly only the variability of the power low component, while $r_{HK'}, r_{JK'}$ can be affected both variable component in both side of the 1μm minimum. It is also consistent with above vision that r_{JH} keeps somewhat high value while $r_{HK'}, r_{JK'}$ are lower than 0 in the $0.6 < z < 1$ region of fig.5.23, though the significance of this feature cannot be concluded because of the lack of the data accuracy.

Bottom of fig.5.23 shows the $r_{JH}, r_{HK'}, r_{JK'}$ of the subsamples made by dividing the radio loud sample with the criterion of $0 < z < 0.1, 0.1 < z < 0.3, 0.3 < z < 0.6$ and $0.6 < z < 1.0$. The accuracy of $r_{JH}, r_{HK'}, r_{JK'}$ of the radio loud subsamples tend to become higher with z becoming larger. The radio loud sample number of $0 < z < 0.1$ is too small, therefore the calculation doesn't execute more. The confident interval of the radio loud sample of $0.1 < z < 0.3$ is still wide, and it is impossible to judge whether the correlation is good or not. On the other hand, both $r_{JH}, r_{HK'}, r_{JK'}$ and their accuracy are remarkably high at high z region of $0.3 < z < 0.6, 0.6 < z < 1.0$.

The accuracy of $r_{JH}, r_{HK'}, r_{JK'}$ of the radio quiet sample is high in the region of $0 < z <$

$0.1, 0.1 < z < 0.3$, and is clearly down in the region of larger z. what is clear contrast with radio quiet. So it is impossible to test whether the features of z dependence of $r_{JH}, r_{HK'}, r_{JK'}$ found in the radio quiet or radio loud sample exist in the other. Therefore, it is concluded that significant difference of the correlation of the variability at different band wasn't found between the radio loud and radio quiet sample.

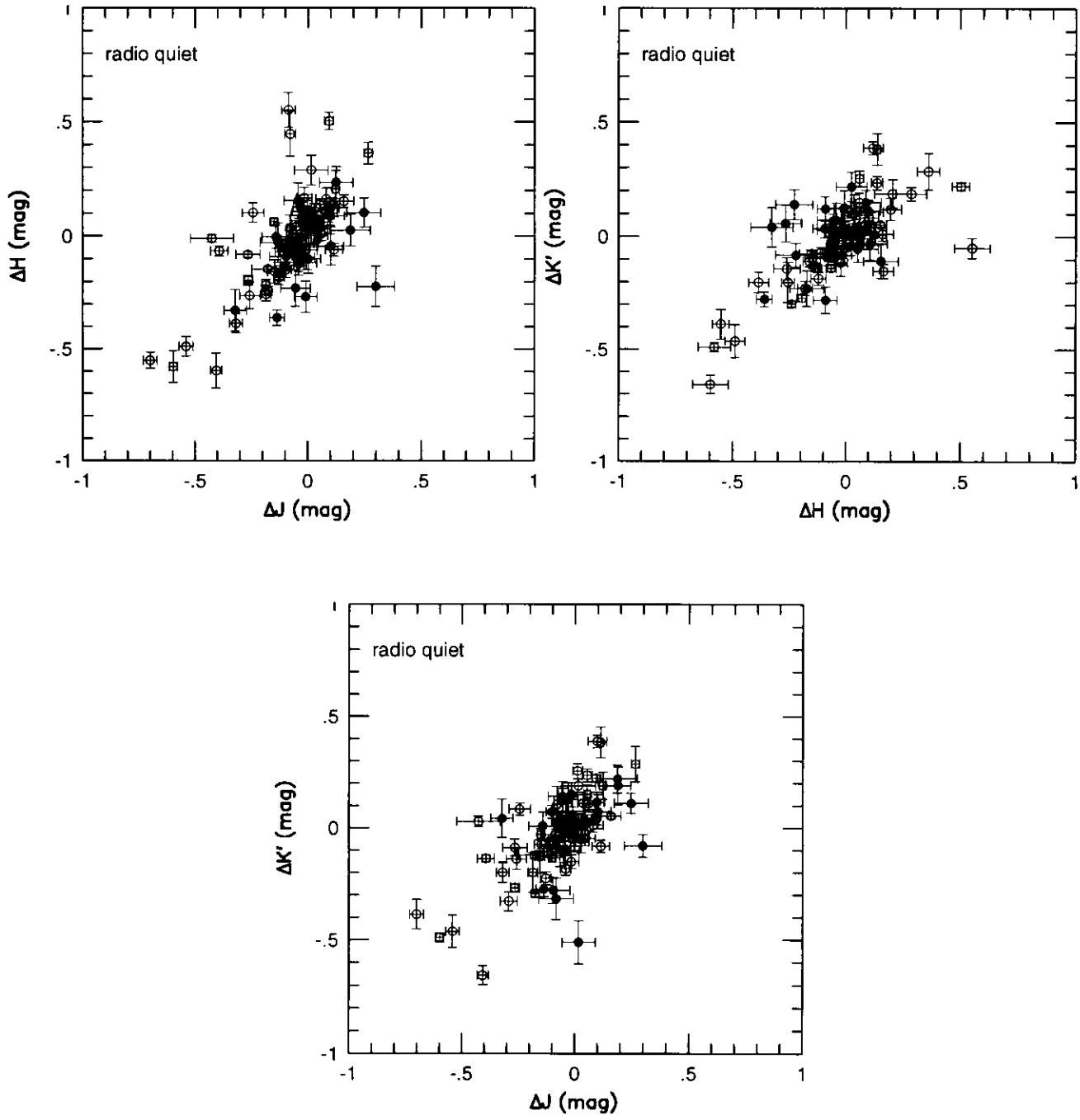

Figure 5.21: Correlation of the variability of J and H, H and K', J and K' band for each radio quiet object. Filled circle represents the sample with short rest frame interval of the observation $100days < \Delta t < 400days$ and long. Open circle represents same but with long interval $400days < \Delta t < 800days$.

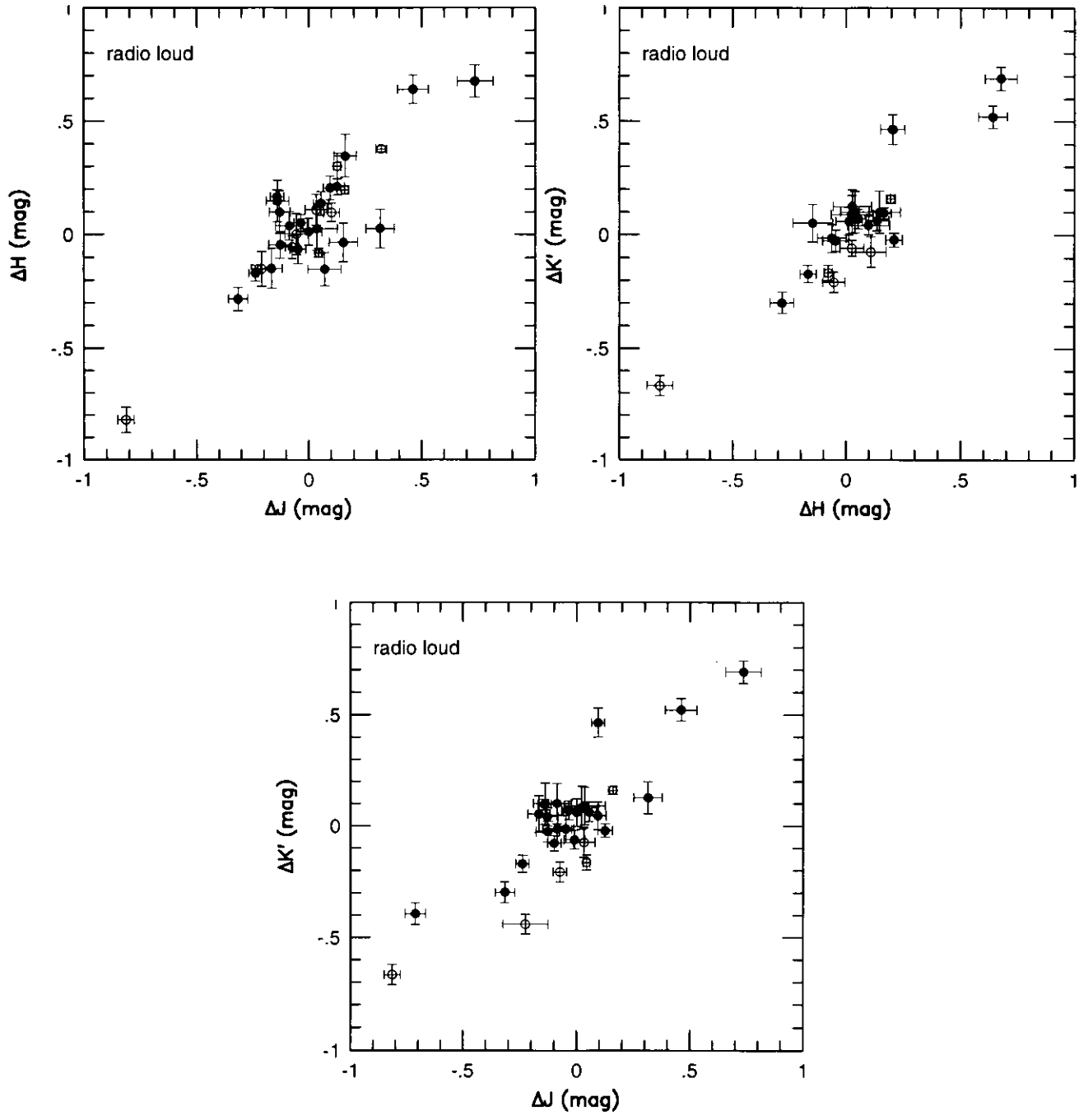

Figure 5.22: Correlation of the variability of J and H, H and K', J and K' band for each radio loud object. Filled circle represents the sample with short rest frame interval of the observation $100days < \Delta t < 400days$ and long. Open circle represents same but with long interval $400days < \Delta t < 800days$.

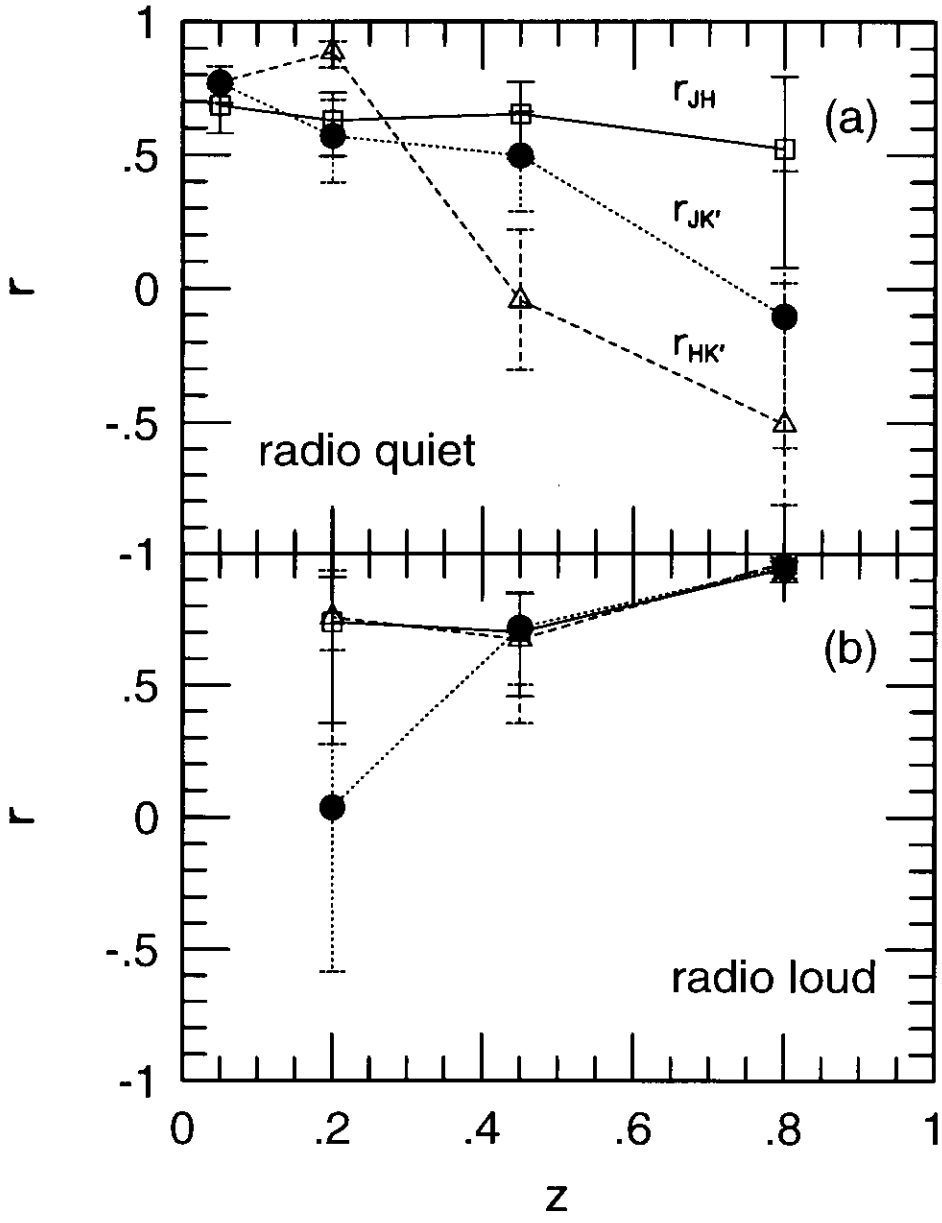

Figure 5.23: Top figure shows the correlation coefficient r of each subsamples made by dividing the radio quiet sample by z. Open square, open triangle and filled circle represents r_{JH}, $r_{HK'}$ and $r_{JK'}$, respectively. Bottom figure shows same but for the radio loud staple.

sample	data num	r	68.3% confidence interval	σ_x(average)	σ_y(average)
all					
J,H	127	0.74	0.70-0.78	0.040	0.050
H,K'	111	0.81	0.77-0.84	0.047	0.044
J,K'	118	0.71	0.66-0.76	0.040	0.046
quiet					
J,H	91	0.65	0.59- 0.71	0.039	0.047
H,K'	84	0.72	0.66- 0.77	0.045	0.041
J,K'	85	0.65	0.59- 0.71	0.037	0.043
loud					
J,H	31	0.88	0.83- 0.91	0.044	0.060
H,K'	24	0.91	0.87- 0.94	0.058	0.053
J,K'	30	0.86	0.80- 0.90	0.047	0.054

Table 5.8: Correlation coefficient r of the J and H, H and K', J and K' band for the all sample, the radio quiet sample and the radio loud sample. $\sigma(x), \sigma(y)$ represents the average error of the variability data of compared band.

sample	r_{JH}	$r_{HK'}$	$r_{JK'}$	r_0	$P(\%)$
radio quiet					
$0 < z < 0.1$	0.69(36)	0.77(38)	0.77(38)	0.75	31.5
$0.1 < z < 0.1$	0.63(29)	0.89 (23)	0.57(22)	$0.72^{(1)}$	96.8
$0.3 < z < 0.6$	0.65(19)	-0.04(17)	0.50(19)	0.42	58.1
$0.6 < z < 1$	0.52(7)	-0.51(6)	-0.11(6)	0.03	68.3
radio loud					
$0 < z < 0.1$	-(2)	-(3)	-(2)	-	-
$0.1 < z < 0.1$	0.74(6)	0.76(5)	0.04(5)	0.60	46.0
$0.3 < z < 0.6$	0.70(10)	0.67(8)	0.72(11)	0.70	1.17
$0.6 < z < 1$	0.94(12)	0.97(9)	0.95(12)	0.95	12.9

Table 5.9: The result of the equivalence test of the correlation coefficient $r_{JH}, r_{HK'}, r_{JK'}$ where $r_{JH}, r_{HK'}, r_{JK'}$ is assumed to be equal each other. r_0 is the estimation of real correlation coefficient in the case of the equivalence is accepted. P is the probability to reject the hypothesis. The radio loud sample of $0 < z < 0.1$ is too few, therefore the test isn't done. caution (1): The value of r_0 isn't adequate since the equivalence is rejected.

5.2.5 time scale of variability of AGN

In this section, how the variability develops is discussed. There is possibility to estimate how the variability develops by using the combination of the data observed at the 1st and 3rd term and the 2nd and 3rd term because their observation intervals are differ about factor 2.

However, it is impossible ,for example, to consider about geometry of emitting region from light curve because frequent repeat of observation was not done in this work. Furthermore, it is also impossible to estimate the time scale or the variability for each objects even as the unique solution because each objects were observed only two times.

The aim of this section is to estimate the time scale of the variability of AGN and to consider the relation between the time scale and parameters that characterize AGN.

All sample was divided into subsample with short rest frame interval ($100 < \Delta t' < 400$) and long interval($400 < \Delta t' < 800$) by $\Delta t' = \Delta t/(1+z)$. The ensemble variability was estimated for each obtained subsamples. The result is shown in fig??. Open triangle, square and circle represent the ensemble variability of J, H and K' band. Fig5.24(b) show the ensemble variability of radio quiet and radio loud sample estimated by divided by $\Delta t'$ as the same way. Open triangle, square and circle represent the ensemble variability of J, H and K' band of radio quiet, and filled symbol represent as same but for radio loud sample. Only variability data estimated with more than two reference stars and their accuracy was better than 0.1mag was used to determine those ensemble variability.

To estimate how the variability develops,

$$V1(t) = A_0(t/(1+z))^p \tag{5.6}$$

and

$$V2(t) = B_0\left\{1 - \exp\left[-\frac{t}{\tau(1+z)}\right]\right\} \tag{5.7}$$

were introduced. It is impossible to plot many data on the time sequence in this work, therefore the numbers of the parameters that characterize how the variability develops is strongly limited. So it is preferable that the equation to fit the development of variability is simple and include few free parameters. There are only p or τ as the parameter to characterize the time scale of variability development and A_0 or B_0 to characterize the amplitude of variability in eq.(5.10)and eq.(5.7) and they are very simple.

It is natural that the variability obtained by two times observation increases and the increasing velocity doesn't accelerate with with the rest frame interval becoming longer. And it is clear that the variability of AGN is 0 if the rest frame interval is 0. Both eq.(5.10) and eq.(5.7) have those features. Former increase with divergence, while later increase but with asymptote with the rest

frame interval becoming longer.

eq.(5.10) was applied to the ensemble variability of all sample, radio quiet and radio loud sample and estimation of the parameters in the form and t heir confidence intervals was done. The result is shown at table5.10. p was varied numerically and A_0 was obtained by least square method on every time on the estimation. The best fitted parameter is shown at the 2nd and 3rd column of table5.10. The 4th and 5th column is the confidence interval with 95% and 99% confidential level. The confidence interval was estimated by numerical method assuming the χ^2 distribution. The last column shows the result of the χ^2 test of how the data is dispersing from the best fit curve. Table5.10 also shows the result of the same estimation but for the subsample that was made by dividing radio loud or radio quiet sample by M_B or z.

The lower limit of p of 95% and 99% confidential level for all radio loud sample was negative value by fitting, for example. However, the negative parameter isn't preferable because the ensemble variability should be 0 when the observation interval was 0. Therefore 0 was given for the lower limit of the confidence interval. The best fitted value of p was negative value at $0.3 < z < 0.6$ radio quiet, however, 0 was given for p too. The upper limit was obtained and shown in the table for even such samples.

p reflecting the time scale is related to the feature of variability, and $p = 1/2$ is correspond to the random walk and $p = 1$ is correspond to linear growing where the time scale is much longer the the observation interval. The table shows that p of all sample, radio quiet and radio loud sample include $p = 1/2$ in their 95% and 99% confidence interval. This fact means that the hypothesis where the variability of those sample is like random walk is accepted at such confidence level test. On the other hand, even the 99% confidence interval doesn't include $p = 1$ for all sample, radio loud sample. This fact means that the hypothesis where the variability of all or radio loud sample is like linear is rejected at 99% confidence level.

Table5.11 shows the result of the same estimation and test but by eq.(5.10). If the best optimized value or the limit of confidence interval of τ became negative, 0 was given as above case. Those value may diverse when the data allows the linear increasing in eq.(5.10).

It is understood from table 5.10 and table 5.11 that the optimized curves are accepted for all sample, radio quiet sample and radio loud sample. This result means that increasing of ensemble variability of J,H and K' band is described by single curve for each samples. Therefore it is concluded that the difference related observed band was found in the time scale of variability increasing for the each samples. However, the conclusion is natural result of other features of this work, one of them is almost simultaneous observation in J,H and K' band, and another is that ensemble variability at each band is comparable each other shown in sec.5.2.2. It is hard to distinguish whether the function of variability developing is eq.(5.10) or eq.(5.7, what is understood from that fitting by both eq.(5.10) and eq.(5.7) go well. Further test was done using the sample divided by $\Delta t'$, but significant difference by function type was not found.

p of radio loud sample in this work is smaller than that of radio quiet, as shown in table5.10. $p = 0, 21$ for all radio loud and $p < 0.3$ for radio loud samples divided by z or M_B. On the other hand, for all radio quiet $p = 0.63$ and $p > 0.7$ for radio quiet samples divided by z or M_B except the case where the estimation didn't go well like $0.3 < M_B < 0.6$. The time scale of the increasing of the ensemble variability becomes faster when p becomes smaller at eq.(5.10). Therefore, it is suggested that the time scale of the radio loud sample is shorter than that of radio quiet sample.

However, the accuracy of p obtained as the result of those estimation, what is understood by table.5.10. The 95% confidence interval of p estimated for all radio loud sample includes p estimated for all radio quiet. The confidence interval of p for the sample divided by M_B or z is more extended. Therefore, the difference of p found in the analysis in this section could not concluded to be significant. The cause of such low accuracy of p estimation could be thought that not only the error of each ensemble variability but also the observation interval of the data is limited. The data are localized around 2 places in fig.5.24. So the fitting becomes like unique solution, and it becomes hard to distinguish the form of function to describe increasing of the ensemble variability. Therefore, it is not impossible to conclude that increasing of the ensemble variability is described by above function even if the data of this work was explained by those function.

It is preferable that there are many data on time axis to discuss the time scale and the function form of how to increase the ensemble variability. For example, if the ensemble variability with rest frame interval of 3 years is added to the data of this work, the fitting that is not like unique solution becomes possible. The data that expand the range of the interval of this work is better if new observation is added. For example, if additional observation is done from fall in 200 to spring in 2001, total data set covers the observation interval of 1, 2 and 4 years. However, there is still possibility that result as the parameters or the function form with enough accuracy is not obtained, if the time scale of variability of the sample is too long. However it isn't efficient to observe for 10 years to determine the function form of the increasing of the ensemble variability. On the other hand, it is interesting plan to observe two times with short interval and add the result to the data of this work. The effect of the difference of the form or parameters of the function is remarkably appears at region of $\Delta t/(1+z) \sim 100$ or shorter. By two times observation with such interval, it may becomes possible to confirm the different time dependence of the variability between the radio quiet and radio loud sample, or to limit the emission and variability of AGN by determining the function form of the time dependence of the variability. Another merit of this plan is to be able to done the observation in 1 season.

It is possible to improve the accuracy of the parameters by fitting with eq.(5.10) or eq.(5.7) if the accuracy of each ensemble variability at (5.24),(5.25),(5.26) is improved. However, not only higher SNR of the observation but also much more sample is necessary to realize above plan. The way to improve merely the accuracy of each data needs powerful telescope, much observation time and man power, however, the information to determine the function form cannot be obtained, therefore what is not good way.

Top of fig.5.27 show p obtained the analysis of this section with the optical data from other work. Filled circle, triangle and square correspond the all sample, radio loud and radio quiet sample respectively. The vertical errorbar means the 68.3% confidence interval. The abscissas axis is wavelength and the abscissas errorbar shows dispersion of wavelength of the sample. Bottom of the figure shows as same but for τ of $B_0\left\{1-\exp\left[-\frac{t}{\tau(1+z)}\right]\right\}$. Open square represents the result of Cristiani et.al(1996). Open hexagon represents as same but fitted with also z as the fitting parameter.

As discussed above, it is impossible to conclude that the difference of p or τ in the all sample, radio quiet and radio loud sample in this work is significant because the accuracy of those parameters isn't enough. However, it is interesting that both of p and τ value show faster variability in order of radio loud, all sample, radio quiet sample in this work. $p = 0.69 \pm 0.03$ obtained by Cristiani et.al(1996) is similar to the value of the radio quiet sample of this work. τ of Cristiani et.al(1996) is larger than that of the radio quiet sample of this work. However, the upper confidence interval of the radio quiet sample extend widely, as is understood from that the estimation allows linear increasing of the ensemble variability, and the confidence interval includes the value of Cristiani et.al(1996). Reflecting those features, the difference of p and τ between Cristiani et.al(1996) and the radio quiet of this work was not found, while found between Cristiani et.al(1996) and the value of the radio loud sample of this work.

From the point of view of emission and variability by the dust reverberation, it is natural that the time scale of infrared variability is longer than that of UV or optical because especially fast variability becomes dull by the effect of the geometry of dust torus. In contrast, it is hard to explain by the dust reverberation model that the infrared variability is faster than UV or optical. If infrared variability that is as fast as, or faster than UV or optical variability, there is possibility to limit or reject the emission and variability by the dust reverberation mechanism.

Neugebauer et al(1989) discussed the relation between the time scale of the variability and observing wavelength at infrared wavelength region. The time scale of variability at near infrared is estimated $\sim$ years because the emitting region is limited near the central source. So detection of the near infrared variability with time scale $\sim$ years doesn't mean the contribution of nonthermal component at least direct. On the other hand, the time scale of variability at 10μm band is estimated $\sim$100 years, therefore it was discussed that detection of the variability at 10μm band was efficient method to show the nonthermal component.

And the results of the 10μm monitoring of 25 quasars were shown in Neugebauer & Matthews(1999) and it was concluded that the variability was found for some radio loud objects and one radio quiet object PG 1226+023 at 10μm band.

As discussed in this section, it is thought to be hard to confirm or limit the emission and variability mechanism from only near infrared variability of AGN. However, there is possibility to confirm or limit the mechanism by comparing the time scale of near infrared variability to those of UV or optical, or detecting the variability more shorter time scale even at near infrared wavelength. p and τ of the radio loud sample obtained in this section correspond to faster vari-

ability than the values of Cristiani et.al(1996), while p and τ of radio quiet don't differ from the values of Cristiani et.al(1996) significantly. Those result suggest the possibility of contribution by nonthermal component in infrared emission and variability of radio loud AGN. However, caution is necessary on the interpretation of the result because ensemble variability of different sample was compared and therefore not focused parameter might affect the result. It is expected that the comparison of the time scale between UV,optical and infrared wavelength for each objects will become possible when multi-color detail monitoring of many sample is done by the MAGNUM project.

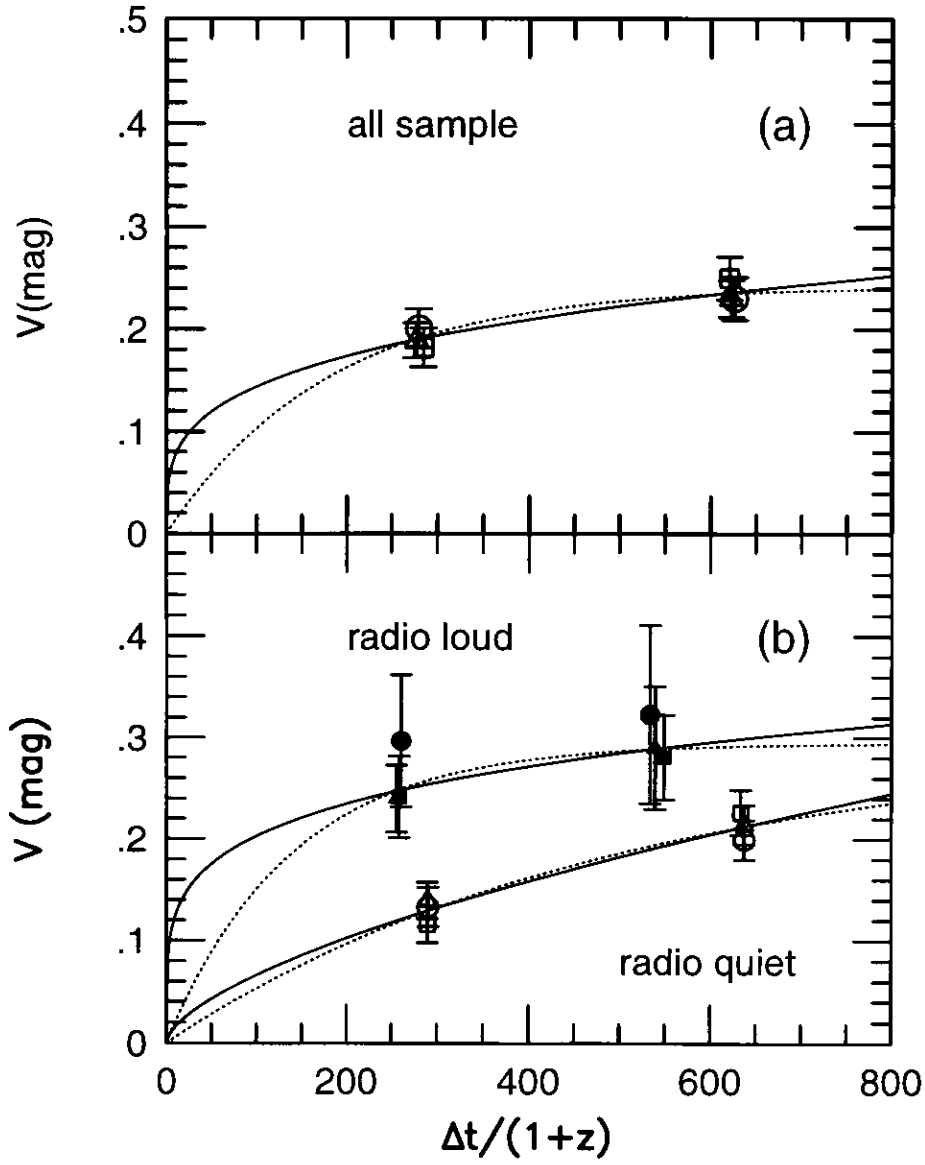

Figure 5.24: (a)Relation between the ensemble variability of the all sample and the rest frame interval of the observation. The sample is divided by the interval as $100days < \Delta t' < 400days$ and $400days < \Delta t' < 800days$. Solid and dashed line represents the result of fitting by $A_0(t/(1+z))^p$ and $B_0\left\{1-\exp\left[-\frac{t}{\tau(1+z)}\right]\right\}$, respectively. Open triangle, square and circle represents the ensemble variability at J, H and K' band. (b)Same as (a) but for the radio quiet and the radio loud sample. Open triangle, square and circle represents the ensemble variability of the radio quiet sample at J, H and K' band, and filled triangle, square and circle represents the ensemble variability of the radio loud sample at J, H and K' band, respectively.

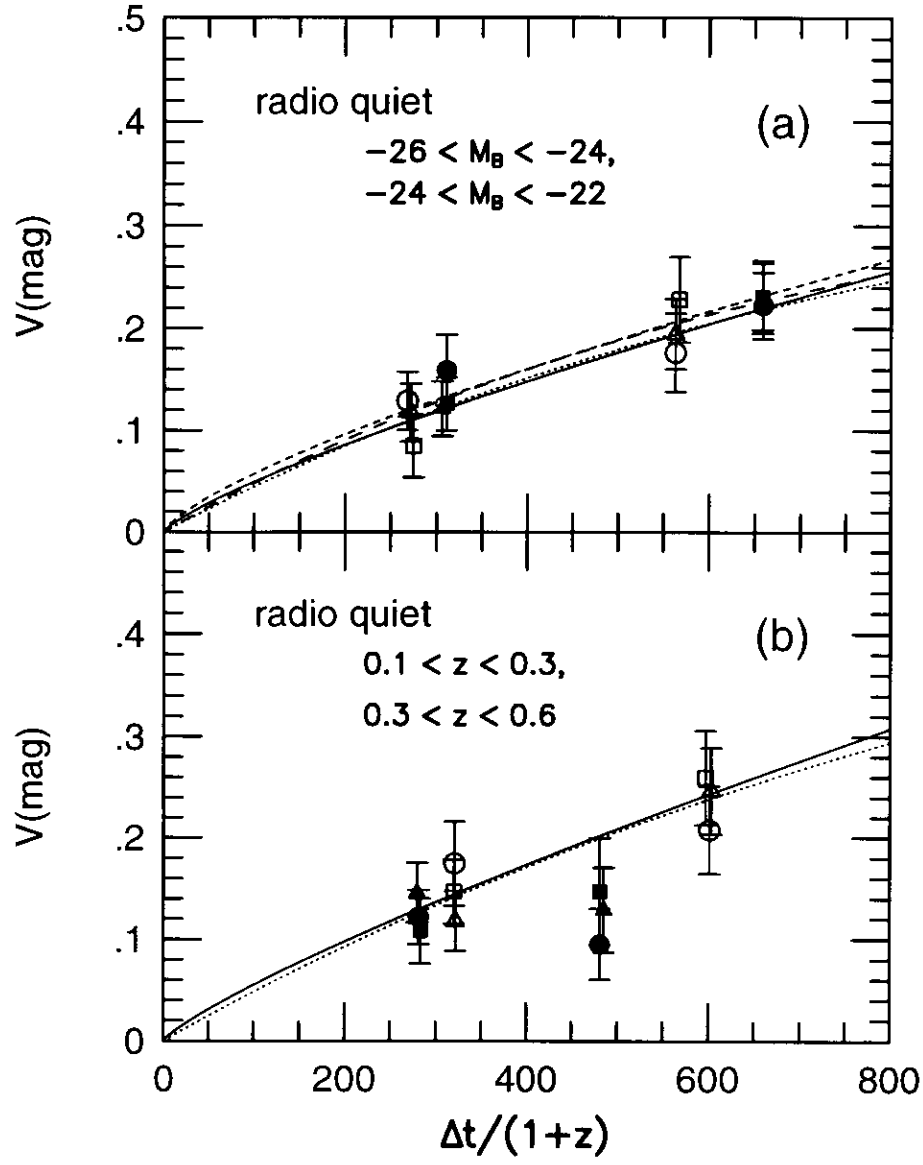

Figure 5.25: (a)Relation between the ensemble variability of the radio quiet subsamples divided by M_B and the rest frame interval of the observation. The sample is divided by the interval as $100days < \Delta t' < 400days$ and $400days < \Delta t' < 800days$. Open triangle, square and circle represents the ensemble variability of the subsample of $-26 < M_B < -24$ at J, H and K' band, and filled triangle, square and circle represents those of $-24 < M_B < -22$ at J, H and K' band. Solid and dotted line represents the result of fitting by $A_0(t/(1+z))^p$ and $B_0\left\{1-\exp\left[-\frac{t}{\tau(1+z)}\right]\right\}$ for $-26 < M_B < -24$ sample. Long and short dashed line represents same but for $-24 < M_B < -22$ sample. (b)Relation between the ensemble variability of the radio quiet subsamples divided by z. Open triangle, square and circle represents the ensemble variability of the subsample of $0.1 < z < 0.3$ at J, H and K' band, and filled triangle, square and circle represents those of $0.3 < z < 0.6$ at J, H and K' band. Solid and dotted line represents the result of fitting by $A_0(t/(1+z))^p$ and $B_0\left\{1-\exp\left[-\frac{t}{\tau(1+z)}\right]\right\}$ for $0.1 < z < 0.3$ sample.

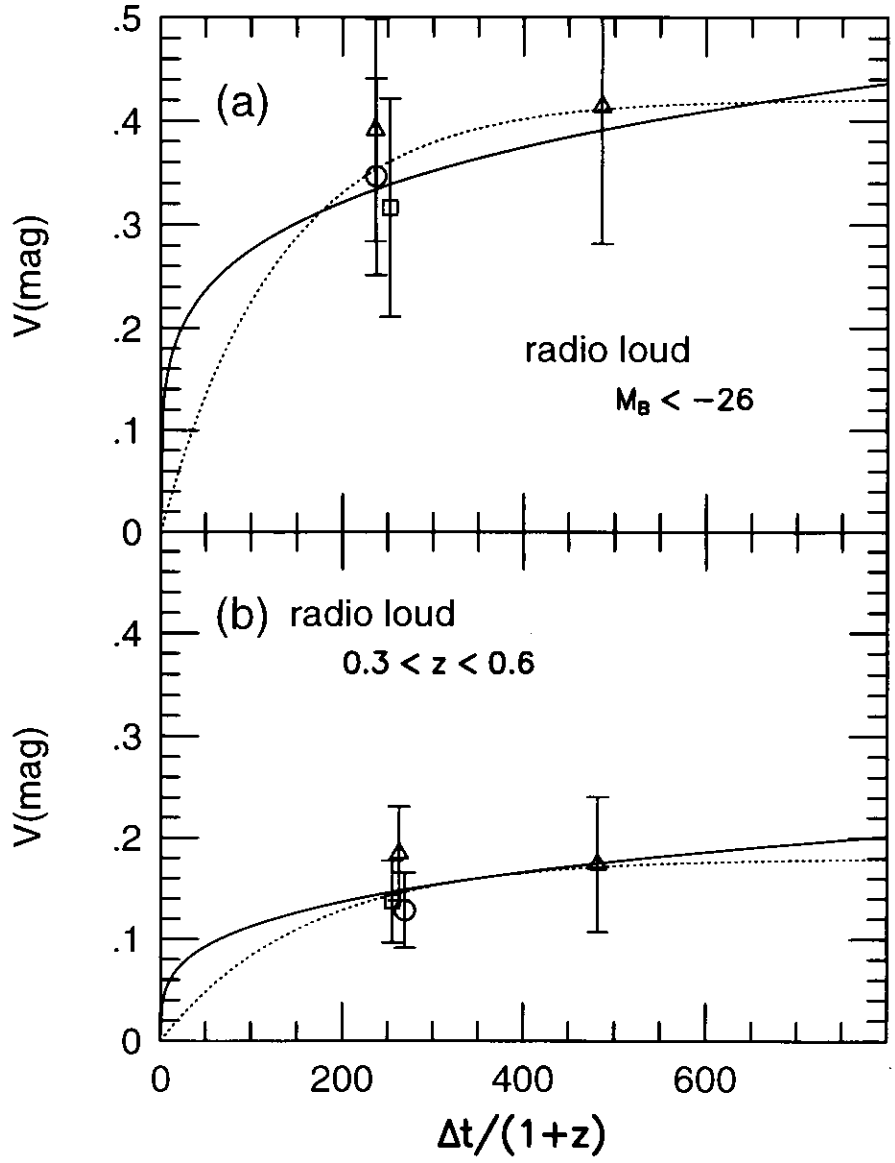

Figure 5.26: (a)Relation between the ensemble variability of the radio loud subsamples divided by M_B and the rest frame interval of the observation. The sample is divided by the interval as $100days < \Delta t' < 400days$ and $400days < \Delta t' < 800days$. Open triangle, square and circle represents the ensemble variability of the subsample of $-26 < M_B < -24$ at J, H and K' band. Solid and dotted line represents the result of fitting by $A_0(t/(1+z))^p$ and $B_0\left\{1-\exp\left[-\frac{t}{\tau(1+z)}\right]\right\}$ for $M_B < -26$ sample. (b)Relation between the ensemble variability of the radio loud subsamples divided by z. Open triangle, square and circle represents the ensemble variability of the subsample of $0.1 < z < 0.3$ at J, H and K' band.

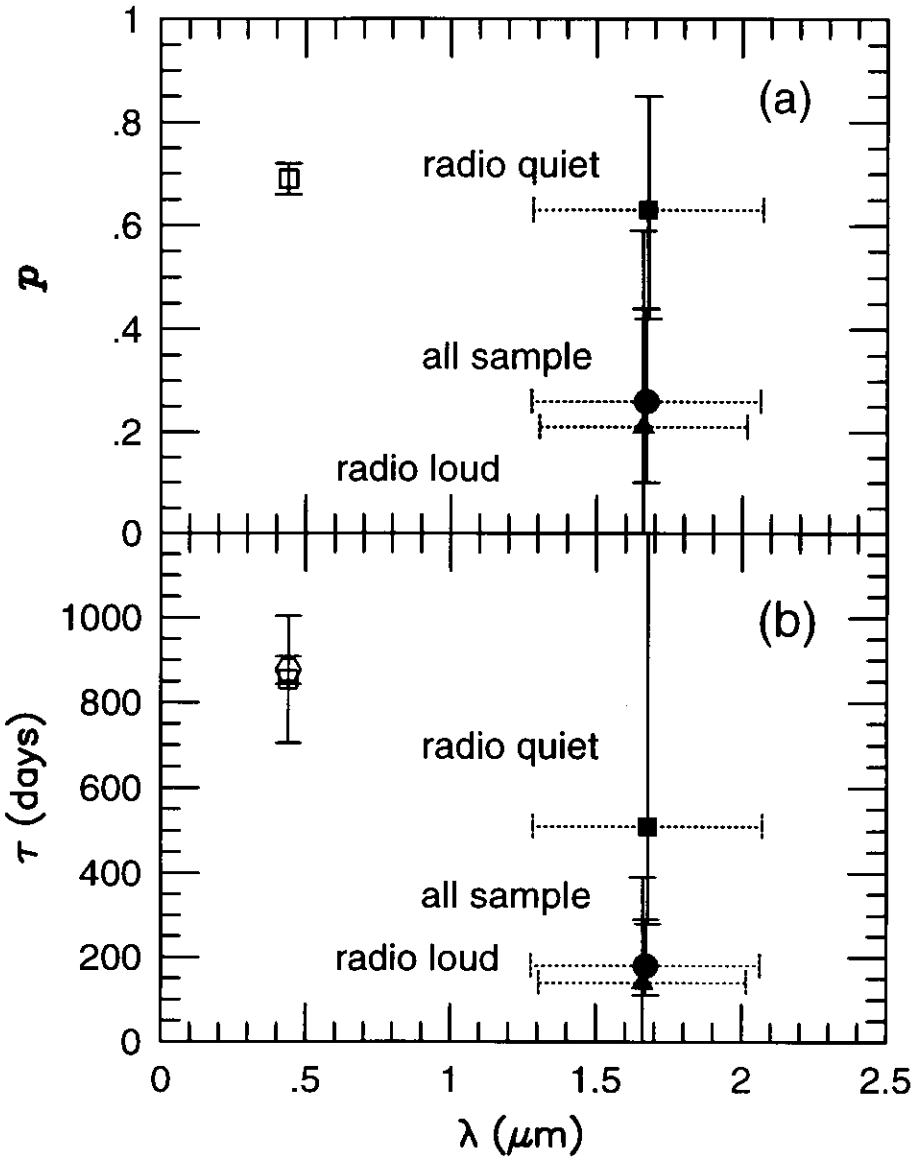

Figure 5.27: (a)p obtained as the result to apply $A_0(t/(1+z))^p$ to the ensemble variability of the all sample, the radio quiet sample and the radio loud sample. Filled circle, triangle and square represents the all sample, the radio quiet sample and the radio loud sample. The abscissas axis means wavelength and the dotted bar represents the standard deviations that reflect the expansion of the data that is localized at the place of J,H and K' band. The errorbars of the vertical axis represent the 68.3% confidence interval. Open square shows p of Cristiani et.al(1996) obtained shorter wavelength. (b)Same as (a) but for τ of $B_0\left\{1-\exp\left[-\frac{t}{\tau(1+z)}\right]\right\}$. Open square shows τ of Cristiani et.al(1996), and open hexagon shows also τ of Cristiani et.al(1996) but the case where z is added to fitting parameters.

sample	p	A_0	confidence interval of p(95%)	confidence interval of p(99%)	P(%)
all sample	0.26	0.044	$0^{(1)} \sim 0.53$	$0^{(1)} \sim 0.60$	12.5
radio quiet	0.63	0.0036	$0.30 \sim 1.0$	$0.22 \sim 1.09$	22.7
radio loud	0.21	0.077	$0^{(1)} \sim 0.79$	$0^{(1)} \sim 0.91$	6.3
radio quiet					
$-32 < Mv < -26$	-	-	-	-	-
$-26 < Mv < -24$	0.79	0.0012	$0.11 \sim 1.59$	$0^{(1)} \sim 1.83$	28.3
$-24 < Mv < -22$	0.73	0.0020	$0.17 \sim 1.40$	$0.05 \sim 1.57$	6.4
$-22 < Mv < -18$	-	-	-	-	-
$0.0 < z < 0.1$	-	-	-	-	-
$0.1 < z < 0.3$	0.83	0.0012	$0.09 \sim 1.67$	$0^{(1)} \sim 1.92$	27.9
$0.3 < z < 0.6$	$0^{(2)}$	$0.13^{(2)}$	$0^{(1)} \sim 1.08$	$0^{(1)} \sim 1.36$	20.6
$0.6 < z < 1.0$	-	-	-	-	-
radio loud					
$-32 < Mv < -26$	0.22	0.10	$0^{(1)} \sim 1.32$	$0^{(1)} \sim 1.94$	13.4
$-26 < Mv < -24$	-	-	-	-	-
$-24 < Mv < -22$	-	-	-	-	-
$-22 < Mv < -18$	-	-	-	-	-
$0.0 < z < 0.1$	-	-	-	-	-
$0.1 < z < 0.3$	-	-	-	-	-
$0.3 < z < 0.6$	0.28	0.031	$0^{(1)} \sim 1.56$	$0^{(1)} \sim 1.90$	38.4
$0.6 < z < 1.0$	-	-	-	-	-

Table 5.10: The result of the test and estimation of the parameters of $A_0(t/(1+z))^p$ that describe the development of the ensemble variability. Blank means that the test and estimation is impossible because the data of different interval aren't exist. Caution(1): p=0 is included in the confidence interval. Caution(2): The optimized p becomes negative at the radio quiet sample in $0.3 < z < 0.6$, however, p=0 is given and A_0 is optimized for p=0. The upper limits are obtained even for those cases.

sample	τ	B_0	confidence interval of τ(95%)	confidence interval of τ(00%)	P(%)
all sample	180	0.24	$50 \sim 370$	$0^{(4)} \sim 440$	12.9
radio quiet	510	0.30	$200 \sim {}^{(3)}$	$170 \sim {}^{(3)}$	6.4
radio loud	140	0.29	$0^{(4)} \sim 820$	$0^{(4)} \sim 2040$	22.5
radio quiet					
$-32 < Mv < -26$	-	-	-	-	-
$-26 < Mv < -24$	870	0.41	$110 \sim {}^{(3)}$	$0 \sim {}^{(3)}$	28.5
$-24 < Mv < -22$	760	0.39	$150 \sim {}^{(3)}$	$100 \sim {}^{(3)}$	6.4
$-22 < Mv < -18$	-	-	-	-	-
$0.0 < z < 0.1$	-	-	-	-	-
$0.1 < z < 0.3$	1240	0.62	$110 \sim {}^{(3)}$	$0 \sim {}^{(3)}$	27.9
$0.3 < z < 0.6$	$0^{(5)}$	$0.13^{(5)}$	$0^{(4)} \sim {}^{(3)}$	$0^{(4)} \sim {}^{(3)}$	-
$0.6 < z < 1.0$	-	-	-	-	-
radio loud					
$-32 < Mv < -26$	130	0.42	$0 {}^{(3)} \sim {}^{(4)}$	$0 {}^{(3)} \sim {}^{(4)}$	14.3
$-26 < Mv < -24$	-	-	-	-	-
$-24 < Mv < -22$	-	-	-	-	-
$-22 < Mv < -18$	-	-	-	-	-
$0.0 < z < 0.1$	-	-	-	-	-
$0.1 < z < 0.3$	-	-	-	-	-
$0.3 < z < 0.6$	160	0.18	$0 {}^{(3)} \sim {}^{(4)}$	$0 {}^{(3)} \sim {}^{(4)}$	38.6
$0.6 < z < 1.0$	-	-	-	-	-

Table 5.11: The result of the test and estimation of the parameters of $B_0 \exp\left[-\frac{t}{\tau(1+z)}\right]$ that describe the development of the ensemble variability. Blank means that the test and estimation is impossible because the data of different interval aren't exist. (3): Linear development of the ensemble variability is accepted at the χ^2 test, therefore the upper limit of τ isn't defined. (4): τ=0 is included in the confidence interval. (5): The optimized p becomes negative at the radio quiet sample in $0.3 < z < 0.6$, however, τ=0 is given and B_0 is optimized for τ=0.

5.3 relation between near infrared emission and variability and radio activity

As described above, difference of the near infrared variability of AGN in this work is remarkable when radio quiet and radio loud sample are compared. Obtained features of the near infrared variability of radio quiet and radio loud sample are following.

1. amplitude of ensemble variability: smaller in radio quiet sample, larger in radio loud sample.
2. wavelength dependence of ensemble variability: not found in both radio quiet and radio loud sample
3. luminosity dependence of ensemble variability: not found in raw data of radio quiet sample. Consider that contamination of host galaxy component is more in darker objects, negative correlation between Mv and variability is suggested. Positive correlation is found in raw data of radio loud sample, that is clearly different from raw data of radio quit.
4. correlation of variabilities of different band: r_{HK} is significantly higher than $r_{JH}, r_{JK'}$ for radio quiet at $0.1<z<0.3$. $r_{JH}, r_{JK'}, r_{HK'}$ of radio loud are high value of ~ 0.95 at $0.6<z$
5. time scale of variability: characteristic parameters of the time scale correspond faster in radio loud sample in this work than radio quiet. However the differences are not enough significant.

2,3,4 of those for radio quiet sample is consistent with the dust reverberation model as discussed in each section. However, it is hard to explain the difference of luminosity dependence of the variability between radio quiet and radio loud by simple dust reverberation mechanism.

Therefore, nonthermal component as a substitute of thermal radiation from hot dust is worth to be considered. For example shown in Sanders et al.1989, nonthermal component from more compact region than dust distribution can vary larger and faster than the thermal radiation.

Hereafter, a working hypothesis, which dust reverberation model well explain emission and variability of radio quiet AGN however it cannot explain those of radio loud AGN because of their nonthermal component, is discussed and checked. First, radio activity of the sample that the dust reverberation model explain well observed light curve is checked and the probability to apply the model for radio quiet and loud sample is discussed. Next, subsamples of radio loud AGN and origin of nonthermal component in the ensemble of this work are considered.

<radio activity of dust reverberation sample>

It is very effective method to confirm that emission and variability of a AGN is originated by the dust reverberation to monitor both UV,optical and infrared light curve and detect the infrared time delay.

Dust reverberation model was applied to light curves of some AGN and explained them somewhat well, though observations is hard and the samples are not enough because those observation usually needs multi instrument and long observation time.

- GQ comae: Result of monitoring project over 3 years were shown in Sitko et al(1993). The data was from U to L band, and UV variability was compared with variability of other band. Δt was estimated about 250 days at K band. Indication of larger Δt at L band.
- Fairall 9: Clavel,Wamstecker & Glass(1989) showed far-UV by IUE, optical and JHKL monitor data. UV variability of factor 33 was observed. δt ~400 days was found. Dust reverberation model was applied by Barvanis(1992). Possibility of nonthermal component was pointed out in Neslon(1996a).
- NGC 3783: Glass(1992) showed the result of JHKL monitoring over 15 years. Δt of 80~90 days was lead by comparison with UV variability. And stability of shape of the variable component was concluded.
- NGC 744: Dust reverberation model fitted V and K band light curves best in the sample of Nelson(1996a). The delay of K from V was determined as Δt=32±7 days.
- NGC 4151: By Okyanskii 1993.
- NGC 1566: Multi-wavelength variabilities were compiled from X ray to near infrared. *Deltat* of 50 days was obtained though cross correlation function was not shown.

$f_{\nu 6cm}/f_{\nu V}$ of above sample was estimated to check radio activity of those objects. The result is shown in table5.12. f_V was used here, where usually value around 1μm was used, because f_V was available for all of the sample. All the ratios are small for all sample in the table and fill the condition to be regarded as radio quiet in this work $f_{\nu 6cm}/f_{\nu V}$ <10. z,M_B,f_{6cm} and f_V was obtained from VV catalog.

The sample shown in table5.12 is compilation of independent work and therefore completeness or systematic criterion could not be expected in sample selection. Observation detail and accuracy is also different each other. The sample shown in table5.12 tends to be nearby blight objects. It is possible that the sample was biased to radio quiet as the result of selection optimized for observation. Furthermore, it is also possible that the observation that was successfully explained by dust reverberation was biased and reported. In fact Mark 744 was the sample that was explained by dust reverberation best in sample of Nelson(1996a),discussed following.

Therefore, effect of the bias should be thought large. However, it is interesting that all the sample in table5.12 is radio quiet.

Many Seyfert 1 AGN and quasar was monitored at V and K band in Nelson(1996a,thesis). The main interest of his thesis was on modeling of variability of each object, however, his data is very useful because it includes the example where the dust reverberation model was tried to explain the curve but could not. Table (4.6) shows the result of trying to detect the variability of V ,K band and their time lag for 51 samples. Radio activity was estimated for those sample by the same method with $f_{\nu 6cm}/f_{\nu V}$. The result is shown in table5.3. The 1st column is name of objects of VV8 catalog and the object that was not detected at radio is marked with $*$. z,M_B by VV catalog are following. Val_V, Val_K show the result of detection of variability by Nelson. "Y" means detected ,"N" means not detected and "?" means unknown. In column of "cor", "Y" is the case of correlation between V and K band variabilities was found, "N" is of not found. In column of "Lag", "Y" is the case of the delay of K band variabilities from V band was found, "N" is of not found and "L" means that limiting succeeded. The most right column shows the radio activity $f_{\nu 6cm}/f_{\nu V}$ determined in this work.

Fig5.16 shows summary of localization of the objects that are well explained by dust reverberation model in Nelson(1996a)'s sample. Number of the object that is variable in both V and K band is shown in the 2nd line. The 3rd line shows the number of the object where the time delay of the K band variability was obtained. It is shown from fig5.16 that the 6 sample where the time delay was obtained is limited in only radio quiet sample nevertheless detection rate of the variability is almost equal for radio quiet and radio loud sample. It gives some ambiguous that 2 of the 6 samples are the objects that was not detected in radio. However, even if the 2 ambiguous sample is neglected, all of 4 remained sample are radio quiet. Unfortunately, the difference between 6/29 that is ratio of the sample where the time delay was obtained in radio quiet and 0/3 that is in radio loud cannot be concluded with significance. It is efficient to increase the data of radio loud sample to confirm or reject these tendency.

<subsamples of radio loud AGN>

In this section, possibility of contribution of the nonthermal component is discussed. The ensemble is used to estimate the amplitude of the variability of AGN. Therefore, when there are some nonthermal components in the emission and the ensemble variability of radio loud, not only the case where each radio loud sample have some nonthermal component but also the case where some extreme sample have remarkable component and others are thermal is possible. So subsamples of radio loud AGN is researched following. Krolik(1999)was referred for the classification of them.

Radio loud sample is sometimes divided into flat spectrum radio loud and steep spectrum radio loud by their SED in radio wavelength (for example, Sanders et al.1989). when the SED of radio wavelength for many AGN are fitted by $\alpha = f_\nu \propto \nu^\alpha$, α distribute in the region of -1$\sim$0. The sample of -0.5$< \alpha$ is classified as flat spectrum radio loud and the sample of α-0.5 is classified as steep spectrum radio loud. There is correlation between the flatness of AGN and their morphology. SED in radio of extended lobe-dominant source is usually described by steep spectrum, while SED of core-dominant source tends to be flatter. Correlation between large variability and polarization seen in the subsample that is Bl lac, high polarized QSO,OVV and flat spectrum that is extended toward 100Ghz(Tornikoski et al.1993, Landau et al.1986). However, the flatness of SED can change when focused wavelength is changed. It is shown that flat source searched at 4850MHz is significantly more than searched at 408MHz in Maslowski et al(1984).

Radio loud sample is also divided by their morphology. For robe-dominant radio loud, light compact sources are sometimes seen at the outer side of the robe. On the other hand, there are objects of which robe is brighter at near central source. Fanaroff and Riley(1974) divided robe-dominant sample into two groups by the distribution of brightness of robe. FR1 is the object where the distance of the brightest spots on both side of central source is smaller than a half of total size, while FR2 is larger. Feature that jet brightness closer to center becomes brighter is seen at FR1, and the jet is seen on both side of the central source. It is also feature of FR1 that curved jet is sometimes seen. For FR2, jet is darker than outer robe and sometimes seen only one side of the central source. FR1 and FR2 can be divided clearly by their luminosity. The borderline can be described with $L_{1.4GHz} \propto L_{opt}^2$ where $L_{1.4GHz}$, L_{opt}^2 is the luminosity at 1.4GHz and optical respectively. Most of FR2 distributed in the brighter side of the borderline at radio, and most of FR1 darker side(Ledlow and Owen 1996).

Concerning the variability of radio loud AGN, similarity of structure function of the variability of flat source and BL lac is pointed out (Hughes,Aller & Aller 1992, Lainela & Valtaoja 1993). Variability with the time scale from a few week to 10 years was researched and the power spectrum was like f^{-1} at high frequency, and flat at low frequency like white noise.

As shown above, radio loud sample was divided into various subsamples by SED, morphology, polarization, variability. It is thought that there are features that variability is large and fast and nonthermal component contribute to emission and variability for OVV, high polarized QSO and BL lac. It is consistent with the features of variability obtained in this work that the ensemble of radio loud in this work is contaminated by such objects. It is possible that the emission and variability is originated by thermal mechanism in usual radio loud while some remarkable object like above is mixed. Another possibility is that contribution of nonthermal component is general property of radio loud AGN in contrast with radio quiet. It is necessary to distinguish those tow possibility to consider the property of for each objects.

< relation between variability and flatness of radio SED >

OVV, high polarized QSO and BL lac object are candidate that bring nonthermal component to ensemble emission and variability, as pointed out in previous section. Large and fast variability, large polarization, flatness of SED at radio are the features of those objects. Especially, flatness of radio SED is useful because the information is available for many objects. In this section, the radio loud sample of this work is more divided into flat radio loud and steep radio loud by the flatness of radio SED, and variability of each group is discussed.

At first the division was executed. Flux data at 6cm and 11cm in VV catalog were used to determine the flatness of SED at radio. α is obtained by fitting by $f \propto \nu^{\alpha}$. The sample with $\alpha < -0.5$ was regarded as steep sample, while $-0.5 < \alpha$ sample was regarded as flat. The flatness was determined for most of radio loud AGN in this work though 11cm flux of some objects were unknown. Fig5.28(a) shows distribution of α and M_B. Open triangle and square represents short interval ($100 < \Delta t/(1+z) < 400$) steep and flat spectrum radio loud sample. Filled symbol represents same but long interval ($400 < \Delta t/(1+z) < 800$)sample. Obtained α mainly distribute from -1 to 0, however, some of them extend to 1. There is possibility that simple measurement error caused this feature, while variability of flux is also possible cause. Fig5.28(b) shows relation between α and z.

Figure (5.29a) shows the ensemble variability of flat and the steep sample. Open square and triangle show the value of the flat and steep sample.

Figure (5.29b) is an ensemble variability when the sample is divided by the observation interval in rest frame similarly to doing up to now. Open triangle and square represents short interval ($100 < \Delta t/(1+z) < 400$) steep and flat spectrum radio loud sample, and filled square represents long interval($400 < \Delta t/(1+z) < 800$) flat sample. Long interval steep sample was less, and sample number of each band was smaller than 5, so the ensemble variability was not determined.

The ensemble variability of radio loud sample divided by M_B is shown in fig5.30(a). The way of dividing was different from those of up to now a little because the sample number was smaller than past case. Combination of flat sample with short($100 < \Delta t/(1+z) < 400$) and long ($400 < \Delta t/(1+z) < 800$) interval was regarded as the initial sample. And the dividing by M_B was limited into only two groups, which was M_B<-25 sample and -25<M_B sample. It is understood from fig(a) that the ratio of sample with long interval and short interval is comparable and remarkable difference is not seen as the result of the dividing by border of M_B=-25mag.

On the other hand, fig5.30(b) shows the ensemble variability of steep sample with short interval into two groups, which was M_B<-25 sample and -25<M_B sample. Steep sample with long interval was only a few, and localized in the side of M_B<-25mag. Therefore only the short interval sample was regarded as the initial sample and dividing of them was executed into two groups which was M_B<-25 sample and -25<M_B sample and the ensemble variability was estimated.

First, it is examined whether there is a difference in the ensemble variability of the different band. A remarkable wavelength dependence is not seen in the ensemble variability of each sample in figure5.29 and figure5.30. Table 5.17 shows the result of the test that examine whether significant difference is found in the ensemble variability of different band. The technique was same to the way up to now. a of $V = C\lambda^a$ was changed and C was estimated in every case of a, and χ^2 test was done, finally the 95% or 99% confidence interval was determined. The first column of the table means the testing sample. It is understood from the table that a=0 is in the confidence interval for all case. This fact means that the hypothesis that there are no band dependence of the ensemble variability in those test is accepted. However, the confidence interval is expanded at the sample like M_B>-25 mag flat radio loud because of lack of accuracy. In these case, interpretation should be done as not rejected rather than accepted though the result of the test doesn't change.

Next, difference of the ensemble variability in different subsample is considered. $V_{\bar{\lambda}}$ was estimated as the weighted average of the ensemble variability at J,H and K' band and it was used as the index of variability at near infrared, those process was equal to those for the previous section. It was aim of these operations to gain SNR by average and to be simple by reducing 3 parameters into 1.

Table5.18 shows the result of examination whether there is significant difference in the $V_{\bar{\lambda}}$ of different subsamples. The examinations were done by χ^2 test with 1 freedom for 2 values of $V_{\bar{\lambda}}$. The first column means compared two samples. The 2nd,3rd and 4th column is the best fitted C_0 and its error and χ^2. The 5th column shows the probability to reject the hypothesis that compared $V_{\bar{\lambda}}$ are equal. In following discussion, the confidence level was set as 5%(P=95%).

The first line of the table5.18 shows the result of comparison of $V_{\bar{\lambda}}$ between all flat radio loud and steep radio loud sample. P=99.9%, and therefore the data is concluded as enough significantly different. It is shown that the variability of flat group is larger than steep group from fig5.30. The result of the examination for tow subsamples made by dividing flat sample into M_B<-25 sample and -25<M_B sample is shown in the 4th line. Long interval sample and short interval sample was mixed and used here as counterplan for the lack of sample. However, the ratio of sample with different interval was comparable, therefore the influence of this effect for the result would be small. P>99.9% , and therefore the data is concluded as enough significantly different here too. It is shown that the variability of brighter group at M_B is larger from fig5.30. The 5th line is the result for tow subsamples made by dividing steep sample with short interval($100 < \Delta t/(1+z) < 400$) into M_B<-25 sample and -25<M_B sample. The difference is also significant and it is shown that the variability of brighter group at M_B is larger from fig5.30 too. The result of the examination for M_B<-25mag flat sample and M_B<-25mag short interval steep sample is shown in the 6th line. Caution is necessary to mixing $400 < \Delta t/(1+z) < 800$ sample at only flat sample, however it is understood that $V_{\bar{\lambda}}$ of flat sample is statistically larger.

On the other hand, no significant difference of $V_{\bar{\lambda}}$ was found between dark flat and steep sample of M_B>-25mag (7th line of table??). $V_{\bar{\lambda}}$ of those samples are not different significantly from the value of radio quiet with -24<M_B<-22mag and $100 < \Delta t/(1+z) < 400$.

It is understood from fig5.29(b) that the ensemble variabilities of flat sample of $100 < \Delta t/(1+z) < 400$ and $400 < \Delta t/(1+z) < 800$ are almost equal. This fact suggests that the time scale of variability of flat sample is shorter than ,for example, radio quiet. However, it is hard to estimate the time scale of variability with further divided flat subsample by M_B or to estimate for steep sample because of lack of sample number.

The variability of bright(M_B<-25) flat sample is main cause of the features that the variability of radio loud was larger than radio quiet, and had positive correlation with their luminosity. However, positive correlation between the variability and luminosity is also significant in steep sample. And concerning blight (M_B<-25) sample, the variability of bright steep sample is significantly larger than radio quiet though smaller than flat sample.

Therefore, it is natural interpretation that the positive correlation between the variability and luminosity is common property of radio loud sample though it is more remarkable at flat sample. Another interpretation is that above features are unique property of flat sample, and resemble features seen in steep samples are caused by the contamination of flat sample. It is shown by fig5.28 that the separation of the flat radio loud and steep radio loud is not as clear as the separation of radio loud and radio quiet. Error of the flux data used to determine α can be able to bring miss classification, of course. Furthermore, the variability of radio flux is also the candidate of the cause of miss classification. There is possibility to obtain different α from real value by the variability even the shape of SED is not variable because the flux data used to determine α were not observed always simultaneously.

<summary>

At the opening of this section, the hypothesis that dust reverberation model well explain emission and variability of radio quiet AGN however it cannot explain those of radio loud AGN because of their nonthermal component is assumed. It was discussed whether there was the fact that support or reject the hypothesis using the result of this work and other papers, and the results like following were obtained. Those results support, or are consistent with, the hypothesis shown above.

- Radio activities of the objects individually reported of which light curves were well explained by dust reverberation were examined. All of them were radio quiet.
- Radio activities of the objects in Nelson(1996a,thesis) were also examined. All of the objects of which time delay of infrared light curve were radio quiet too, nevertheless the detection sensitivity of variability was almost equal at radio quiet and radio loud sample.
- There was no significant difference between the variability of dark(M_B>-25mag) flat and steep radio loud. Those values also didn't differ significantly from value of radio quiet.

- For blight(M_B<-25mag) flat and steep sample, the variability was significantly larger than dark flat and steep sample, what was not seen in radio quiet.
- The variability of blight(M_B<-25mag) flat sample was larger than bright that of steep sample, and any other subsample of this work.
- Maybe the time scale of the variability of flat sample was shorter than radio quiet sample. The time scale of the variability of steep sample or M_B dependence of variability time scale of flat sample was unknown.

The results of the research are consistent with the hypothesis that assume that the emission and variability mechanism of radio quiet AGN is dominated by dust reverberation. The objects that were monitored at both UV,optical and infrared are small number. These sample are all radio quiet, but localized in nearby objects and maybe under their complicated bias. In this work, the observation of more widespread sample($0 < z < 1$, -20<M_B<-30) could be done as the result of that the observation of each object was limited only two times. However, it is impossible to test the dust reverberation for each object in this work because the ensemble is necessary to estimate the variability. Those works and this work can be regarded as complementary to each other from the point of view to examine the dust reverberation model in detail or in widespread sample.

It turned out that the features of variability found in the radio loud sample of this work was mainly caused by blight flat radio loud. It is known that objects such as OVV,high polarized QSO,BL lac is flat radio loud AGN. Therefore, it is reasonable interpretation that at least some of the flat sample are such objects and their nonthermal component make the dust reverberation not be adopted (As for non thermal emissions of those objects, for example, Robson et al.1993, and for Bloom et al.1994).

On the other hand, the condition is complicated about steep radio loud sample. The infrared bump like radio quiet sample was found in the SED of steep radio loud and they were sometimes interpreted by the thermal radiation(Sanders et al.1989). However, the positive correlation between the variability and the luminosity in steep sample like flat sample though the feature was not as remarkable as flat sample. It is suggested the possibility that there is nonthermal component in the emission of steep radio loud because the feature seen in flat sample was also found in steep sample. There is a possibility that nonthermal component contributes to the variability more strongly than thermal component comparing to the small ratio because the variability of nonthermal component can be larger than thermal. There is the possibility to explain both infrared bump in the steep sample reported before and the variability contributed by nonthermal component in this model. Furthermore, There is also possible that the feature of nonthermal component was not identified in total SED if the shape of SED of the nonthermal component was specific.

However, it is also possible explanation that the feature of the variability of steep radio loud is originated by contamination of flat sample and therefore only apparent. To distinguish those probability is difficult for this work. The MAGNUM project is in preparation where each of many AGN is monitored in multi wavelengths and the mechanism of emission and variability is researched for each object.

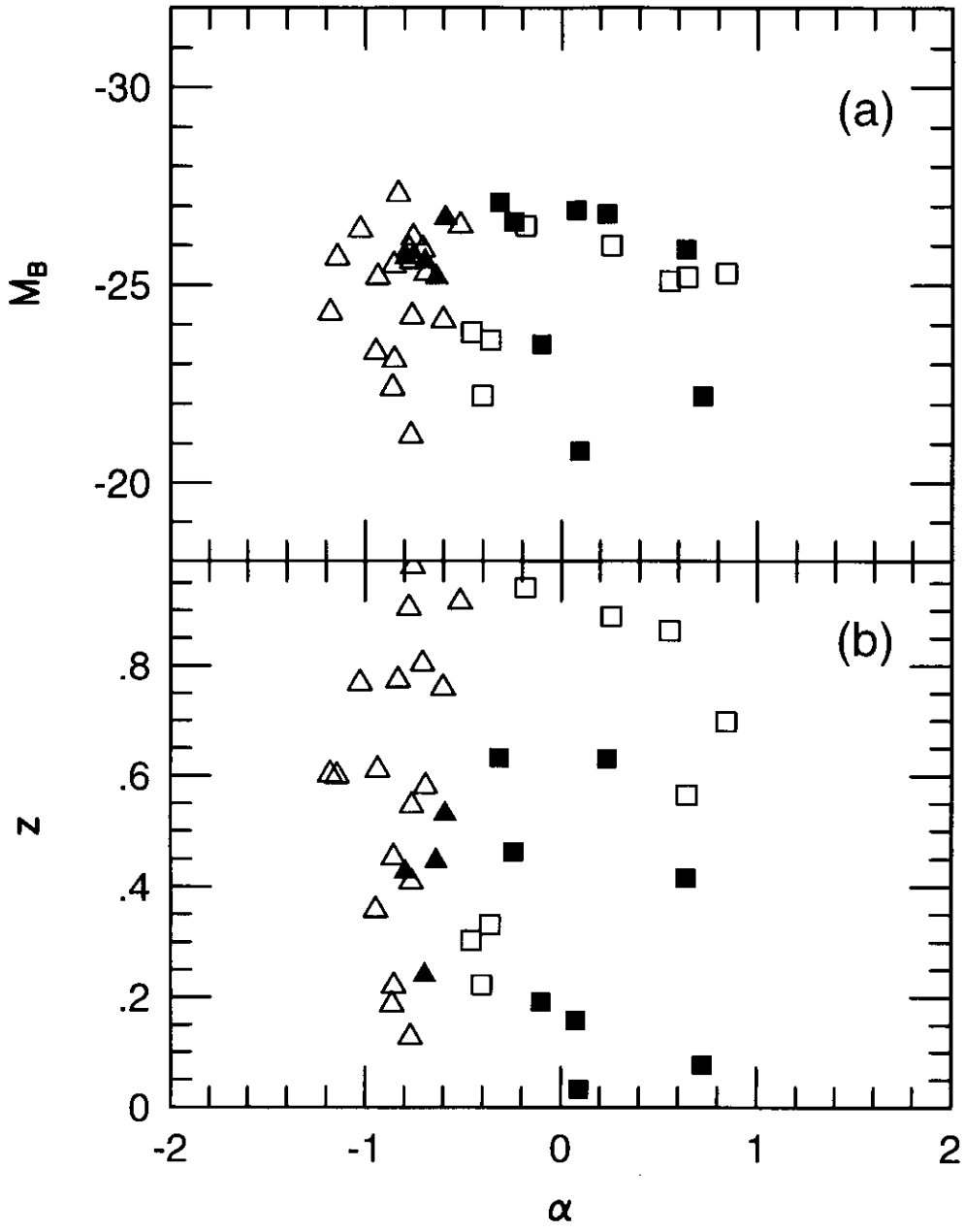

Figure 5.28: (a) The distribution of α and M_B. Open triangle and square represents the steep and flat spectrum radio loud with short rest frame interval of $100 days < \Delta t' < 400 days$, while filled triangle and square represents also the steep and flat spectrum radio loud but with long rest frame interval of $400 days < \Delta t' < 800 days$. (b) The distribution of α and z.

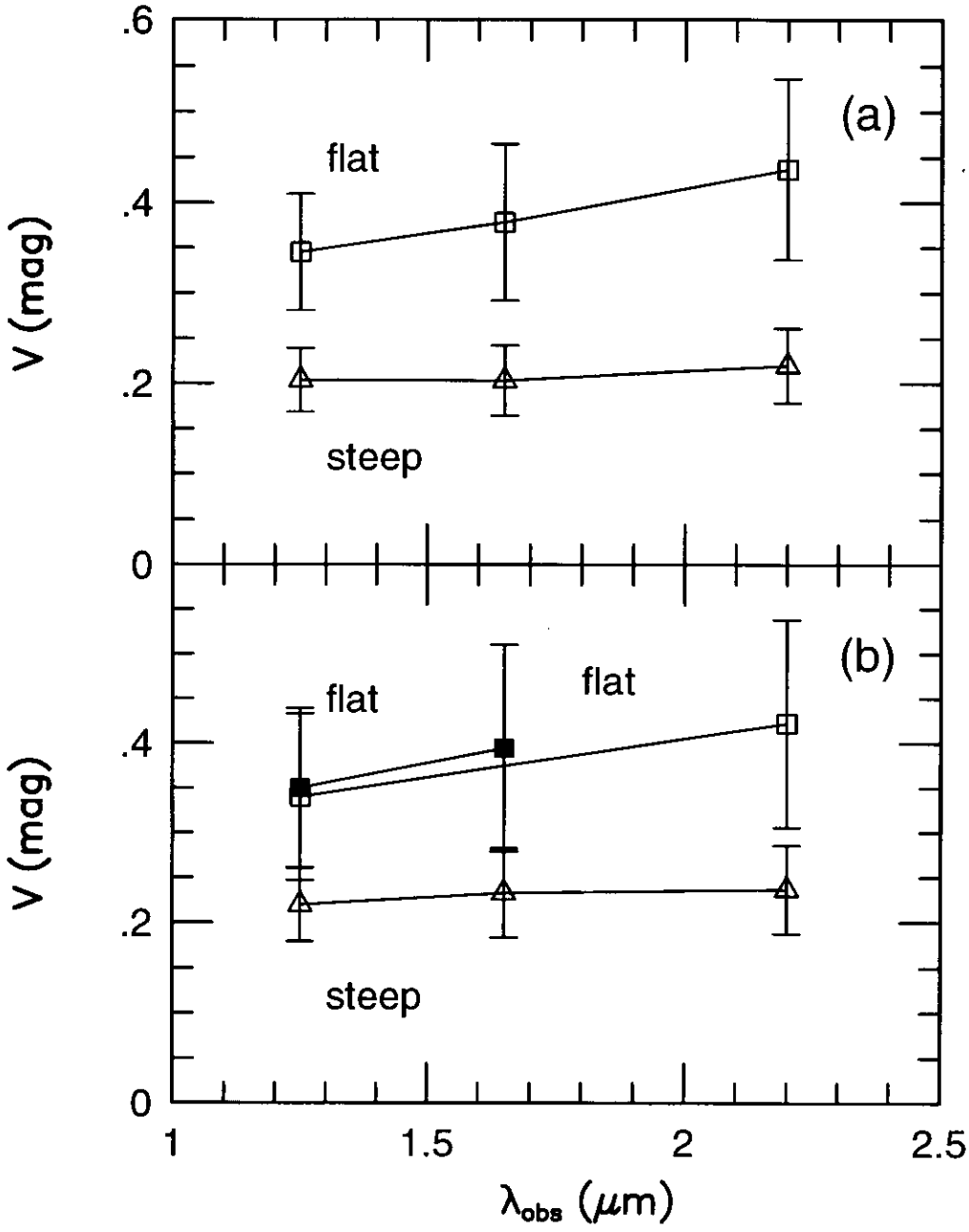

Figure 5.29: The ensemble variability of the flat and steep spectrum radio loud sample. (a)Open square and triangle represents the flat and steep sample. (b)Open square and filled square represents the flat samples with short interval of $100days < \Delta t' < 400days$ and with long interval of $400say < \Delta t' < 800days$. Open triangle represents the steep sample with short interval of $100days < \Delta t' < 400days$.

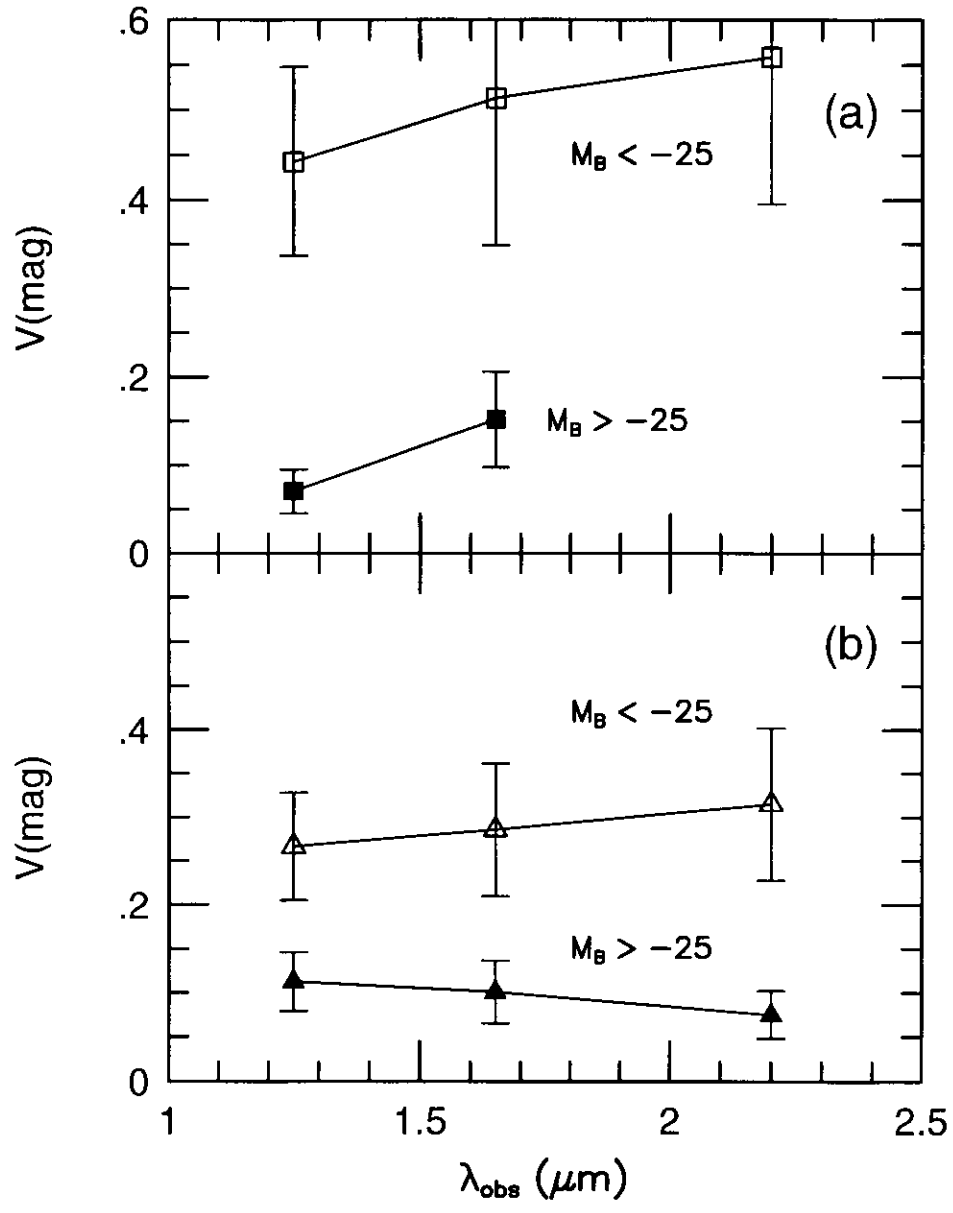

Figure 5.30: (a) Open square represents the ensemble variability of the flat spectrum radio loud sample with M_B<-25mag. Filled square represents same but for sample with M_B>-25mag. (b)Open triangle represents the ensemble variability of the steep spectrum radio loud sample with M_B<-25mag and $100 days < \Delta t' < 400 days$. Filled square represents same but for sample with M_B>-25mag and $100 days < \Delta t' < 400 days$.

object	z	M_B	$f_{\nu 6cm}/f_{\nu V}$
GQ COM	0.165	-24.4	0.0
*F 9	0.046	-23.0	0.0
NGC 3783	0.009	-19.7	0.7
MARK 744	0.010	-19.3	0.0
NGC 4151	0.003	-18.7	2.3
NGC 1566	0.004	-18.0	3.7

Table 5.12: The examples of which the light curves at UV-optical and infrared wavelength are explained by the dust reverberation model. $f_{\nu 6cm}/f_{\nu V}$ is used to estimate the radio activity. $f_{\nu 6cm}/f_{\nu V}$ of the objects in the table tends to be small, and are filled the condition to be regarded as radio quiet. The data os z, M_B, $f_{6cm}(Jy)$, $f_V(Jy)$ are obtained from VV catalog.

Table 5.13: The result of the test of radio activity for the sample shown in Nelson(1996).

object	z	M_B	Val_V	Val_K	cor	lag	$f_{\nu 6cm}/f_{\nu V}$
KUV 18217+6419	0.297	-27.1	Y	Y	N	N	9.8
3C 120	0.033	-20.8	Y	Y	N	N	1505.6
3C 273.0	0.158	-26.9	Y	Y	Y	N	1692.7
3C 445.0	0.057	-20.8	N	Y	N	N	1171.2
AKN 120	0.033	-22.2	Y	Y	Y	L	0.0
I Zw 1	0.061	-23.4	Y	N	N	N	0.0
II Zw 136	0.063	-23.0	Y	Y	N	N	0.0
III Zw 2	0.090	-22.7	Y	Y	N	N	175.6
IRAS 03450+0055	0.031	-21.3	Y	Y	Y	Y	2.0
IRAS 07598+6508	0.148	-22.3	N	Y	N	N	27.7
UGC 12138	0.025	-20.6	Y	N	N	N	0.0
*MCG 2-58-22	0.023	—	Y	Y	N	N	—
MCG 08.11.11	0.020	-20.0	Y	Y	Y	L	15.9
MARK 9	0.039	-22.1	N	Y	N	N	0.0
*MARK 10	0.030	-21.1	Y	Y	?	?	0.0
MARK 79	0.022	-20.9	Y	Y	N	N	0.0
MARK 231	0.041	-22.3	N	N	N	N	39.8
MARK 304	0.067	-23.0	Y	N	N	N	0.0
MARK 315	0.040	-21.3	N	Y	N	N	0.0
MARK 335	0.025	-21.7	Y	Y	N	N	0.0
MARK 376	0.056	-22.5	Y	Y	?	?	0.0
MARK 478	0.077	-23.4	N	Y	N	N	0.0
MARK 509	0.035	-23.3	Y	Y	N	L	0.0
NGC 7603	0.029	-21.5	Y	Y	N	N	1.1
*MARK 543	0.026	-20.6	?	Y	Y	Y	0.0
MARK 590	0.027	-21.6	Y	Y	?	?	0.0
MARK 618	0.035	-21.5	N	Y	N	N	0.0
*MARK 704	0.029	-21.4	Y	Y	N	N	0.0
MARK 705	0.028	-21.0	Y	Y	Y	Y	2.0
MARK 739E	0.030	-21.4	Y	Y	?	N	0.0
MARK 744	0.010	-19.3	Y	Y	Y	Y	0.0
MARK 766	0.012	-20.0	Y	Y	N	N	0.8
MARK 876	0.129	-23.5	Y	N	N	N	0.0
*MARK 975	0.050	-21.8	Y	Y	Y	Y	0.0
MARK 1152	0.052	-21.7	Y	Y	N	N	0.0
MARK 1239	0.019	-20.3	N	N	N	N	1.6
MARK 1298	0.060	-22.8	N	Y	N	N	0.0
MARK 1383	0.086	-23.4	Y	Y	N	N	0.0
*MARK 1392	0.036	-21.3	Y	Y	N	N	0.0
NGC 1275	0.017	-21.9	N	N	N	N	519.2
NGC 2639	0.011	-21.3	N	Y	N	N	0.8

Table 5.14: continued

object	z	M_B	Val_V	Val_K	cor	lag	$f_{\nu 6cm}/f_{\nu V}$
NGC 4051	0.002	-16.8	Y	Y	Y	L	1.2
NGC 4151	0.003	-18.7	Y	Y	?	N	2.3
NGC 4593	0.009	-19.7	Y	Y	N	N	0.0
NGC 5548	0.017	-20.7	Y	Y	N	N	0.9
NGC 6814	0.006	-17.5	Y	Y	Y	Y	0.0
NGC 7469	0.017	-21.6	Y	Y	N	N	2.8
PG 0844+349	0.064	-23.1	Y	Y	N	N	0.0
PG 1116+215	0.177	-25.3	Y	N	N	N	0.0
PG 1211+143	0.085	-24.1	Y	Y	N	N	0.0
PG 1351+64	0.088	-24.1	N	N	N	N	4.4

Table 5.15: Object name, z and M_B from VV catalog are shown from the left column. The object not detected at radio is marked by $*$ Val_V, Val_K is the result of detection of the variability at V and K band by Nelson(1996), and Y,N and ? represents detected, not detected and ambiguous, respectively. cor is the result of detection of correlation of both lightcurves Lag is the result of detection of correlation of the time lag and L represents to obtain the limit. The data of $f_{6cm}(Jy)$, $f_V(Jy)$ are obtained from VV catalog.

radio activity	radio qiet	radio loud	ambiguous
sample	43	5	3
variability detected	29	3	1
time delay obtained	6	0	0

Table 5.16: The result of the relation between radio activity and the suitability of the dust reverberation model. The second line represents the object in which the variability is detected at both V and K band.

sample	C_0	a_0	confidence interval of a(95%)	confidence interval of a(99%)
flat radio loud	0.253	0.246	-0.633 $\sim$ 1.008	-0.918 $\sim$ 1.212
steep radio loud	0.182	0.081	-0.649 $\sim$ 0.755	-0.863 $\sim$ 0.934
flat radio loud,				
$100 < \Delta t' < 400$	0.256	0.227	-0.694 $\sim$ 1.144	-1.161 $\sim$ 1.605
$400 < \Delta t' < 800$	0.242	0.296	-2.047 $\sim$ 2.344	-3.395 $\sim$ 3.260
steep radio loud,				
$100 < \Delta t' < 400$	0.200	0.078	-0.710 $\sim$ 0.793	-0.951 $\sim$ 0.986
$400 < \Delta t' < 800$	—	—	—	—
flat radio loud,				
$M_B < -25$	0.329	0.247	-0.957 $\sim$ 1.237	-1.454 $\sim$ 1.544
$M_B > -25$	0.006	1.923	-1.305 $\sim$ 4.999	-4.451 $\sim$ 4.999
steep radio loud,$100 < \Delta t' < 400$				
$M_B < -25$	0.213	0.177	-0.943 $\sim$ 1.123	-1.351 $\sim$ 1.398
$M_B > -25$	0.194	-0.424	-2.041 $\sim$ 0.842	-2.904 $\sim$ 1.306

Table 5.17: The result of the test and the estimation of wavelength dependence of the ensemble variability for the flat,steep radio loud and other their subsamples. The steep sample with long observation interval of $400 days < \Delta t' < 800 days$ is few, therefore blank.

compared samples	C_0	σ_{C0}	χ^2	P(%)
flat /steep	0.240	0.020	10.615164	99.9
flat,$100 < \Delta t' < 400$, /flat,$400 < \Delta t' < 800$	0.370	0.051	0.003041	4.4
flat, $100 < \Delta t' < 400$ /steep, $400 < \Delta t' < 800$	0.245	0.025	3.465026	93.7
flat,$M_B < -25$, /flat,$M_B > -25$	0.116	0.022	24.272392	>99.9
steep,$100 < \Delta t' < 400, M_B < -25$, /steep,$100 < \Delta t' < 400, M_B > -25$	0.123	0.017	17.557811	>99.9
flat,$M_B < -25$, /steep,$M_B < -25$, $100 < \Delta t' < 400$	0.328	0.037	5.171503	97.7
flat,$M_B > -25$, /steep,$M_B > -25$, $100 < \Delta t' < 400$	0.090	0.014	0.077112	21.9
quiet,$-24 < M_B < -22$, /flat,$M_B < -25$	0.115	0.013	2.753600	90.3
quiet,$-24 < M_B < -22$, /steep,$M_B < -25$, $100 < \Delta t' < 400$	0.114	0.012	2.470579	88.4

Table 5.18: The result of the test and the estimation of the difference of $V_{\overline{\lambda}}$ between various subsamples.

Chapter 6

conclusion

Results of near infrared(J,H,K' band) variability observations of 226 AGN are shown in this thesis. Samples are mainly QSO and Seyfert 1 AGN, and are radio quiet samples and radio quiet samples. Redshift(z) of the samples are from 0 to 1, and absolute magnitudes at V band(Mv) are from -30mag to -20mag. Each objects were broad line observed 2 times and the variabilities were measured by differential photometry. Ensemble variabilities of all samples were typically 0.2 mag regardless of observed band.

To detect high sensitivity and high accuracy, method of differential photometry specialized for this work was developed. Existence of systematic error σ_f turned out that was maybe originated by the error of flat fielding more than a few 10 pixel scale. The average of σ_f was about 0.03mag for J,H and K' band and no wavelength dependence was found, what was consistent with the error estimated by dithering of photmetric standard star frames. Influence of the PSF variation to the result of the differential photometry was estimated since AGN were not always point sources and therefore there was possibility that the influence was not canceled even with differential photometry. And it was turned out that the influence of the PSF variation was 0.01mag or less and was smaller than other main errors in this work. Estimating those systematic errors, 3 arcsec aperture that was comparable to the seeing size of this work could be adopted. As the result, determination of the variability of AGN with smaller statistic error than in the photometry using the photmetric standards too. The differential photometry was also applied to the reference objects around AGN and accuracy of the error estimation of the differential photometry in this work was checked. It was confirmed that the error estimation was quantitatively reasonable for J,H and K' band by the test.

z<0.3 AGN was distributed from typical galaxies position to typical QSO positioning near infrared J-H,H-K' 2 color diagram. In these samples, from Seyfert 1 to 1.5 samples were plotted from typical galaxies to typical QSO position, but from Seyfert 1.8 to 2.0 samples were plotted about typical galaxies position. And, bright AGN at V band absolute magnitude(Mv) tended to be plotted near typical QSO position and dark AGN tended to be plotted near typical galaxies position. These differences by Seyfert type or Mv were consistent to AGN's unified model. On the other hand, radio activities of samples were estimated by V band and 6 cm radio fluxes and but

positions on 2 color diagram were not separated. The near infrared colors estimated by smaller aperture(about 3 arcsec) were more QSO like than larger the colors by larger aperture(about 15arcsec). This tendency was more remarkable at dark object than at bright object, and this fact could be explained by nucleus and host galaxy color gradient.

Because only 2 times observations were done for each objects in this work, ensemble of variability data were calculated and features of AGN variability was estimated. For all samples, radio loud or radio quiet samples, and more divided by rest frame observation interval,Mv,Z, ensemble variability dependence on observed band was tested and clear dependence like in from UV to optical study was rejected in this near infrared work.

And ensemble variability dependence on radio activity, rest frame observation interval,Mv,z were tested. The variability of radio loud samples were larger than radio quiet variability was shown. In radio loud samples, more luminous samples shown larger variability than dark samples. For radio loud samples of this work, the variability of bright at Mv and high z objects were intrinsic large, but to separate the effect of z and Mv was difficult.

For radio quiet samples, variability of higher z samples tended small variability, but only variability of high z and short rest frame interval samples was concluded because of cosmological time delay. And significant Mv dependence was not found for radio quiet samples. When effect of host galaxies in the photometry apertuers, because dark samples were more effected by host galaxies by J-H,H-K' color analysis, the dependence of variability of AGN themselves and luminosity was negative. So probability exist that negative correlation between variability and luminosity discussed in optical work was consistent.

By adding this work result to other work in optical and UV wavelength, wave length range of statistic variability of AGN could be expanded about 2 times wider. Wavelength dependence of variability was not found which was seen in Uv and optical data and variability of near infrared was smaller or comparable to Uv and optical data. These result were consistent to AGN's hot dust thermal emission in near infrared wavelength.

For each AGN, significance of variabilities at J,H,K' band were estimated by ratio of variability to error. Distributions of the significance of J,H,K' band were resemble for each other. More than $2\sigma(3\sigma)$ variability samples were 58%(44%) by average of J,H,K' values of all samples whose error was smaller than 0.1 mag.

Difference of variability significance of the subsamples divided by their error to 3 was clear. The distribution of the lowest accuracy group(0.05mag $< \sigma <$0.1mag) was localized toward smaller significance side. On the other hand, more than $2\sigma(3\sigma)$ variability samples were high ratio of 80%(68%) for the highest accuracy group($\sigma <$0.03mag). The distribution of the group with 0.03mag$< \sigma <$0.05mag accuracy was intermediate shape. No observed band dependence was found in those distributions. The ratio of AGN with certain variability grew larger when the accuracy of the data became higher, and feature of saturation was found. As the simplest interpretation, it was concluded that maybe all quasars and Seyfert 1 AGN were variable objects.

The observation of this work was only 2 times for each objects, and some conditions of the observation link aperture of telescope or seeing were worse than some other works, however, higher ratio of the certain variability detected objects was realize. It was guessed that this feature was caused by the differential photometry with small aperture because main systematic error were canceled, SN was heightened and AGN component was dipped from host galaxy especially nearby AGN.

For all samples,radio quiet and radio loud samples, correlation coefficient r between different band variability were estimated. These values were r=0.6 $\sim$ 0.9. Radio quiet samples were splitted by z, and z dependence of r was tested by these subsamples. $r_{HK'}$ was significantly higher than $r_{JH}, r_{JK'}$ at $0.1, z < 0.3$ though error of r was large at some z regions. $r_{JH}, r_{JK'} and r_{HK's}$ z dependence of radio quiet samples was explained by radiation and variability by dust reverberation.

For radio loud samples, $r_{JH}, r_{JK'} and r_{HK's}$high redshift object in this work($0.6 < z < 1$) were high value about 0.95. Errors of $r_{JH}, r_{JK'} and r_{HK's}$ of radio loud samples were large at low redshift($0 < z, 0.3$) against radio quiet samples. So to distinguish existence of z dependence found in radio quiet samples for radio loud samples couldn't done.

Using samples whose rest frame observation interval were about 1, 2 years, time evolutions of ensemble variability were estimated. 2 form of function $A_0(t/(1+z))^p$ and $B_0[1-\exp(-t/\tau(1+z))]$ were used for fitting. For all samples, the radio quiet and the radio loud samples and the splitted samples of those by Mv or z, significant difference by observed band were not found. Time scale of radio loud samples was shorter than radio quiet as the value of the parameters. But the difference of the time scales of radio quiet and radio loud samples couldn't concluded as significant because the errors were large.

The features found in this work were consistent with the dust reverberation model. However, it was difficult for the simple dust reverberation model that the Mv dependence of variabilities of radio quiet and radio loud were significantly different each other.

Radio activities were checked for the objects where the time delay between optical and infrared light curves was determined, and all of them tested in this work were radio quiet. Furthermore, the radio activities of sample of Nelson 1996 were also checked. It was turned out that all objects where the time delay could be determined was radio quiet nevertheless the detection rate of the variability was almost equal between radio quiet and radio loud.

In the radio loud samples, ensemble variabilities of flat spectrum samples were significantly larger than steep spectrum samples. It is known that OVV,high polarized QSO, BL lac object are subsamples of radio loud and variabilities of nonthermal component of those objects are fast and large. Therefore it is reasonable that the feature of flat samples is caused by contamination of nonthermal emission of such objects into the ensemble variability.

On the other hand, ensemble variability of the steep radio loud sample was significantly larger than that of radio quiet though smaller than flat radio loud. Positive correlation between lumi-

nosity and the ensemble variability was found in steep sample similar to flat sample. Therefore, it is possible that nonthermal component exist steep radio loud sample too and the mechanism of emission and variability is different from those of radio quiet though the degree is weaker than flat radio loud sample. As another explanation, it is also possible that those features of steep sample are caused by contamination of some flat sample into steep sample because of incompleteness of the separation of flatness.

Bibliography

[1] Alonso-Herrero,A., Ward,M.J. & Kotilainen,J.K. 1996, MNRAS, 278, 902

[2] Baribaud,T., Alloin,D., Glass,I. & Pelat,D. 1992, A&A, 256, 375

[3] Barvainis,R. 1992, ApJ, 400, 502

[4] Bloom,S.D., Marscher,A.P., Gear,.K., Terasranta,H., Valtaoja,E., Aller,H.D. & Aller,M.F. 1994, AJ, 108, 398

[5] Borgeest,U. & Schramm,K.-J. 1994, A&A, 284, 764

[6] Cid Fernandes,R.,J., Aretxaga,I. & Terlevich,R. 1996, MNRAS, 282, 1191

[7] Clavel,J., Wamsteker,W. & Glass,I. S. 1989, ApJ, 337, 236

[8] Cristiani,S., Trentini,S., La Franca,F. & Andreani,P. 1997, A&A, 321, 123

[9] Cristiani,S., Trentini,S., La Franca,F., Aretxaga,I., Andreani,P., Vio, R. & Gemmo, A. 1996, A&A, 306, 395

[10] Cutri,R.M., Wisniewski,W.Z., Rieke,G.H. & Lebofsky,M.J. 1985, ApJ, 296, 423

[11] Di Clemente,A., Giallongo,E., Natali,G., Trevese,D. & Vagnetti,F. 1996ApJ, 463, 466

[12] Edelson R.A. et al. 1996, ApJ, 470, 364

[13] Fanaroff,B.L. & Riley,J.M. 1974, MNRAS, 167P, 31

[14] Garcia,A., Sodr,L., Jablonski,F.,J. & Terlevich,R.,J. 1999, MNRAS, 309, 803

[15] Giallongo,E., Trevese,D. & Vagnetti,F. 1991, ApJ, 377, 345

[16] Givcon,U., Maoz,D., Kaspi,S., Netzer,H. & Smith,P.,S. 1999, MNRAS, 306, 637

[17] Glass,I.S. 1992, MNRAS, 256, 23

[18] Glass,I.S. 1997, MNRAS, 292L,50

[19] Glass,I.S. 1998, MNRAS, 297, 18

[20] Hook,I. M., McMahon,R.G., Boyle,B.J. & Irwin,M.J. 1994,MNRAS, 268, 305

[21] Hughes,P.A., Aller,H.D. & Aller,M.F. 1992, ApJ, 396, 469

[22] Hunt,L. K., Malkan,M.A., Salvati,M., Mandolesi,N., Palazzi,E. & Wade,R. 1997, ApJS, 108, 229

[23] Kobayashi,Y, Sato,S, Yamashita,T., Shiba,H. & Takami,H. 1993, ApJ, 404, 94

[24] Kotilainen,J. K. & Ward,M.J. 1994, MNRAS, 266, 953

[25] Kotilainen,J.K., Ward,M.J., Boisson,C., Depoy,D.L. & Smith,M.G. 1992, MNRAS, 256, 149

[26] Kotilainen,J.K., Ward,M.J., Boisson,C., Depoy,D.L., Smith,M.G. & Bryant,L.R. 1992, MNRAS, 256, 125

[27] Krolik,J.H., Active galactic nuclei : from the central black hole to the galactic environment, Prinston Series in Astrophysics

[28] Lainela,M. & Valtaoja,E. 1993, ApJ, 416, 485

[29] Landau,R., Golisch,B., Jones,T.J., Jones,T.W., Pedelty,J., Rudnick,L., Sitko,M.L., Kenney,J., Roellig,T., Salonen,E., Urpo,S., Schmidt,G., Neugebauer,G., Matthews,K., Elias,J.H., Impey,C., Clegg,P. & Harris,S. 1986, ApJ, 308, 78

[30] Ledlow,M.J. & Owen,F.N. 1996, AJ, 112, 9

[31] Longo,G., Vio,R., Paura,P., Provenzale,A. & Rifatto,A. 1996, A&A, 312, 424

[32] Maslowski,J., Pauliny-Toth,I.I.K., Witzel,A. & Kuehr,H. 1984, A&A, 139, 85

[33] Minezaki,T. 1997,thesis

[34] Nelson,B.,O. 1996, ApJ, 465L, 87

[35] Nelson,B.,O. 1996, thesis

[36] Netzer,H., Heller, A., Loinger,F., Alexander,T., Baldwin,J.A., Wills,B.J., Han,M., Fruch,M., & Higdon,J.L. 1996, MNRAS, 279, 429

[37] Neugebauer,G. & Matthews,K. 1999, AJ, 118, 35

[38] Neugebauer,G., Soifer,B.T., Matthews,K. & Elias,J. H. 1989, AJ, 97, 957

[39] Oknyanskii,V.L. 1993, Astron.Lett., 19, 416

[40] Pier,E.A. & Krolik,J.H. 1992, ApJ, 401, 99

[41] Pier,E.A. & Krolik,J.H. 1993, ApJ, 418, 673

[42] Robson,E.I., Gear,W.K., Clegg,P.E., Ade,P.A.R., Smith,M.G., Griffin,M.J., Nolt,I.G., Radostitz,J.V. & Howard,R.J. 1983, Natur, 305, 194

[43] Robson,E.I., Litchfield,S.J., Gear,W.K., Hughes,D.H., Sandell,G., Courvoisier,T. J.-L., Paltani,S., Valtaoja,E., Terasranta,H., Tornikoski,M., Steppe,H. & Wright,M.C.H. 1993, MNRAS, 262, 249

[44] Sanders,D.B., Phinney,E.S., Neugebauer,G., Soifer,B.T. & Matthews,K. 1989, ApJ, 347, 29S

[45] Sembay,S., Hanson,C.G. & Coe,M.J. 1987, MNRAS, 226, 137

[46] Sitko,M.L., Sitko,A.K., Siemiginowska,A. & Szczerba,R. 1993, ApJ, 409, 139

[47] Tornikoski,M., Valtaoja,E., Terasranta,H., Lainela,M., Bramwell,M. & Botti,L.C.L. 1993, AJ, 105, 1680

[48] Trevese,D., Kron,R.G., Majewski,S.R., Bershady,M.A. & Koo,D.C. 1994, ApJ, 433, 494

[49] Veron-Cetty,M.P., Veron,P., Quasars and Active Galactic Nuclei (8th Ed.). ESO Sci. Rep., 18, 1 (1998)

[50] Winkler,H., Glass,I. S., van Wyk,F., Marang,F., Jones,J.H.S., Buckley,D.A.H. & Sekiguchi,K. 1992, MNRAS, 257, 659

Appendix A

table

A.1 observed object list

Table A.1: observed object list

num	name	RA				dec			z	M_B	radio type
1	PB 5669	0	0	12.0	+	0	2	24	0.479	-24.6	U
2	Q 2357+019A	0	0	23.7	+	2	12	41	0.81	-26.8	U
3	PB 5677	0	0	42.9	+	0	55	39	0.949	-25.4	U
4	PB 5723	0	5	47.5	+	2	3	2	0.234	-24.2	U
5	PB 5853	0	18	22.1	+	1	19	1	0.16	-22.8	U
6	Q 0019+0022B	0	21	46.4	+	0	38	59	0.661	-25.0	U
7	PB 5932	0	24	44.1	+	0	32	21	0.404	-25.1	U
8	MS 00377-0156	0	40	17.9	-	1	40	15	0.296	-23.6	U
9	Q 0057+0000	1	0	2.3	+	0	16	42	0.776	-26.3	U
10	Q 0058+0218	1	1	20.1	+	2	34	30	0.929	-26.4	U
11	PHL 964	1	3	33.5	+	10	10	34	0.465	-24.1	U
12	Q 0110-0047	1	13	10.4	-	0	31	34	0.412	-23.1	U
13	B2 0110+29	1	13	24.2	+	29	58	16	0.363	-24.8	L
14	PKS 0130+24	1	33	24.6	+	24	27	40	0.452	-25.5	L
15	UM 341	1	34	18.2	+	0	15	37	0.401	-25.1	U
16	3C 47.0	1	36	24.5	+	20	57	26	0.425	-24.0	L
17	PHL 1070	1	37	18.7	+	3	38	30	0.079	-21.9	U
18	PHL 1093	1	39	57.2	+	1	31	47	0.258	-23.9	L
19	KUV 01507-0744	1	53	11.0	-	7	28	57	0.3	-24.9	U
20	PHL 1226	1	54	28.1	+	4	48	17	0.404	-25.0	U
21	UM 381	1	57	9.7	-	1	47	29	0.91	-26.7	U
22	UM 153	1	58	38.9	+	3	47	44	0.66	-26.0	U
23	MARK 1018	2	6	16.0	-	0	17	29	0.043	-21.3	U
24	RXS J02070+2930	2	7	2.2	+	29	30	45	0.110	-23.1	U
25	MARK 586	2	7	49.8	+	2	42	55	0.155	-24.2	Q
26	PKS 0214+10	2	17	7.7	+	11	4	9	0.408	-25.6	L
27	PB 9130	2	17	29.4	-	3	8	9	0.323	-24.8	U
28	B3 0219+443	2	22	17.7	+	44	32	57	0.850	-26.6	L
29	KUV 02292+3227	2	32	10.4	+	32	39	46	0.356	-24.7	U
30	MARK 1179	2	33	22.4	+	27	56	14	0.038	-20.3	Q
31	NGC 985	2	34	37.8	-	8	47	15	0.043	-22.4	Q
32	MS 02328-0400	2	35	19.2	-	3	47	15	0.376	-24.0	U
33	4C 41.04	2	35	56.1	+	41	23	16	0.500	-25.1	L
34	Q 0235+0121	2	38	10.0	+	1	34	19	0.393	-24.0	U
35	Q 0238-0142	2	41	12.7	-	1	29	17	0.346	-24.3	U

Table A.2: observed object list: continued

num	name	RA				dec			z	M_B	radio type
36	PB 6856	2	42	40.3	+	0	57	27	0.569	-26.1	U
37	US 3150	2	46	51.9	-	0	59	31	0.467	-25.2	U
38	MS 02448+1928	2	47	40.8	+	19	40	58	0.176	-23.4	U
39	Q 0248+0207	2	51	10.3	+	2	19	20	0.489	-23.6	U
40	US 3254	2	52	21.0	+	0	5	59	0.811	-26.6	U
41	US 3333	2	55	5.6	+	0	25	22	0.354	-24.5	U
42	US 3376	2	56	16.5	-	1	26	38	0.879	-27.1	U
43	S 0254+0101	2	56	46.9	+	1	13	48	0.177	-22.0	U
44	US 3472	2	59	37.5	+	0	37	36	0.532	-25.6	U
45	S 0257-0027	2	59	51.8	-	0	15	22	0.102	-19.7	U
46	Q 0258+0227	3	0	44.1	+	2	39	41	0.892	-25.4	U
47	US 3543	3	2	6.8	-	0	1	20	0.641	-24.6	U
48	Q 0300-0018	3	3	15.7	-	0	7	2	0.703	-25.0	U
49	US 3605	3	4	22.4	+	0	22	32	0.635	-25.8	U
50	Q 0305+0222	3	8	14.1	+	2	34	23	0.590	-24.9	U
51	PKS 0306+102	3	9	3.7	+	10	29	16	0.863	-25.1	Q
52	Q 0307-0015	3	9	39.4	-	0	3	40	0.770	-26.1	U
53	PKS 0310+013	3	12	43.6	+	1	33	17	0.664	-24.6	L
54	MS 03120+1405	3	14	48.4	+	14	16	27	0.744	-25.5	U
55	Q 0313+0126	3	16	31.3	+	1	37	30	0.956	-25.2	U
56	B2 0321+33	3	24	41.2	+	34	10	45	0.062	-22.2	L
57	PKS 0336-01	3	39	31.0	-	1	46	36	0.852	-24.9	L
58	KUV 03399-0014	3	42	26.4	-	0	4	27	0.384	-24.5	U
59	3C 93.0	3	43	30.1	+	4	57	49	0.357	-23.3	L
60	MS 03419+0451	3	44	34.5	+	5	0	38	0.756	-25.4	U
61	PKS 0353+027	3	55	59.0	+	2	56	24	0.602	-24.3	L
62	MS 03574+1046	4	0	11.7	+	10	55	11	0.182	-23.2	U
63	3C 109.0	4	13	40.4	+	11	12	15	0.306	-22.5	L
64	MS 04124-0802	4	14	52.7	-	7	55	40	0.037	-21.1	Q
65	3C 110	4	17	16.7	-	5	53	45	0.773	-27.3	L
66	PKS 0420-01	4	23	15.8	-	1	20	33	0.915	-26.5	L
67	3C 120	4	33	11.1	+	5	21	15	0.033	-20.8	L
68	IRAS 04448-0513	4	47	20.2	-	5	8	15	0.044	-21.2	U
69	Q 0446+0130	4	49	7.5	+	1	35	29	0.811	-24.6	U
70	NGC 1685	4	52	34.2	-	2	56	57	0.014	-18.4	Q
71	UGC 3223	4	59	9.4	+	4	58	30	0.018	-19.9	U
72	2E 0507+1626	5	10	45.5	+	16	29	56	0.017	-19.4	U
73	3C 135.0	5	14	8.4	+	0	56	33	0.127	-21.2	L
74	AKN 120	5	16	11.4	-	0	9	0	0.033	-22.2	Q
75	1E 0514-0030	5	16	33.5	-	0	27	14	0.291	-25.1	U

Table A.3: observed object list: continued

num	name	RA				dec			z	M_B	radio type
76	3C 138.0	5	21	9.9	+	16	38	21	0.759	-24.1	L
77	3C 147.0	5	42	36.3	+	49	51	7	0.545	-24.2	L
78	4C 16.14	5	51	18.8	+	16	36	40	0.474	-25.4	L
79	MCG 08.11.11	5	54	53.6	+	46	26	21	0.020	-20.0	A
80	OH-010	6	7	59.7	-	8	34	49	0.872	-25.4	L
81	3C 154.0	6	13	50.2	+	26	4	36	0.580	-25.3	L
82	MC 0657+176	7	0	31.4	+	17	35	53	0.722	-24.8	L
83	3C 175.0	7	13	2.3	+	11	46	15	0.768	-26.4	L
84	B2 0709+37	7	13	9.4	+	36	56	7	0.487	-26.8	A
85	MARK 376	7	14	15.1	+	45	41	56	0.056	-22.5	Q
86	B3 0729+391	7	33	20.8	+	39	5	5	0.663	-24.7	L
87	S4 0731+47	7	35	2.2	+	47	50	8	0.782	-25.5	L
88	PKS 0736+01	7	39	18.0	+	1	37	4	0.191	-23.5	L
89	OI 363	7	41	10.7	+	31	11	59	0.630	-26.8	L
90	MARK 79	7	42	32.8	+	49	48	35	0.022	-20.9	Q
91	B2 0742+31	7	45	41.6	+	31	42	56	0.462	-26.6	L
92	PKS 0743-006	7	45	54.0	-	0	44	18	0.994	-27.1	L
93	GC 0742+33	7	45	59.3	+	33	13	34	0.610	-25.2	L
94	RXS J07491+2842	7	49	10.7	+	28	42	14	0.345	-24.7	U
95	RXS J07498+3454	7	49	48.2	+	34	54	44	0.132	-22.1	U
96	PKS 0748+126	7	50	52.1	+	12	31	5	0.889	-26.0	L
97	MARK 382	7	55	25.3	+	39	11	10	0.034	-20.5	U
98	B2 0752+25A	7	55	37.0	+	25	42	39	0.446	-25.2	L
99	B3 0754+394	7	58	0.1	+	39	20	29	0.096	-24.1	Q
100	KUV 07549+4228	7	58	19.8	+	42	19	35	0.21	-24.2	U
101	UGC 4155	8	0	20.6	+	26	36	51	0.025	-22.7	U
102	MARK 1210	8	4	6.0	+	5	6	51	0.013	-19.9	Q
103	MS 08019+2129	8	4	52.8	+	21	20	50	0.118	-23.4	U
104	3C 192.0	8	5	35.0	+	24	9	51	0.060	-22.3	L
105	MS 08080+4840	8	11	37.2	+	48	31	33	0.700	-25.3	L
106	3C 196.0	8	13	36.0	+	48	13	3	0.871	-25.6	L
107	B2 0810+32	8	14	9.3	+	32	37	31	0.842	-25.9	L
108	PKS 0812+02	8	15	23.0	+	1	54	58	0.402	-24.7	L
109	RX J08166+2941	8	16	36.1	+	29	41	33	0.262	-23.7	U
110	3C 197	8	17	35.1	+	22	37	17	0.980	-26.2	L
111	RXS J08223+3305	8	22	18.6	+	33	5	26	0.125	-21.2	U
112	KUV 08217+4235	8	25	8.3	+	42	25	15	0.19	-23.8	U
113	4C 44.17	8	25	17.6	+	44	36	27	0.904	-25.9	L
114	KUV 08267+4027	8	30	0.2	+	40	16	47	0.89	-27.3	U
115	B2 0827+24	8	30	52.1	+	24	11	0	0.941	-26.5	L

Table A.4: observed object list: continued

num	name	RA				dec			z	M_B	radio type
116	PG 0832+251	8	35	35.9	+	24	59	41	0.331	-25.7	U
117	OJ 256	8	36	23.0	+	27	28	52	0.765	-24.9	L
118	US 1329	8	36	58.9	+	44	26	2	0.249	-25.7	U
119	MARK 1218	8	38	11.1	+	24	53	45	0.028	-21.1	Q
120	Q 0835+4744	8	38	40.5	+	47	34	10	0.697	-24.1	U
121	3C 207.0	8	40	47.6	+	13	12	23	0.684	-24.6	L
122	KUV 08377+4136	8	40	58.7	+	41	25	19	0.69	-26.4	U
123	PG 0844+349	8	47	42.5	+	34	45	5	0.064	-23.1	Q
124	55W 179	8	47	44.6	+	44	26	11	0.463	-22.9	U
125	CSO 2	8	49	2.5	+	30	2	35	0.660	-26.1	U
126	US 1742	8	49	59.5	+	43	16	47	0.693	-25.9	U
127	LB 8741	8	50	29.4	+	18	53	49	0.568	-25.6	U
128	MS 08475+2813	8	50	35.8	+	28	2	12	0.330	-23.6	U
129	US 1786	8	51	16.2	+	42	43	29	0.487	-25.0	U
130	MS 08495+0805	8	52	15.1	+	7	53	34	0.063	-21.9	U
131	MS 08498+2820	8	52	48.8	+	28	8	29	0.197	-21.9	U
132	MS 08502+2825	8	53	17.8	+	28	13	49	0.922	-26.3	L
133	US 1867	8	53	34.2	+	43	49	1	0.513	-25.9	U
134	MARK 391	8	54	46.4	+	39	32	19	0.013	-19.6	Q
135	NGC 2683 U1	8	55	2.5	+	32	39	19	0.621	-25.6	U
136	LB 8948	8	57	6.3	+	19	8	54	0.331	-24.0	U
137	LB 8960	8	57	33.1	+	16	0	17	0.828	-26.3	U
138	US 2068	8	59	24.3	+	46	37	18	0.923	-27.1	U
139	KUV 09012+4019	9	4	23.3	+	40	7	3	0.412	-25.1	U
140	US 44	9	7	23.6	+	17	16	17	0.098	-22.3	U
141	1E 0906+4254	9	9	26.6	+	42	42	29	0.242	-22.4	U
142	4C 05.38	9	14	1.8	+	5	7	50	0.303	-23.8	L
143	MARK 704	9	18	26.0	+	16	18	20	0.029	-21.4	U
144	RXS J09189+3016	9	18	56.0	+	30	16	57	0.146	-21.8	U
145	RX J09190+3502B	9	19	1.4	+	35	3	7	2.23	-28.3	U
146	E 0917+341	9	21	2.7	+	33	53	45	0.227	-22.4	U
147	RX J09249+2527	9	24	59.1	+	25	27	39	0.269	-23.6	U
148	PG 0923+201	9	25	54.7	+	19	54	4	0.190	-24.5	Q
149	MARK 705	9	26	3.3	+	12	44	3	0.028	-21.0	Q
150	B2 0923+39	9	27	3.0	+	39	2	21	0.698	-25.3	L
151	RX J09273+3045	9	27	18.5	+	30	45	36	0.527	-24.9	U
152	MS 09309+2128	9	33	47.7	+	21	14	36	0.172	-23.4	Q
153	US 737	9	35	2.6	+	43	31	11	0.456	-25.8	U
154	MARK 707	9	37	1.1	+	1	5	43	0.051	-20.8	Q
155	TON 1078	9	37	1.9	+	34	25	0	0.908	-28.0	U

Table A.5: observed object list: continued

num	name	RA				dec			z	M_B	radio type
156	PG 0936+396	9	39	44.6	+	39	24	2	0.458	-26.0	U
157	US 822	9	40	33.7	+	46	23	15	0.699	-25.6	U
158	MS 09398+0952	9	42	33.4	+	9	38	36	0.205	-21.9	U
159	HS 0940+4820	9	44	4.4	+	48	6	44	0.393	-23.8	U
160	2E 0944+4629	9	47	17.8	+	46	15	8	0.35	-23.1	U
161	US 995	9	48	59.4	+	43	35	18	0.226	-24.3	U
162	HS 0946+4845	9	50	0.5	+	48	31	30	0.590	-26.1	U
163	MARK 1239	9	52	19.1	-	1	36	44	0.019	-20.3	Q
164	US 1107	9	55	39.8	+	45	32	17	0.259	-24.3	A
165	PG 0953+415	9	56	52.3	+	41	15	41	0.239	-25.6	Q
166	3C 232	9	58	20.9	+	32	24	2	0.530	-26.7	L
167	NGC 3080	9	59	55.8	+	13	2	40	0.035	-20.9	Q
168	IRAS 09595-0755	10	2	0.0	-	8	9	44	0.055	-22.1	U
169	KUV 09597+3343	10	2	34.9	+	33	28	16	0.95	-27.4	U
170	KUV 10000+3255	10	2	54.6	+	32	40	39	0.83	-27.1	U
171	TON 28	10	4	2.6	+	28	55	36	0.329	-25.4	U
172	PG 1001+05	10	4	20.1	+	5	13	1	0.161	-23.6	Q
173	PKS 1004+13	10	7	26.2	+	12	48	56	0.240	-25.6	L
174	RXS J10079+4918	10	7	56.3	+	49	18	8	0.149	-21.4	U
175	TON 488	10	10	0.7	+	30	3	21	0.26	-25.1	U
176	4C 41.21	10	10	27.5	+	41	32	38	0.613	-26.6	L
177	Q 1008+0058	10	10	44.4	+	0	43	31	0.18	-23.7	U
178	CSO 37	10	11	17.3	+	32	28	7	0.41	-25.0	U
179	TON 1187	10	13	3.1	+	35	51	22	0.079	-23.0	U
180	PG 1011-040	10	14	20.7	-	4	18	39	0.058	-22.2	Q
181	PKS 1011+23	10	14	47.1	+	23	1	18	0.565	-25.2	L
182	PG 1012+008	10	14	54.9	+	0	33	37	0.185	-24.3	Q
183	Q 1013+0124	10	15	57.0	+	1	9	13	0.779	-26.9	L
184	MARK 720	10	17	38.0	+	6	58	16	0.045	-21.1	U
185	Q 1015-0121	10	18	11.0	-	1	36	2	0.319	-23.1	U
186	PG 1016+336	10	19	49.5	+	33	22	4	0.024	-19.9	U
187	MS 10182+2010	10	20	55.1	+	19	54	47	0.250	-22.4	U
188	B2 1028+31	10	30	59.1	+	31	2	56	0.177	-23.1	L
189	MS 10461+1411	10	48	46.2	+	13	54	53	0.290	-22.6	U
190	Q 1047+067	10	49	36.8	+	6	29	22	0.148	-23.1	U
191	MS 10470+3537	10	49	49.3	+	35	22	5	0.161	-22.8	U
192	CSO 292	10	50	53.7	+	34	43	38	0.147	-23.2	U
193	PG 1049-005	10	51	51.5	-	0	51	17	0.357	-25.7	Q
194	MARK 634	10	58	1.2	+	20	29	14	0.066	-21.9	U
195	RXS J11006+4316	11	0	37.5	+	43	0	11	0.32	-23.5	U

Table A.6: observed object list: continued

num	name	RA				dec			z	M_B	radio type
196	RXS J11008+2839	11	0	52.4	+	28	38	1	0.243	-24.1	U
197	MARK 728	11	1	1.8	+	11	2	50	0.036	-19.9	A
198	TOL 1059+105	11	1	57.9	+	10	17	39	0.034	-21.0	U
199	1059.6+0157	11	2	8.7	+	1	41	11	0.394	-23.4	U
200	PKS 1103-006	11	6	31.8	-	0	52	53	0.426	-25.7	L
201	MC 1104+167	11	7	15.1	+	16	28	3	0.632	-27.1	L
202	PG 1112+431	11	15	6.0	+	42	49	50	0.302	-25.2	U
203	PG 1114+445	11	17	6.3	+	44	13	34	0.144	-23.7	Q
204	PG 1115+407	11	18	30.4	+	40	25	55	0.154	-23.9	Q
205	PG 1116+215	11	19	8.8	+	21	19	18	0.177	-25.3	Q
206	MARK 734	11	21	47.1	+	11	44	19	0.049	-22.0	Q
207	RXS J11240+3110	11	24	0.6	+	31	10	0	0.109	-21.2	U
208	PG 1121+422	11	24	39.2	+	42	1	45	0.234	-24.2	U
209	A1 27	11	26	43.0	+	15	45	55	0.431	-25.7	U
210	MARK 423	11	26	48.5	+	35	15	4	0.032	-21.4	Q
211	US 2450	11	27	36.4	+	26	54	50	0.378	-24.9	U
212	MARK 1298	11	29	16.7	-	4	24	8	0.060	-22.8	Q
213	MARK 1447	11	30	29.1	+	49	34	58	0.096	-22.8	U
214	B2 1128+31	11	31	9.4	+	31	14	7	0.289	-25.3	L
215	3C 261	11	34	54.5	+	30	5	26	0.614	-24.5	L
216	MARK 739E	11	36	29.3	+	21	35	46	0.030	-21.4	Q
217	MCG 06.26.012	11	39	13.7	+	33	55	54	0.032	-21.0	U
218	MARK 744	11	39	42.6	+	31	54	34	0.010	-19.3	Q
219	WAS 26	11	41	16.1	+	21	56	22	0.063	-23.0	U
220	CG 855	11	44	30.0	+	36	53	9	0.04	-20.7	U
221	MS 11435-0411	11	46	3.9	-	4	28	1	0.133	-22.7	U
222	MC 1146+111	11	48	47.9	+	10	54	59	0.863	-26.9	A
223	CBS 147	11	50	9.5	+	34	56	31	0.251	-25.0	U
224	PG 1151+117	11	53	49.3	+	11	28	30	0.176	-24.2	Q
225	CBS 151	11	54	28.5	+	34	7	8	0.461	-24.3	U
226	4C 29.45	11	59	31.9	+	29	14	45	0.729	-28.6	L
227	GQ COM	12	4	42.1	+	27	54	12	0.165	-24.4	Q
228	UGC 7064	12	4	43.4	+	31	10	38	0.024	-21.0	U
229	Q 1211+0848	12	13	57.2	+	8	32	3	0.810	-26.3	U
230	PG 1211+143	12	14	17.7	+	14	3	13	0.085	-24.1	Q
231	WAS 49B	12	14	17.9	+	29	31	43	0.064	-22.5	Q
232	PKS 1216-010	12	18	35.0	-	1	19	54	0.415	-25.9	L
233	MARK 1320	12	19	8.8	-	1	48	29	0.103	-24.0	U
234	PG 1216+069	12	19	20.9	+	6	38	38	0.334	-26.0	Q
235	Q 1220+0939	12	23	17.8	+	9	23	8	0.681	-25.6	U

Table A.7: observed object list: continued

num	name	RA				dec			z	M_B	radio type
236	MS 12209+1601	12	23	30.8	+	15	45	8	0.081	-21.8	U
237	B2 1223+25	12	25	39.5	+	24	58	36	0.268	-23.8	L
238	2E 1224+0930	12	27	16.5	+	9	14	9	0.731	-23.9	U
239	3C 273.0	12	29	6.7	+	2	3	8	0.158	-26.9	L
240	Q 1228-0130	12	30	51.0	-	1	47	4	0.706	-25.2	U
241	TON 1542	12	32	3.6	+	20	9	30	0.064	-22.4	Q
242	CSO 150	12	33	41.7	+	31	1	2	0.290	-25.3	U
243	IC 3528	12	34	55.9	+	15	33	56	0.046	-22.0	U
244	MC 1233+108	12	36	4.6	+	10	34	50	0.664	-24.3	L
245	Q 1235+0216	12	38	13.1	+	2	0	19	0.672	-25.6	U
246	NGC 4593	12	39	39.4	-	5	20	39	0.009	-19.7	Q
247	WAS 61	12	42	10.6	+	33	17	1	0.045	-21.8	U
248	Q 1240+1546	12	42	38.5	+	15	29	35	0.07	-22.1	U
249	CBS 63	12	42	58.1	+	29	24	1	0.397	-25.0	U
250	Q 1240+1746	12	43	26.5	+	17	29	35	0.549	-24.7	U
251	4C 45.26	12	49	23.5	+	44	44	49	0.803	-25.9	L
252	MS 12480-0600A	12	50	37.7	-	6	17	23	0.305	-22.6	U
253	CSO 769	12	52	42.5	+	28	12	47	0.85	-27.0	U
254	MS 12545+2209	12	56	59.0	+	21	53	47	0.187	-23.3	U
255	MARK 783	13	2	58.9	+	16	24	28	0.067	-22.0	Q
256	US 272	13	6	34.3	+	30	49	34	0.422	-23.1	U
257	3C 281	13	7	54.0	+	6	42	14	0.599	-25.7	L
258	MS 13061-0115	13	8	45.6	-	1	30	54	0.111	-21.1	U
259	PG 1307+085	13	9	47.0	+	8	19	49	0.155	-24.6	Q
260	CSO 835	13	10	23.3	+	29	55	34	0.71	-25.0	U
261	B2 1308+32	13	10	28.7	+	32	20	44	0.997	-28.6	L
262	PG 1309+355	13	12	17.7	+	35	15	23	0.184	-24.7	A
263	RXS J13129+2628	13	12	59.6	+	26	28	26	0.060	-21.0	U
264	Q 1316+0103	13	18	43.9	+	0	47	33	0.394	-23.5	U
265	MARK 1347	13	22	55.5	+	8	9	42	0.050	-22.3	Q
266	Q 1326-0516	13	29	28.6	-	5	31	36	0.580	-27.2	U
267	MS 13285+3135	13	30	53.2	+	31	19	32	0.241	-22.9	U
268	Q 1330-0156	13	33	19.5	-	2	12	16	0.889	-25.2	U
269	1333.3+2604	13	35	39.4	+	25	49	8	0.414	-23.8	U
270	Q 1334-0232	13	37	12.8	-	2	47	54	0.722	-25.7	U
271	IRAS 13349+2438	13	37	18.8	+	24	23	4	0.107	-24.1	Q
272	Q 1338-0030	13	40	44.5	-	0	45	17	0.385	-24.8	U
273	TON 730	13	43	56.6	+	25	38	52	0.087	-22.1	Q
274	MARK 69	13	46	8.1	+	29	38	10	0.076	-21.9	U
275	1343.9+2828	13	46	14.4	+	28	13	55	0.659	-25.1	U

Table A.8: observed object list: continued

num	name	RA				dec			z	M_B	radio type
276	MARK 662	13	54	6.4	+	23	25	49	0.055	-21.6	Q
277	PG 1352+183	13	54	35.6	+	18	5	18	0.152	-24.0	Q
278	MARK 463E	13	56	2.8	+	18	22	19	0.051	-22.4	A
279	PG 1402+261	14	5	16.2	+	25	55	34	0.164	-24.5	Q
280	PG 1404+226	14	6	21.9	+	22	23	47	0.098	-23.1	Q
281	OQ 208	14	7	0.4	+	28	27	15	0.077	-22.2	L
282	Q 1404-0455	14	7	30.8	-	5	10	10	15.79	___	U
283	PG 1407+265	14	9	23.9	+	26	18	21	0.94	-28.0	Q
284	PG 1411+442	14	13	48.3	+	44	0	14	0.089	-23.7	Q
285	PG 1415+451	14	17	0.8	+	44	56	6	0.114	-23.5	Q
286	NGC 5548	14	17	59.6	+	25	8	13	0.017	-20.7	Q
287	H 1419+480	14	21	29.7	+	47	47	24	0.072	-22.8	U
288	MS 14201+2956	14	22	20.5	+	29	42	55	0.053	-21.7	U
289	B2 1420+32	14	22	30.3	+	32	23	10	0.685	-25.7	L
290	MARK 471	14	22	55.3	+	32	51	3	0.034	-21.3	U
291	B 1422+231	14	24	38.1	+	22	56	1	3.62	-30.7	Q
292	2E 1423+2008	14	26	13.4	+	19	55	25	0.21	-24.6	U
293	MARK 813	14	27	25.0	+	19	49	52	0.131	-24.1	U
294	B2 1425+26	14	27	35.7	+	26	32	14	0.366	-26.0	A
295	MARK 1383	14	29	6.6	+	1	17	6	0.086	-23.4	Q
296	MARK 684	14	31	4.9	+	28	17	14	0.046	-21.9	U
297	MS 14315+0526	14	34	5.5	+	5	13	27	0.152	-21.9	U
298	MARK 474	14	34	52.4	+	48	39	43	0.041	-20.7	U
299	PG 1435-067	14	38	16.2	-	6	58	20	0.129	-23.4	Q
300	MARK 478	14	42	7.5	+	35	26	23	0.077	-23.4	Q
301	PG 1444+407	14	46	46.0	+	40	35	6	0.267	-25.4	Q
302	Q 1446-0035	14	49	30.5	-	0	47	46	0.254	-22.9	U
303	PG 1448+273	14	51	8.8	+	27	9	27	0.065	-23.0	Q
304	MS 14564+2147	14	58	42.7	+	21	36	10	0.062	-22.1	U
305	MS 15005+2552	15	2	47.3	+	25	40	21	0.191	-22.1	U
306	MARK 841	15	4	1.2	+	10	26	16	0.036	-22.2	Q
307	MARK 840	15	4	8.5	+	14	31	26	0.118	-23.3	U
308	PKS 1509+022	15	12	15.8	+	2	3	16	0.222	-22.2	L
309	MS 15198-0633	15	22	28.8	-	6	44	41	0.084	-23.3	Q
310	LB 9695	15	24	46.4	+	25	43	52	0.55	-23.9	U
311	OR 139	15	25	2.9	+	11	7	44	0.331	-23.6	L
312	QNZ5:02	15	25	6.6	+	2	24	26	0.340	-23.8	U
313	MARK 1098	15	29	40.5	+	30	29	8	0.035	-20.8	U
314	NGC 5940	15	31	18.1	+	7	27	28	0.033	-20.9	Q
315	KUV 15524+2153	15	54	32.7	+	21	43	47	0.285	-24.2	U

Table A.9: observed object list: continued

num	name	RA				dec			z	M_B	radio type
316	MS 16118-0323	16	14	29.0	-	3	31	10	0.298	-23.7	U
317	MARK 877	16	20	11.3	+	17	24	28	0.114	-23.4	Q
318	PG 1634+706	16	34	29.0	+	70	31	33	1.337	-30.3	Q
319	RXS J16446+2619	16	44	42.5	+	26	19	13	0.145	-22.6	U
320	TEX 1652+151	16	54	51.9	+	15	2	57	0.29	-23.3	L
321	2E 1654+3514	16	56	14.0	+	35	10	15	0.80	-26.2	U
322	PKS 1725+044	17	28	24.9	+	4	27	5	0.293	-23.9	L
323	PKS 1739+18C	17	42	7.0	+	18	27	20	0.186	-22.4	L
324	TEX 1750+175	17	52	46.0	+	17	34	21	0.507	-25.9	L
325	OX 169	21	43	35.5	+	17	43	49	0.211	-24.7	L
326	PG 2233+134	22	36	7.7	+	13	43	55	0.325	-24.9	Q
327	PB 5155	22	46	45.7	+	0	36	30	0.973	-26.7	U
328	3C 459.0	23	16	35.2	+	4	5	18	0.220	-23.1	L
329	Q 2350-007B	23	53	21.6	-	0	28	42	0.761	-25.1	U
330	PB 5577	23	53	24.1	+	0	3	57	0.561	-25.3	U
331	Q 2352+0025	23	54	57.1	+	0	42	20	0.271	-23.3	U

A.2 variability of AGN

Table A.10: vriability data of AGN

	name	ΔJ	$\sigma_{\Delta J}$	n_J	ΔH	$\sigma_{\Delta H}$	n_H	$\Delta K'$	$\sigma_{\Delta K'}$	$n_{K'}$	date1	date2
1	PB 5669	——	——	—	0.366	0.126	6	-0.004	0.058	6	961203	980105
5	PB 5853	0.017	0.073	5	——	——	—	-0.511	0.096	8	961203	980121
7	PB 5932	0.048	0.037	10	0.037	0.055	5	0.162	0.105	9	961201	980126
8	MS 00377-0156	0.097	0.063	2	0.088	0.078	8	——	——	—	961203	980106
14	PKS 0130+24	0.315	0.062	11	0.028	0.085	10	0.126	0.072	9	961201	980121
15	UM 341	-0.030	0.082	1	——	——	—	0.031	0.076	1	961201	971227
19	KUV 01507-0744	-0.054	0.065	3	-0.229	0.081	3	0.141	0.066	2	961125	971231
20	PHL 1226	-0.142	0.063	5	-0.004	0.051	4	0.007	0.063	6	961201	980116
21	UM 381	0.027	0.034	3	0.053	0.091	3	-0.054	0.059	4	961208	980104
22	UM 153	0.096	0.033	9	0.100	0.053	9	0.115	0.045	7	961208	980105
23	MARK 1018	0.011	0.022	7	0.061	0.019	5	0.254	0.033	2	960211	980105
24	RXS J02070+2930	-0.041	0.023	7	-0.122	0.033	5	-0.183	0.029	5	960211	980105
25	MARK 586	-0.079	0.024	8	0.448	0.098	6	0.000	0.204	6	960207	980105
26	PKS 0214+10	-0.098	0.030	6	-0.072	0.108	8	-0.078	0.034	7	961208	971227
27	PB 9130	0.544	0.100	1	0.126	0.102	2	0.062	0.106	1	961125	961201
28	B3 0219+443	-0.139	0.050	26	0.148	0.091	21	0.100	0.093	13	961222	980131
32	MS 02328-0400	0.187	0.087	4	0.025	0.070	6	0.218	0.064	4	961221	980116
34	Q 0235+0121	-0.002	0.066	5	0.108	0.075	5	-0.032	0.070	3	961202	980104
35	Q 0238-0142	0.246	0.074	5	0.103	0.064	5	0.109	0.045	5	961208	980217
37	US 3150	-0.259	0.073	5	——	——	—	——	——	—	961125	980106
38	MS 02448+1928	-0.101	0.025	8	-0.056	0.035	6	0.071	0.029	7	961201	971227
42	US 3376	-0.114	0.129	1	——	——	—	——	——	—	961222	970222
44	US 3472	-0.096	0.075	5	-0.090	0.053	4	-0.280	0.059	6	961222	971231
45	S 0257-0027	0.070	0.142	7	-0.336	0.192	7	0.000	0.060	6	970209	980121
50	Q 0305+0222	-0.044	0.062	6	0.156	0.076	6	-0.108	0.074	5	961202	980209
51	PKS 0306+102	——	——	—	——	——	—	0.859	0.083	5	961223	980126
54	MS 03120+1405	-0.030	0.044	8	-0.007	0.085	7	0.127	0.075	7	961209	980129
56	B2 0321+33	0.159	0.015	24	0.197	0.019	19	0.158	0.018	12	960205	980105
59	3C 93.0	-0.126	0.052	9	-0.045	0.058	10	-0.025	0.047	10	970204	980105
61	PKS 0353+027	0.000	0.057	11	0.013	0.059	16	0.060	0.062	13	970122	980116
62	MS 03574+1046	-0.137	0.034	4	-0.361	0.035	7	-0.276	0.032	6	961201	971224
64	MS 04124-0802	-0.123	0.015	6	-0.162	0.030	7	-0.107	0.024	5	960206	971227
65	3C 110	-0.048	0.035	8	-0.063	0.064	5	-0.014	0.061	7	960202	971231
66	PKS 0420-01	0.736	0.079	7	0.677	0.070	6	0.690	0.051	4	961208	971224
67	3C 120	0.044	0.014	14	-0.079	0.018	11	-0.165	0.034	6	960205	971227
68	IRAS 04448-0513	0.053	0.014	9	0.060	0.021	8	0.150	0.043	6	960205	971227
69	Q 0446+0130	——	——	—	——	——	—	0.123	0.085	8	970120	980131
71	UGC 3223	-0.305	0.110	3	-0.058	0.016	9	——	——	—	960206	971227
72	2E 0507+1626	0.007	0.083	1	——	——	—	0.468	0.152	1	960206	971227
73	3C 135.0	-0.035	0.030	18	0.053	0.037	17	0.070	0.042	16	961207	971231
74	AKN 120	-0.177	0.072	22	-0.145	0.011	16	-0.124	0.014	11	960205	980106
75	1E 0514-0030	0.080	0.044	19	0.163	0.048	14	0.011	0.031	18	960211	971224
76	3C 138.0	-0.070	0.067	48	——	——	—	——	——	—	970106	980124
77	3C 147.0	-0.237	0.029	24	-0.168	0.036	25	-0.171	0.039	18	961221	980105
78	4C 16.14	-0.491	0.198	70	——	——	—	——	——	—	961207	980208
79	MCG 08.11.11	-0.483	0.012	59	-0.668	0.011	24	-0.628	0.055	16	960203	980106
81	3C 154.0	0.126	0.032	62	0.212	0.035	61	-0.022	0.030	50	961209	971231
82	MC 0657+176	0.022	0.075	57	——	——	—	0.081	0.097	40	970106	980206

Table A.11: vriability data of AGN: continued

	name	ΔJ	$\sigma_{\Delta J}$	n_J	ΔH	$\sigma_{\Delta H}$	n_H	$\Delta K'$	$\sigma_{\Delta K'}$	$n_{K'}$	date1	date2
83	3C 175.0	0.094	0.029	3	0.205	0.052	12	0.465	0.065	10	961129	980104
84	B2 0709+37	0.315	0.067	17	-0.284	0.040	16	-0.377	0.046	20	960202	980105
85	MARK 376	0.112	0.011	33	0.140	0.012	25	0.383	0.069	15	960203	980105
88	PKS 0736+01	0.100	0.035	20	0.098	0.040	20	-2.699	0.111	1	960131	971218
89	OI 363	-0.210	0.045	19	-0.150	0.076	18	2.187	1.157	3	960131	980106
91	B2 0742+31	-0.225	0.099	18	-0.200	0.102	18	-0.441	0.043	13	960124	971224
93	GC 0742+33	0.070	0.074	19	-0.150	0.073	19	——	——	—	961221	980121
95	RXS J07498+3454	-0.016	0.060	9	0.090	0.069	5	0.149	0.055	6	961203	980105
96	PKS 0748+126	0.461	0.069	13	0.641	0.063	13	0.521	0.050	16	970126	980116
98	B2 0752+25A	-0.055	0.051	6	0.003	0.090	3	-0.182	0.124	2	960131	971231
99	B3 0754+394	0.173	0.146	17	0.126	0.107	5	0.058	0.011	11	960124	980105
101	UGC 4155	-0.086	0.059	14	-0.068	0.013	12	-0.030	0.014	6	960206	971224
102	MARK 1210	-0.150	0.015	25	0.063	0.014	17	-0.030	0.026	15	960205	980105
103	MS 08019+2129	-0.030	0.022	12	-0.032	0.030	6	0.000	0.027	6	960124	971218
104	3C 192.0	-0.144	0.138	3	-0.118	0.139	2	0.020	0.087	1	961203	971218
105	MS 08080+4840	-0.166	0.048	16	-0.147	0.087	14	0.052	0.083	16	961231	980210
109	RX J08166+2941	0.291	0.097	15	——	——	—	0.604	0.107	15	961207	980119
110	3C 197	0.094	0.036	20	0.072	0.105	17	0.044	0.063	16	970126	980126
111	RXS J08223+3305	-0.005	0.038	4	0.061	0.070	4	-0.008	0.042	6	970220	980116
112	KUV 08217+4235	——	——	—	——	——	—	-0.037	0.127	2	961129	971231
113	4C 44.17	0.161	0.049	12	0.347	0.094	14	0.377	0.428	12	970127	980209
115	B2 0827+24	-0.712	0.046	14	-0.302	0.111	13	-0.394	0.049	14	961207	980116
116	PG 0832+251	-0.148	0.032	9	-0.155	0.051	8	-0.075	0.019	9	960124	971224
118	US 1329	-0.541	0.030	10	-0.489	0.044	6	-0.463	0.073	7	960202	971225
119	MARK 1218	-0.094	0.028	2	-0.456	0.128	3	-0.179	0.139	3	960205	971224
122	KUV 08377+4136	-0.516	0.079	10	0.573	0.148	9	——	——	—	961222	980208
123	PG 0844+349	-0.067	0.018	9	-0.023	0.030	6	-0.115	0.059	3	960202	971224
124	55W 179	——	——	—	——	——	—	-0.196	0.179	2	970212	980318
125	CSO 2	-0.034	0.032	6	0.128	0.052	9	0.008	0.044	8	961207	980106
127	LB 8741	0.188	0.057	15	——	——	—	0.188	0.084	8	961207	980124
129	US 1786	——	——	—	0.118	0.111	1	0.127	0.061	8	961222	980121
131	MS 08498+2820	0.001	0.056	7	-0.100	0.064	11	-0.068	0.294	4	970219	980130
132	MS 08502+2825	0.036	0.090	12	0.026	0.094	12	0.089	0.084	10	961202	980129
133	US 1867	-0.258	0.045	7	-0.262	0.059	8	-0.141	0.048	4	960207	971225
135	NGC 2683 U1	0.343	0.303	3	-0.149	0.139	4	0.162	0.085	4	961208	980119
136	LB 8948	-0.023	0.051	7	0.057	0.047	8	0.035	0.023	6	961207	971224
137	LB 8960	0.058	0.054	7	——	——	—	0.294	0.109	7	961207	980130
138	US 2068	-0.149	0.039	4	——	——	—	0.006	0.127	4	961129	980121
139	KUV 09012+4019	-0.005	0.159	5	——	——	—	0.115	0.041	7	970222	980403
140	US 44	-0.045	0.025	9	-0.050	0.027	8	-0.094	0.031	5	970211	971227
141	1E 0906+4254	-0.010	0.049	11	-0.267	0.070	12	0.058	0.081	7	961230	980302
142	4C 05.38	-0.009	0.046	7	-0.133	0.140	6	-0.062	0.042	4	961202	980102
143	MARK 704	0.036	0.025	3	0.048	0.021	3	0.111	0.036	4	960203	971224
144	RXS J09189+3016	-0.185	0.132	10	-0.173	0.075	9	-0.228	0.078	9	970220	980126
146	E 0917+341	-0.053	0.078	2	-0.032	0.073	2	-0.169	0.121	2	970223	980302
148	PG 0923+201	-0.186	0.021	6	-0.257	0.030	4	-0.201	0.088	3	960201	971225
149	MARK 705	0.093	0.019	8	0.503	0.038	13	0.221	0.017	10	960206	971224
150	B2 0923+39	0.020	0.065	3	-0.293	0.106	1	——	——	—	961221	980315

Table A.12: vriability data of AGN: continued

	name	ΔJ	$\sigma_{\Delta J}$	n_J	ΔH	$\sigma_{\Delta H}$	n_H	$\Delta K'$	$\sigma_{\Delta K'}$	$n_{K'}$	date1	date2
152	MS 09309+2128	-1.315	1.016	2	-0.721	0.120	1	-0.473	0.160	1	961130	971227
153	US 737	-0.016	0.034	13	0.167	0.046	13	-0.152	0.031	12	960202	971227
154	MARK 707	——	——	—	0.199	0.047	2	0.120	0.048	3	960203	971224
155	TON 1078	0.033	0.041	5	0.025	0.057	4	0.051	0.087	1	960202	980105
156	PG 0936+396	-0.122	0.064	7	-0.657	0.205	4	-0.398	0.239	3	960202	980212
157	US 822	0.016	0.037	4	0.069	0.056	4	0.016	0.049	5	961209	980126
159	HS 0940+4820	——	——	—	0.117	0.212	4	0.108	0.051	6	961229	980129
160	2E 0944+4629	0.100	0.057	9	-0.043	0.084	8	0.072	0.077	11	970102	980210
161	US 995	0.023	0.038	7	0.077	0.047	4	0.081	0.162	3	960210	971227
162	HS 0946+4845	-0.322	0.049	3	-0.328	0.093	3	0.041	0.086	3	961129	980210
164	US 1107	-0.470	0.044	2	-0.517	0.054	3	-0.673	0.123	2	961129	980116
165	PG 0953+415	-0.128	0.024	7	-0.181	0.032	6	-0.226	0.030	4	960202	971218
166	3C 232	-0.073	0.030	7	-0.054	0.049	4	-0.207	0.045	7	960202	980105
167	NGC 3080	0.122	0.015	14	0.207	0.079	10	0.188	0.061	7	960203	971224
168	IRAS 09595-0755	-0.555	0.018	8	——	——	—	-0.730	0.075	1	960211	971225
170	KUV 10000+3255	0.248	0.272	4	——	——	—	-0.362	0.224	5	961130	980206
172	PG 1001+05	0.015	0.074	8	0.288	0.066	5	0.188	0.029	5	960210	971224
173	PKS 1004+13	0.393	0.153	5	0.026	0.052	4	-0.058	0.035	3	960201	971218
174	RXS J10079+4918	0.205	0.051	3	0.147	0.161	3	0.277	0.130	3	970220	980119
175	TON 488	0.733	0.072	3	——	——	—	——	——	—	960130	960405
177	Q 1008+0058	-0.186	0.244	2	0.026	0.097	1	-0.112	0.137	2	960210	961130
179	TON 1187	-0.050	0.030	8	-0.057	0.038	7	0.037	0.020	9	960130	971224
180	PG 1011-040	0.053	0.021	12	0.139	0.025	11	0.235	0.029	6	960211	971225
181	PKS 1011+23	-0.315	0.043	5	-0.283	0.052	6	-0.298	0.048	6	961208	980121
182	PG 1012+008	-0.014	0.376	8	-0.114	0.038	5	-0.070	0.024	7	960201	971218
190	Q 1047+067	——	——	—	-0.029	0.059	4	0.022	0.039	3	961130	971225
191	MS 10470+3537	0.298	0.082	5	-0.222	0.090	4	-0.081	0.052	4	961229	980116
193	PG 1049-005	0.045	0.043	8	0.002	0.050	9	-0.047	0.034	4	960212	971218
194	MARK 634	0.074	0.073	1	——	——	—	——	——	—	960203	971225
196	RXS J11008+2839	0.095	0.308	3	0.000	0.222	2	0.083	0.078	2	970222	980119
197	MARK 728	0.174	0.039	9	0.062	0.053	4	0.270	0.039	5	960203	971225
198	TOL 1059+105	-0.292	0.037	5	-0.319	0.262	5	-0.329	0.042	7	960205	971227
199	1059.6+0157	——	——	—	——	——	—	-0.043	0.081	5	970103	980206
200	PKS 1103-006	0.032	0.048	7	0.110	0.068	6	-0.074	0.066	5	960212	980105
201	MC 1104+167	-0.815	0.036	8	-0.821	0.057	8	-0.666	0.045	12	960202	980119
204	PG 1115+407	-0.154	0.021	7	-0.015	0.182	8	-0.130	0.074	8	960212	980403
205	PG 1116+215	-0.053	0.026	4	0.041	0.027	4	——	——	—	960202	980106
206	MARK 734	-0.041	0.016	5	-0.013	0.027	6	0.038	0.084	3	960205	971224
210	MARK 423	0.134	0.133	1	——	——	—	——	——	—	960206	980102
211	US 2450	-0.007	0.036	8	-0.094	0.053	7	0.036	0.039	9	970222	980124
212	MARK 1298	-0.174	0.211	5	——	——	—	0.213	0.203	3	960206	980124
213	MARK 1447	0.114	0.038	6	-0.060	0.027	6	-0.083	0.028	6	960205	971224
217	MCG 06.26.012	0.090	0.023	2	——	——	—	0.139	0.107	2	960205	971224
218	MARK 744	-0.142	0.155	2	——	——	—	-0.091	0.186	1	960206	980124
219	WAS 26	-0.086	0.030	9	0.552	0.076	7	-0.050	0.044	5	960202	971218
220	CG 855	-0.234	0.039	3	-0.145	0.105	1	-0.170	0.133	1	960205	980102
222	MC 1146+111	0.090	0.047	7	——	——	—	-0.209	0.139	5	961208	980307
227	GQ COM	-0.244	0.048	7	0.103	0.043	8	0.083	0.027	6	960131	971218

Table A.13: vriability data of AGN: continued

	name	ΔJ	$\sigma_{\Delta J}$	n_J	ΔH	$\sigma_{\Delta H}$	n_H	$\Delta K'$	$\sigma_{\Delta K'}$	$n_{K'}$	date1	date2
228	UGC 7064	-0.393	0.038	8	-0.065	0.022	3	-0.138	0.014	5	960212	980102
230	PG 1211+143	0.158	0.043	4	0.153	0.029	3	0.052	0.012	3	960131	980124
232	PKS 1216-010	-0.335	0.075	8	-0.401	0.104	4	——	——	—	960202	980121
233	MARK 1320	-0.701	0.031	5	-0.551	0.036	5	-0.388	0.066	3	960211	971227
235	Q 1220+0939	0.138	0.070	4	-0.183	0.143	4	——	——	—	961221	980130
236	MS 12209+1601	-0.319	0.029	6	-0.386	0.044	8	-0.201	0.045	6	960206	980121
238	2E 1224+0930	-0.129	0.052	2	-0.021	0.105	1	-0.114	0.226	2	970120	980131
239	3C 273.0	0.320	0.024	5	0.378	0.013	4	0.251	0.256	7	960130	980124
241	TON 1542	-0.031	0.071	5	-0.061	0.067	4	0.028	0.030	4	960206	980102
242	CSO 150	-0.135	0.059	9	——	——	—	-0.009	0.082	4	960130	960221
243	IC 3528	0.126	0.067	5	——	——	—	-1.787	0.222	1	960206	971225
247	WAS 61	-0.598	0.018	5	-0.580	0.071	6	-0.490	0.020	8	960211	980102
248	Q 1240+1546	0.077	0.113	3	0.180	0.102	1	-0.151	0.199	1	960206	980102
249	CBS 63	——	——	—	——	——	—	0.021	0.137	2	970223	980212
250	Q 1240+1746	-0.082	0.076	6	-0.163	0.106	7	-0.319	0.092	6	961231	980318
251	4C 45.26	0.276	0.090	5	——	——	—	0.245	0.133	4	961221	980202
257	3C 281	0.153	0.063	3	-0.033	0.085	3	-0.154	0.109	3	970223	980130
260	CSO 835	-0.172	0.092	2	0.116	0.144	1	——	——	—	970201	970206
262	PG 1309+355	0.020	0.128	4	1.578	0.488	4	0.124	0.114	2	960202	980301
263	RXS J13129+2628	0.090	0.017	9	0.096	0.034	6	0.043	0.030	6	961229	980129
264	Q 1316+0103	-0.131	0.082	7	-0.029	0.088	9	0.028	0.181	9	970130	980210
265	MARK 1347	-0.010	0.013	10	-0.059	0.014	9	-0.048	0.015	7	960206	980126
266	Q 1326-0516	-0.070	0.026	5	-0.005	0.049	5	0.030	0.037	5	960130	980131
267	MS 13285+3135	0.367	0.111	5	0.320	0.169	2	0.363	0.162	2	970220	980124
271	IRAS 13349+2438	-0.079	0.013	7	0.035	0.057	3	0.106	0.079	2	960210	980124
272	Q 1338-0030	0.563	0.949	2	0.144	0.101	1	-0.063	0.103	1	970223	980130
273	TON 730	0.097	0.042	6	0.121	0.044	6	0.388	0.029	6	960206	971218
274	MARK 69	0.023	0.027	5	0.063	0.266	4	——	——	—	960205	980302
276	MARK 662	-0.084	0.099	2	-0.077	0.131	2	——	——	—	960206	980131
278	MARK 463E	0.016	0.015	7	0.066	0.039	5	-0.056	0.129	7	960206	980131
279	PG 1402+261	0.265	0.019	6	0.363	0.048	3	0.285	0.080	2	960210	980126
280	PG 1404+226	-0.097	0.023	6	-0.147	0.034	5	-0.093	0.031	4	960210	980302
281	OQ 208	0.126	0.016	8	0.302	0.058	6	0.128	0.156	1	960206	980126
283	PG 1407+265	-0.055	0.038	5	-0.090	0.038	5	0.123	0.054	5	960131	980212
284	PG 1411+442	-0.108	0.013	5	-0.071	0.014	6	-0.061	0.014	4	960210	980302
285	PG 1415+451	-0.047	0.016	10	-0.059	0.022	10	-0.025	0.031	5	960210	980302
286	NGC 5548	——	——	—	0.100	0.133	1	0.189	0.376	4	960212	980131
287	B 1419+480	-0.175	0.015	11	-0.241	0.019	10	-0.297	0.014	9	960212	980302
290	MARK 471	0.038	0.013	6	0.029	0.055	5	0.021	0.026	4	960212	980302
291	B 1422+231	0.077	0.019	8	0.108	0.033	7	0.072	0.027	5	970219	980301
292	2E 1423+2008	——	——	—	——	——	—	0.003	0.100	1	960210	980102
293	MARK 813	-0.187	0.017	6	-0.216	0.026	6	-0.208	0.104	2	960130	980208
294	B2 1425+26	0.021	0.060	6	0.203	0.338	3	——	——	—	960130	980212
295	MARK 1383	-0.266	0.054	2	-0.081	0.013	3	-0.089	0.038	2	960222	980202
296	MARK 684	-0.426	0.096	14	-0.010	0.016	9	0.028	0.024	5	960206	980126
298	MARK 474	0.059	0.027	12	0.010	0.029	8	0.110	0.028	7	960212	980301
300	MARK 478	-0.090	0.135	14	-0.126	0.013	10	-0.138	0.016	12	960210	980302
301	PG 1444+407	-0.169	0.030	7	-0.026	0.027	8	-0.005	0.024	8	960210	960405

Table A.14: vriability data of AGN: continued

	name	ΔJ	$\sigma_{\Delta J}$	n_J	ΔH	$\sigma_{\Delta H}$	n_H	$\Delta K'$	$\sigma_{\Delta K'}$	$n_{K'}$	date1	date2
302	Q 1446-0035	0.124	0.073	5	0.234	0.069	5	0.050	0.112	3	970206	980315
303	PG 1448+273	-0.074	0.014	13	-0.061	0.017	8	-0.001	0.021	8	960210	980302
304	MS 14564+2147	-0.407	0.025	9	-0.597	0.078	11	-0.657	0.041	6	960212	980302
306	MARK 841	0.363	0.037	6	0.391	0.330	2	——	——	—	960212	980202
308	PKS 1509+022	0.054	0.034	10	0.138	0.052	13	0.063	0.044	9	970224	980315
309	MS 15198-0633	-0.265	0.020	14	-0.194	0.022	11	-0.270	0.018	9	960222	980307
310	LB 9695	-0.284	0.085	11	——	——	—	——	——	—	970130	980317
311	OR 139	-0.086	0.061	7	0.039	0.063	7	0.100	0.091	8	970128	980206
312	QNZ5:02	0.003	0.054	9	0.023	0.070	8	-0.037	0.046	6	970223	980212
313	MARK 1098	-0.100	0.012	13	-0.136	0.015	12	-0.135	0.018	5	960210	980202
314	NGC 5940	-0.153	0.014	14	-0.237	0.139	9	-0.123	0.019	4	960222	980131
315	KUV 15524+2153	-0.082	0.038	11	-0.014	0.038	13	-0.081	0.043	10	970222	980316
318	PG 1634+706	0.074	0.011	9	0.055	0.017	9	——	——	—	970222	980307
319	RXS J16446+2619	-0.042	0.080	8	-0.117	0.055	9	0.127	0.308	8	970211	980316
320	TEX 1652+151	-0.130	0.047	15	0.100	0.093	14	0.041	0.042	13	970220	980316
321	2E 1654+3514	——	——	—	0.215	0.133	8	-0.067	0.108	8	970220	980318
323	PKS 1739+18C	-0.141	0.029	24	0.167	0.031	22	0.095	0.024	13	970224	980307
328	3C 459.0	-0.085	0.063	4	0.248	0.102	5	-0.014	0.062	3	961125	971231
330	PB 5577	-0.192	0.098	5	0.047	0.116	3	-0.079	0.113	3	961202	971227
331	Q 2352+0025	0.052	0.048	8	0.033	0.053	7	0.022	0.035	6	961223	971231

A.3 magnitude of AGN

Table A.15: J,H,K' band magnitude of AGN with 7,10 pix apertuers

	name	J_7	σ_J	H_7	σ_H	K'_7	$\sigma_{K'}$	J_{10}	σ_J	H_{10}	σ_H	K'_{10}	$\sigma_{K'}$	date
1	PB 5669	16.24	0.09	15.45	0.10	14.60	0.08	16.09	0.10	15.29	0.13	14.43	0.10	961203
		—	—	15.81	0.23	14.75	0.10	—	—	15.15	0.19	15.19	0.22	980105
2	Q 2357+019A	16.62	0.12	16.41	0.27	—	—	16.59	0.17	16.21	0.34	—	—	961202
3	PB 5677	16.89	0.11	16.16	0.12	—	—	16.87	0.15	16.27	0.20	—	—	970106
4	PB 5723	15.90	0.08	15.03	0.10	14.07	0.08	15.83	0.11	15.13	0.17	14.34	0.16	961222
5	PB 5853	16.08	0.09	15.31	0.11	14.53	0.10	16.04	0.12	15.18	0.14	14.29	0.13	961203
		15.90	0.08	—	—	14.21	0.04	15.92	0.11	—	—	14.10	0.06	980121
6	Q 0019+0022B	—	—	—	—	16.01	0.26	—	—	—	—	15.80	0.32	961230
7	PB 5932	15.75	0.05	15.16	0.09	14.19	0.08	15.69	0.07	15.26	0.14	14.20	0.13	961201
		15.85	0.06	15.11	0.07	14.21	0.04	15.82	0.08	15.04	0.11	14.12	0.06	980126
8	MS 00377-0156	16.19	0.09	15.34	0.10	14.21	0.06	16.27	0.12	15.43	0.16	14.20	0.09	961203
		16.31	0.10	15.32	0.08	—	—	16.34	0.15	15.18	0.11	—	—	980106
9	Q 0057+0000	15.95	0.07	15.63	0.16	15.30	0.21	15.89	0.10	15.67	0.24	15.29	0.32	961202
10	Q 0058+0218	16.63	0.09	15.83	0.14	14.94	0.10	16.49	0.12	15.27	0.13	14.65	0.12	961202
11	PHL 964	16.85	0.09	15.84	0.10	15.30	0.11	17.11	0.16	15.65	0.12	15.31	0.17	961223
12	Q 0110-0047	17.06	0.11	16.16	0.14	15.30	0.10	17.29	0.20	16.25	0.24	15.21	0.14	970120
13	B2 0110+29	16.33	0.09	15.69	0.14	14.51	0.10	16.19	0.11	16.11	0.30	14.47	0.16	961202
14	PKS 0130+24	16.07	0.06	15.31	0.09	14.47	0.08	16.03	0.09	15.28	0.14	14.44	0.12	961201
		16.17	0.07	15.30	0.07	14.64	0.06	16.18	0.09	15.15	0.09	14.49	0.08	980121
15	UM 341	15.56	0.04	14.83	0.06	13.67	0.04	15.43	0.05	14.86	0.09	13.77	0.07	961201
		15.55	0.06	14.78	0.07	13.61	0.04	15.60	0.10	14.90	0.12	13.52	0.06	971227
16	3C 47.0	16.14	0.05	15.21	0.06	14.27	0.05	16.11	0.06	15.15	0.07	14.29	0.07	961223
17	PHL 1070	14.69	0.06	13.89	0.04	13.10	0.04	14.59	0.05	13.80	0.04	13.03	0.04	961203
18	PHL 1093	15.28	0.05	14.40	0.06	13.62	0.04	15.27	0.06	14.46	0.09	13.69	0.07	961202
19	KUV 01507-0744	15.69	0.08	14.77	0.10	14.07	0.07	15.69	0.13	14.63	0.12	13.99	0.09	971231
20	PHL 1226	15.78	0.05	14.92	0.06	14.08	0.06	15.61	0.06	14.75	0.08	14.05	0.09	961201
		15.72	0.06	14.91	0.06	14.04	0.05	15.56	0.08	14.79	0.08	13.96	0.06	980116
21	UM 381	15.27	0.04	15.01	0.10	14.20	0.08	15.26	0.06	15.09	0.16	14.21	0.13	961208
		15.32	0.06	15.00	0.08	14.06	0.06	15.32	0.07	15.05	0.12	14.03	0.08	980104
22	UM 153	15.34	0.05	14.80	0.08	14.15	0.09	15.36	0.07	14.81	0.12	14.28	0.15	961208
		15.55	0.05	14.98	0.08	14.26	0.05	15.59	0.08	15.08	0.13	14.28	0.08	980105
23	MARK 1018	12.29	0.02	11.45	0.02	11.02	0.01	12.13	0.02	11.28	0.02	10.92	0.02	960211
		12.32	0.03	11.55	0.02	11.04	0.01	12.16	0.04	11.41	0.02	10.90	0.02	980105
24	RXS J02070+2930	14.22	0.03	13.22	0.04	12.62	0.03	14.12	0.04	13.09	0.05	12.62	0.05	960211
		14.12	0.04	13.24	0.04	12.40	0.03	14.04	0.05	13.14	0.06	12.26	0.05	980105
25	MARK 586	14.51	0.06	13.74	0.06	12.67	0.04	14.54	0.08	13.74	0.09	12.64	0.06	960207
		14.30	0.04	13.68	0.06	12.76	0.05	14.22	0.06	13.61	0.09	12.96	0.09	980105
26	PKS 0214+10	14.96	0.04	14.30	0.05	13.59	0.04	14.94	0.06	14.29	0.08	13.52	0.06	961208
		14.95	0.04	14.26	0.04	13.58	0.04	14.91	0.06	14.28	0.07	13.59	0.06	971227
27	PB 9130	14.33	0.01	14.03	0.03	13.45	0.04	13.38	0.01	12.93	0.02	12.61	0.03	961201
28	B3 0219+443	16.17	0.08	15.48	0.12	14.79	0.15	16.33	0.15	15.34	0.16	14.59	0.20	961222
		16.01	0.07	15.80	0.10	14.91	0.06	16.03	0.08	15.81	0.13	14.88	0.08	980131
29	KUV 02292+3227	—	—	—	—	14.05	0.10	—	—	—	—	13.97	0.14	961222
30	MARK 1179	13.08	0.02	12.25	0.02	11.97	0.02	12.91	0.02	12.12	0.02	11.89	0.03	960211
31	NGC 985	12.42	0.03	11.55	0.02	10.83	0.01	12.35	0.04	11.46	0.02	10.78	0.02	980105
32	MS 02328-0400	16.04	0.11	15.49	0.13	14.29	0.09	15.91	0.13	15.73	0.22	14.29	0.13	961221
		16.32	0.10	15.49	0.09	14.37	0.07	16.50	0.18	15.73	0.17	14.28	0.09	980116
33	4C 41.04	15.89	0.07	15.12	0.09	14.42	0.10	15.90	0.10	15.22	0.14	14.24	0.13	961222
34	Q 0235+0121	15.99	0.07	14.87	0.08	14.33	0.09	16.15	0.12	14.82	0.11	14.58	0.17	961202
		15.88	0.08	15.16	0.09	14.02	0.06	15.82	0.10	15.00	0.12	13.89	0.08	980104
35	Q 0238-0142	16.25	0.08	15.21	0.09	14.36	0.09	16.34	0.14	15.11	0.13	14.34	0.14	961208
		16.27	0.08	15.16	0.08	14.12	0.06	16.25	0.12	15.01	0.10	14.04	0.06	980217
36	PB 6856	15.23	0.03	14.71	0.05	14.08	0.06	15.21	0.04	14.58	0.07	14.09	0.10	961201
37	US 3150	15.86	0.06	—	—	14.48	0.06	15.82	0.08	—	—	14.40	0.08	980106
38	MS 02448+1928	15.13	0.03	14.52	0.05	13.33	0.03	15.15	0.04	14.42	0.07	13.40	0.05	961201
		15.07	0.04	14.34	0.05	13.44	0.04	15.06	0.06	14.39	0.08	13.43	0.05	971227
39	Q 0248+0207	—	—	—	—	16.43	0.26	—	—	—	—	16.07	0.28	970102
40	US 3254	15.79	0.05	15.83	0.19	15.02	0.15	15.67	0.07	15.95	0.33	15.08	0.24	961201
41	US 3333	16.47	0.11	15.51	0.10	14.43	0.14	16.80	0.23	15.61	0.17	14.31	0.19	980106
42	US 3376	15.81	0.09	15.28	0.12	—	—	15.84	0.13	15.32	0.19	—	—	961222

Table A.16: J,H,K' band magnitude of AGN with 7,10 pix apertuers: continued

	name	J_{12}	σ_J	H_{12}	σ_H	K'_{12}	$\sigma_{K'}$	J_{15}	σ_J	H_{15}	σ_H	K'_{15}	$\sigma_{K'}$	date
		15.72	0.09	15.38	0.13	—	—	15.72	0.14	15.28	0.17	—	—	970222
43	S 0254+0101	15.51	0.13	14.71	0.10	14.00	0.07	15.43	0.13	14.70	0.10	13.94	0.07	961230
44	US 3472	15.16	0.05	14.56	0.06	13.57	0.06	15.05	0.06	14.62	0.10	13.64	0.09	961222
		15.23	0.04	14.61	0.07	13.54	0.04	15.29	0.07	14.76	0.11	13.50	0.06	971231
45	S 0257-0027	16.33	0.08	15.70	0.12	14.87	0.07	16.23	0.10	16.10	0.25	14.80	0.10	980121
46	Q 0258+0227	17.30	0.21	15.98	0.15	—	—	17.14	0.28	15.67	0.17	—	—	970127
47	US 3543	—	—	—	—	16.14	0.32	—	—	—	—	15.76	0.35	970128
48	Q 0300-0018	16.77	0.12	16.71	0.27	15.14	0.11	16.30	0.12	17.22	0.67	14.92	0.14	970130
49	US 3605	16.16	0.07	15.26	0.10	14.71	0.12	16.18	0.11	15.54	0.20	14.62	0.17	961208
50	Q 0305+0222	16.31	0.07	15.31	0.09	14.87	0.09	15.99	0.08	14.92	0.09	14.44	0.09	961202
		16.26	0.13	15.68	0.09	14.89	0.08	15.91	0.13	15.45	0.11	14.58	0.10	980209
51	PKS 0306+102	16.92	0.10	—	—	15.14	0.11	16.71	0.12	—	—	15.17	0.16	961223
		—	—	17.10	0.23	16.21	0.18	—	—	17.52	0.53	16.49	0.35	980126
52	Q 0307-0015	16.54	0.10	15.55	0.14	14.73	0.12	16.66	0.18	15.12	0.15	14.41	0.14	961208
53	PKS 0310+013	—	—	—	—	15.30	0.11	—	—	—	—	15.36	0.18	970126
54	MS 03120+1405	16.50	0.11	15.71	0.14	15.49	0.19	16.69	0.17	15.36	0.16	15.45	0.28	961209
		16.30	0.05	16.02	0.08	15.36	0.09	16.28	0.08	16.03	0.13	15.27	0.13	980129
55	Q 0313+0126	17.15	0.14	—	—	—	—	17.02	0.19	—	—	—	—	970130
56	B2 0321+33	13.46	0.07	12.58	0.03	11.85	0.02	13.39	0.10	12.54	0.05	11.83	0.02	960205
		13.57	0.03	12.74	0.03	11.97	0.02	13.50	0.04	12.65	0.04	11.91	0.04	980105
57	PKS 0336-01	15.76	0.07	14.86	0.07	—	—	15.72	0.09	14.88	0.11	—	—	970224
58	KUV 03399-0014	15.99	0.07	15.26	0.10	14.73	0.12	15.91	0.10	15.03	0.13	14.70	0.18	961208
59	3C 93.0	16.14	0.06	15.15	0.06	14.38	0.06	16.10	0.08	15.05	0.08	14.27	0.08	970204
		16.32	0.09	15.13	0.08	14.36	0.06	16.31	0.14	14.99	0.10	14.31	0.08	980105
60	MS 03419+0451	16.82	0.10	16.06	0.13	15.80	0.16	16.80	0.14	15.84	0.17	15.70	0.23	970201
61	PKS 0353+027	16.57	0.06	15.67	0.07	15.06	0.07	16.51	0.07	15.51	0.09	15.08	0.10	970122
		16.59	0.10	15.55	0.08	15.09	0.10	16.66	0.17	15.54	0.12	15.14	0.16	980116
62	MS 03574+1046	14.90	0.02	14.10	0.03	13.10	0.03	14.95	0.03	14.11	0.05	13.08	0.04	961201
		14.79	0.06	13.87	0.06	12.92	0.03	14.75	0.08	13.93	0.08	12.91	0.05	971224
63	3C 109.0	14.61	0.02	13.55	0.03	12.43	0.02	14.62	0.03	13.53	0.03	12.42	0.02	970219
64	MS 04124-0802	12.97	0.02	12.12	0.04	11.19	0.02	12.93	0.01	12.08	0.03	11.18	0.01	960206
		12.82	0.01	11.90	0.01	11.04	0.01	12.78	0.02	11.90	0.03	11.02	0.02	971227
65	3C 110	15.11	0.06	14.68	0.10	14.28	0.14	15.14	0.09	14.48	0.13	14.46	0.26	960202
		15.01	0.04	14.86	0.09	13.96	0.06	14.97	0.06	14.83	0.12	13.92	0.08	971231
66	PKS 0420-01	15.11	0.03	14.29	0.05	13.31	0.03	15.18	0.05	14.40	0.08	13.24	0.04	961208
		16.30	0.22	15.40	0.21	14.25	0.11	16.96	0.62	15.46	0.34	14.20	0.17	971224
67	3C 120	12.28	0.07	11.33	0.03	10.43	0.02	12.18	0.10	11.25	0.05	10.38	0.01	960205
		12.32	0.01	11.29	0.01	10.31	0.01	12.23	0.01	11.21	0.02	10.28	0.01	971227
68	IRAS 04448-0513	13.09	0.07	12.19	0.03	11.56	0.02	12.99	0.10	12.13	0.05	11.55	0.02	960205
		13.11	0.01	12.25	0.02	11.73	0.02	13.03	0.02	12.17	0.03	11.69	0.03	971227
69	Q 0446+0130	16.80	0.08	16.35	0.12	15.31	0.10	16.81	0.12	16.06	0.15	15.23	0.15	970120
		—	—	—	—	15.46	0.09	—	—	—	—	15.48	0.13	980131
70	NGC 1685	12.93	0.05	12.17	0.02	11.87	0.02	12.75	0.05	11.98	0.02	11.70	0.02	960212
71	UGC 3223	12.24	0.02	11.48	0.04	11.14	0.02	11.97	0.01	11.20	0.02	10.90	0.01	960206
		12.18	0.01	11.38	0.01	10.92	0.01	11.91	0.01	11.14	0.02	10.70	0.02	971227
72	2E 0507+1626	12.79	0.02	11.89	0.04	11.11	0.02	12.66	0.01	11.78	0.02	11.07	0.01	960206
		12.76	0.01	11.92	0.02	11.12	0.02	12.66	0.02	11.82	0.03	11.05	0.02	971227
73	3C 135.0	15.09	0.10	14.28	0.09	13.61	0.06	15.07	0.10	14.16	0.09	13.45	0.07	961207
		14.99	0.03	14.28	0.05	13.83	0.04	14.96	0.05	14.23	0.06	13.79	0.06	971231
74	AKN 120	11.84	0.07	10.93	0.03	10.13	0.02	11.75	0.10	10.87	0.05	10.08	0.01	960205
		11.71	0.02	10.84	0.01	10.08	0.01	11.63	0.02	10.78	0.02	10.04	0.02	980106
75	1E 0514-0030	15.03	0.06	14.14	0.07	13.09	0.05	15.18	0.10	13.99	0.10	13.08	0.07	960211
		15.28	0.08	14.46	0.08	13.22	0.04	15.31	0.13	14.57	0.14	13.30	0.07	971224
76	3C 138.0	17.05	0.11	—	—	15.37	0.11	16.86	0.14	—	—	15.38	0.16	970106
		17.07	0.11	16.38	0.12	15.53	0.09	17.01	0.13	16.60	0.23	15.50	0.13	980124
77	3C 147.0	15.39	0.07	14.68	0.07	14.09	0.06	15.40	0.08	14.76	0.09	14.08	0.09	961221
		15.47	0.05	14.67	0.05	14.13	0.05	15.56	0.08	14.63	0.07	14.09	0.08	980105
78	4C 16.14	18.25	0.62	—	—	—	—	18.85	1.67	—	—	—	—	961207
		16.87	0.14	16.30	0.16	15.90	0.18	16.17	0.11	15.93	0.17	15.64	0.21	980208
79	MCG 08.11.11	11.85	0.04	11.02	0.04	10.30	0.02	11.65	0.04	10.84	0.04	10.19	0.02	960203

Table A.17: J,H,K' band magnitude of AGN with 7,10 pix apertuers: continued

	name	J_{12}	σ_J	H_{12}	σ_H	K'_{12}	$\sigma_{K'}$	J_{15}	σ_J	H_{15}	σ_H	K'_{15}	$\sigma_{K'}$	date
		11.63	0.03	10.64	0.01	9.76	0.01	11.47	0.02	10.53	0.02	9.69	0.02	980106
80	OH-010	13.34	0.04	12.68	0.02	12.39	0.03	13.33	0.02	12.66	0.02	12.36	0.02	970125
81	3C 154.0	15.43	0.07	14.56	0.09	14.03	0.05	15.45	0.09	14.60	0.11	14.00	0.07	961209
		15.32	0.06	14.44	0.06	13.74	0.05	15.41	0.09	14.47	0.08	13.74	0.07	971231
82	MC 0657+176	17.15	0.11	—	—	15.44	0.13	17.03	0.15	—	—	15.22	0.16	970106
		17.62	0.19	16.65	0.14	15.84	0.16	18.36	0.54	16.59	0.20	15.92	0.26	980206
83	3C 175.0	14.42	0.04	14.09	0.05	13.66	0.07	13.74	0.03	13.30	0.05	12.99	0.06	961129
		14.24	0.05	13.80	0.04	13.39	0.04	13.59	0.04	13.17	0.03	12.86	0.03	980104
84	B2 0709+37	14.81	0.05	14.44	0.07	14.07	0.09	14.78	0.07	14.49	0.11	14.27	0.16	960202
		14.95	0.05	14.34	0.05	13.97	0.06	14.94	0.07	14.23	0.07	14.09	0.10	980105
85	MARK 376	12.64	0.04	11.69	0.04	10.70	0.02	12.56	0.04	11.65	0.04	10.67	0.02	960203
		12.79	0.03	11.85	0.02	10.90	0.01	12.71	0.04	11.80	0.02	10.88	0.02	980105
86	B3 0729+391	—	—	16.67	0.19	15.41	0.12	—	—	16.65	0.29	15.19	0.15	970130
87	S4 0731+47	15.92	0.09	15.85	0.11	15.32	0.13	15.77	0.09	15.85	0.16	15.55	0.24	970128
88	PKS 0736+01	14.49	0.11	13.64	0.09	14.03	0.12	14.37	0.10	13.54	0.08	13.80	0.13	960131
		—	—	13.77	0.07	12.72	0.04	—	—	13.83	0.09	12.67	0.05	971218
89	OI 363	15.76	0.13	15.02	0.16	13.83	0.11	15.86	0.17	15.06	0.23	13.72	0.12	960131
		15.31	0.04	14.81	0.05	14.07	0.04	15.25	0.05	14.76	0.07	14.10	0.07	980106
90	MARK 79	11.86	0.22	11.18	0.01	10.34	0.01	11.68	0.23	11.08	0.01	10.27	0.02	971225
91	B2 0742+31	14.61	0.05	13.88	0.05	13.06	0.03	14.59	0.05	13.83	0.05	13.10	0.04	960124
		14.62	0.05	13.83	0.05	13.04	0.04	14.72	0.08	13.92	0.08	13.10	0.06	971224
92	PKS 0743-006	14.69	0.04	14.29	0.07	13.89	0.06	12.92	0.04	12.50	0.05	12.11	0.02	961202
93	GC 0742+33	17.00	0.14	15.66	0.11	14.86	0.12	16.87	0.19	15.56	0.14	14.80	0.16	961221
		17.11	0.10	15.77	0.07	—	—	17.00	0.13	15.61	0.09	—	—	980121
94	RXS J07491+2842	16.27	0.07	15.19	0.08	14.30	0.07	16.40	0.12	15.11	0.11	14.31	0.11	961208
95	RXS J07498+3454	14.93	0.06	14.41	0.06	13.49	0.05	14.85	0.06	14.34	0.08	13.43	0.07	961203
		14.96	0.04	14.25	0.05	13.42	0.03	14.87	0.06	14.19	0.07	13.44	0.05	980105
96	PKS 0748+126	15.73	0.03	15.14	0.05	14.35	0.05	15.75	0.05	15.19	0.08	14.34	0.07	970126
		16.23	0.10	15.61	0.11	14.84	0.09	16.35	0.16	15.57	0.16	14.79	0.14	980116
97	MARK 382	13.30	0.04	12.59	0.04	12.15	0.02	13.16	0.04	12.46	0.04	12.02	0.03	960203
98	B2 0752+25A	15.55	0.12	14.81	0.13	13.80	0.11	15.52	0.13	14.79	0.17	13.83	0.13	960131
		15.50	0.06	14.87	0.07	14.05	0.06	15.51	0.09	15.00	0.11	13.98	0.09	971231
99	B3 0754+394	12.88	0.05	12.01	0.04	11.03	0.01	12.86	0.04	11.99	0.03	11.03	0.01	960124
		13.00	0.03	12.10	0.02	11.08	0.01	12.99	0.04	12.10	0.03	11.06	0.02	980105
100	KUV 07549+4228	14.75	0.22	14.21	0.09	13.01	0.03	14.85	0.25	14.15	0.13	12.99	0.05	971225
101	UGC 4155	12.12	0.02	11.40	0.04	11.03	0.02	11.94	0.01	11.23	0.02	10.88	0.01	960206
		12.19	0.04	11.41	0.02	10.99	0.01	12.01	0.04	11.24	0.02	10.84	0.02	971224
102	MARK 1210	12.29	0.07	11.57	0.03	11.15	0.02	12.07	0.10	11.36	0.05	10.99	0.01	960205
		12.33	0.03	11.58	0.02	11.14	0.01	12.10	0.04	11.38	0.02	10.96	0.02	980105
103	MS 08019+2129	14.26	0.05	13.49	0.04	12.66	0.02	14.16	0.04	13.43	0.04	12.58	0.03	960124
		14.18	0.06	13.48	0.05	12.77	0.04	14.08	0.07	13.42	0.06	12.77	0.06	971218
104	3C 192.0	13.63	0.05	12.92	0.03	12.56	0.03	13.54	0.04	12.80	0.03	12.48	0.03	961203
		13.62	0.06	12.94	0.05	12.52	0.03	13.50	0.07	12.78	0.05	12.43	0.04	971218
105	MS 08080+4840	16.78	0.08	16.48	0.18	15.57	0.15	16.93	0.12	16.51	0.28	15.44	0.22	961231
		16.65	0.08	16.19	0.10	15.62	0.10	16.63	0.11	16.12	0.14	15.57	0.15	980210
106	3C 196.0	15.69	0.04	15.45	0.07	14.86	0.06	15.59	0.06	15.37	0.09	14.73	0.09	970201
107	B2 0810+32	17.46	0.16	—	—	15.97	0.23	17.37	0.23	—	—	15.54	0.24	970127
108	PKS 0812+02	15.37	0.10	14.73	0.10	13.94	0.07	15.21	0.10	14.57	0.11	13.92	0.09	961207
109	RX J08166+2941	16.32	0.13	15.66	0.18	14.55	0.11	16.43	0.18	15.97	0.35	14.39	0.15	961207
		16.69	0.14	—	—	14.86	0.11	16.99	0.26	—	—	14.98	0.19	980119
110	3C 197	16.01	0.04	15.98	0.10	15.16	0.10	15.92	0.05	16.13	0.18	14.99	0.13	970126
		16.13	0.04	15.77	0.07	15.04	0.06	16.09	0.06	15.50	0.08	14.91	0.08	980126
111	RXS J08223+3305	15.68	0.10	14.89	0.08	14.20	0.06	15.76	0.12	14.92	0.11	14.14	0.09	970220
		15.56	0.05	15.02	0.06	14.31	0.06	15.62	0.08	15.07	0.10	14.32	0.09	980116
112	KUV 08217+4235	15.16	0.04	14.40	0.06	13.72	0.06	15.11	0.06	14.35	0.08	13.70	0.09	961129
		14.91	0.04	14.24	0.06	13.57	0.05	14.87	0.06	14.19	0.07	13.63	0.08	971231
113	4C 44.17	16.43	0.07	16.25	0.14	15.62	0.16	16.48	0.11	16.14	0.20	15.56	0.23	970127
		16.92	0.15	16.40	0.12	15.97	0.16	17.16	0.22	16.38	0.18	16.08	0.26	980209
114	KUV 08267+4027	15.89	0.07	15.49	0.13	15.02	0.18	15.83	0.10	15.58	0.22	14.71	0.20	961129
115	B2 0827+24	15.89	0.11	15.30	0.13	14.35	0.09	15.90	0.13	14.95	0.14	14.20	0.12	961207

Table A.18: J,H,K' band magnitude of AGN with 7,10 pix apertuers: continued

	name	J_{12}	σ_J	H_{12}	σ_H	K'_{12}	$\sigma_{K'}$	J_{15}	σ_J	H_{15}	σ_H	K'_{15}	$\sigma_{K'}$	date
		15.48	0.05	14.79	0.04	14.09	0.05	15.47	0.07	14.77	0.06	14.16	0.07	980116
116	PG 0832+251	14.59	0.05	13.82	0.05	12.68	0.02	14.56	0.04	13.78	0.05	12.69	0.03	960124
		14.32	0.05	13.67	0.05	12.65	0.03	14.27	0.06	13.79	0.08	12.71	0.04	971224
117	OJ 256	—	—	—	—	16.38	0.20	—	—	—	—	15.95	0.22	970120
118	US 1329	14.73	0.05	14.09	0.05	13.33	0.04	14.68	0.06	14.01	0.07	13.17	0.06	960202
		14.47	0.22	14.01	0.07	13.24	0.04	14.44	0.24	13.96	0.10	13.14	0.06	971225
119	MARK 1218	12.28	0.07	11.57	0.03	11.16	0.02	12.04	0.10	11.35	0.05	10.98	0.01	960205
		12.30	0.04	11.51	0.03	11.02	0.02	12.10	0.04	11.33	0.02	10.87	0.03	971224
120	Q 0835+4744	—	—	—	—	15.69	0.11	—	—	—	—	15.60	0.16	970102
121	3C 207.0	16.51	0.06	15.68	0.09	15.09	0.09	16.52	0.09	15.45	0.10	15.11	0.13	961223
122	KUV 08377+4136	16.32	0.10	16.06	0.21	—	—	16.07	0.12	16.36	0.44	—	—	961222
		16.24	0.05	15.82	0.07	14.91	0.08	16.05	0.06	15.58	0.08	14.73	0.10	980208
123	PG 0844+349	13.26	0.04	12.61	0.02	11.95	0.02	13.22	0.04	12.58	0.03	11.92	0.03	960202
		13.34	0.04	12.61	0.03	11.88	0.03	13.31	0.05	12.59	0.04	11.82	0.05	971224
124	55W 179	—	—	—	—	16.06	0.15	—	—	—	—	14.73	0.07	970212
		17.00	0.17	16.60	0.24	15.77	0.26	15.21	0.07	14.74	0.09	14.55	0.13	980318
125	CSO 2	15.36	0.10	15.27	0.12	13.97	0.07	15.34	0.10	15.32	0.17	13.86	0.09	961207
		15.47	0.04	15.12	0.05	14.16	0.05	15.31	0.05	14.97	0.07	14.07	0.08	980106
126	US 1742	16.62	0.11	16.17	0.21	15.14	0.15	16.91	0.22	16.40	0.39	15.09	0.23	961202
127	LB 8741	16.74	0.15	—	—	15.01	0.16	16.80	0.21	—	—	15.27	0.30	961207
		16.64	0.09	15.98	0.10	15.04	0.06	16.70	0.12	16.08	0.16	14.95	0.09	980124
128	MS 08475+2813	16.76	0.11	16.04	0.19	14.97	0.11	16.85	0.17	15.75	0.23	14.91	0.16	961209
129	US 1786	—	—	15.51	0.12	14.37	0.10	—	—	15.48	0.18	14.42	0.16	961222
		16.33	0.11	15.65	0.08	14.46	0.04	16.08	0.13	15.77	0.13	14.41	0.06	980121
130	MS 08495+0805	13.58	0.03	12.82	0.03	12.21	0.03	13.46	0.03	12.70	0.03	12.16	0.04	960211
131	MS 08498+2820	16.86	0.08	15.99	0.10	15.60	0.11	16.68	0.10	16.01	0.16	15.71	0.19	970219
		16.67	0.08	15.93	0.08	15.60	0.12	16.67	0.12	15.88	0.11	15.76	0.21	980130
132	MS 08502+2825	16.61	0.09	15.97	0.16	15.57	0.17	16.79	0.16	15.75	0.20	15.80	0.32	961202
		16.80	0.07	16.08	0.09	15.71	0.10	16.81	0.10	16.09	0.13	16.06	0.21	980129
133	US 1867	15.25	0.07	14.55	0.09	13.54	0.07	14.97	0.08	14.30	0.11	13.39	0.10	960207
		15.08	0.23	14.51	0.07	13.61	0.04	14.91	0.25	14.44	0.11	13.41	0.06	971225
134	MARK 391	12.05	0.02	11.34	0.04	11.01	0.02	11.85	0.01	11.15	0.02	10.83	0.01	960206
135	NGC 2683 U1	16.60	0.10	16.20	0.19	15.04	0.13	16.52	0.14	16.15	0.27	14.89	0.18	961208
		17.00	0.17	15.72	0.14	15.02	0.11	17.05	0.25	15.51	0.17	15.17	0.19	980119
136	LB 8948	15.50	0.10	14.30	0.09	13.01	0.05	15.40	0.10	14.26	0.09	13.00	0.06	961207
		15.71	0.12	14.35	0.10	13.12	0.04	16.04	0.24	14.37	0.15	13.11	0.06	971224
137	LB 8960	16.15	0.12	—	—	14.90	0.16	16.04	0.13	—	—	14.52	0.17	961207
		16.36	0.07	15.77	0.07	15.16	0.08	16.39	0.09	15.71	0.11	15.14	0.12	980130
138	US 2068	16.03	0.08	—	—	14.67	0.14	16.06	0.12	—	—	14.49	0.18	961129
		15.83	0.05	15.47	0.08	14.70	0.05	15.85	0.07	15.33	0.10	14.62	0.07	980121
139	KUV 09012+4019	16.04	0.09	15.12	0.10	13.89	0.06	16.34	0.18	15.18	0.17	13.85	0.09	970222
		16.19	0.07	15.09	0.05	14.22	0.05	16.20	0.10	15.11	0.08	14.19	0.07	980403
140	US 44	14.57	0.04	13.96	0.04	13.21	0.04	14.02	0.03	13.42	0.03	12.79	0.04	970211
		14.63	0.03	13.93	0.04	13.15	0.03	14.01	0.03	13.43	0.04	12.82	0.03	971227
141	1E 0906+4254	16.46	0.15	15.57	0.12	14.68	0.09	16.35	0.16	15.29	0.13	14.47	0.11	961230
		16.45	0.06	15.56	0.06	14.98	0.06	16.33	0.08	15.40	0.08	15.12	0.10	980302
142	4C 05.38	15.28	0.05	14.81	0.08	13.72	0.04	15.13	0.06	14.73	0.11	13.67	0.06	961202
		15.50	0.08	14.86	0.09	13.84	0.06	15.60	0.13	15.27	0.21	14.02	0.11	980102
143	MARK 704	12.28	0.04	11.36	0.04	10.49	0.02	12.16	0.04	11.27	0.04	10.43	0.02	960203
		12.46	0.04	11.50	0.03	10.64	0.01	12.33	0.04	11.39	0.02	10.58	0.03	971224
144	RXS J09189+3016	16.00	0.11	15.35	0.11	14.92	0.11	15.90	0.13	15.30	0.16	15.07	0.19	970220
		15.87	0.06	15.12	0.09	14.80	0.08	15.75	0.09	14.96	0.12	14.96	0.15	980126
145	RX J09190+3502B	17.31	0.18	17.37	0.52	—	—	17.40	0.28	17.47	0.88	—	—	961203
146	E 0917+341	16.41	0.09	15.69	0.12	15.37	0.14	16.29	0.13	15.44	0.15	15.43	0.22	970223
		16.42	0.07	15.68	0.08	14.94	0.06	16.36	0.10	15.61	0.11	14.89	0.09	980302
147	RX J09249+2527	16.14	0.09	15.17	0.11	14.41	0.05	16.12	0.11	15.21	0.16	14.35	0.07	961209
148	PG 0923+201	14.19	0.03	13.32	0.03	12.22	0.03	14.06	0.03	13.19	0.04	12.17	0.03	960201
		13.85	0.22	13.21	0.04	12.11	0.02	13.70	0.24	13.10	0.05	12.09	0.04	971225
149	MARK 705	12.42	0.02	11.55	0.04	10.93	0.02	12.35	0.03	11.49	0.02	10.89	0.01	960206
		12.53	0.04	11.70	0.03	11.10	0.02	12.44	0.04	11.61	0.03	11.08	0.03	971224

Table A.19: J,H,K' band magnitude of AGN with 7,10 pix apertuers: continued

	name	J_{12}	σ_J	H_{12}	σ_H	K'_{12}	$\sigma_{K'}$	J_{15}	σ_J	H_{15}	σ_H	K'_{15}	$\sigma_{K'}$	date
150	B2 0923+39	15.22	0.07	14.93	0.09	13.95	0.06	13.80	0.07	13.58	0.07	13.33	0.05	961221
		15.09	0.04	14.53	0.06	—	—	13.65	0.03	13.25	0.03	—	—	980315
151	RX J09273+3045	17.06	0.13	16.57	0.19	15.71	0.19	16.98	0.18	16.32	0.24	15.28	0.20	961208
152	MS 09309+2128	14.55	0.03	13.91	0.04	13.03	0.03	14.57	0.05	13.86	0.06	12.88	0.05	961130
		14.52	0.02	13.70	0.03	13.06	0.03	14.49	0.04	13.63	0.04	13.02	0.04	971227
153	US 737	15.24	0.06	14.25	0.06	13.65	0.06	15.17	0.08	14.21	0.09	13.70	0.09	960202
		15.13	0.05	14.46	0.07	13.41	0.03	15.08	0.07	14.35	0.09	13.36	0.05	971227
154	MARK 707	—	—	13.29	0.04	12.72	0.03	—	—	13.18	0.05	12.69	0.04	960203
		14.14	0.05	13.53	0.05	12.80	0.04	14.02	0.05	13.43	0.07	12.65	0.05	971224
155	TON 1078	15.00	0.06	14.93	0.11	13.77	0.07	14.96	0.08	15.02	0.19	13.60	0.09	960202
		15.05	0.05	14.70	0.07	14.10	0.06	15.06	0.07	14.58	0.10	14.11	0.10	980105
156	PG 0936+396	16.10	0.11	15.60	0.17	14.96	0.18	16.07	0.16	15.26	0.19	15.20	0.35	960202
		16.22	0.06	15.90	0.11	14.64	0.08	16.07	0.08	16.18	0.22	14.57	0.11	980212
157	US 822	16.26	0.09	15.54	0.11	15.03	0.10	16.26	0.11	15.41	0.14	15.28	0.20	961209
		16.23	0.05	15.65	0.07	15.03	0.06	16.24	0.07	15.65	0.10	15.08	0.09	980126
158	MS 09398+0952	16.60	0.07	15.55	0.08	15.02	0.07	16.50	0.09	15.46	0.11	15.01	0.11	970131
159	HS 0940+4820	16.79	0.13	15.95	0.19	14.85	0.07	16.61	0.14	15.65	0.21	14.69	0.09	961229
		17.04	0.08	16.58	0.19	15.12	0.06	16.79	0.10	16.43	0.26	15.06	0.08	980129
160	2E 0944+4629	16.38	0.04	15.95	0.09	15.41	0.11	15.53	0.03	15.04	0.06	14.60	0.08	970102
		16.59	0.08	15.93	0.08	15.39	0.08	15.64	0.06	14.97	0.06	14.71	0.07	980210
161	US 995	15.14	0.04	14.21	0.05	13.57	0.06	15.22	0.06	14.08	0.07	13.57	0.09	960210
		15.24	0.05	14.51	0.06	13.79	0.05	15.22	0.08	14.61	0.11	13.88	0.09	971227
162	HS 0946+4845	16.32	0.10	15.44	0.12	14.55	0.13	16.63	0.21	15.27	0.16	14.74	0.24	961129
		16.17	0.07	15.40	0.06	14.98	0.07	16.22	0.08	15.35	0.08	15.38	0.15	980210
163	MARK 1239	11.90	0.05	10.61	0.02	9.49	0.01	11.86	0.05	10.60	0.01	9.48	0.01	960212
164	US 1107	15.59	0.06	14.78	0.07	13.97	0.08	15.50	0.08	14.89	0.12	14.13	0.13	961129
		15.33	0.05	14.63	0.05	13.91	0.04	15.19	0.06	14.70	0.09	13.89	0.06	980116
165	PG 0953+415	14.36	0.04	13.64	0.04	12.72	0.03	14.36	0.05	13.62	0.05	12.75	0.05	960202
		14.25	0.07	13.52	0.06	12.48	0.03	14.29	0.08	13.39	0.06	12.34	0.04	971218
166	3C 232	14.96	0.05	14.38	0.07	13.89	0.08	14.97	0.07	14.38	0.10	13.76	0.10	960202
		14.93	0.04	14.27	0.05	13.71	0.04	15.05	0.07	14.20	0.07	13.66	0.06	980105
167	NGC 3080	12.92	0.04	12.20	0.04	11.70	0.02	12.72	0.04	12.03	0.04	11.54	0.02	960203
		13.00	0.04	12.29	0.03	11.79	0.02	12.79	0.04	12.10	0.03	11.61	0.04	971224
168	IRAS 09595-0755	13.35	0.02	12.56	0.02	12.14	0.02	13.06	0.03	12.29	0.03	11.89	0.03	960211
		13.25	0.22	12.53	0.03	11.84	0.02	13.00	0.23	12.30	0.03	11.60	0.04	971225
169	KUV 09597+3343	—	—	16.03	0.23	15.39	0.26	—	—	15.65	0.24	15.48	0.44	970222
170	KUV 10000+3255	16.32	0.13	—	—	15.13	0.22	16.19	0.17	—	—	14.74	0.24	961130
		16.37	0.09	16.02	0.08	15.23	0.08	16.49	0.13	16.00	0.12	15.19	0.11	980206
171	TON 28	14.63	0.04	13.94	0.04	12.90	0.03	14.57	0.06	13.95	0.07	12.92	0.04	960202
172	PG 1001+05	15.34	0.04	14.35	0.06	13.11	0.04	15.35	0.07	14.31	0.09	13.05	0.06	960210
		15.39	0.10	14.84	0.14	13.30	0.04	15.52	0.17	14.83	0.21	13.27	0.07	971224
173	PKS 1004+13	13.90	0.03	13.48	0.03	12.78	0.04	13.90	0.03	13.45	0.04	12.77	0.05	960201
		14.23	0.07	13.57	0.05	12.62	0.03	14.33	0.09	13.52	0.06	12.62	0.05	971218
174	RXS J10079+4918	15.54	0.09	14.79	0.06	14.22	0.05	15.50	0.09	14.92	0.09	14.22	0.08	970220
		15.79	0.07	15.08	0.07	14.66	0.09	15.78	0.08	15.05	0.09	14.57	0.12	980119
175	TON 488	15.38	0.11	14.53	0.12	13.91	0.11	15.34	0.12	14.58	0.16	13.87	0.13	960130
		15.65	0.07	14.74	0.07	14.10	0.09	15.67	0.08	14.71	0.09	14.05	0.12	960405
176	4C 41.21	15.60	0.07	—	—	13.96	0.08	15.56	0.10	—	—	13.77	0.10	961130
177	Q 1008+0058	14.62	0.03	13.88	0.04	12.94	0.04	14.55	0.04	13.72	0.05	12.90	0.05	960210
		14.81	0.03	13.99	0.05	12.97	0.03	14.68	0.05	14.09	0.08	12.94	0.05	961130
178	CSO 37	17.14	0.19	16.11	0.23	—	—	17.02	0.26	16.25	0.39	—	—	961202
179	TON 1187	14.11	0.10	13.45	0.07	12.63	0.08	14.13	0.09	13.45	0.08	12.64	0.07	960130
		14.21	0.05	13.56	0.05	12.60	0.03	14.29	0.07	13.61	0.08	12.60	0.04	971224
180	PG 1011-040	13.48	0.02	12.74	0.02	12.15	0.02	13.38	0.03	12.61	0.03	12.14	0.04	960211
		13.41	0.22	12.93	0.03	12.21	0.03	13.27	0.24	12.88	0.04	12.11	0.05	971225
181	PKS 1011+23	15.14	0.03	14.54	0.04	14.24	0.05	12.81	0.02	12.24	0.03	12.13	0.01	961208
		14.65	0.04	14.51	0.05	13.89	0.03	12.75	0.04	12.42	0.02	12.18	0.01	980121
182	PG 1012+008	14.24	0.03	13.51	0.03	12.55	0.04	14.22	0.03	13.44	0.04	12.46	0.04	960201
		14.20	0.06	13.54	0.06	12.55	0.03	14.20	0.08	13.52	0.08	12.54	0.04	971218
183	Q 1013+0124	15.50	0.08	14.88	0.14	14.49	0.18	15.40	0.11	14.48	0.15	14.65	0.31	961130

Table A.20: J,H,K' band magnitude of AGN with 7,10 pix apertuers: continued

	name	J_{12}	σ_J	H_{12}	σ_H	K'_{12}	$\sigma_{K'}$	J_{15}	σ_J	H_{15}	σ_H	K'_{15}	$\sigma_{K'}$	date
184	MARK 720	13.23	0.04	12.55	0.04	12.20	0.02	13.10	0.04	12.43	0.04	12.06	0.03	960203
185	Q 1015-0121	16.22	0.09	15.29	0.08	14.92	0.10	16.17	0.13	15.03	0.09	14.77	0.13	961231
186	PG 1016+336	13.33	0.02	12.49	0.04	11.93	0.02	13.19	0.01	12.37	0.03	11.88	0.02	960206
187	MS 10182+2010	16.68	0.09	16.09	0.10	15.25	0.09	16.69	0.14	16.31	0.20	15.57	0.20	970224
188	B2 1028+31	14.66	0.03	13.83	0.04	13.15	0.04	14.64	0.04	13.71	0.05	13.18	0.06	961130
189	MS 10461+1411	16.16	0.07	15.25	0.05	14.73	0.06	16.19	0.10	15.20	0.07	14.87	0.11	970224
190	Q 1047+067	—	—	14.25	0.07	13.37	0.05	—	—	14.32	0.11	13.42	0.08	961130
		14.80	0.22	14.19	0.06	13.17	0.03	14.71	0.24	14.04	0.08	13.06	0.04	971225
191	MS 10470+3537	14.98	0.10	14.41	0.13	13.85	0.06	14.91	0.10	14.29	0.14	13.84	0.09	961229
		15.00	0.04	14.34	0.06	13.71	0.06	14.95	0.05	14.22	0.09	13.74	0.09	980116
192	CSO 292	14.91	0.03	13.99	0.04	13.31	0.04	14.79	0.05	13.90	0.06	13.41	0.07	961130
193	PG 1049-005	14.82	0.06	13.96	0.06	12.94	0.04	14.78	0.08	14.06	0.11	12.95	0.07	960212
		14.81	0.10	14.01	0.09	12.89	0.04	14.98	0.15	14.12	0.14	12.81	0.06	971218
194	MARK 634	13.54	0.04	12.77	0.04	12.16	0.02	13.41	0.04	12.66	0.04	12.05	0.03	960203
		13.32	0.22	12.76	0.03	12.26	0.03	13.17	0.23	12.60	0.03	12.15	0.05	971225
195	RXS J11006+4316	16.24	0.06	15.22	0.06	14.24	0.04	16.22	0.08	15.28	0.10	14.23	0.07	970201
196	RXS J11008+2839	15.70	0.07	15.05	0.09	14.13	0.08	15.74	0.10	15.08	0.14	14.14	0.12	970222
		15.91	0.07	15.21	0.09	14.21	0.06	15.99	0.10	15.56	0.16	14.24	0.08	980119
197	MARK 728	13.36	0.04	12.66	0.04	12.12	0.02	13.27	0.04	12.58	0.04	12.06	0.03	960203
		13.21	0.22	12.72	0.03	12.31	0.03	13.10	0.23	12.66	0.04	12.24	0.05	971225
198	TOL 1059+105	14.23	0.08	13.55	0.05	13.32	0.06	14.17	0.11	13.45	0.07	13.47	0.11	960205
		14.23	0.03	13.60	0.03	13.19	0.03	14.13	0.04	13.58	0.04	13.17	0.04	971227
199	1059.6+0157	—	—	—	—	15.76	0.14	—	—	—	—	15.68	0.20	970103
		17.12	0.14	16.13	0.12	15.31	0.09	17.22	0.22	16.20	0.19	15.18	0.12	980206
200	PKS 1103-006	15.40	0.09	14.49	0.09	13.87	0.09	15.37	0.12	14.52	0.15	13.79	0.14	960212
		15.53	0.07	14.76	0.08	13.75	0.05	15.65	0.11	14.82	0.13	13.71	0.07	980105
201	MC 1104+167	15.19	0.06	14.50	0.07	14.12	0.09	15.23	0.08	14.45	0.10	14.11	0.14	960202
		15.15	0.05	14.50	0.06	14.12	0.05	15.23	0.05	14.58	0.07	14.29	0.09	980119
202	PG 1112+431	15.84	0.12	15.09	0.17	14.37	0.16	16.64	0.39	15.06	0.26	14.26	0.22	960211
203	PG 1114+445	13.97	0.01	13.09	0.03	—	—	13.94	0.02	13.04	0.03	—	—	960210
204	PG 1115+407	14.33	0.05	13.45	0.03	12.62	0.03	14.24	0.06	13.38	0.04	12.55	0.04	960212
		14.23	0.04	13.45	0.03	12.47	0.03	14.18	0.05	13.37	0.03	12.42	0.04	980403
205	PG 1116+215	13.49	0.04	12.50	0.02	11.36	0.02	13.46	0.04	12.52	0.02	11.38	0.02	960202
		13.63	0.03	12.77	0.02	11.64	0.02	13.59	0.03	12.79	0.04	11.61	0.03	980106
206	MARK 734	13.31	0.07	12.50	0.03	11.87	0.02	13.25	0.10	12.38	0.05	11.81	0.02	960205
		13.10	0.04	12.35	0.03	11.71	0.02	13.06	0.04	12.33	0.03	11.67	0.03	971224
207	RXS J11240+3110	14.80	0.11	13.93	0.08	13.51	0.04	14.75	0.10	13.89	0.08	13.53	0.05	970206
208	PG 1121+422	14.98	0.06	14.16	0.05	13.07	0.04	14.94	0.08	14.09	0.07	12.96	0.06	960212
209	AI 27	15.70	0.07	14.72	0.09	13.75	0.08	15.73	0.11	14.75	0.14	13.66	0.11	960210
210	MARK 423	12.48	0.02	11.74	0.04	11.41	0.02	12.29	0.01	11.57	0.02	11.24	0.01	960206
		12.47	0.02	11.80	0.01	11.44	0.03	12.27	0.02	11.61	0.02	11.26	0.03	980102
211	US 2450	15.76	0.06	15.31	0.08	14.64	0.08	15.77	0.08	15.31	0.12	14.89	0.15	970222
		15.83	0.08	15.14	0.05	14.52	0.04	15.84	0.08	15.09	0.08	14.43	0.06	980124
212	MARK 1298	12.92	0.02	11.98	0.04	11.10	0.02	12.88	0.02	11.97	0.03	11.08	0.01	960206
		12.97	0.07	—	—	11.22	0.01	12.96	0.06	—	—	11.20	0.01	980124
213	MARK 1447	13.96	0.07	13.19	0.04	12.66	0.03	13.57	0.10	12.84	0.05	12.44	0.03	960205
		13.85	0.04	13.10	0.04	12.54	0.03	13.54	0.05	12.81	0.04	12.25	0.04	971224
214	B2 1128+31	14.85	0.04	14.15	0.05	—	—	14.76	0.04	14.08	0.06	—	—	960201
215	3C 261	17.01	0.13	16.07	0.13	15.01	0.10	16.98	0.19	15.93	0.18	14.62	0.11	961231
216	MARK 739E	12.23	0.02	11.48	0.04	10.90	0.02	12.00	0.01	11.24	0.02	10.70	0.01	960206
217	MCG 06.26.012	13.63	0.07	12.88	0.04	12.31	0.03	13.33	0.10	12.63	0.05	12.08	0.03	960205
		13.65	0.04	—	—	12.34	0.03	13.38	0.05	—	—	12.10	0.04	971224
218	MARK 744	11.84	0.02	11.06	0.04	10.63	0.02	11.63	0.01	10.86	0.02	10.48	0.01	960206
		11.82	0.07	11.09	0.02	10.67	0.01	11.60	0.06	10.90	0.03	10.51	0.01	980124
219	WAS 26	13.89	0.04	13.08	0.03	12.58	0.03	13.83	0.04	12.95	0.03	12.57	0.04	960202
		14.06	0.06	13.37	0.05	12.64	0.04	13.99	0.07	13.22	0.06	12.56	0.05	971218
220	CG 855	13.41	0.07	12.68	0.03	12.14	0.03	13.23	0.10	12.48	0.05	12.00	0.03	960205
		13.37	0.03	12.69	0.03	12.23	0.04	13.15	0.03	12.47	0.03	12.14	0.05	980102
221	MS 11435-0411	14.90	0.04	14.04	0.04	13.37	0.05	14.81	0.04	13.94	0.05	13.35	0.06	970211
222	MC 1146+111	16.37	0.07	—	—	15.66	0.27	16.23	0.09	—	—	15.53	0.37	961208

Table A.21: J,H,K' band magnitude of AGN with 7.10 pix apertuers: continued

	name	J_{12}	σ_J	H_{12}	σ_H	K'_{12}	$\sigma_{K'}$	J_{15}	σ_J	H_{15}	σ_H	K'_{15}	$\sigma_{K'}$	date
		16.53	0.07	16.13	0.08	15.40	0.08	16.56	0.09	16.18	0.12	15.45	0.12	980307
223	CBS 147	15.72	0.08	15.75	0.23	13.98	0.08	15.55	0.10	16.12	0.49	14.00	0.12	960202
224	PG 1151+117	14.92	0.11	14.21	0.09	13.20	0.08	14.92	0.10	14.46	0.12	13.42	0.10	960131
225	CBS 151	17.10	0.16	16.12	0.21	16.63	0.36	16.76	0.16	15.80	0.23	16.14	0.36	961229
226	4C 29.45	14.12	0.04	13.36	0.04	12.50	0.05	14.10	0.05	13.31	0.06	12.43	0.07	980102
227	GQ COM	14.63	0.11	13.77	0.08	12.63	0.08	14.56	0.10	13.79	0.09	12.60	0.06	960131
		14.63	0.07	13.77	0.07	12.93	0.04	14.64	0.09	13.65	0.09	12.97	0.07	971218
228	UGC 7064	12.25	0.05	11.49	0.02	11.08	0.01	12.02	0.05	11.27	0.01	10.88	0.01	960212
		12.24	0.02	11.52	0.01	11.07	0.02	12.00	0.02	11.29	0.01	10.87	0.02	980102
229	Q 1211+0848	16.48	0.08	15.90	0.14	15.99	0.26	16.54	0.13	15.73	0.19	15.61	0.28	961208
230	PG 1211+143	13.12	0.11	12.34	0.08	11.35	0.07	13.11	0.09	12.35	0.06	11.35	0.05	960131
		13.26	0.07	12.44	0.03	11.40	0.01	13.28	0.06	12.42	0.03	11.41	0.01	980124
231	WAS 49B	13.90	0.02	13.24	0.05	12.66	0.03	13.63	0.02	12.93	0.03	12.42	0.03	960206
232	PKS 1216-010	16.49	0.15	15.24	0.15	14.51	0.13	16.30	0.19	15.00	0.18	14.56	0.21	960202
		16.11	0.06	15.34	0.09	—	—	16.10	0.08	15.49	0.16	—	—	980121
233	MARK 1320	14.41	0.03	13.80	0.05	13.04	0.05	14.36	0.04	13.80	0.07	12.93	0.07	960211
		14.54	0.03	13.71	0.03	13.33	0.03	14.51	0.04	13.62	0.05	13.31	0.05	971227
234	PG 1216+069	13.94	0.03	13.36	0.03	12.92	0.04	12.21	0.02	11.68	0.01	11.57	0.02	980102
235	Q 1220+0939	16.50	0.13	16.24	0.27	—	—	16.36	0.16	15.80	0.28	—	—	961221
		16.86	0.10	16.11	0.11	15.53	0.10	16.79	0.15	16.09	0.17	15.48	0.14	980130
236	MS 12209+1601	14.84	0.04	14.21	0.07	13.69	0.06	14.80	0.05	14.32	0.09	13.61	0.09	960206
		14.83	0.05	14.08	0.04	13.73	0.03	14.77	0.05	14.02	0.04	13.71	0.04	980121
237	B2 1223+25	16.09	0.06	—	—	—	—	16.04	0.09	—	—	—	—	970222
238	2E 1224+0930	16.76	0.07	16.23	0.11	15.39	0.09	16.67	0.09	16.14	0.16	15.33	0.14	970120
		16.49	0.08	16.36	0.15	14.94	0.06	16.46	0.10	16.35	0.21	14.78	0.08	980131
239	3C 273.0	11.58	0.10	10.77	0.07	9.71	0.07	11.56	0.09	10.76	0.06	9.69	0.06	960130
		11.91	0.07	11.08	0.02	9.98	0.01	11.91	0.05	11.09	0.02	9.99	0.01	980124
240	Q 1228-0130	—	—	—	—	15.75	0.16	—	—	—	—	16.18	0.37	970126
241	TON 1542	13.38	0.02	12.57	0.04	11.88	0.02	13.27	0.01	12.46	0.03	11.79	0.02	960206
		13.31	0.03	12.55	0.02	11.86	0.03	13.21	0.03	12.46	0.03	11.80	0.04	980102
242	CSO 150	15.85	0.13	—	—	14.76	0.19	15.90	0.16	—	—	14.86	0.30	960130
		15.86	0.08	15.17	0.09	14.58	0.09	15.76	0.10	15.15	0.13	14.54	0.14	960221
243	IC 3528	13.05	0.02	12.32	0.04	11.82	0.02	12.79	0.01	12.06	0.02	11.62	0.01	960206
		12.84	0.22	12.31	0.02	11.85	0.02	12.57	0.23	12.07	0.02	11.67	0.03	971225
244	MC 1233+108	16.77	0.06	16.09	0.09	15.52	0.10	16.73	0.08	15.73	0.09	15.63	0.18	970106
245	Q 1235+0216	16.08	0.10	15.30	0.14	—	—	15.89	0.12	14.86	0.14	—	—	961221
246	NGC 4593	11.03	0.05	10.18	0.06	9.70	0.03	10.79	0.05	9.96	0.04	9.52	0.02	980131
247	WAS 61	13.34	0.02	12.54	0.02	11.83	0.01	13.31	0.03	12.51	0.02	11.82	0.02	960211
		13.26	0.03	12.52	0.02	11.66	0.03	13.24	0.03	12.51	0.04	11.68	0.04	980102
248	Q 1240+1546	14.21	0.02	13.51	0.05	13.05	0.04	14.20	0.03	13.44	0.04	12.98	0.05	960206
		14.26	0.04	13.52	0.04	13.15	0.04	14.19	0.05	13.42	0.05	13.06	0.06	980102
249	CBS 63	—	—	16.32	0.23	15.69	0.22	—	—	16.52	0.42	15.85	0.40	970223
		—	—	—	—	15.67	0.13	—	—	—	—	15.88	0.25	980212
250	Q 1240+1746	16.59	0.10	16.30	0.17	16.06	0.25	16.46	0.13	16.33	0.28	16.48	0.57	961231
		16.71	0.14	15.98	0.15	15.17	0.12	16.65	0.20	15.97	0.22	15.15	0.17	980318
251	4C 45.26	16.76	0.12	16.52	0.25	15.24	0.15	17.06	0.22	16.72	0.45	15.05	0.19	961221
		16.70	0.07	—	—	15.81	0.14	16.57	0.09	—	—	15.71	0.19	980202
252	MS 12480-0600A	—	—	—	—	14.66	0.05	—	—	—	—	14.48	0.07	970212
253	CSO 769	—	—	16.70	0.34	14.71	0.14	—	—	16.81	0.59	14.30	0.15	970223
254	MS 12545+2209	—	—	—	—	12.80	0.03	—	—	—	—	12.53	0.03	970223
255	MARK 783	14.20	0.02	13.56	0.05	12.89	0.03	14.18	0.03	13.60	0.05	12.92	0.04	960206
256	US 272	—	—	16.34	0.19	15.62	0.15	—	—	16.40	0.31	15.70	0.24	970128
257	3C 281	16.41	0.13	15.38	0.11	15.06	0.19	16.62	0.24	15.30	0.16	15.09	0.30	970223
		16.25	0.07	15.48	0.09	15.10	0.07	16.25	0.10	15.33	0.11	15.07	0.11	980130
258	MS 13061-0115	15.83	0.12	15.54	0.15	15.06	0.12	15.73	0.12	16.01	0.30	15.38	0.24	970206
259	PG 1307+085	14.04	0.10	13.47	0.08	12.47	0.07	14.02	0.09	13.42	0.08	12.39	0.07	960130
260	CSO 835	16.74	0.10	—	—	—	—	16.67	0.14	—	—	—	—	970201
		16.53	0.13	16.42	0.21	—	—	16.35	0.14	16.25	0.26	—	—	970206
261	B2 1308+32	16.08	0.10	15.49	0.18	—	—	16.01	0.14	15.44	0.26	—	—	960201
262	PG 1309+355	13.99	0.04	13.33	0.03	12.48	0.03	13.94	0.04	13.33	0.04	12.47	0.03	960202

Table A.22: J,H,K' band magnitude of AGN with 7,10 pix apertuers: continued

	name	J_{12}	σ_J	H_{12}	σ_H	K'_{12}	$\sigma_{K'}$	J_{15}	σ_J	H_{15}	σ_H	K'_{15}	$\sigma_{K'}$	date
		14.08	0.02	13.48	0.03	12.55	0.03	14.05	0.03	13.46	0.04	12.59	0.05	980301
263	RXS J13129+2628	13.96	0.10	13.42	0.11	13.04	0.04	13.78	0.09	13.20	0.11	12.96	0.05	961229
		14.09	0.02	13.41	0.02	13.02	0.02	13.91	0.02	13.23	0.02	12.87	0.02	980129
264	Q 1316+0103	17.26	0.17	15.85	0.14	14.85	0.07	17.41	0.30	15.88	0.22	14.70	0.09	970130
		16.92	0.11	15.78	0.09	14.96	0.07	17.02	0.17	15.66	0.12	14.79	0.09	980210
265	MARK 1347	13.00	0.02	12.16	0.04	11.56	0.02	12.80	0.01	11.99	0.02	11.45	0.01	960206
		13.01	0.02	12.18	0.02	11.51	0.02	12.82	0.02	12.03	0.02	11.40	0.02	980126
266	Q 1326-0516	14.76	0.10	14.10	0.09	13.18	0.08	14.77	0.10	14.00	0.11	13.24	0.09	960130
		14.71	0.06	14.10	0.07	13.26	0.04	14.78	0.06	14.20	0.08	13.28	0.05	980131
267	MS 13285+3135	16.12	0.10	15.40	0.09	14.69	0.09	15.95	0.11	15.34	0.13	14.61	0.13	970220
		16.76	0.23	15.82	0.33	15.30	0.39	16.68	0.31	15.68	0.44	15.21	0.55	980124
268	Q 1330-0156	—	—	—	—	15.97	0.16	—	—	—	—	15.96	0.25	970127
269	1333.3+2604	16.81	0.09	16.29	0.18	15.01	0.09	16.82	0.12	16.64	0.38	15.11	0.15	970125
270	Q 1334-0232	16.60	0.08	—	—	15.51	0.14	16.49	0.10	—	—	15.72	0.25	970222
271	IRAS 13349+2438	12.88	0.01	11.85	0.02	10.53	0.01	12.87	0.01	11.83	0.02	10.53	0.01	960210
		12.84	0.07	11.87	0.02	10.62	0.01	12.81	0.05	11.84	0.03	10.60	0.01	980124
272	Q 1338-0030	16.04	0.08	15.08	0.09	14.37	0.11	16.11	0.14	14.83	0.11	14.48	0.18	970223
		16.03	0.06	15.34	0.08	14.45	0.04	15.97	0.08	15.15	0.11	14.31	0.06	980130
273	TON 730	14.12	0.02	13.34	0.05	12.58	0.03	14.10	0.02	13.28	0.04	12.51	0.03	960206
		14.24	0.07	13.47	0.06	12.87	0.04	14.16	0.08	13.29	0.06	12.76	0.05	971218
274	MARK 69	14.12	0.07	13.56	0.04	13.04	0.04	14.01	0.10	13.56	0.07	12.93	0.06	960205
		14.45	0.04	13.70	0.03	13.24	0.03	14.42	0.04	13.67	0.04	13.23	0.05	980302
275	1343.9+2828	17.41	0.20	16.37	0.23	16.19	0.29	17.86	0.46	16.36	0.34	16.18	0.45	970127
276	MARK 662	13.35	0.02	12.63	0.04	12.13	0.02	13.32	0.02	12.58	0.03	12.11	0.02	960206
		13.31	0.05	12.52	0.06	11.97	0.04	13.27	0.05	12.48	0.05	11.95	0.03	980131
277	PG 1352+183	14.79	0.03	14.22	0.06	13.28	0.05	14.77	0.05	14.27	0.10	13.29	0.08	960210
278	MARK 463E	12.70	0.02	11.58	0.04	10.34	0.02	12.48	0.01	11.43	0.02	10.28	0.01	960206
		12.74	0.05	11.54	0.06	10.32	0.03	12.52	0.05	11.40	0.05	10.27	0.02	980131
279	PG 1402+261	14.12	0.02	13.06	0.03	11.87	0.02	14.15	0.03	13.05	0.03	11.86	0.02	960210
		14.46	0.03	13.46	0.03	12.21	0.03	14.48	0.03	13.50	0.05	12.23	0.03	980126
280	PG 1404+226	14.54	0.03	13.92	0.05	13.14	0.04	14.48	0.04	13.93	0.07	13.19	0.07	960210
		14.61	0.03	13.97	0.04	13.11	0.03	14.58	0.04	14.03	0.05	13.21	0.04	980302
281	OQ 208	13.22	0.02	12.39	0.04	11.69	0.02	13.07	0.01	12.30	0.02	11.63	0.02	960206
		13.37	0.02	12.54	0.02	11.79	0.02	13.21	0.02	12.40	0.03	11.72	0.02	980126
282	Q 1404-0455	—	—	15.14	0.17	14.64	0.18	—	—	15.60	0.38	14.34	0.20	960130
283	PG 1407+265	14.92	0.11	14.49	0.09	13.90	0.10	14.95	0.10	14.49	0.11	13.86	0.12	960131
		14.79	0.04	14.52	0.05	14.41	0.09	14.75	0.05	14.44	0.07	14.73	0.19	980212
284	PG 1411+442	13.33	0.01	12.51	0.02	11.56	0.01	13.31	0.01	12.47	0.02	11.56	0.02	960210
		13.27	0.03	12.44	0.02	11.48	0.02	13.25	0.03	12.41	0.02	11.47	0.02	980302
285	PG 1415+451	13.89	0.01	13.03	0.02	12.24	0.02	13.86	0.02	13.04	0.03	12.26	0.03	960210
		13.94	0.03	12.97	0.02	12.13	0.02	13.94	0.03	12.97	0.03	12.11	0.03	980302
286	NGC 5548	11.53	0.05	10.71	0.02	10.06	0.01	11.36	0.05	10.56	0.01	9.97	0.01	960212
		11.52	0.05	10.71	0.06	10.14	0.03	11.36	0.05	10.56	0.04	10.03	0.02	980131
287	H 1419+480	13.38	0.05	12.48	0.02	11.66	0.01	13.36	0.05	12.43	0.02	11.67	0.02	960212
		13.29	0.03	12.32	0.02	11.39	0.02	13.29	0.03	12.33	0.02	11.38	0.02	980302
288	MS 14201+2956	13.65	0.05	12.86	0.02	12.39	0.03	13.50	0.05	12.71	0.03	12.30	0.04	960212
289	B2 1420+32	16.87	0.10	15.87	0.12	15.44	0.12	16.87	0.16	15.56	0.14	15.40	0.19	970201
290	MARK 471	12.37	0.05	11.64	0.02	11.29	0.01	12.18	0.05	11.48	0.02	11.15	0.01	960212
		12.41	0.02	11.66	0.01	11.31	0.02	12.23	0.02	11.50	0.01	11.14	0.02	980302
291	B 1422+231	13.79	0.02	13.24	0.03	12.59	0.02	13.74	0.02	13.18	0.03	12.50	0.02	970219
		13.77	0.02	13.21	0.03	12.53	0.03	13.72	0.02	13.12	0.03	12.42	0.04	980301
292	2E 1423+2008	14.70	0.03	13.80	0.04	12.71	0.03	14.67	0.05	13.78	0.06	12.65	0.04	960210
		—	—	—	—	12.96	0.05	—	—	—	—	12.90	0.08	980102
293	MARK 813	13.89	0.10	13.24	0.07	12.37	0.07	13.89	0.09	13.26	0.07	12.41	0.07	960130
		13.83	0.02	13.08	0.03	12.22	0.03	13.80	0.02	13.12	0.04	12.24	0.04	980208
294	B2 1425+26	14.96	0.10	14.20	0.09	13.62	0.09	14.99	0.10	14.22	0.10	13.65	0.11	960130
		15.06	0.05	14.30	0.05	13.58	0.05	14.99	0.06	14.23	0.06	13.49	0.07	980212
295	MARK 1383	13.06	0.01	12.22	0.02	11.32	0.01	13.01	0.01	12.18	0.02	11.30	0.01	960222
		12.94	0.03	12.15	0.02	11.25	0.01	12.87	0.02	12.13	0.01	11.24	0.01	980202
296	MARK 684	12.75	0.02	12.02	0.04	11.51	0.02	12.61	0.01	11.90	0.02	11.41	0.01	960206

Table A.23: J,H,K' band magnitude of AGN with 7,10 pix apertuers: continued

	name	J_{12}	σ_J	H_{12}	σ_H	K'_{12}	$\sigma_{K'}$	J_{15}	σ_J	H_{15}	σ_H	K'_{15}	$\sigma_{K'}$	date
		12.81	0.02	12.06	0.02	11.53	0.02	12.67	0.02	11.94	0.02	11.43	0.02	980126
297	MS 14315+0526	15.84	0.07	14.88	0.07	14.63	0.09	15.80	0.09	14.81	0.10	14.54	0.13	961231
298	MARK 474	13.25	0.05	12.54	0.02	12.14	0.02	13.09	0.05	12.38	0.02	11.99	0.03	960212
		13.33	0.02	12.61	0.02	12.23	0.02	13.18	0.02	12.45	0.02	12.10	0.03	980301
299	PG 1435-067	14.61	0.03	13.82	0.05	12.76	0.03	14.65	0.05	13.91	0.08	12.70	0.05	960222
300	MARK 478	13.05	0.01	12.11	0.02	11.16	0.01	13.02	0.01	12.09	0.02	11.16	0.01	960210
		13.04	0.03	11.99	0.01	11.06	0.02	13.01	0.02	11.98	0.01	11.07	0.02	980302
301	PG 1444+407	14.82	0.03	13.85	0.04	12.78	0.03	14.82	0.05	13.90	0.07	12.84	0.05	960210
		14.56	0.06	13.88	0.05	12.82	0.04	14.47	0.07	13.95	0.06	12.82	0.05	960405
302	Q 1446-0035	15.66	0.12	15.02	0.12	14.40	0.07	15.33	0.11	14.72	0.13	14.34	0.10	970206
		16.02	0.05	15.39	0.08	14.52	0.07	15.71	0.06	15.27	0.11	14.44	0.10	980315
303	PG 1448+273	13.58	0.01	12.88	0.02	12.13	0.02	13.52	0.02	12.84	0.03	12.09	0.03	960210
		13.66	0.03	12.87	0.02	12.23	0.03	13.61	0.03	12.83	0.03	12.25	0.04	980302
304	MS 14564+2147	14.71	0.06	13.94	0.06	13.12	0.05	14.58	0.06	13.92	0.08	13.02	0.06	960212
		14.52	0.03	13.67	0.02	12.85	0.02	14.50	0.03	13.70	0.03	12.81	0.02	980302
305	MS 15005+2552	15.77	0.04	14.82	0.05	14.19	0.04	15.78	0.06	14.62	0.06	14.11	0.06	970219
306	MARK 841	12.88	0.05	12.14	0.02	11.71	0.01	12.81	0.05	12.09	0.02	11.64	0.02	960212
		13.21	0.03	12.45	0.02	11.64	0.01	13.14	0.02	12.40	0.02	11.60	0.02	980202
307	MARK 840	14.32	0.03	13.56	0.02	12.77	0.02	14.29	0.03	13.56	0.02	12.77	0.02	980317
308	PKS 1509+022	15.67	0.05	14.90	0.04	14.11	0.03	15.55	0.06	14.90	0.05	14.02	0.04	970224
		15.81	0.05	14.99	0.05	14.25	0.07	15.71	0.07	14.90	0.07	14.32	0.12	980315
309	MS 15198-0633	14.10	0.02	13.36	0.03	12.59	0.02	14.00	0.03	13.34	0.05	12.51	0.03	960222
		13.97	0.05	13.15	0.03	12.40	0.02	13.91	0.05	13.07	0.03	12.36	0.03	980307
310	LB 9695	17.29	0.16	—	—	—	—	17.20	0.22	—	—	—	—	970130
		17.08	0.10	16.28	0.10	15.28	0.08	17.03	0.14	16.34	0.17	15.41	0.13	980317
311	OR 139	16.56	0.12	15.44	0.09	14.58	0.07	16.70	0.17	15.33	0.11	14.61	0.10	970128
		16.36	0.10	15.47	0.09	14.92	0.07	16.22	0.13	15.44	0.14	14.90	0.10	980206
312	QNZ5:02	15.69	0.05	14.83	0.06	13.96	0.05	15.55	0.07	14.69	0.08	13.93	0.07	970223
		15.64	0.09	14.86	0.08	14.05	0.07	15.40	0.10	14.81	0.12	14.08	0.11	980212
313	MARK 1098	13.03	0.01	12.25	0.02	11.75	0.01	12.90	0.01	12.15	0.02	11.64	0.02	960210
		12.95	0.02	12.19	0.02	11.66	0.01	12.82	0.02	12.06	0.01	11.58	0.01	980202
314	NGC 5940	12.95	0.01	12.20	0.02	11.82	0.01	12.63	0.01	11.89	0.02	11.52	0.02	960222
		12.92	0.05	12.17	0.06	11.73	0.04	12.61	0.05	11.88	0.05	11.46	0.03	980131
315	KUV 15524+2153	15.80	0.05	15.00	0.06	14.14	0.06	15.69	0.07	14.88	0.07	14.15	0.09	970222
		15.80	0.06	15.06	0.04	14.15	0.04	15.70	0.07	15.03	0.06	14.03	0.05	980316
316	MS 16118-0323	16.09	0.07	15.16	0.05	14.26	0.05	16.15	0.11	15.13	0.08	14.25	0.08	980403
317	MARK 877	14.42	0.04	13.48	0.03	12.42	0.02	14.42	0.05	13.52	0.04	12.43	0.03	980403
318	PG 1634+706	13.43	0.03	12.68	0.02	12.49	0.02	13.43	0.02	12.68	0.02	12.49	0.03	970222
		13.42	0.05	12.67	0.02	12.44	0.02	13.43	0.05	12.68	0.03	12.41	0.02	980307
319	RXS J16446+2619	15.70	0.06	14.88	0.06	14.31	0.08	15.75	0.08	14.82	0.09	14.31	0.12	970211
		15.53	0.05	14.83	0.04	14.15	0.04	15.48	0.06	14.81	0.05	14.18	0.06	980316
320	TEX 1652+151	15.66	0.10	14.72	0.07	14.10	0.05	15.54	0.10	14.53	0.08	13.95	0.07	970220
		15.57	0.05	14.86	0.04	14.17	0.04	15.46	0.06	14.72	0.06	14.07	0.05	980316
321	2E 1654+3514	—	—	15.75	0.19	15.03	0.14	—	—	15.58	0.24	14.96	0.21	970220
		16.51	0.10	16.22	0.13	15.18	0.09	16.31	0.11	16.16	0.18	15.17	0.13	980318
322	PKS 1725+044	15.43	0.05	14.62	0.04	13.93	0.03	15.30	0.06	14.51	0.05	13.78	0.05	980403
323	PKS 1739+18C	14.93	0.05	14.22	0.04	13.37	0.03	14.93	0.06	14.26	0.06	13.47	0.05	970224
		14.97	0.06	14.40	0.06	13.51	0.04	14.96	0.07	14.49	0.09	13.55	0.06	980307
324	TEX 1750+175	15.80	0.07	15.12	0.06	14.68	0.08	15.72	0.09	15.08	0.09	14.71	0.13	980403
325	OX 169	14.95	0.07	14.14	0.07	13.33	0.09	14.99	0.12	14.00	0.09	13.46	0.15	980116
326	PG 2233+134	15.91	0.14	14.77	0.12	14.00	0.07	15.86	0.21	14.84	0.20	14.02	0.11	980121
327	PB 5155	16.11	0.07	15.61	0.15	14.88	0.12	16.22	0.12	15.72	0.25	14.87	0.19	961223
328	3C 459.0	15.44	0.07	14.81	0.11	13.77	0.06	15.42	0.10	14.75	0.15	13.65	0.08	971231
329	Q 2350-007B	16.58	0.07	16.38	0.16	15.97	0.24	16.55	0.11	16.45	0.27	16.32	0.51	970102
330	PB 5577	—	—	15.67	0.14	14.95	0.14	—	—	15.48	0.18	15.10	0.25	961202
		16.29	0.09	15.59	0.09	14.58	0.06	16.34	0.15	15.62	0.15	14.51	0.09	971227
331	Q 2352+0025	15.58	0.05	14.60	0.06	13.65	0.05	15.52	0.06	14.60	0.09	13.50	0.05	961223
		15.60	0.06	14.56	0.07	13.80	0.05	15.51	0.09	14.49	0.09	13.80	0.07	971231

Table A.24: J,H,K' band magnitude of AGN with 12,15 pix apertuers

	name	J_{12}	σ_J	H_{12}	σ_H	K'_{12}	$\sigma_{K'}$	J_{15}	σ_J	H_{15}	σ_H	K'_{15}	$\sigma_{K'}$	date
1	PB 5669	15.96	0.12	15.26	0.16	14.28	0.12	15.78	0.14	15.13	0.20	14.16	0.14	961203
		—	—	14.87	0.19	15.67	0.44	—	—	14.63	0.21	17.21	2.51	980105
2	Q 2357+019A	16.67	0.24	16.37	0.50	—	—	16.62	0.31	16.08	0.53	—	—	961202
3	PB 5677	16.83	0.19	16.10	0.22	—	—	16.64	0.22	15.87	0.25	—	—	970106
4	PB 5723	15.98	0.16	15.22	0.24	14.57	0.25	16.13	0.26	14.99	0.27	14.87	0.45	961222
5	PB 5853	16.05	0.15	15.11	0.17	14.26	0.16	16.07	0.20	15.06	0.23	14.27	0.22	961203
		15.92	0.14	—	—	14.06	0.07	15.94	0.19	—	—	13.99	0.09	980121
6	Q 0019+0022B	—	—	—	—	15.55	0.33	—	—	—	—	15.27	0.35	961230
7	PB 5932	15.66	0.09	15.35	0.20	14.18	0.17	15.69	0.12	15.30	0.27	14.04	0.20	961201
		15.76	0.10	15.04	0.14	14.00	0.07	15.67	0.12	14.90	0.17	13.85	0.08	980126
8	MS 00377-0156	16.15	0.13	15.31	0.18	14.18	0.11	16.08	0.17	15.39	0.28	14.17	0.15	961203
		16.22	0.17	14.93	0.12	—	—	16.26	0.24	14.66	0.13	—	—	980106
9	Q 0057+0000	15.83	0.12	15.85	0.36	15.04	0.33	15.81	0.16	15.77	0.47	14.80	0.36	961202
10	Q 0058+0218	16.57	0.16	15.17	0.15	14.61	0.14	16.92	0.29	15.05	0.18	14.50	0.18	961202
11	PHL 964	17.07	0.20	15.71	0.17	15.21	0.20	17.33	0.35	15.66	0.22	15.52	0.36	961223
12	Q 0110-0047	17.36	0.27	16.36	0.34	15.20	0.18	17.44	0.41	16.41	0.49	15.09	0.23	970120
13	B2 0110+29	16.21	0.15	16.70	0.66	14.34	0.18	16.16	0.19	17.40	1.73	14.13	0.20	961202
14	PKS 0130+24	15.89	0.10	15.15	0.16	14.50	0.17	15.80	0.13	15.34	0.26	14.40	0.21	961201
		16.13	0.11	15.09	0.11	14.32	0.08	16.14	0.14	15.13	0.16	14.22	0.11	980121
15	UM 341	15.36	0.06	14.98	0.13	13.87	0.10	15.26	0.08	15.05	0.20	14.03	0.16	961201
		15.61	0.13	14.95	0.16	13.51	0.08	15.60	0.18	15.13	0.25	13.40	0.09	971227
16	3C 47.0	16.23	0.09	15.22	0.10	14.34	0.09	16.36	0.13	15.19	0.14	14.33	0.13	961223
17	PHL 1070	14.58	0.05	13.77	0.05	12.99	0.05	14.57	0.06	13.69	0.06	12.95	0.07	961203
18	PHL 1093	15.29	0.07	14.48	0.10	13.79	0.10	15.31	0.09	14.47	0.13	13.96	0.16	961202
19	KUV 01507-0744	15.57	0.15	14.33	0.12	13.77	0.10	15.43	0.18	14.04	0.13	13.54	0.10	971231
20	PHL 1226	15.50	0.07	14.70	0.10	14.04	0.11	15.44	0.10	14.62	0.12	14.14	0.17	961201
		15.53	0.09	14.76	0.10	13.91	0.07	15.60	0.14	14.68	0.12	13.87	0.09	980116
21	UM 381	15.26	0.08	15.09	0.21	14.14	0.16	15.27	0.11	15.17	0.31	14.11	0.21	961208
		15.35	0.09	15.16	0.17	14.03	0.10	15.37	0.12	15.20	0.24	14.00	0.13	980104
22	UM 153	15.27	0.08	14.73	0.14	14.32	0.20	15.28	0.11	14.51	0.16	14.46	0.31	961208
		15.59	0.09	15.04	0.16	14.29	0.11	15.53	0.12	14.98	0.21	14.26	0.14	980105
23	MARK 1018	12.07	0.02	11.22	0.02	10.89	0.01	12.04	0.03	11.17	0.02	10.87	0.02	960211
		12.11	0.04	11.35	0.03	10.88	0.02	12.08	0.04	11.37	0.03	10.86	0.03	980105
24	RXS J02070+2930	14.13	0.05	13.05	0.06	12.65	0.07	14.17	0.07	12.94	0.08	12.65	0.09	960211
		14.02	0.06	13.12	0.07	12.21	0.06	14.06	0.07	13.10	0.09	12.19	0.07	980105
25	MARK 586	14.68	0.10	13.79	0.11	12.62	0.07	14.95	0.18	13.89	0.17	12.66	0.10	960207
		14.18	0.06	13.54	0.10	12.98	0.12	14.16	0.08	13.52	0.14	12.95	0.16	980105
26	PKS 0214+10	14.80	0.06	14.15	0.09	13.41	0.07	14.44	0.06	14.01	0.10	13.09	0.08	961208
		14.73	0.06	14.17	0.08	13.52	0.07	14.44	0.07	13.85	0.08	13.42	0.09	971227
27	PB 9130	13.28	0.01	12.81	0.02	12.49	0.03	13.23	0.01	12.78	0.03	12.42	0.04	961201
28	B3 0219+443	16.55	0.23	15.29	0.19	14.48	0.23	16.53	0.31	15.28	0.27	14.72	0.39	961222
		15.99	0.10	16.02	0.20	14.81	0.10	15.96	0.12	16.41	0.38	14.71	0.12	980131
29	KUV 02292+3227	—	—	—	—	14.06	0.19	—	—	—	—	14.05	0.27	961222
30	MARK 1179	12.84	0.03	12.04	0.02	11.86	0.03	12.73	0.03	11.96	0.03	11.78	0.04	960211
31	NGC 985	12.33	0.04	11.42	0.02	10.78	0.02	12.34	0.04	11.39	0.02	10.77	0.03	980105
32	MS 02328-0400	15.88	0.16	15.72	0.28	14.32	0.17	15.76	0.19	15.88	0.45	14.40	0.25	961221
		16.56	0.24	15.88	0.24	14.31	0.12	16.95	0.46	15.93	0.35	14.30	0.15	980116
33	4C 41.04	15.99	0.14	15.37	0.21	14.08	0.15	16.11	0.22	15.40	0.30	13.80	0.16	961222
34	Q 0235+0121	16.26	0.17	14.71	0.12	14.95	0.30	16.56	0.30	14.49	0.14	16.07	1.16	961202
		15.71	0.11	14.86	0.13	13.80	0.09	15.55	0.13	14.74	0.16	13.59	0.10	980104
35	Q 0238-0142	16.41	0.19	15.07	0.16	14.29	0.17	16.82	0.38	15.10	0.22	14.22	0.23	961208
		16.24	0.15	15.02	0.13	13.96	0.07	16.25	0.20	14.96	0.18	13.90	0.09	980217
36	PB 6856	15.23	0.05	14.60	0.09	14.11	0.13	15.29	0.08	14.52	0.12	14.20	0.19	961201
37	US 3150	15.89	0.10	—	—	14.39	0.10	16.00	0.16	—	—	14.25	0.13	980106
38	MS 02448+1928	15.09	0.05	14.36	0.08	13.44	0.07	15.01	0.06	14.28	0.10	13.47	0.10	961201
		15.02	0.07	14.38	0.10	13.42	0.07	15.15	0.11	14.46	0.14	13.44	0.10	971227
39	Q 0248+0207	—	—	—	—	16.15	0.39	—	—	—	—	16.38	0.67	970102
40	US 3254	15.60	0.08	16.24	0.55	15.03	0.29	15.46	0.10	16.35	0.84	15.22	0.48	961201
41	US 3333	17.30	0.47	15.69	0.24	14.19	0.22	17.67	0.90	15.63	0.31	14.00	0.25	980106
42	US 3376	15.78	0.16	15.27	0.24	—	—	15.73	0.22	15.13	0.29	—	—	961222

Table A.25: J,H,K' band magnitude of AGN with 12,15 pix apertuers: continued

	name	J_{12}	σ_J	H_{12}	σ_H	K'_{12}	$\sigma_{K'}$	J_{15}	σ_J	H_{15}	σ_H	K'_{15}	$\sigma_{K'}$	date
		15.64	0.16	15.07	0.18	—	—	15.47	0.19	15.00	0.24	—	—	970222
43	S 0254+0101	15.45	0.13	14.68	0.10	13.88	0.07	15.44	0.14	14.64	0.11	13.80	0.09	961230
44	US 3472	14.98	0.07	14.70	0.13	13.65	0.12	14.85	0.09	14.80	0.20	13.81	0.18	961222
		15.28	0.09	14.89	0.15	13.49	0.07	15.37	0.13	15.22	0.28	13.48	0.09	971231
45	S 0257-0027	16.17	0.12	16.39	0.42	14.64	0.11	16.18	0.16	17.81	2.14	14.53	0.14	980121
46	Q 0258+0227	17.25	0.39	15.52	0.19	—	—	17.67	0.81	15.16	0.19	—	—	970127
47	US 3543	—	—	—	—	15.59	0.38	—	—	—	—	15.74	0.61	970128
48	Q 0300-0018	15.45	0.07	15.75	0.22	14.57	0.13	13.48	0.02	12.96	0.03	12.71	0.03	970130
49	US 3605	16.21	0.15	15.73	0.31	14.52	0.20	16.26	0.22	16.07	0.57	14.43	0.25	961208
50	Q 0305+0222	15.91	0.09	14.79	0.10	14.51	0.13	15.83	0.11	14.61	0.12	14.38	0.16	961202
		15.79	0.14	15.48	0.14	14.53	0.11	15.59	0.16	15.55	0.19	14.47	0.14	980209
51	PKS 0306+102	16.76	0.16	—	—	15.11	0.20	16.61	0.20	—	—	14.83	0.21	961223
		—	—	18.24	1.32	16.98	0.71	—	—	17.84	1.26	17.00	1.00	980126
52	Q 0307-0015	17.04	0.33	14.91	0.15	14.20	0.15	17.40	0.63	14.73	0.18	13.88	0.15	961208
53	PKS 0310+013	—	—	—	—	15.40	0.24	—	—	—	—	15.67	0.42	970126
54	MS 03120+1405	16.91	0.25	15.17	0.17	15.48	0.36	17.69	0.69	15.02	0.20	16.23	1.01	961209
		16.30	0.10	16.00	0.16	15.31	0.17	16.23	0.13	16.20	0.27	15.39	0.25	980129
55	Q 0313+0126	16.91	0.22	—	—	—	—	16.64	0.24	—	—	—	—	970130
56	B2 0321+33	13.37	0.10	12.52	0.06	11.84	0.03	13.36	0.11	12.53	0.07	11.82	0.04	960205
		13.46	0.04	12.60	0.04	11.86	0.04	13.42	0.05	12.60	0.05	11.82	0.06	980105
57	PKS 0336-01	15.70	0.11	14.81	0.13	—	—	15.66	0.15	14.80	0.18	—	—	970224
58	KUV 03399-0014	15.93	0.12	14.95	0.15	14.71	0.23	15.92	0.17	14.83	0.19	14.96	0.41	961208
59	3C 93.0	16.13	0.10	15.00	0.10	14.30	0.10	16.17	0.14	14.85	0.12	14.35	0.14	970204
		16.30	0.17	14.92	0.12	14.34	0.11	16.57	0.30	14.86	0.16	14.30	0.14	980105
60	MS 03419+0451	16.74	0.17	15.68	0.19	15.73	0.30	16.55	0.20	15.46	0.21	15.72	0.41	970201
61	PKS 0353+027	16.43	0.09	15.42	0.10	15.07	0.13	16.19	0.09	15.19	0.12	14.97	0.17	970122
		16.91	0.27	15.48	0.14	15.32	0.24	16.97	0.39	15.36	0.18	15.21	0.29	980116
62	MS 03574+1046	14.99	0.04	14.10	0.07	13.06	0.05	15.06	0.06	14.12	0.09	13.07	0.07	961201
		14.76	0.10	13.92	0.10	12.97	0.06	14.70	0.13	13.85	0.13	13.09	0.09	971224
63	3C 109.0	14.64	0.03	13.54	0.04	12.42	0.02	14.69	0.04	13.55	0.05	12.43	0.03	970219
64	MS 04124-0802	12.90	0.02	12.07	0.03	11.18	0.01	12.88	0.02	12.07	0.03	11.19	0.02	960206
		12.78	0.02	11.89	0.04	11.02	0.03	12.80	0.03	11.88	0.04	11.09	0.04	971227
65	3C 110	15.24	0.12	14.45	0.16	14.54	0.36	15.39	0.19	14.39	0.20	15.22	0.94	960202
		14.96	0.08	14.87	0.16	13.89	0.10	14.92	0.10	15.02	0.24	13.97	0.14	971231
66	PKS 0420-01	15.19	0.07	14.40	0.10	13.15	0.05	15.18	0.09	14.47	0.14	12.97	0.06	961208
		17.09	0.89	15.38	0.40	14.28	0.23	16.67	0.82	15.14	0.45	14.45	0.36	971224
67	3C 120	12.14	0.10	11.22	0.05	10.36	0.01	12.10	0.10	11.18	0.06	10.34	0.01	960205
		12.20	0.02	11.18	0.04	10.27	0.02	12.19	0.02	11.17	0.03	10.31	0.03	971227
68	IRAS 04448-0513	12.96	0.10	12.10	0.05	11.54	0.02	12.93	0.11	12.07	0.06	11.56	0.03	960205
		13.00	0.02	12.14	0.05	11.71	0.05	13.01	0.03	12.08	0.05	11.75	0.06	971227
69	Q 0446+0130	16.81	0.15	15.93	0.17	15.12	0.17	16.65	0.18	15.62	0.18	14.90	0.19	970120
		—	—	—	—	15.61	0.19	—	—	—	—	15.34	0.21	980131
70	NGC 1685	12.67	0.06	11.92	0.03	11.63	0.03	12.60	0.06	11.84	0.03	11.59	0.04	960212
71	UGC 3223	11.84	0.01	11.07	0.02	10.78	0.01	11.70	0.02	10.93	0.02	10.66	0.01	960206
		11.78	0.02	11.02	0.04	10.58	0.02	11.66	0.02	10.90	0.03	10.47	0.03	971227
72	2E 0507+1626	12.58	0.02	11.73	0.02	11.06	0.02	12.45	0.02	11.64	0.02	11.01	0.02	960206
		12.61	0.03	11.78	0.04	11.02	0.03	12.56	0.04	11.77	0.04	11.02	0.05	971227
73	3C 135.0	15.00	0.10	14.06	0.10	13.35	0.09	14.93	0.11	13.89	0.10	13.16	0.09	961207
		14.86	0.05	14.21	0.07	13.75	0.07	14.76	0.07	14.12	0.09	13.70	0.09	971231
74	AKN 120	11.72	0.10	10.85	0.05	10.06	0.01	11.71	0.10	10.83	0.06	10.05	0.01	960205
		11.61	0.02	10.77	0.02	10.04	0.02	11.61	0.04	10.78	0.04	10.06	0.03	980106
75	1E 0514-0030	15.21	0.14	14.04	0.13	13.07	0.09	15.41	0.22	14.14	0.19	12.97	0.11	960211
		15.39	0.17	14.56	0.18	13.37	0.09	15.71	0.30	14.57	0.24	13.50	0.14	971224
76	3C 138.0	16.39	0.12	—	—	15.37	0.21	14.75	0.05	—	—	14.17	0.10	970106
		16.69	0.13	16.23	0.21	15.38	0.15	14.97	0.06	14.51	0.06	15.22	0.18	980124
77	3C 147.0	15.48	0.09	14.73	0.11	14.11	0.11	15.49	0.12	14.76	0.14	14.08	0.14	961221
		15.64	0.10	14.60	0.08	14.17	0.11	15.68	0.13	14.55	0.10	14.24	0.16	980105
78	4C 16.14	16.93	0.37	—	—	—	—	16.41	0.32	—	—	—	—	961207
		15.73	0.09	15.38	0.13	15.21	0.18	15.34	0.09	14.98	0.13	14.85	0.19	980208
79	MCG 08.11.11	11.53	0.04	10.74	0.04	10.13	0.02	11.41	0.04	10.63	0.04	10.07	0.02	960203

Table A.26: J,H,K' band magnitude of AGN with 12,15 pix apertuers: continued

	name	J_{12}	σ_J	H_{12}	σ_H	K'_{12}	$\sigma_{K'}$	J_{15}	σ_J	H_{15}	σ_H	K'_{15}	$\sigma_{K'}$	date
		11.39	0.02	10.48	0.02	9.67	0.02	11.32	0.04	10.44	0.04	9.64	0.03	980106
80	OH-010	13.32	0.02	12.66	0.02	12.35	0.02	13.32	0.02	12.67	0.02	12.33	0.02	970125
81	3C 154.0	15.47	0.10	14.62	0.13	14.02	0.10	15.31	0.12	14.57	0.17	14.09	0.14	961209
		15.37	0.11	14.44	0.10	13.73	0.09	15.29	0.14	14.26	0.12	13.74	0.11	971231
82	MC 0657+176	16.72	0.15	—	—	15.04	0.18	16.04	0.11	—	—	14.65	0.17	970106
		18.19	0.59	16.41	0.22	15.92	0.33	16.95	0.27	15.72	0.17	15.39	0.29	980206
83	3C 175.0	13.47	0.04	13.03	0.04	12.72	0.06	13.43	0.04	12.95	0.05	12.62	0.07	961129
		13.34	0.04	12.96	0.04	12.73	0.04	13.29	0.04	12.86	0.04	12.67	0.05	980104
84	B2 0709+37	14.73	0.08	14.44	0.13	14.52	0.26	14.70	0.10	14.38	0.17	14.71	0.43	960202
		14.92	0.08	14.28	0.09	14.10	0.12	15.03	0.11	14.34	0.13	14.12	0.17	980105
85	MARK 376	12.54	0.04	11.64	0.04	10.66	0.02	12.51	0.04	11.64	0.04	10.65	0.02	960203
		12.69	0.04	11.78	0.03	10.89	0.02	12.70	0.04	11.78	0.03	10.89	0.03	980105
86	B3 0729+391	—	—	16.86	0.45	15.00	0.16	—	—	17.38	1.01	14.84	0.19	970130
87	S4 0731+47	15.68	0.10	16.08	0.25	15.73	0.36	15.60	0.11	16.85	0.68	16.76	1.30	970128
88	PKS 0736+01	14.30	0.09	13.54	0.10	13.77	0.15	14.28	0.10	13.53	0.12	13.98	0.25	960131
		—	—	13.92	0.13	12.64	0.06	—	—	13.89	0.17	12.59	0.08	971218
89	OI 363	15.74	0.18	14.90	0.25	13.57	0.13	15.31	0.17	14.60	0.26	13.33	0.14	960131
		15.09	0.06	14.64	0.08	14.02	0.08	14.81	0.07	14.39	0.09	14.00	0.11	980106
90	MARK 79	11.68	0.16	11.02	0.03	10.26	0.01	11.67	0.08	10.98	0.02	10.23	0.02	971225
91	B2 0742+31	14.50	0.05	13.73	0.05	13.11	0.05	14.33	0.05	13.58	0.06	13.14	0.07	960124
		14.67	0.08	13.92	0.10	13.01	0.07	14.51	0.10	13.87	0.13	13.00	0.10	971224
92	PKS 0743-006	11.35	0.04	11.00	0.05	10.79	0.02	10.79	0.04	10.56	0.06	10.45	0.02	961202
93	GC 0742+33	16.87	0.24	15.50	0.16	14.88	0.22	17.10	0.40	15.37	0.20	14.84	0.30	961221
		16.97	0.16	15.40	0.09	—	—	16.96	0.22	15.25	0.11	—	—	980121
94	RXS J07491+2842	16.39	0.15	15.14	0.15	14.27	0.13	16.53	0.24	15.07	0.19	14.21	0.17	961208
95	RXS J07498+3454	14.80	0.06	14.40	0.10	13.44	0.08	14.74	0.08	14.39	0.14	13.54	0.13	961203
		14.87	0.07	14.22	0.09	13.43	0.07	14.89	0.09	14.39	0.14	13.47	0.09	980105
96	PKS 0748+126	15.73	0.06	15.18	0.10	14.43	0.10	15.63	0.08	15.16	0.14	14.47	0.14	970126
		16.48	0.24	15.52	0.20	14.85	0.18	16.55	0.34	15.36	0.24	14.79	0.23	980116
97	MARK 382	13.11	0.04	12.42	0.04	11.96	0.03	13.05	0.04	12.38	0.05	11.89	0.04	960203
98	B2 0752+25A	15.45	0.15	14.86	0.23	13.87	0.17	15.23	0.16	15.11	0.39	14.08	0.28	960131
		15.44	0.10	15.08	0.15	13.99	0.11	15.31	0.12	15.27	0.24	13.94	0.14	971231
99	B3 0754+394	12.85	0.03	11.98	0.03	11.03	0.01	12.84	0.03	11.98	0.03	11.04	0.02	960124
		12.98	0.04	12.11	0.03	11.06	0.03	12.98	0.04	12.14	0.04	11.03	0.03	980105
100	KUV 07549+4228	15.00	0.20	14.12	0.16	13.00	0.06	15.37	0.23	14.21	0.23	13.00	0.08	971225
101	UGC 4155	11.88	0.01	11.18	0.02	10.82	0.01	11.83	0.02	11.14	0.02	10.76	0.01	960206
		11.96	0.03	11.18	0.03	10.80	0.01	11.93	0.05	11.13	0.02	10.78	0.03	971224
102	MARK 1210	11.98	0.10	11.27	0.05	10.94	0.01	11.92	0.10	11.21	0.06	10.91	0.02	960205
		12.02	0.04	11.31	0.02	10.90	0.02	11.97	0.04	11.27	0.02	10.88	0.02	980105
103	MS 08019+2129	14.11	0.04	13.41	0.04	12.50	0.03	14.08	0.04	13.42	0.05	12.41	0.04	960124
		14.03	0.08	13.37	0.08	12.78	0.07	13.95	0.08	13.41	0.11	12.83	0.10	971218
104	3C 192.0	13.44	0.04	12.70	0.03	12.42	0.04	13.06	0.04	12.42	0.03	12.18	0.04	961203
		13.41	0.06	12.70	0.05	12.36	0.05	13.11	0.05	12.49	0.06	12.17	0.05	971218
105	MS 08080+4840	16.97	0.16	16.35	0.31	15.48	0.28	17.41	0.31	16.35	0.43	15.80	0.51	961231
		16.65	0.14	16.33	0.22	15.60	0.19	16.62	0.18	16.37	0.32	15.53	0.25	980210
106	3C 196.0	15.56	0.06	15.31	0.11	14.76	0.11	15.54	0.08	15.38	0.16	14.98	0.19	970201
107	B2 0810+32	17.20	0.26	—	—	15.44	0.29	17.54	0.49	—	—	15.45	0.40	970127
108	PKS 0812+02	15.10	0.11	14.35	0.11	13.87	0.11	15.01	0.12	14.29	0.13	13.94	0.15	961207
109	RX J08166+2941	16.58	0.25	16.18	0.53	14.32	0.17	17.25	0.60	16.09	0.68	14.32	0.24	961207
		17.37	0.47	—	—	15.22	0.30	18.49	1.82	—	—	15.33	0.45	980119
110	3C 197	15.88	0.06	16.10	0.22	15.05	0.17	15.79	0.08	16.45	0.43	14.92	0.21	970126
		16.10	0.08	15.37	0.09	14.82	0.09	16.09	0.11	15.08	0.10	14.64	0.10	980126
111	RXS J08223+3305	15.74	0.14	14.86	0.13	14.03	0.10	15.03	0.11	14.40	0.12	13.72	0.10	970220
		15.63	0.10	15.09	0.12	14.33	0.11	14.97	0.08	14.48	0.10	14.14	0.13	980116
112	KUV 08217+4235	15.02	0.07	14.37	0.10	13.65	0.10	14.88	0.08	14.22	0.11	13.55	0.13	961129
		14.78	0.07	14.16	0.09	13.66	0.10	14.68	0.09	14.09	0.12	13.68	0.13	971231
113	4C 44.17	16.42	0.13	15.90	0.20	15.45	0.26	16.37	0.17	15.66	0.22	15.44	0.36	970127
		17.44	0.32	16.28	0.21	15.90	0.29	17.59	0.50	15.99	0.22	16.04	0.45	980209
114	KUV 08267+4027	15.88	0.14	15.95	0.39	14.64	0.25	15.87	0.18	17.04	1.49	14.77	0.39	961129
115	B2 0827+24	15.80	0.15	14.78	0.14	14.13	0.14	15.51	0.15	14.56	0.16	13.95	0.17	961207

Table A.27: J,H,K' band magnitude of AGN with 12,15 pix apertuers: continued

	name	J_{12}	σ_J	H_{12}	σ_H	K'_{12}	$\sigma_{K'}$	J_{15}	σ_J	H_{15}	σ_H	K'_{15}	$\sigma_{K'}$	date
		15.51	0.09	14.83	0.08	14.25	0.10	15.42	0.12	14.67	0.09	14.25	0.13	980116
116	PG 0832+251	14.55	0.04	13.77	0.05	12.69	0.04	14.58	0.05	13.74	0.06	12.69	0.05	960124
		14.29	0.07	13.86	0.11	12.79	0.05	14.26	0.09	14.11	0.18	12.91	0.08	971224
117	OJ 256	—	—	—	—	15.29	0.15	—	—	—	—	14.86	0.14	970120
118	US 1329	14.60	0.07	13.89	0.08	13.03	0.06	14.54	0.09	13.75	0.10	12.99	0.09	960202
		14.47	0.18	13.85	0.12	13.06	0.07	14.48	0.13	13.74	0.15	13.02	0.09	971225
119	MARK 1218	11.95	0.10	11.26	0.05	10.92	0.01	11.88	0.10	11.18	0.06	10.86	0.02	960205
		12.02	0.03	11.27	0.03	10.83	0.02	11.96	0.05	11.22	0.03	10.81	0.04	971224
120	Q 0835+4744	—	—	—	—	15.46	0.18	—	—	—	—	15.68	0.31	970102
121	3C 207.0	16.67	0.13	15.37	0.12	15.10	0.17	16.75	0.20	15.10	0.13	15.14	0.24	961223
122	KUV 08377+4136	15.88	0.13	17.16	1.17	—	—	15.73	0.16	16.44	0.84	—	—	961222
		15.98	0.07	15.46	0.10	14.69	0.12	15.80	0.09	15.26	0.11	14.44	0.14	980208
123	PG 0844+349	13.22	0.05	12.58	0.03	11.90	0.03	13.21	0.05	12.60	0.04	11.88	0.04	960202
		13.31	0.04	12.60	0.05	11.81	0.05	13.40	0.06	12.67	0.06	11.81	0.07	971224
124	55W 179	—	—	—	—	14.44	0.07	—	—	—	—	14.30	0.08	970212
		14.67	0.06	14.46	0.09	14.19	0.12	14.60	0.07	14.35	0.10	14.10	0.15	980318
125	CSO 2	15.33	0.11	15.37	0.22	13.89	0.11	15.33	0.13	15.41	0.31	13.68	0.12	961207
		15.25	0.06	14.94	0.09	14.11	0.10	15.19	0.08	14.87	0.12	14.13	0.14	980106
126	US 1742	17.11	0.33	16.87	0.76	15.03	0.28	17.38	0.59	18.09	3.27	14.87	0.33	961202
127	LB 8741	16.70	0.25	—	—	15.53	0.48	16.72	0.34	—	—	15.43	0.61	961207
		16.80	0.16	16.12	0.21	14.88	0.11	16.81	0.22	15.90	0.24	14.72	0.13	980124
128	MS 08475+2813	16.82	0.20	15.69	0.27	14.83	0.18	16.63	0.23	15.45	0.30	14.73	0.23	961209
129	US 1786	—	—	15.37	0.21	14.36	0.20	—	—	15.28	0.27	14.46	0.30	961222
		15.92	0.14	16.02	0.21	14.36	0.07	15.83	0.17	16.23	0.36	14.26	0.09	980121
130	MS 08495+0805	13.35	0.04	12.62	0.04	12.16	0.05	12.71	0.03	12.25	0.03	11.95	0.06	960211
131	MS 08498+2820	16.67	0.13	16.11	0.22	15.63	0.23	16.59	0.17	16.15	0.31	15.86	0.39	970219
		16.62	0.14	15.83	0.13	16.15	0.39	16.64	0.19	15.69	0.16	16.55	0.78	980130
132	MS 08502+2825	16.80	0.20	15.45	0.20	15.87	0.44	15.92	0.13	14.67	0.14	14.97	0.27	961202
		16.77	0.13	16.09	0.17	16.05	0.27	15.67	0.07	15.02	0.09	15.23	0.18	980129
133	US 1867	14.86	0.09	14.45	0.16	13.35	0.12	14.77	0.11	14.75	0.29	13.30	0.15	960207
		14.95	0.19	14.46	0.14	13.39	0.06	15.05	0.16	14.52	0.20	13.37	0.09	971225
134	MARK 391	11.78	0.01	11.08	0.02	10.76	0.01	11.72	0.02	11.03	0.02	10.70	0.01	960206
135	NGC 2683 U1	16.48	0.18	15.93	0.29	14.69	0.19	16.43	0.23	15.65	0.31	14.68	0.26	961208
		17.21	0.37	15.28	0.17	15.16	0.24	17.15	0.48	15.12	0.20	15.46	0.43	980119
136	LB 8948	15.33	0.11	14.14	0.10	12.95	0.06	15.18	0.12	14.13	0.12	12.89	0.07	961207
		15.87	0.27	14.23	0.16	13.11	0.06	15.97	0.40	14.15	0.21	13.08	0.09	971224
137	LB 8960	16.09	0.16	—	—	14.34	0.19	16.00	0.19	—	—	14.20	0.23	961207
		16.41	0.12	15.67	0.13	15.36	0.19	16.54	0.17	15.66	0.18	15.37	0.26	980130
138	US 2068	16.03	0.15	—	—	14.44	0.22	15.92	0.19	—	—	14.13	0.24	961129
		15.87	0.08	15.21	0.11	14.56	0.08	15.83	0.09	15.09	0.14	14.43	0.10	980121
139	KUV 09012+4019	16.37	0.23	15.19	0.22	13.79	0.11	16.46	0.35	15.19	0.30	13.71	0.14	970222
		16.32	0.14	15.03	0.10	14.19	0.08	16.36	0.20	14.79	0.11	14.19	0.12	980403
140	US 44	13.62	0.03	12.97	0.03	12.45	0.04	13.50	0.03	12.84	0.03	12.33	0.05	970211
		13.49	0.02	12.92	0.04	12.40	0.03	13.45	0.03	12.88	0.05	12.38	0.04	971227
141	1E 0906+4254	16.31	0.18	15.21	0.14	14.38	0.12	16.22	0.21	15.00	0.16	14.24	0.14	961230
		16.29	0.10	15.29	0.09	15.14	0.13	16.35	0.14	15.18	0.11	15.19	0.19	980302
142	4C 05.38	15.02	0.07	14.73	0.13	13.67	0.08	14.81	0.07	14.51	0.15	13.60	0.11	961202
		15.89	0.20	15.55	0.35	14.09	0.16	15.90	0.28	15.53	0.47	14.22	0.23	980102
143	MARK 704	12.11	0.04	11.24	0.04	10.41	0.02	12.08	0.04	11.21	0.04	10.40	0.02	960203
		12.28	0.04	11.34	0.03	10.56	0.02	12.27	0.05	11.33	0.03	10.57	0.03	971224
144	RXS J09189+3016	15.83	0.14	15.15	0.17	15.47	0.34	15.73	0.17	14.97	0.20	15.63	0.55	970220
		15.62	0.10	14.86	0.14	15.15	0.22	15.42	0.11	14.62	0.15	15.33	0.36	980126
145	RX J09190+3502B	17.29	0.33	17.52	1.18	—	—	16.77	0.28	20.33	21.61	—	—	961203
146	E 0917+341	16.39	0.18	15.32	0.18	15.54	0.32	16.26	0.21	15.26	0.23	15.84	0.58	970223
		16.29	0.12	15.55	0.13	14.93	0.12	16.01	0.13	15.35	0.15	14.90	0.16	980302
147	RX J09249+2527	16.26	0.14	15.14	0.19	14.33	0.08	16.40	0.20	15.18	0.26	14.33	0.11	961209
148	PG 0923+201	13.96	0.03	13.09	0.04	12.14	0.03	13.91	0.04	12.97	0.05	12.12	0.04	960201
		13.68	0.16	13.07	0.07	12.04	0.04	13.72	0.09	13.03	0.09	12.02	0.06	971225
149	MARK 705	12.31	0.03	11.44	0.02	10.86	0.01	12.27	0.04	11.38	0.02	10.84	0.01	960206
		12.37	0.04	11.56	0.03	11.07	0.03	12.32	0.05	11.50	0.03	11.07	0.04	971224

Table A.28: J,H,K' band magnitude of AGN with 12,15 pix apertuers: continued

	name	J_{12}	σ_J	H_{12}	σ_H	K'_{12}	$\sigma_{K'}$	J_{15}	σ_J	H_{15}	σ_H	K'_{15}	$\sigma_{K'}$	date
150	B2 0923+39	12.60	0.07	12.17	0.06	12.03	0.04	12.39	0.06	12.00	0.06	11.84	0.04	961221
		12.78	0.03	12.33	0.02	—	—	12.48	0.03	12.04	0.02	—	—	980315
151	RX J09273+3045	16.83	0.20	16.35	0.32	15.00	0.19	16.79	0.27	16.25	0.40	14.58	0.18	961208
152	MS 09309+2128	14.59	0.06	13.88	0.08	12.82	0.05	14.70	0.09	14.03	0.13	12.75	0.07	961130
		14.54	0.05	13.62	0.06	13.05	0.05	14.64	0.07	13.64	0.07	13.10	0.07	971227
153	US 737	15.22	0.10	14.17	0.10	13.83	0.13	15.18	0.14	14.08	0.13	13.82	0.18	960202
		15.06	0.09	14.28	0.11	13.34	0.06	15.22	0.14	14.26	0.15	13.32	0.08	971227
154	MARK 707	—	—	13.13	0.05	12.69	0.05	—	—	13.11	0.06	12.73	0.07	960203
		13.93	0.05	13.35	0.08	12.62	0.06	13.83	0.07	13.25	0.10	12.58	0.08	971224
155	TON 1078	14.90	0.09	15.34	0.32	13.51	0.11	14.91	0.12	15.39	0.47	13.39	0.14	960202
		15.07	0.09	14.43	0.11	14.07	0.12	15.19	0.13	14.33	0.14	14.01	0.15	980105
156	PG 0936+396	16.09	0.21	14.93	0.18	15.93	0.88	15.93	0.25	14.88	0.24	15.73	1.02	960202
		16.06	0.10	16.35	0.33	14.57	0.15	16.07	0.14	16.62	0.58	14.39	0.17	980212
157	US 822	16.27	0.13	15.45	0.18	15.35	0.27	16.22	0.16	15.29	0.21	15.74	0.54	961209
		16.29	0.09	15.77	0.15	15.27	0.14	16.44	0.14	15.72	0.19	15.71	0.28	980126
158	MS 09398+0952	16.60	0.12	15.49	0.14	15.10	0.15	16.52	0.15	15.48	0.19	15.18	0.22	970131
159	HS 0940+4820	16.45	0.15	15.58	0.24	14.56	0.10	16.50	0.20	15.35	0.26	14.42	0.12	961229
		16.72	0.12	16.17	0.26	15.06	0.11	16.57	0.15	15.99	0.31	15.20	0.17	980129
160	2E 0944+4629	15.43	0.04	14.98	0.07	14.54	0.10	15.33	0.05	14.92	0.09	14.52	0.13	970102
		15.53	0.07	14.78	0.06	14.63	0.08	15.46	0.07	14.64	0.08	14.55	0.10	980210
161	US 995	15.11	0.08	13.96	0.08	13.57	0.12	14.82	0.08	13.65	0.08	13.43	0.15	960210
		15.17	0.10	14.60	0.14	13.89	0.12	14.78	0.09	14.33	0.14	13.99	0.17	971227
162	HS 0946+4845	16.75	0.29	15.18	0.19	14.92	0.36	17.00	0.51	15.02	0.23	14.54	0.35	961129
		16.25	0.10	15.42	0.10	15.75	0.27	16.15	0.12	15.42	0.14	16.81	0.97	980210
163	MARK 1239	11.86	0.05	10.60	0.02	9.49	0.01	11.86	0.06	10.61	0.02	9.50	0.01	960212
164	US 1107	15.49	0.10	14.87	0.15	14.09	0.16	15.36	0.12	14.88	0.21	14.05	0.22	961129
		15.13	0.07	14.64	0.10	13.81	0.07	15.08	0.09	14.74	0.15	13.85	0.10	980116
165	PG 0953+415	14.31	0.06	13.60	0.06	12.74	0.06	14.27	0.08	13.66	0.09	12.78	0.08	960202
		14.27	0.08	13.52	0.09	12.24	0.05	14.21	0.09	13.51	0.12	12.16	0.06	971218
166	3C 232	14.97	0.08	14.42	0.13	13.75	0.13	14.96	0.11	14.29	0.16	13.63	0.16	960202
		15.11	0.09	14.19	0.09	13.61	0.08	15.31	0.14	14.17	0.11	13.52	0.09	980105
167	NGC 3080	12.65	0.04	11.98	0.04	11.48	0.03	12.58	0.04	11.93	0.04	11.41	0.03	960203
		12.71	0.04	12.04	0.03	11.55	0.03	12.66	0.05	11.99	0.03	11.50	0.05	971224
168	IRAS 09595-0755	12.90	0.03	12.15	0.03	11.75	0.03	12.75	0.03	12.03	0.03	11.64	0.04	960211
		12.89	0.16	12.19	0.04	11.45	0.03	12.79	0.08	12.09	0.05	11.29	0.04	971225
169	KUV 09597+3343	—	—	15.64	0.31	15.27	0.46	—	—	15.64	0.43	15.52	0.80	970222
170	KUV 10000+3255	16.19	0.22	—	—	14.57	0.26	16.52	0.42	—	—	14.85	0.46	961130
		16.58	0.15	16.07	0.16	15.06	0.12	16.67	0.21	16.04	0.22	14.88	0.14	980206
171	TON 28	14.58	0.07	14.01	0.09	12.94	0.06	14.63	0.09	14.12	0.13	12.93	0.08	960202
172	PG 1001+05	15.30	0.08	14.36	0.12	13.01	0.07	15.27	0.11	14.39	0.17	13.02	0.10	960210
		15.60	0.23	15.08	0.34	13.26	0.08	15.87	0.41	15.62	0.76	13.30	0.11	971224
173	PKS 1004+13	13.91	0.03	13.45	0.05	12.80	0.06	13.90	0.03	13.43	0.07	12.83	0.08	960201
		14.35	0.10	13.57	0.08	12.60	0.06	14.47	0.12	13.58	0.11	12.57	0.07	971218
174	RXS J10079+4918	15.49	0.10	14.93	0.11	14.22	0.10	15.49	0.12	14.92	0.15	14.29	0.14	970220
		15.77	0.10	15.02	0.11	14.68	0.17	15.74	0.14	14.97	0.14	14.57	0.21	980119
175	TON 488	15.26	0.13	14.53	0.19	13.96	0.17	15.22	0.16	14.61	0.28	14.28	0.31	960130
		15.73	0.10	14.66	0.10	14.10	0.17	15.72	0.12	14.65	0.14	14.25	0.26	960405
176	4C 41.21	15.49	0.12	—	—	13.80	0.13	15.55	0.17	—	—	13.79	0.18	961130
177	Q 1008+0058	14.51	0.05	13.62	0.06	12.87	0.06	14.50	0.06	13.55	0.08	12.88	0.09	960210
		14.68	0.06	14.17	0.11	13.01	0.07	14.66	0.08	14.31	0.17	13.09	0.10	961130
178	CSO 37	17.23	0.40	16.64	0.71	—	—	18.30	1.48	15.94	0.52	—	—	961202
179	TON 1187	14.12	0.09	13.42	0.08	12.65	0.08	14.08	0.09	13.46	0.10	12.69	0.09	960130
		14.31	0.08	13.73	0.11	12.64	0.05	14.40	0.11	13.74	0.16	12.64	0.07	971224
180	PG 1011-040	13.36	0.03	12.59	0.04	12.13	0.04	13.35	0.04	12.61	0.05	12.14	0.06	960211
		13.26	0.16	12.88	0.05	12.14	0.06	13.24	0.08	12.90	0.07	12.15	0.08	971225
181	PKS 1011+23	12.35	0.02	11.78	0.03	11.70	0.01	12.31	0.01	11.73	0.03	11.66	0.02	961208
		12.37	0.04	11.84	0.02	11.68	0.01	12.31	0.04	11.75	0.02	11.60	0.02	980121
182	PG 1012+008	14.27	0.04	13.44	0.05	12.46	0.05	14.29	0.05	13.40	0.07	12.53	0.07	960201
		14.20	0.08	13.52	0.11	12.53	0.05	14.18	0.09	13.58	0.15	12.55	0.08	971218
183	Q 1013+0124	15.34	0.13	14.25	0.16	14.72	0.43	15.44	0.19	14.22	0.21	14.54	0.50	961130

Table A.29: J,H,K' band magnitude of AGN with 12,15 pix apertuers: continued

	name	J_{12}	σ_J	H_{12}	σ_H	K'_{12}	$\sigma_{K'}$	J_{15}	σ_J	H_{15}	σ_H	K'_{15}	$\sigma_{K'}$	date
184	MARK 720	13.04	0.04	12.40	0.04	12.02	0.03	12.98	0.04	12.36	0.04	11.96	0.04	960203
185	Q 1015-0121	16.22	0.17	14.92	0.11	14.76	0.17	16.43	0.28	14.71	0.12	14.81	0.24	961231
186	PG 1016+336	13.16	0.02	12.36	0.03	11.89	0.03	13.13	0.03	12.33	0.03	11.92	0.04	960206
187	MS 10182+2010	16.51	0.15	16.29	0.25	15.64	0.27	16.15	0.15	15.90	0.24	15.82	0.44	970224
188	B2 1028+31	14.67	0.05	13.63	0.06	13.23	0.08	14.69	0.07	13.64	0.09	13.41	0.14	961130
189	MS 10461+1411	16.29	0.14	15.11	0.08	15.12	0.18	16.40	0.21	15.01	0.10	15.58	0.37	970224
190	Q 1047+067	—	—	14.27	0.13	13.50	0.10	—	—	14.28	0.18	13.64	0.16	961130
		14.76	0.17	14.01	0.11	13.04	0.04	14.80	0.12	13.97	0.14	13.03	0.06	971225
191	MS 10470+3537	14.91	0.10	14.21	0.14	13.73	0.10	14.84	0.10	14.22	0.18	13.86	0.15	961229
		14.91	0.06	14.15	0.10	13.77	0.12	14.92	0.08	13.99	0.12	13.78	0.15	980116
192	CSO 292	14.72	0.05	13.92	0.08	13.46	0.09	14.66	0.07	13.86	0.11	13.60	0.14	961130
193	PG 1049-005	14.83	0.09	14.09	0.14	12.94	0.08	15.01	0.14	14.20	0.21	12.95	0.12	960212
		14.95	0.18	14.19	0.19	12.86	0.08	15.00	0.25	14.24	0.27	12.83	0.10	971218
194	MARK 634	13.36	0.04	12.61	0.04	11.99	0.03	13.35	0.04	12.58	0.05	11.98	0.04	960203
		13.22	0.16	12.52	0.04	12.17	0.05	13.30	0.08	12.45	0.05	12.20	0.07	971225
195	RXS J11006+4316	16.20	0.10	15.44	0.14	14.24	0.09	16.20	0.14	15.54	0.22	14.27	0.13	970201
196	RXS J11008+2839	15.74	0.12	15.12	0.19	14.11	0.15	15.87	0.19	15.27	0.30	14.05	0.20	970222
		16.03	0.13	15.65	0.23	14.27	0.11	16.09	0.19	16.12	0.47	14.30	0.15	980119
197	MARK 728	13.24	0.04	12.56	0.04	12.06	0.03	13.23	0.04	12.55	0.05	12.07	0.04	960203
		13.15	0.16	12.60	0.05	12.23	0.06	13.19	0.08	12.59	0.07	12.18	0.08	971225
198	TOL 1059+105	14.15	0.12	13.40	0.09	13.57	0.15	14.11	0.14	13.31	0.11	13.76	0.25	960205
		14.08	0.05	13.55	0.06	13.14	0.06	14.07	0.07	13.60	0.07	13.17	0.08	971227
199	1059.6+0157	—	—	—	—	15.70	0.27	—	—	—	—	15.78	0.40	970103
		17.33	0.29	16.19	0.25	15.06	0.14	16.89	0.28	15.86	0.25	14.72	0.15	980206
200	PKS 1103-006	15.18	0.13	14.41	0.17	13.67	0.16	14.79	0.12	13.90	0.15	13.46	0.18	960212
		15.57	0.13	14.85	0.17	13.60	0.08	15.13	0.12	14.68	0.19	13.39	0.09	980105
201	MC 1104+167	15.28	0.11	14.51	0.14	14.06	0.17	15.31	0.15	14.46	0.19	14.04	0.23	960202
		15.22	0.07	14.59	0.09	14.48	0.13	15.25	0.09	14.50	0.12	14.53	0.19	980119
202	PG 1112+431	16.82	0.58	15.13	0.35	14.47	0.35	17.03	0.98	14.98	0.43	14.38	0.44	960211
203	PG 1114+445	13.91	0.03	13.00	0.04	—	—	13.86	0.03	12.91	0.05	—	—	960210
204	PG 1115+407	14.21	0.06	13.37	0.05	12.49	0.05	14.19	0.08	13.39	0.07	12.54	0.07	960212
		14.16	0.05	13.33	0.04	12.41	0.04	14.10	0.06	13.30	0.05	12.39	0.06	980403
205	PG 1116+215	13.44	0.05	12.52	0.03	11.36	0.03	13.44	0.05	12.56	0.03	11.36	0.03	960202
		13.58	0.03	12.81	0.05	11.61	0.03	13.56	0.05	12.83	0.07	11.61	0.05	980106
206	MARK 734	13.23	0.10	12.31	0.06	11.77	0.03	13.24	0.11	12.25	0.06	11.75	0.04	960205
		13.04	0.04	12.35	0.04	11.68	0.03	13.02	0.05	12.38	0.04	11.71	0.05	971224
207	RXS J11240+3110	14.74	0.10	13.85	0.08	13.55	0.06	14.67	0.10	13.77	0.09	13.55	0.07	970206
208	PG 1121+422	14.95	0.09	14.04	0.08	12.86	0.07	14.97	0.12	13.99	0.11	12.70	0.09	960212
209	A1 27	15.73	0.14	14.63	0.16	13.54	0.12	15.63	0.17	14.62	0.21	13.44	0.16	960210
210	MARK 423	12.22	0.01	11.51	0.02	11.19	0.01	12.17	0.02	11.47	0.02	11.15	0.02	960206
		12.24	0.02	11.56	0.02	11.19	0.04	12.23	0.02	11.53	0.03	11.17	0.04	980102
211	US 2450	15.76	0.10	15.48	0.18	15.17	0.25	15.57	0.12	15.18	0.19	15.31	0.40	970222
		15.82	0.09	15.00	0.09	14.42	0.08	15.56	0.10	14.64	0.09	14.17	0.08	980124
212	MARK 1298	12.86	0.02	11.96	0.02	11.07	0.01	12.85	0.03	11.94	0.03	11.05	0.02	960206
		12.96	0.05	—	—	11.21	0.02	12.97	0.05	—	—	11.24	0.02	980124
213	MARK 1447	13.27	0.10	12.54	0.05	12.19	0.03	13.09	0.11	12.39	0.06	12.13	0.05	960205
		13.14	0.04	12.46	0.04	11.95	0.03	13.06	0.06	12.41	0.05	11.89	0.04	971224
214	B2 1128+31	14.67	0.05	14.01	0.08	—	—	14.60	0.06	13.98	0.10	—	—	960201
215	3C 261	17.15	0.28	15.79	0.20	14.64	0.14	20.04	5.55	15.52	0.22	14.68	0.19	961231
216	MARK 739E	11.92	0.01	11.16	0.02	10.63	0.01	11.86	0.02	11.10	0.02	10.57	0.01	960206
217	MCG 06.26.012	13.22	0.10	12.54	0.06	12.00	0.03	13.16	0.11	12.48	0.06	11.92	0.04	960205
		13.29	0.04	—	—	11.92	0.04	13.28	0.06	—	—	11.82	0.06	971224
218	MARK 744	11.53	0.02	10.77	0.02	10.41	0.01	11.41	0.02	10.65	0.02	10.33	0.02	960206
		11.49	0.05	10.80	0.02	10.42	0.01	11.37	0.05	10.70	0.02	10.34	0.02	980124
219	WAS 26	13.80	0.05	12.92	0.04	12.58	0.04	13.82	0.06	12.88	0.05	12.63	0.06	960202
		13.95	0.07	13.20	0.07	12.52	0.06	13.91	0.08	13.12	0.09	12.47	0.07	971218
220	CG 855	13.15	0.10	12.40	0.06	11.97	0.04	13.10	0.11	12.36	0.06	11.95	0.05	960205
		13.11	0.03	12.40	0.04	12.15	0.07	13.05	0.03	12.33	0.05	12.22	0.09	980102
221	MS 11435-0411	14.78	0.05	13.90	0.06	13.32	0.08	14.71	0.07	13.86	0.08	13.30	0.11	970211
222	MC 1146+111	16.19	0.11	—	—	15.41	0.42	16.07	0.14	—	—	15.54	0.66	961208

Table A.30: J,H,K' band magnitude of AGN with 12,15 pix apertuers: continued

	name	J_{12}	σ_J	H_{12}	σ_H	K'_{12}	$\sigma_{K'}$	J_{15}	σ_J	H_{15}	σ_H	K'_{15}	$\sigma_{K'}$	date
		16.65	0.12	16.28	0.17	15.48	0.16	16.63	0.16	16.55	0.31	15.61	0.25	980307
223	CBS 147	15.47	0.12	15.95	0.54	13.99	0.15	15.35	0.14	15.82	0.67	13.76	0.17	960202
224	PG 1151+117	14.92	0.10	14.59	0.16	13.52	0.12	14.97	0.12	14.97	0.30	13.64	0.18	960131
225	CBS 151	16.67	0.18	15.50	0.22	16.07	0.43	16.44	0.20	15.21	0.23	15.63	0.40	961229
226	4C 29.45	14.05	0.06	13.34	0.08	12.46	0.09	14.10	0.08	13.39	0.11	12.49	0.12	980102
227	GQ COM	14.53	0.10	13.84	0.10	12.57	0.07	14.53	0.10	13.82	0.13	12.54	0.08	960131
		14.63	0.10	13.68	0.11	13.01	0.09	14.66	0.12	13.57	0.14	13.23	0.14	971218
228	UGC 7064	11.93	0.05	11.18	0.02	10.79	0.01	11.86	0.06	11.12	0.02	10.73	0.02	960212
		11.93	0.02	11.20	0.02	10.83	0.04	11.89	0.01	11.14	0.02	10.81	0.03	980102
229	Q 1211+0848	16.58	0.17	15.56	0.21	15.77	0.42	16.60	0.24	15.41	0.25	16.00	0.72	961208
230	PG 1211+143	13.11	0.08	12.34	0.06	11.34	0.05	13.11	0.08	12.33	0.06	11.34	0.05	960131
		13.30	0.05	12.39	0.03	11.42	0.02	13.33	0.05	12.36	0.04	11.42	0.03	980124
231	WAS 49B	13.54	0.02	12.82	0.03	12.33	0.04	13.47	0.03	12.77	0.04	12.29	0.05	960206
232	PKS 1216-010	16.24	0.23	14.78	0.19	14.53	0.26	15.92	0.24	14.58	0.22	14.20	0.27	960202
		16.14	0.10	15.56	0.22	—	—	16.08	0.13	15.43	0.26	—	—	980121
233	MARK 1320	14.33	0.05	13.90	0.10	12.90	0.08	14.33	0.07	14.06	0.16	12.82	0.11	960211
		14.49	0.06	13.54	0.06	13.30	0.07	14.43	0.07	13.42	0.06	13.26	0.08	971227
234	PG 1216+069	11.86	0.02	11.37	0.02	11.18	0.04	11.82	0.01	11.33	0.02	11.13	0.02	980102
235	Q 1220+0939	16.23	0.18	15.81	0.36	—	—	16.28	0.25	16.07	0.64	—	—	961221
		16.71	0.17	15.94	0.19	15.48	0.18	16.58	0.21	15.94	0.26	15.50	0.25	980130
236	MS 12209+1601	14.79	0.06	14.35	0.11	13.60	0.11	14.79	0.09	14.45	0.17	13.46	0.14	960206
		14.72	0.06	13.94	0.05	13.66	0.05	14.63	0.06	13.89	0.06	13.60	0.07	980121
237	B2 1223+25	16.09	0.11	—	—	—	—	15.98	0.14	—	—	—	—	970222
238	2E 1224+0930	16.55	0.10	16.17	0.21	15.34	0.17	16.53	0.13	16.23	0.31	15.36	0.25	970120
		16.47	0.12	16.67	0.35	14.60	0.08	16.50	0.17	17.50	1.03	14.41	0.09	980131
239	3C 273.0	11.55	0.08	10.77	0.06	9.68	0.06	11.55	0.08	10.77	0.06	9.68	0.05	960130
		11.91	0.05	11.09	0.02	9.99	0.01	11.92	0.05	11.09	0.02	1—	0.01	980124
240	Q 1228-0130	—	—	—	—	16.37	0.56	—	—	—	—	16.73	1.08	970126
241	TON 1542	13.24	0.02	12.44	0.03	11.76	0.02	13.25	0.03	12.45	0.03	11.73	0.03	960206
		13.20	0.03	12.45	0.04	11.81	0.05	13.21	0.04	12.44	0.05	11.89	0.06	980102
242	CSO 150	16.14	0.23	—	—	14.81	0.37	16.15	0.31	—	—	14.57	0.41	960130
		15.73	0.13	15.06	0.16	14.47	0.17	15.61	0.16	15.02	0.21	14.23	0.19	960221
243	IC 3528	12.72	0.01	11.98	0.02	11.54	0.02	12.67	0.02	11.93	0.02	11.49	0.02	960206
		12.55	0.16	11.99	0.03	11.63	0.03	12.57	0.08	11.94	0.03	11.65	0.04	971225
244	MC 1233+108	16.73	0.10	15.65	0.11	15.69	0.24	16.76	0.14	15.54	0.14	15.95	0.42	970106
245	Q 1235+0216	15.76	0.13	14.64	0.14	—	—	15.79	0.17	14.21	0.14	—	—	961221
246	NGC 4593	10.71	0.05	9.88	0.04	9.45	0.02	10.63	0.04	9.80	0.04	9.40	0.02	980131
247	WAS 61	13.27	0.03	12.50	0.03	11.77	0.03	13.19	0.04	12.49	0.03	11.74	0.04	960211
		13.23	0.03	12.48	0.05	11.68	0.06	13.26	0.04	12.52	0.06	11.76	0.07	980102
248	Q 1240+1546	14.20	0.04	13.40	0.05	13.00	0.06	14.24	0.05	13.43	0.07	13.00	0.09	960206
		14.20	0.06	13.38	0.06	13.09	0.08	14.32	0.08	13.30	0.08	13.20	0.11	980102
249	CBS 63	—	—	16.46	0.51	16.27	0.75	—	—	15.94	0.44	16.56	1.35	970223
		—	—	—	—	16.04	0.37	—	—	—	—	16.97	1.21	980212
250	Q 1240+1746	16.38	0.14	16.65	0.47	16.88	1.03	15.83	0.12	15.78	0.29	16.44	0.94	961231
		16.53	0.23	15.76	0.24	15.01	0.19	15.88	0.18	15.06	0.18	14.97	0.25	980318
251	4C 45.26	17.12	0.30	16.39	0.43	14.83	0.20	17.25	0.46	15.95	0.40	14.54	0.21	961221
		16.39	0.10	—	—	15.53	0.21	16.20	0.12	—	—	15.51	0.28	980202
252	MS 12480-0600A	—	—	—	—	14.37	0.08	—	—	—	—	14.18	0.09	970212
253	CSO 769	—	—	17.81	1.89	14.08	0.15	—	—	20.04	20.36	13.57	0.13	970223
254	MS 12545+2209	—	—	—	—	12.53	0.04	—	—	—	—	12.53	0.05	970223
255	MARK 783	14.18	0.03	13.66	0.06	12.94	0.06	14.21	0.05	13.67	0.09	12.98	0.08	960206
256	US 272	—	—	16.73	0.54	16.11	0.45	—	—	16.43	0.57	15.73	0.44	970128
257	3C 281	17.02	0.44	15.12	0.18	15.33	0.49	18.88	3.37	15.03	0.22	16.47	1.92	970223
		16.23	0.12	15.32	0.14	15.12	0.15	16.26	0.17	15.23	0.18	15.11	0.20	980130
258	MS 13061-0115	15.69	0.13	16.29	0.49	15.59	0.38	15.60	0.14	17.62	2.30	15.77	0.62	970206
259	PG 1307+085	14.03	0.09	13.40	0.09	12.35	0.07	14.06	0.10	13.40	0.10	12.29	0.07	960130
260	CSO 835	16.63	0.17	—	—	—	—	16.54	0.21	—	—	—	—	970201
		16.23	0.15	16.27	0.33	—	—	16.15	0.17	15.97	0.35	—	—	970206
261	B2 1308+32	15.87	0.15	15.35	0.31	—	—	15.78	0.19	15.49	0.49	—	—	960201
262	PG 1309+355	13.94	0.05	13.36	0.05	12.50	0.04	13.90	0.06	13.39	0.06	12.56	0.06	960202

Table A.31: J,H,K' band magnitude of AGN with 12,15 pix apertuers: continued

	name	J_{12}	σ_J	H_{12}	σ_H	K'_{12}	$\sigma_{K'}$	J_{15}	σ_J	H_{15}	σ_H	K'_{15}	$\sigma_{K'}$	date
		14.03	0.03	13.45	0.05	12.62	0.06	14.00	0.04	13.41	0.07	12.66	0.09	980301
263	RXS J13129+2628	13.72	0.08	13.13	0.10	12.94	0.05	13.70	0.08	13.07	0.11	12.94	0.07	961229
		13.86	0.02	13.17	0.03	12.82	0.02	13.84	0.02	13.10	0.03	12.80	0.03	980129
264	Q 1316+0103	17.81	0.55	15.97	0.31	14.57	0.11	22.36	50.33	16.54	0.72	14.38	0.12	970130
		16.98	0.21	15.48	0.13	14.72	0.10	16.90	0.26	15.31	0.15	14.55	0.12	980210
265	MARK 1347	12.73	0.01	11.94	0.02	11.43	0.02	12.68	0.02	11.90	0.02	11.41	0.02	960206
		12.76	0.01	11.99	0.02	11.38	0.02	12.72	0.01	11.95	0.03	11.38	0.02	980126
266	Q 1326-0516	14.79	0.11	14.01	0.13	13.28	0.11	14.84	0.13	14.00	0.17	13.33	0.14	960130
		14.80	0.07	14.22	0.09	13.32	0.06	14.85	0.08	14.24	0.12	13.32	0.08	980131
267	MS 13285+3135	15.84	0.12	15.21	0.14	14.46	0.14	15.56	0.12	14.96	0.16	14.35	0.17	970220
		16.97	0.52	15.98	0.75	15.23	0.72	16.69	0.56	15.82	0.90	14.89	0.73	980124
268	Q 1330-0156	—	—	—	—	15.71	0.26	—	—	—	—	15.55	0.31	970127
269	1333.3+2604	16.80	0.15	17.14	0.77	15.12	0.20	16.78	0.21	18.13	2.66	15.60	0.42	970125
270	Q 1334-0232	16.27	0.11	—	—	15.60	0.29	15.26	0.06	—	—	14.73	0.18	970222
271	IRAS 13349+2438	12.86	0.01	11.84	0.02	10.54	0.01	12.86	0.02	11.84	0.02	10.55	0.01	960210
		12.80	0.05	11.81	0.03	10.59	0.01	12.79	0.05	11.80	0.03	10.57	0.01	980124
272	Q 1338-0030	16.22	0.20	14.72	0.12	14.53	0.25	16.47	0.34	14.58	0.15	14.44	0.31	970223
		15.98	0.10	15.07	0.13	14.28	0.07	16.11	0.15	14.94	0.16	14.23	0.09	980130
273	TON 730	14.11	0.03	13.29	0.05	12.50	0.04	14.16	0.05	13.27	0.07	12.46	0.05	960206
		14.18	0.09	13.34	0.09	12.76	0.07	14.29	0.10	13.30	0.11	12.85	0.10	971218
274	MARK 69	13.96	0.10	13.52	0.08	12.87	0.07	13.89	0.11	13.53	0.10	12.82	0.09	960205
		14.40	0.05	13.61	0.05	13.25	0.06	14.41	0.07	13.59	0.06	13.31	0.09	980302
275	1343.9+2828	17.41	0.39	15.91	0.29	15.95	0.47	16.36	0.21	15.06	0.19	14.80	0.23	970127
276	MARK 662	13.31	0.02	12.57	0.03	12.09	0.03	13.31	0.03	12.58	0.03	12.08	0.04	960206
		13.24	0.05	12.49	0.05	11.94	0.03	13.24	0.05	12.52	0.05	11.93	0.04	980131
277	PG 1352+183	14.74	0.06	14.32	0.13	13.27	0.09	14.69	0.08	14.28	0.17	13.35	0.14	960210
278	MARK 463E	12.41	0.01	11.37	0.02	10.27	0.01	12.37	0.02	11.34	0.02	10.26	0.01	960206
		12.45	0.05	11.35	0.04	10.25	0.02	12.41	0.04	11.33	0.04	10.24	0.02	980131
279	PG 1402+261	14.24	0.04	13.07	0.04	11.88	0.03	14.26	0.05	13.06	0.05	11.92	0.04	960210
		14.54	0.04	13.48	0.06	12.22	0.03	14.60	0.06	13.55	0.09	12.19	0.04	980126
280	PG 1404+226	14.49	0.05	13.96	0.10	13.18	0.08	14.48	0.06	14.00	0.14	13.20	0.12	960210
		14.66	0.05	14.10	0.07	13.28	0.06	14.71	0.08	14.21	0.11	13.47	0.09	980302
281	OQ 208	13.01	0.02	12.26	0.02	11.61	0.02	12.95	0.02	12.26	0.03	11.60	0.03	960206
		13.16	0.02	12.37	0.03	11.69	0.02	13.11	0.02	12.31	0.04	11.65	0.03	980126
282	Q 1404-0455	—	—	16.24	0.87	14.35	0.25	—	—	17.17	2.84	14.29	0.33	960130
283	PG 1407+265	14.97	0.10	14.39	0.12	13.74	0.13	14.96	0.12	14.26	0.14	13.62	0.16	960131
		14.71	0.06	14.39	0.09	14.81	0.26	14.65	0.08	14.26	0.11	15.32	0.57	980212
284	PG 1411+442	13.31	0.02	12.47	0.03	11.56	0.02	13.30	0.02	12.45	0.04	11.59	0.03	960210
		13.23	0.03	12.40	0.02	11.46	0.02	13.21	0.03	12.38	0.03	11.48	0.03	980302
285	PG 1415+451	13.86	0.03	13.06	0.04	12.27	0.03	13.85	0.03	13.07	0.06	12.35	0.05	960210
		13.93	0.03	12.98	0.04	12.09	0.04	13.91	0.04	12.98	0.05	12.08	0.05	980302
286	NGC 5548	11.30	0.05	10.50	0.01	9.92	0.01	11.24	0.06	10.45	0.02	9.89	0.01	960212
		11.30	0.05	10.50	0.04	9.98	0.02	11.24	0.04	10.46	0.04	9.95	0.02	980131
287	H 1419+480	13.35	0.06	12.40	0.02	11.71	0.03	13.34	0.06	12.36	0.03	11.75	0.04	960212
		13.28	0.03	12.33	0.02	11.37	0.02	13.28	0.03	12.32	0.03	11.38	0.03	980302
288	MS 14201+2956	13.46	0.06	12.64	0.03	12.29	0.04	13.41	0.06	12.55	0.04	12.29	0.06	960212
289	B2 1420+32	16.74	0.18	15.54	0.18	15.45	0.25	16.87	0.28	15.50	0.24	15.57	0.39	970201
290	MARK 471	12.11	0.05	11.41	0.02	11.09	0.01	12.06	0.06	11.35	0.02	11.06	0.02	960212
		12.16	0.02	11.45	0.01	11.06	0.02	12.11	0.03	11.41	0.01	11.00	0.02	980302
291	B 1422+231	13.72	0.02	13.15	0.03	12.47	0.02	13.70	0.02	13.14	0.03	12.44	0.03	970219
		13.70	0.02	13.10	0.04	12.38	0.05	13.70	0.03	13.05	0.05	12.33	0.06	980301
292	2E 1423+2008	14.65	0.06	13.79	0.08	12.64	0.05	14.64	0.08	13.72	0.10	12.56	0.06	960210
		—	—	—	—	13.08	0.11	—	—	—	—	13.08	0.15	980102
293	MARK 813	13.90	0.09	13.26	0.08	12.43	0.07	13.90	0.09	13.26	0.09	12.45	0.08	960130
		13.76	0.03	13.17	0.05	12.26	0.05	13.74	0.04	13.22	0.07	12.28	0.07	980208
294	B2 1425+26	14.96	0.11	14.27	0.13	13.87	0.16	14.90	0.12	14.20	0.16	14.12	0.26	960130
		14.94	0.08	14.26	0.08	13.47	0.08	14.99	0.11	14.21	0.11	13.62	0.13	980212
295	MARK 1383	13.00	0.02	12.17	0.02	11.30	0.02	12.99	0.02	12.14	0.03	11.30	0.02	960222
		12.84	0.02	12.13	0.02	11.22	0.01	12.80	0.02	12.12	0.02	11.21	0.02	980202
296	MARK 684	12.55	0.01	11.85	0.02	11.36	0.01	12.50	0.02	11.80	0.02	11.32	0.02	960206

Table A.32: J,H,K' band magnitude of AGN with 12,15 pix apertuers: continued

	name	J_{12}	σ_J	H_{12}	σ_H	K'_{12}	$\sigma_{K'}$	J_{15}	σ_J	H_{15}	σ_H	K'_{15}	$\sigma_{K'}$	date
		12.61	0.01	11.86	0.02	11.38	0.02	12.56	0.01	11.80	0.03	11.33	0.02	980126
297	MS 14315+0526	15.77	0.10	14.71	0.12	14.47	0.15	15.67	0.12	14.55	0.14	14.53	0.22	961231
298	MARK 474	13.04	0.05	12.32	0.02	11.94	0.03	13.01	0.06	12.27	0.03	11.89	0.04	960212
		13.13	0.02	12.41	0.02	12.02	0.03	13.10	0.02	12.39	0.03	11.99	0.04	980301
299	PG 1435-067	14.69	0.06	13.92	0.10	12.67	0.06	14.82	0.10	13.94	0.14	12.62	0.08	960222
300	MARK 478	13.02	0.01	12.08	0.02	11.16	0.01	13.02	0.02	12.07	0.03	11.18	0.02	960210
		13.02	0.02	11.97	0.02	11.07	0.02	13.03	0.03	11.96	0.02	11.07	0.02	980302
301	PG 1444+407	14.83	0.06	13.96	0.09	12.90	0.06	14.85	0.08	14.15	0.15	13.02	0.09	960210
		14.37	0.08	14.03	0.07	12.77	0.06	14.26	0.09	14.09	0.09	12.74	0.07	960405
302	Q 1446-0035	15.11	0.11	14.53	0.13	14.40	0.13	15.01	0.12	14.43	0.16	14.51	0.19	970206
		15.54	0.06	15.14	0.13	14.29	0.11	15.49	0.08	15.09	0.17	14.37	0.17	980315
303	PG 1448+273	13.51	0.02	12.85	0.03	12.11	0.03	13.45	0.03	12.85	0.05	12.13	0.04	960210
		13.61	0.03	12.84	0.04	12.27	0.05	13.59	0.04	12.85	0.05	12.28	0.07	980302
304	MS 14564+2147	14.56	0.08	13.89	0.10	12.98	0.08	14.48	0.09	13.94	0.15	12.93	0.11	960212
		14.49	0.04	13.74	0.04	12.79	0.03	14.50	0.05	13.84	0.06	12.81	0.04	980302
305	MS 15005+2552	15.80	0.07	14.51	0.07	14.12	0.08	15.86	0.10	14.35	0.08	14.09	0.10	970219
306	MARK 841	12.79	0.05	12.05	0.02	11.63	0.02	12.78	0.06	12.05	0.03	11.61	0.03	960212
		13.09	0.02	12.39	0.02	11.58	0.02	13.06	0.02	12.41	0.03	11.57	0.03	980202
307	MARK 840	14.27	0.03	13.57	0.02	12.78	0.02	14.25	0.04	13.57	0.03	12.78	0.02	980317
308	PKS 1509+022	15.29	0.06	14.83	0.06	13.96	0.05	14.81	0.05	14.42	0.06	13.66	0.05	970224
		15.54	0.07	14.72	0.07	14.34	0.15	15.16	0.07	14.36	0.07	14.19	0.18	980315
309	MS 15198-0633	13.94	0.03	13.35	0.06	12.51	0.04	13.91	0.04	13.48	0.10	12.50	0.06	960222
		13.90	0.05	13.01	0.03	12.38	0.03	13.87	0.05	13.00	0.04	12.42	0.04	980307
310	LB 9695	17.20	0.29	—	—	—	—	16.91	0.31	—	—	—	—	970130
		16.88	0.16	16.27	0.20	15.38	0.17	16.69	0.18	16.06	0.23	15.15	0.19	980317
311	OR 139	16.80	0.23	15.16	0.12	14.51	0.12	16.91	0.34	15.09	0.15	14.43	0.15	970128
		16.19	0.14	15.34	0.16	14.88	0.13	16.15	0.18	15.20	0.19	14.72	0.15	980206
312	QNZ5:02	15.28	0.07	14.50	0.08	13.79	0.08	15.07	0.08	14.29	0.10	13.71	0.11	970223
		15.12	0.10	14.56	0.12	14.00	0.13	14.86	0.11	14.42	0.15	13.98	0.18	980212
313	MARK 1098	12.86	0.01	12.10	0.02	11.60	0.02	12.84	0.02	12.07	0.03	11.58	0.03	960210
		12.78	0.02	12.02	0.01	11.54	0.02	12.74	0.02	11.99	0.02	11.53	0.03	980202
314	NGC 5940	12.50	0.02	11.78	0.02	11.41	0.02	12.40	0.02	11.69	0.03	11.33	0.02	960222
		12.47	0.05	11.76	0.04	11.33	0.03	12.35	0.04	11.66	0.04	11.23	0.03	980131
315	KUV 15524+2153	15.64	0.08	14.87	0.09	14.12	0.11	15.56	0.10	14.92	0.13	14.13	0.15	970222
		15.74	0.08	15.05	0.08	13.95	0.06	15.81	0.11	14.99	0.10	13.84	0.07	980316
316	MS 16118-0323	15.82	0.11	14.93	0.09	14.16	0.09	15.18	0.09	14.35	0.07	13.82	0.09	980403
317	MARK 877	14.43	0.06	13.51	0.05	12.41	0.03	14.47	0.08	13.48	0.06	12.41	0.04	980403
318	PG 1634+706	13.44	0.02	12.67	0.02	12.50	0.03	13.43	0.02	12.65	0.03	12.51	0.04	970222
		13.42	0.05	12.68	0.03	12.39	0.03	13.42	0.05	12.70	0.03	12.33	0.04	980307
319	RXS J16446+2619	15.75	0.10	14.80	0.11	14.36	0.16	15.78	0.14	14.70	0.14	14.73	0.31	970211
		15.43	0.06	14.85	0.07	14.24	0.07	15.31	0.07	14.85	0.09	14.29	0.11	980316
320	TEX 1652+151	15.45	0.10	14.51	0.10	13.89	0.08	15.30	0.11	14.29	0.11	13.75	0.10	970220
		15.43	0.07	14.64	0.07	14.00	0.06	15.26	0.08	14.43	0.08	13.93	0.08	980316
321	2E 1654+3514	—	—	15.45	0.28	14.87	0.24	—	—	15.09	0.28	14.55	0.25	970220
		16.16	0.12	16.39	0.28	15.08	0.15	15.80	0.12	16.00	0.27	15.04	0.19	980318
322	PKS 1725+044	15.18	0.06	14.38	0.05	13.72	0.06	15.01	0.07	14.19	0.06	13.57	0.07	980403
323	PKS 1739+18C	14.90	0.07	14.27	0.07	13.51	0.07	14.94	0.09	14.32	0.10	13.61	0.11	970224
		14.99	0.08	14.63	0.13	13.57	0.08	14.97	0.10	14.86	0.22	13.69	0.12	980307
324	TEX 1750+175	15.61	0.10	14.98	0.10	14.88	0.19	15.78	0.16	14.92	0.13	14.92	0.28	980403
325	OX 169	14.94	0.14	13.91	0.10	13.57	0.20	14.87	0.18	13.77	0.12	14.13	0.46	980116
326	PG 2233+134	15.91	0.27	14.71	0.22	14.10	0.15	15.93	0.38	14.74	0.32	14.28	0.24	980121
327	PB 5155	16.50	0.19	15.48	0.25	14.64	0.19	17.01	0.43	15.45	0.34	14.66	0.27	961223
328	3C 459.0	15.36	0.12	14.84	0.21	13.71	0.10	15.30	0.16	15.02	0.33	13.64	0.12	971231
329	Q 2350-007B	16.65	0.15	16.05	0.24	16.69	0.93	16.47	0.18	15.60	0.22	16.84	1.47	970102
330	PB 5577	—	—	15.32	0.20	14.96	0.28	—	—	15.36	0.28	14.72	0.31	961202
		16.29	0.18	15.66	0.20	14.52	0.11	16.12	0.21	15.69	0.28	14.44	0.14	971227
331	Q 2352+0025	15.46	0.07	14.57	0.11	13.48	0.06	15.47	0.09	14.55	0.15	13.40	0.08	961223
		15.56	0.11	14.41	0.10	13.72	0.08	15.71	0.18	14.27	0.12	13.65	0.09	971231

Appendix B

figures

B.1 comparison between the two photometry methods

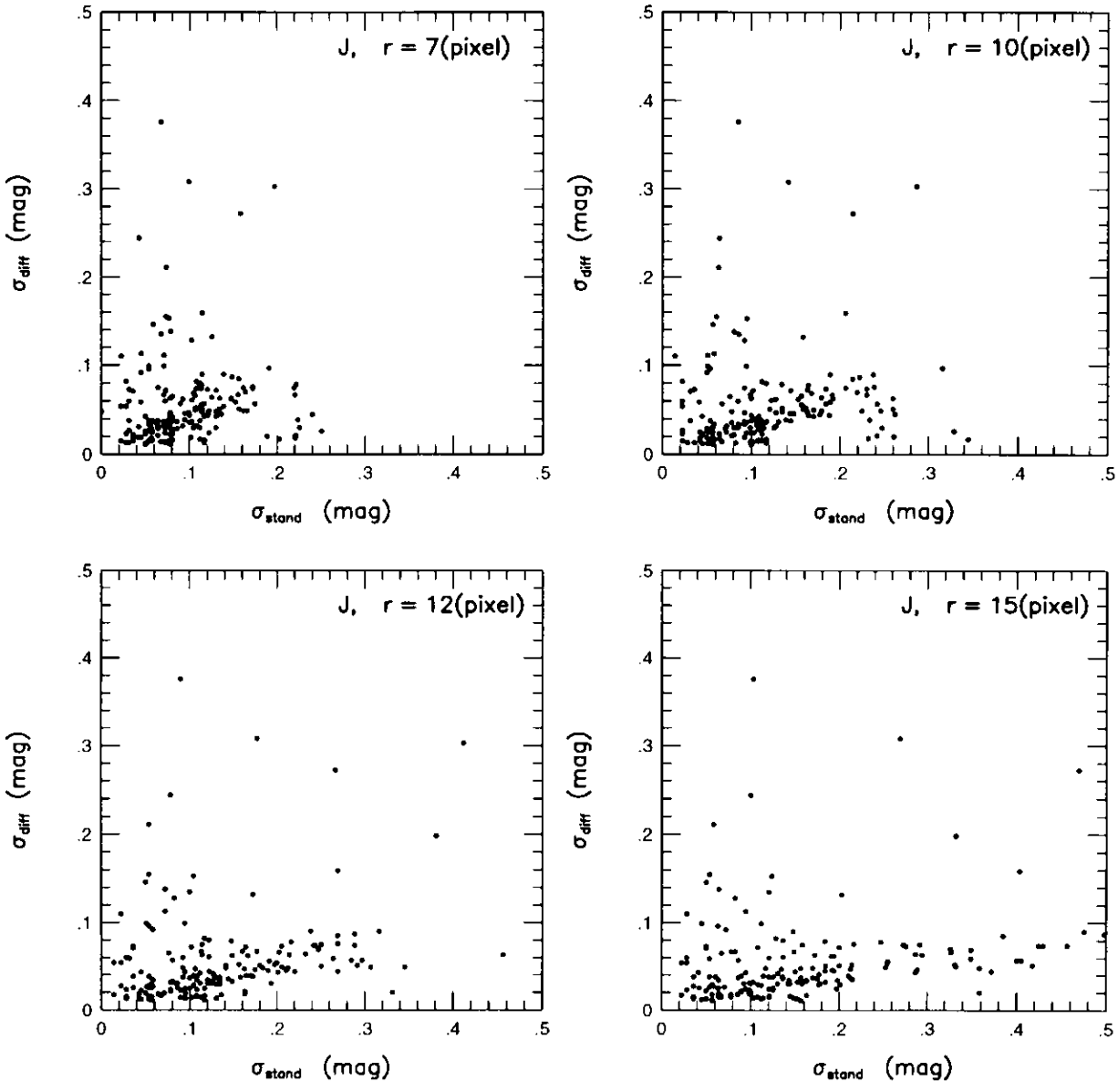

Figure B.1: The relation between the error of the AGN variability in J band determined by the differential photometory σ_{diff} and by the photometory using phtometoric standard σ_{stand}. r shows the apertuer used in the later method.

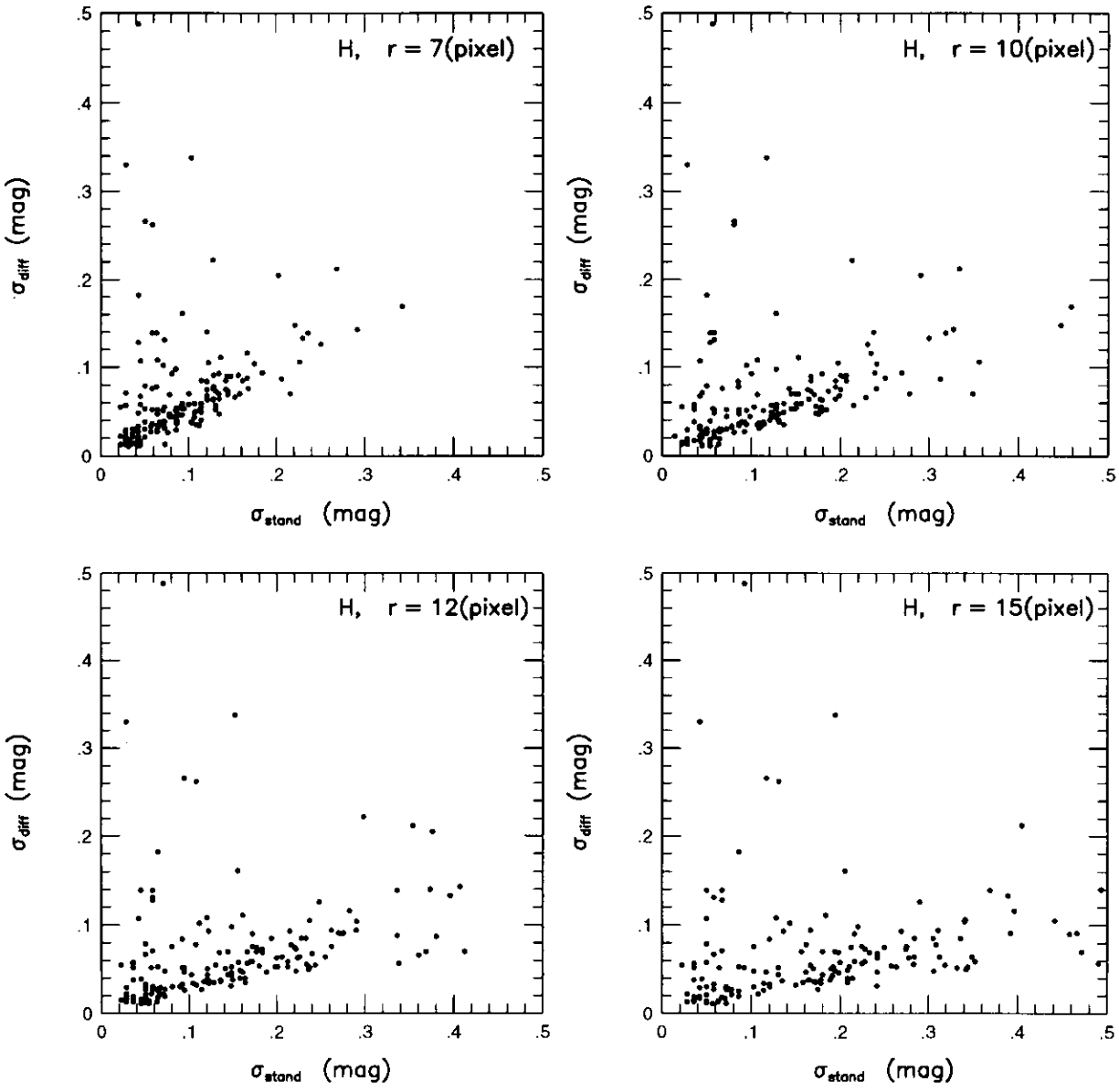

Figure B.2: The relation between the error of the AGN variability in H band determined by the differential photometory σ_{diff} and by the photometory using phtometoric standard σ_{stand}. r shows the apertuer used in the later method.

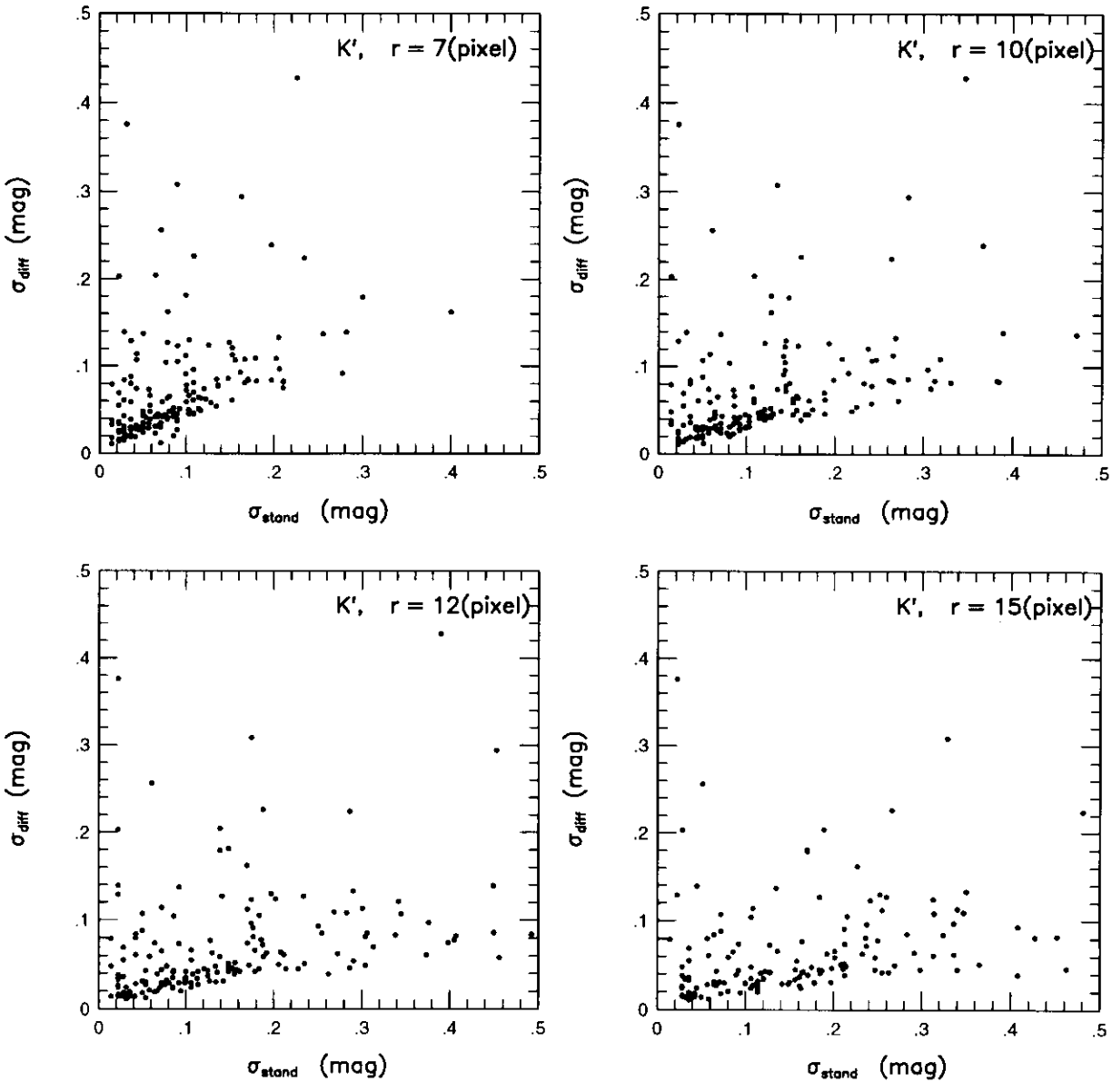

Figure B.3: The relation between the error of the AGN variability in K' band determined by the differential photometory σ_{diff} and by the photometory using phtometoric standard σ_{stand}. r shows the apertuer used in the later method.

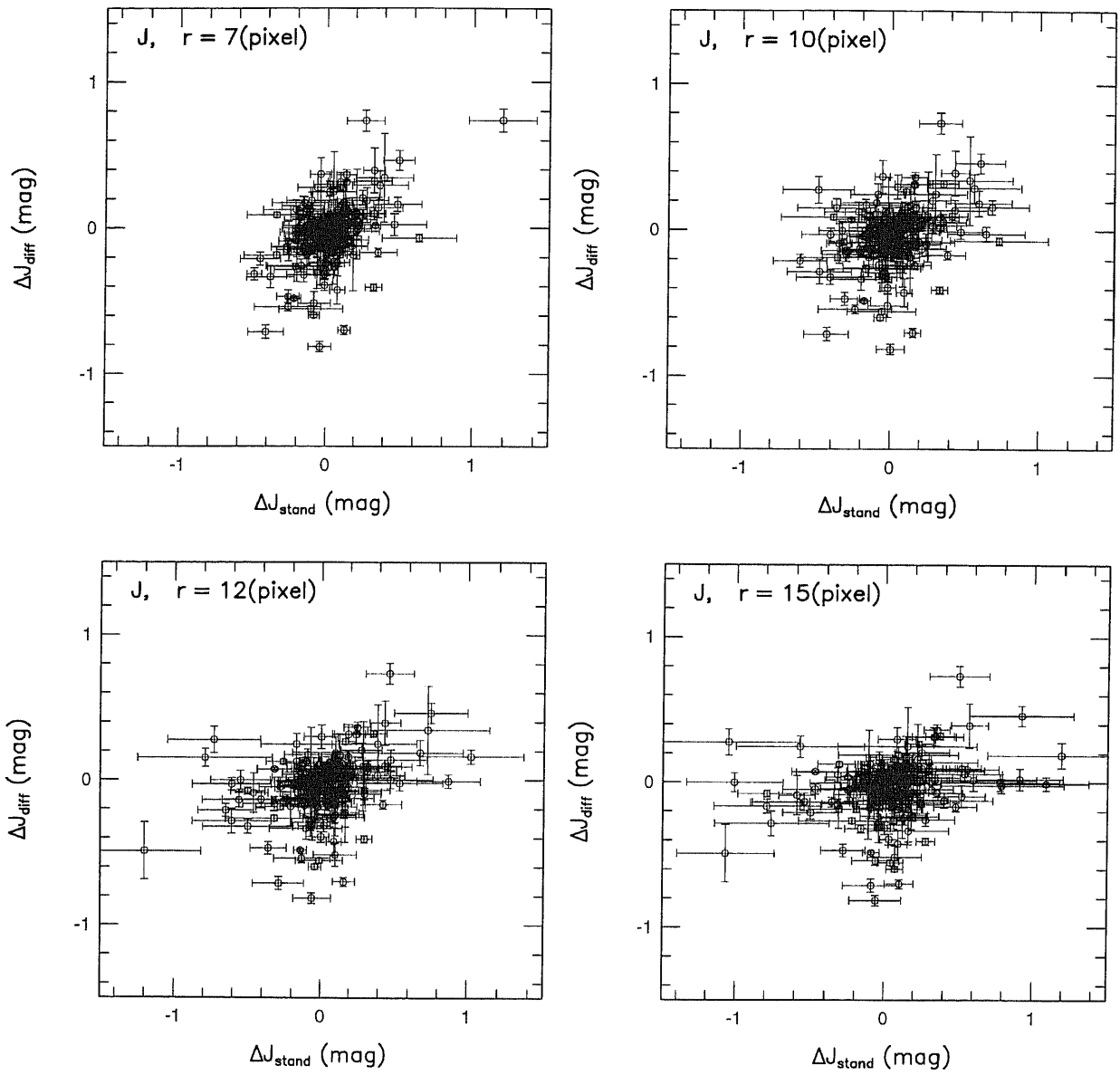

Figure B.4: The relation between the AGN variability in J band determined by the differential photometory Δ_{diff} and by the photometory using phtometoric standard Δ_{stand}. r shows the apertuer used in the later method.

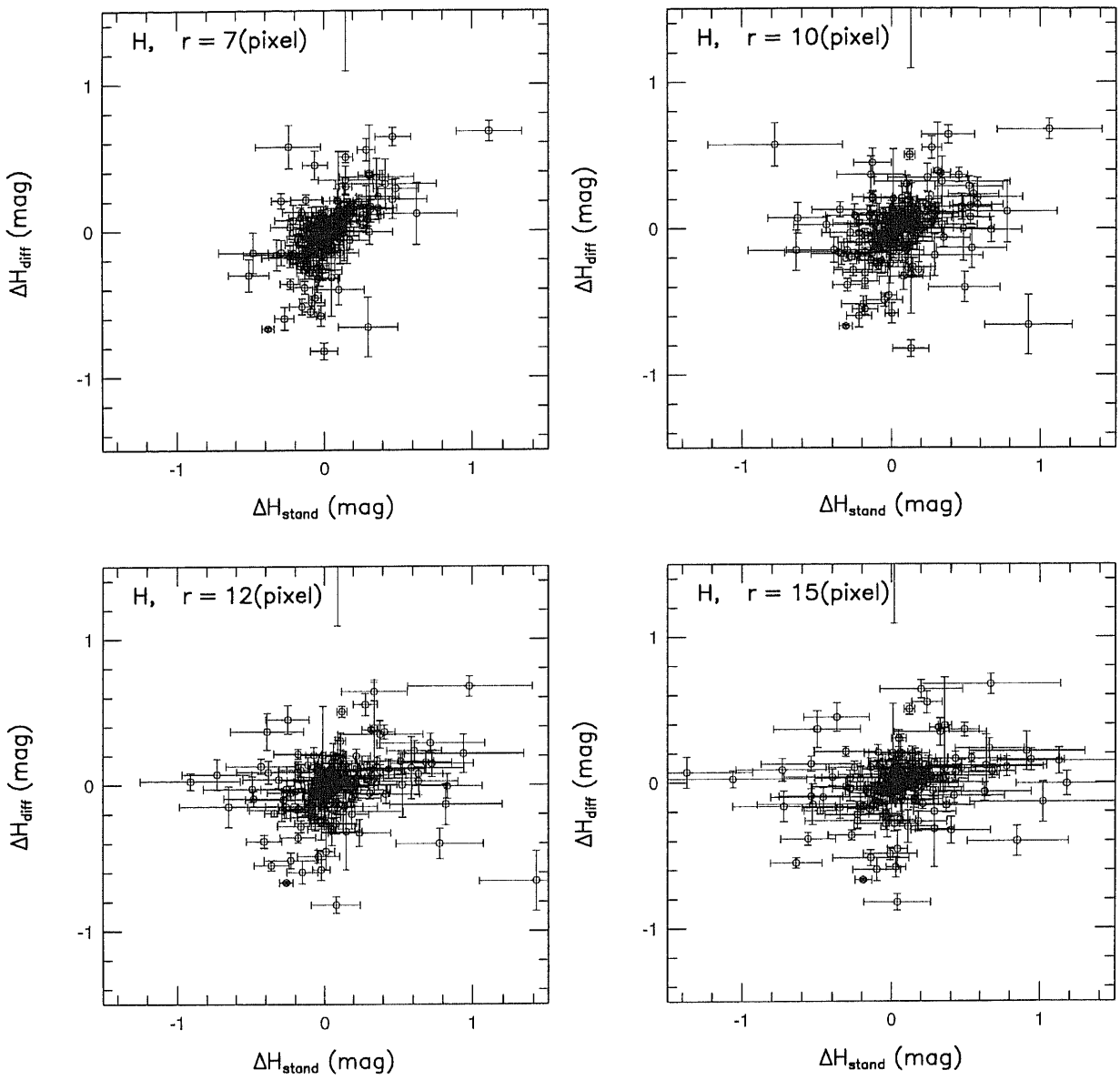

Figure B.5: The relation between the AGN variability in H band determined by the differential photometory Δ_{diff} and by the photometory using phtometoric standard Δ_{stand}. r shows the apertuer used in the later method.

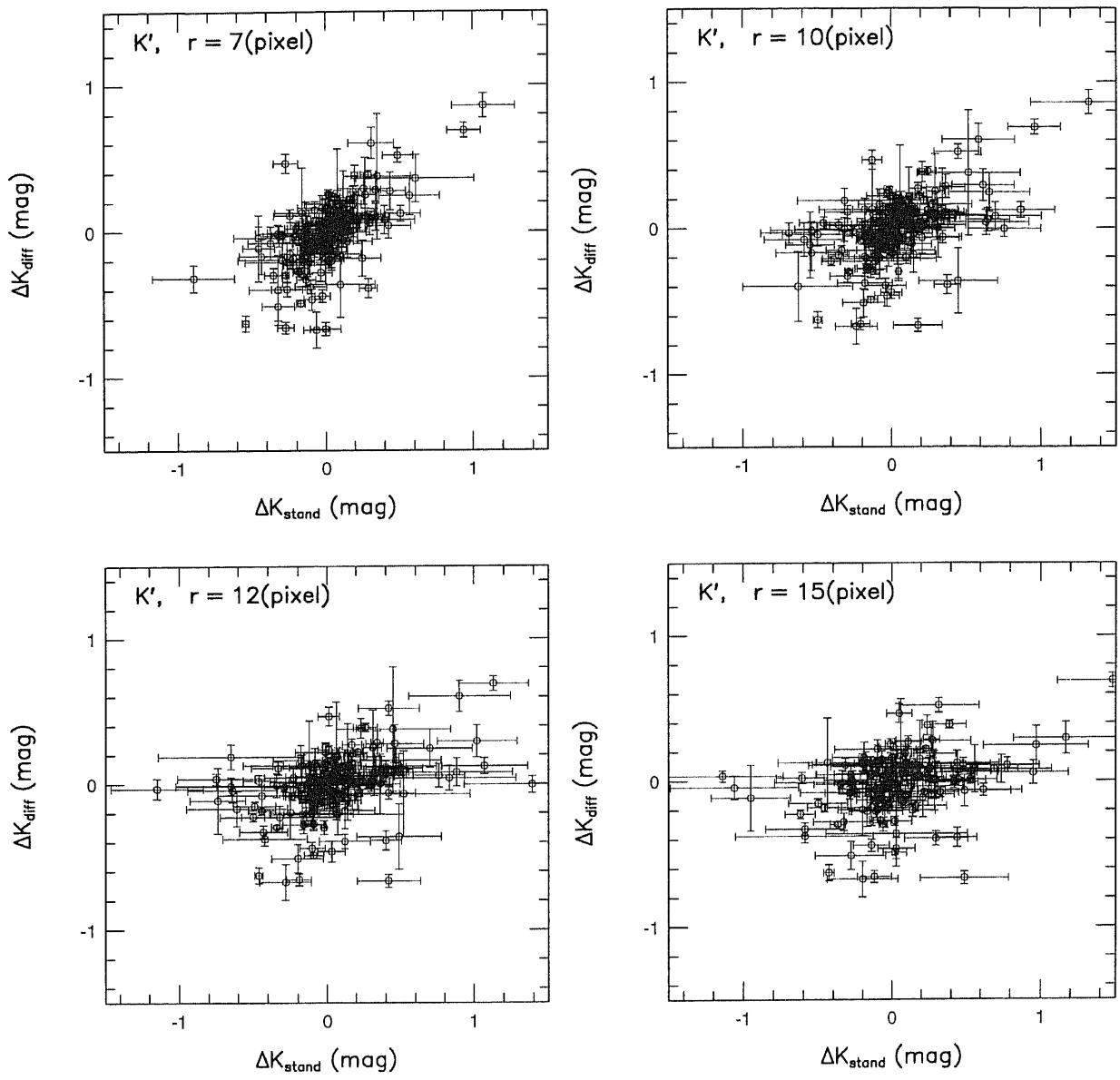

Figure B.6: The relation between the AGN variability in K' band determined by the differential photometory Δ_{diff} and by the photometory using phtometoric standard Δ_{stand}. r shows the apertuer used in the later method.

B.2 variability and other parameter of AGN

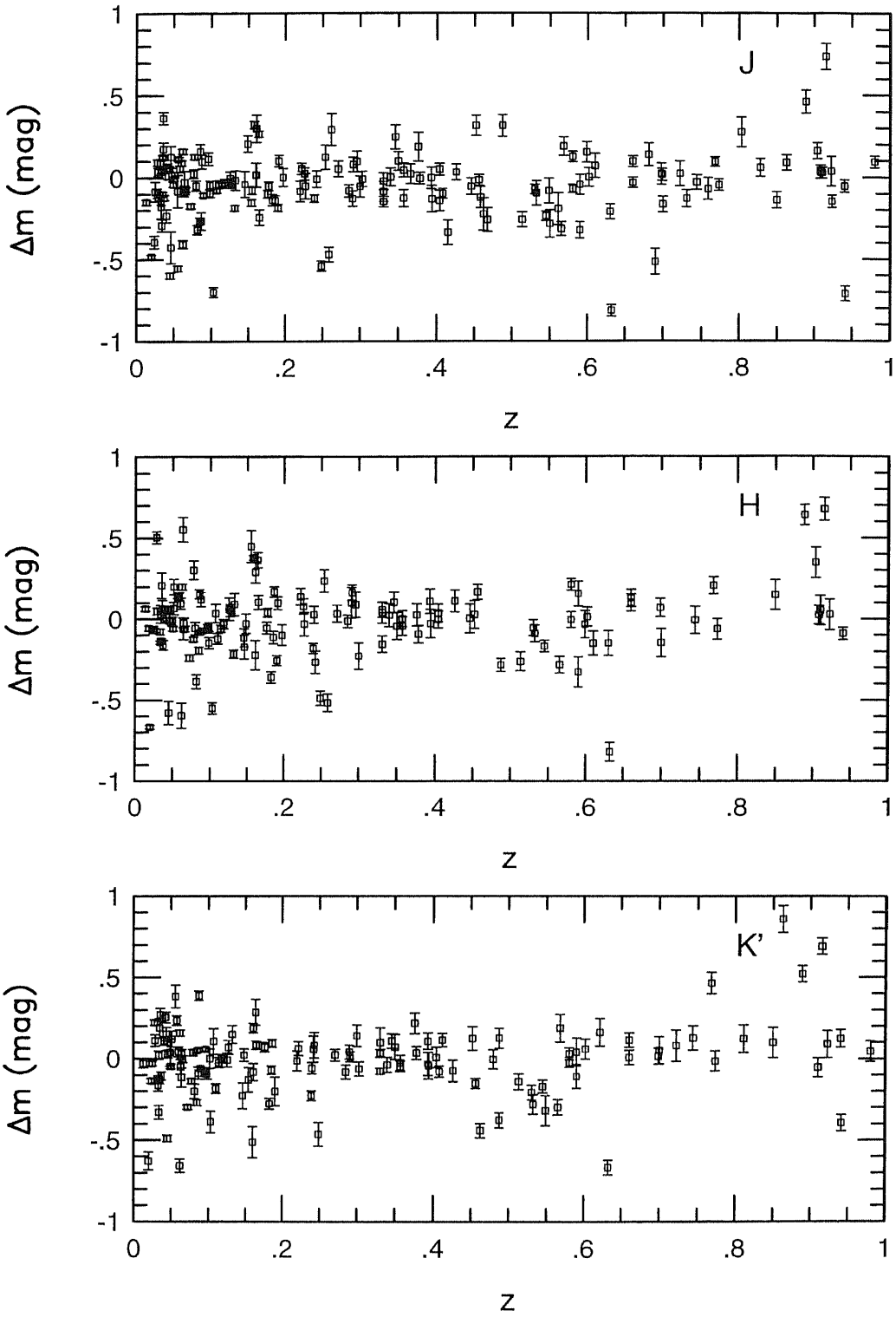

Figure B.7: Relation between variability of AGN at J,H and K' band and redshift. Only the data estimated with more than two reference objects and with accuracy higher than 0.1mag are plotted.

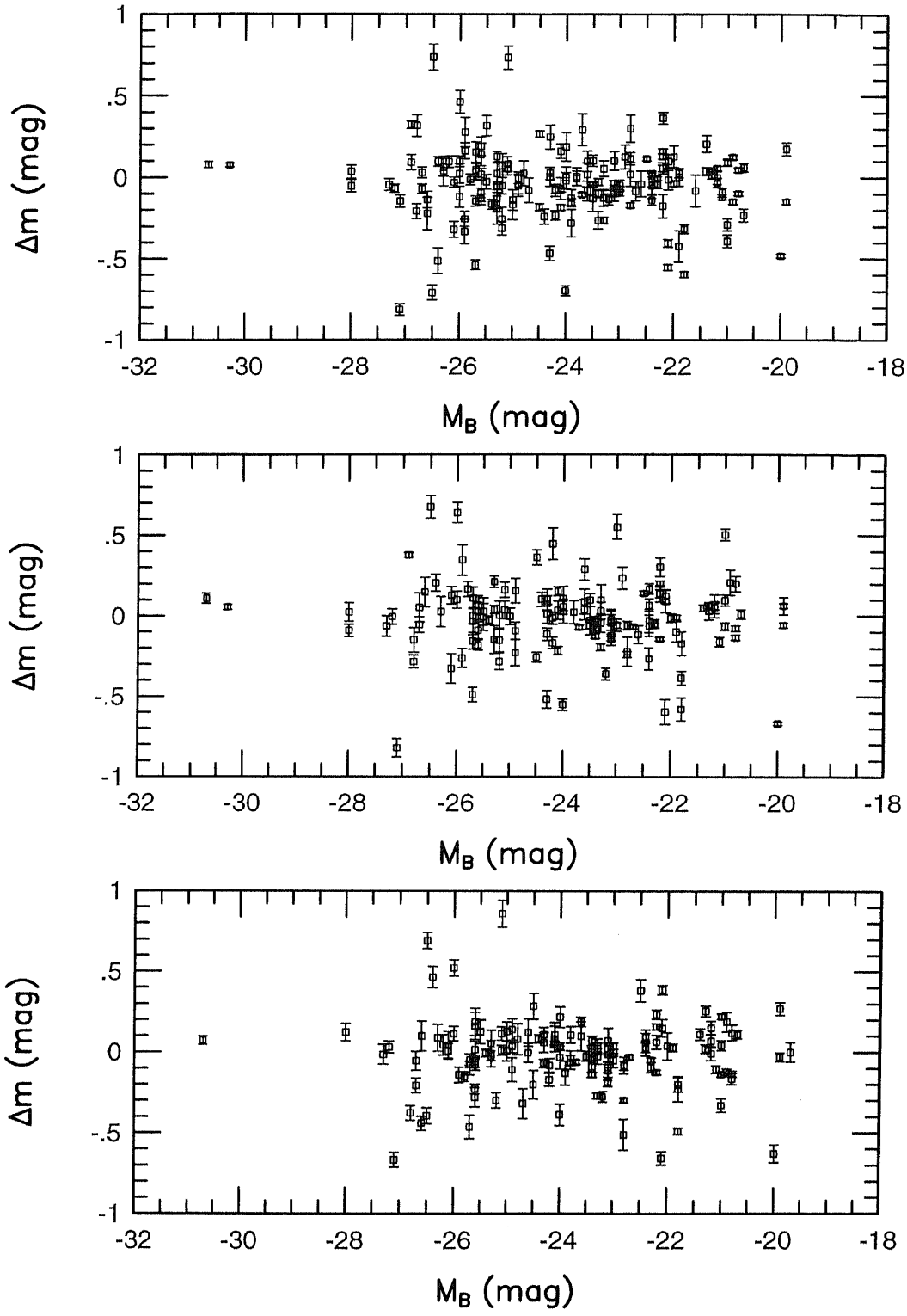

Figure B.8: Relation between variability of AGN at J,H and K' band and B band absolute magnitude M_B. Only the data estimated with more than two reference objects and with accuracy higher than 0.1mag are plotted.

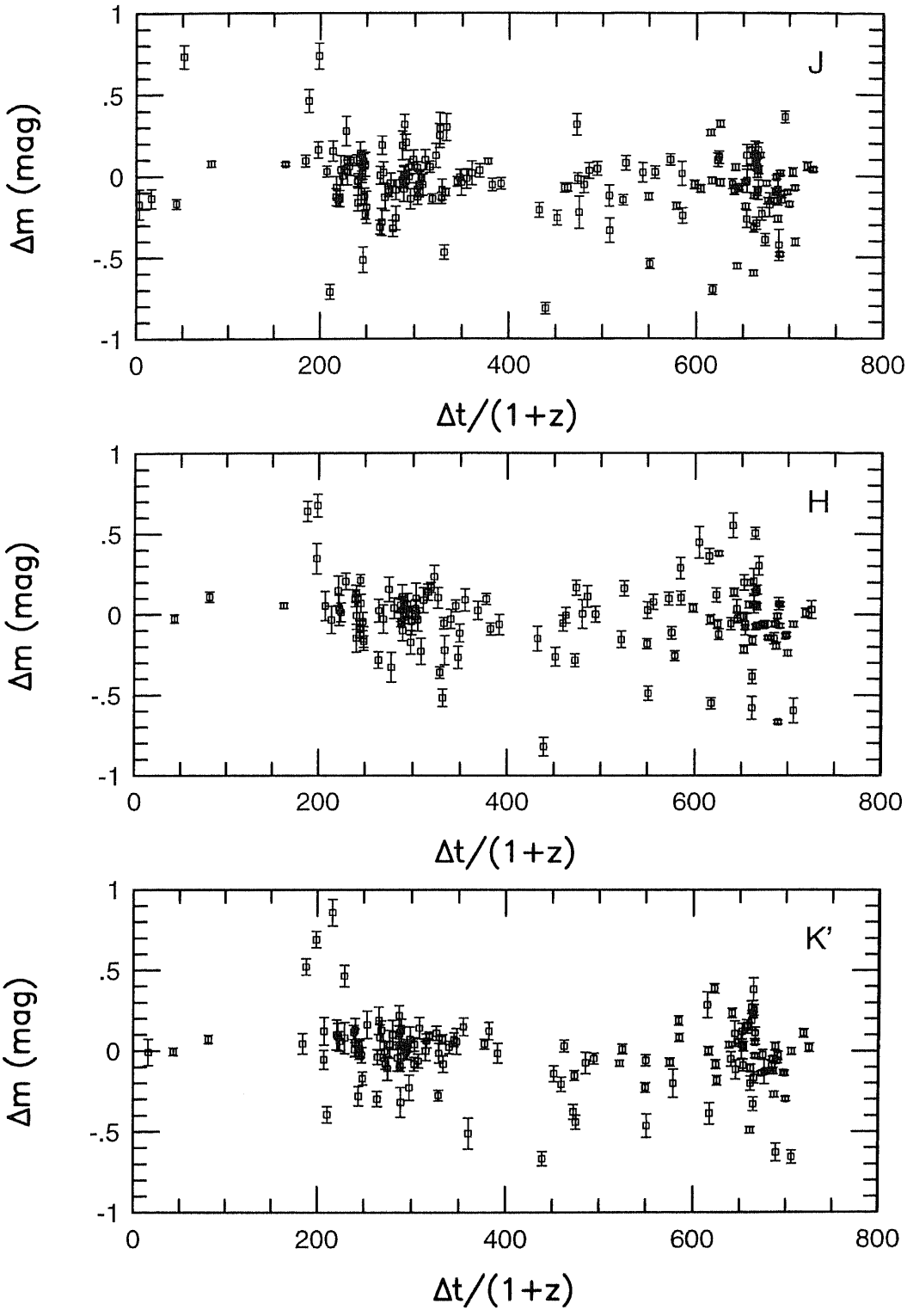

Figure B.9: Relation between variability of AGN at J,H and K' band and rest frame interval of the observation $\Delta t/(1+z)$. Only the data estimated with more than two reference objects and with accuracy higher than 0.1mag are plotted.

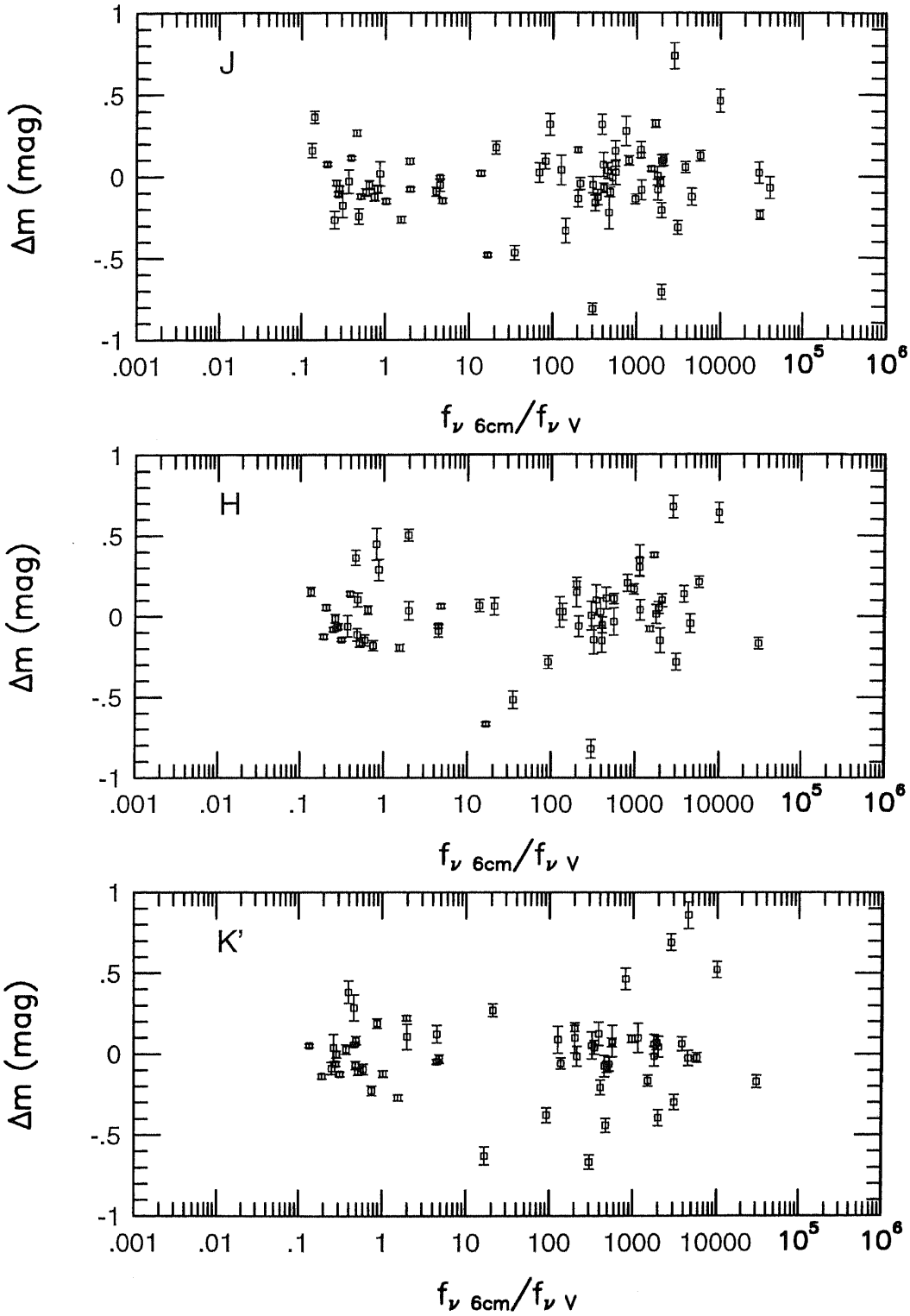

Figure B.10: Relation between variability of AGN at J,H and K' band and radio activity. the radio activity is estimated as the ratio of the flux at 6cm wavelength and at V band $f_{\nu 6cm}/f_{\nu V}$.

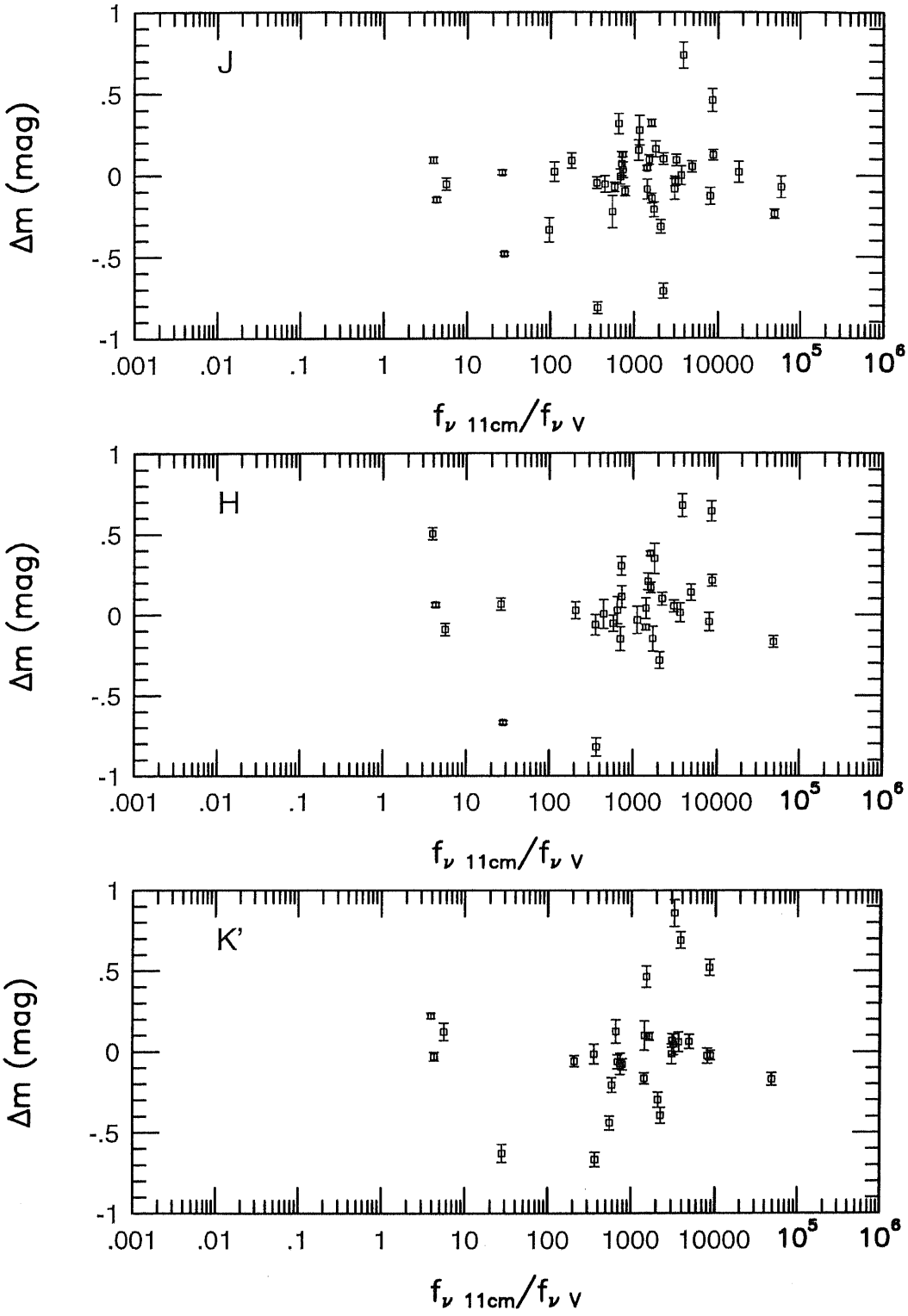

Figure B.11: Relation between variability of AGN at J,H and K' band and radio activity. the radio activity is estimated as the ratio of the flux at 6cm wavelength and at V band $f_{\nu 11cm}/f_{\nu V}$.

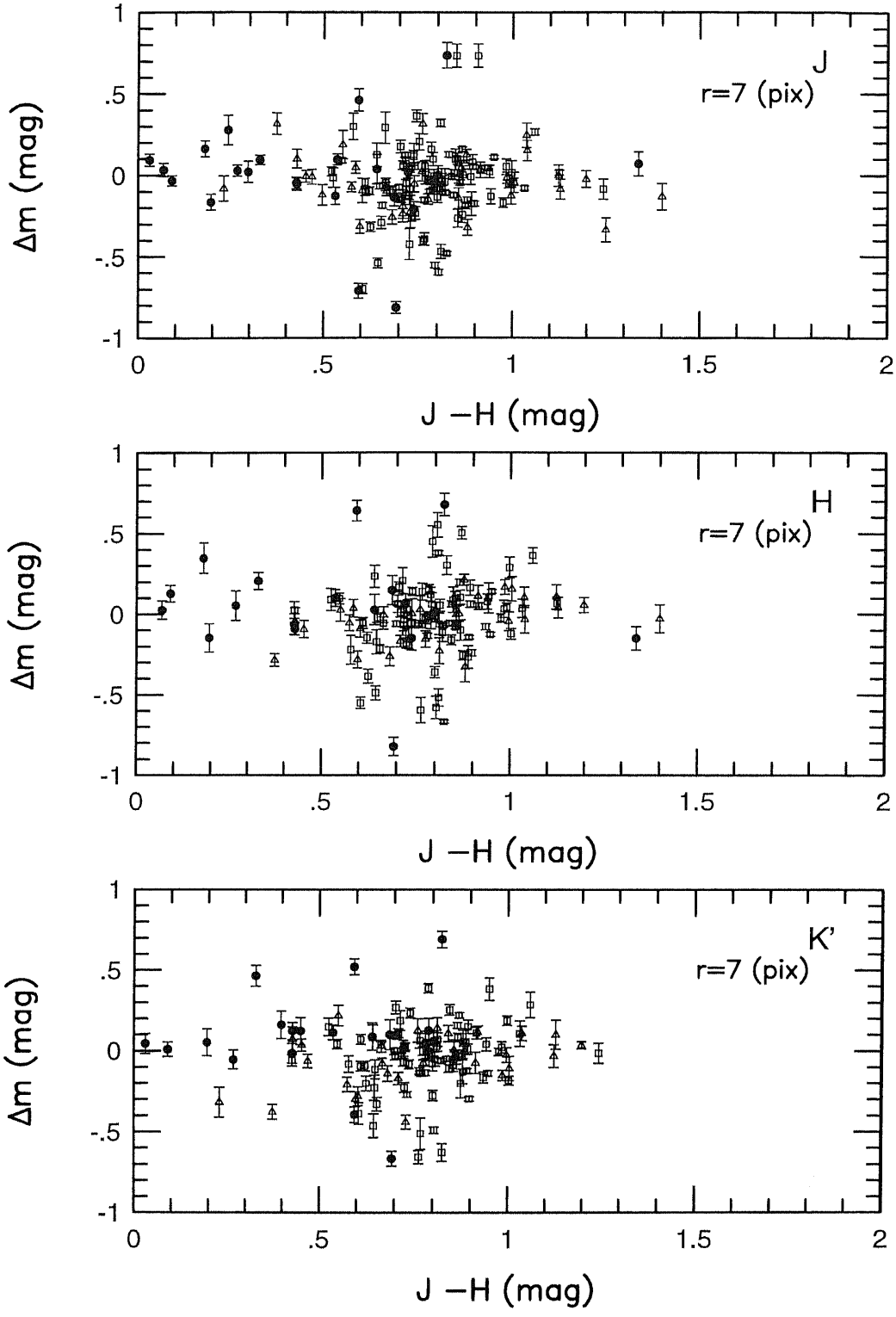

Figure B.12: Relation between variability of AGN at J,H and K' band and radio near infrared color J-H. Only the data estimated with more than two reference objects and with accuracy higher than 0.1mag are plotted.

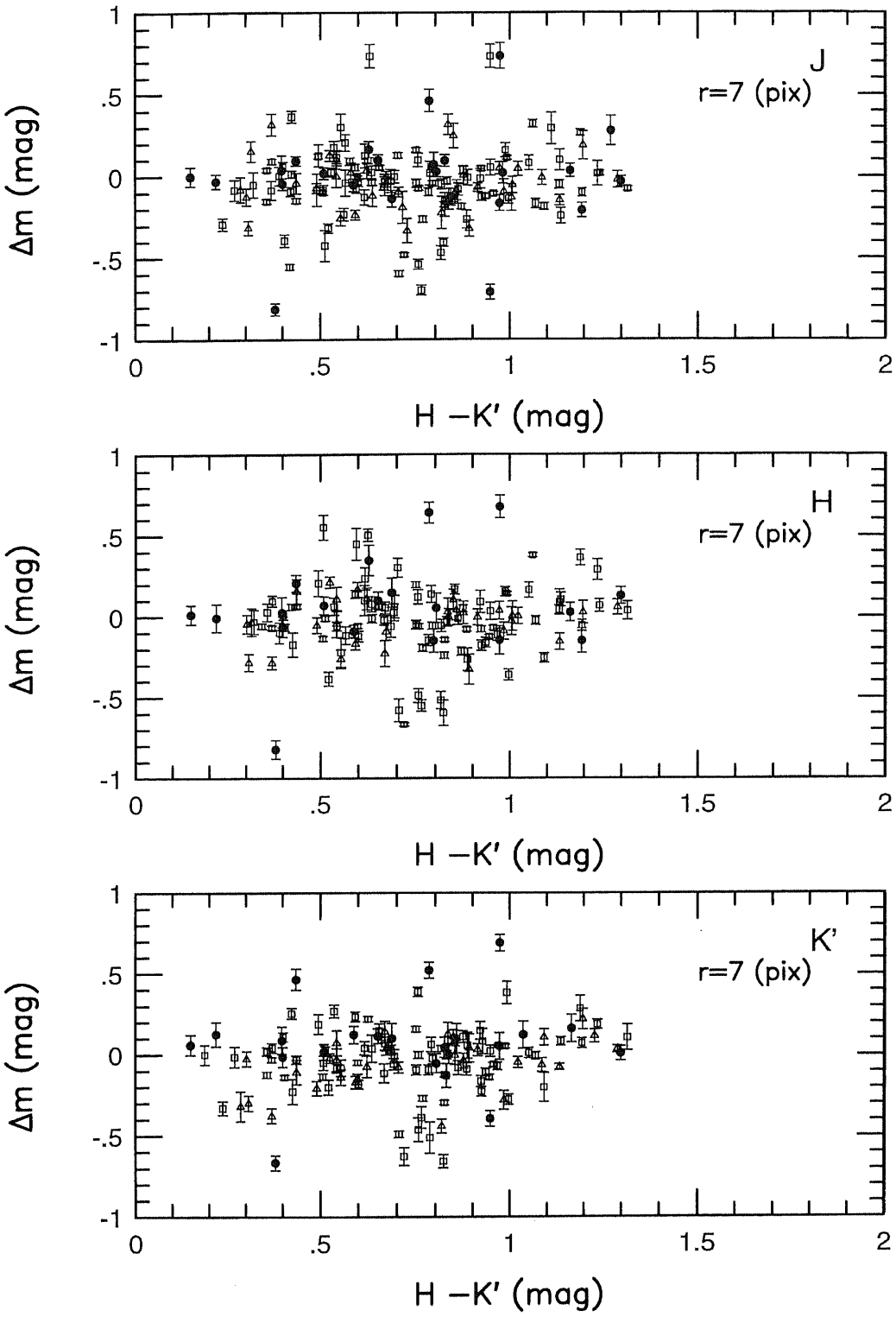

Figure B.13: Relation between variability of AGN at J,H and K' band and radio near infrared color H-K'. Only the data estimated with more than two reference objects and with accuracy higher than 0.1mag are plotted.

B.3 frequency distribution of the probability of having varied

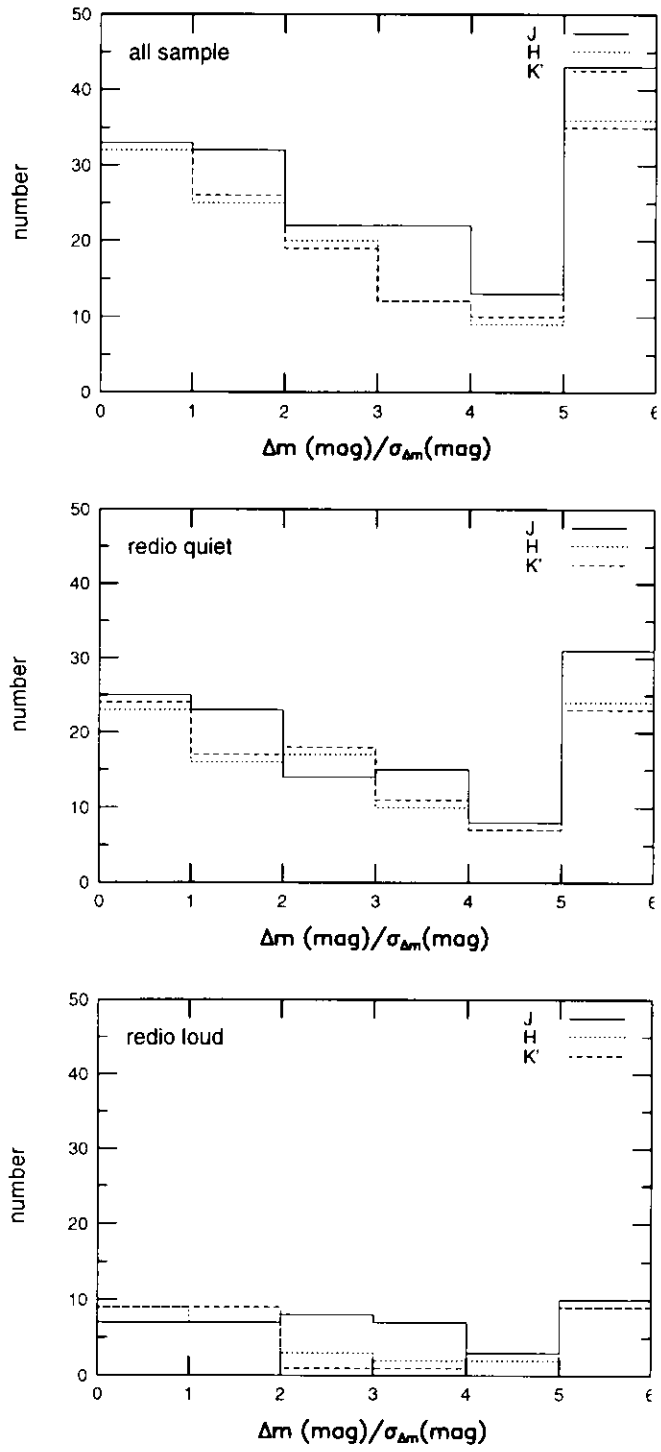

Figure B.14: Frequency distribution of probability of having varied Δm(mag)/$\sigma_{\Delta m}$(mag) for each object at J,H and K' band. Top, middle and bottom figure represents the distribution of the all sample, the radio quiet sample and the radio loud sample respectively. Only the data estimated with more than two reference objects and with accuracy higher than 0.1mag are plotted.

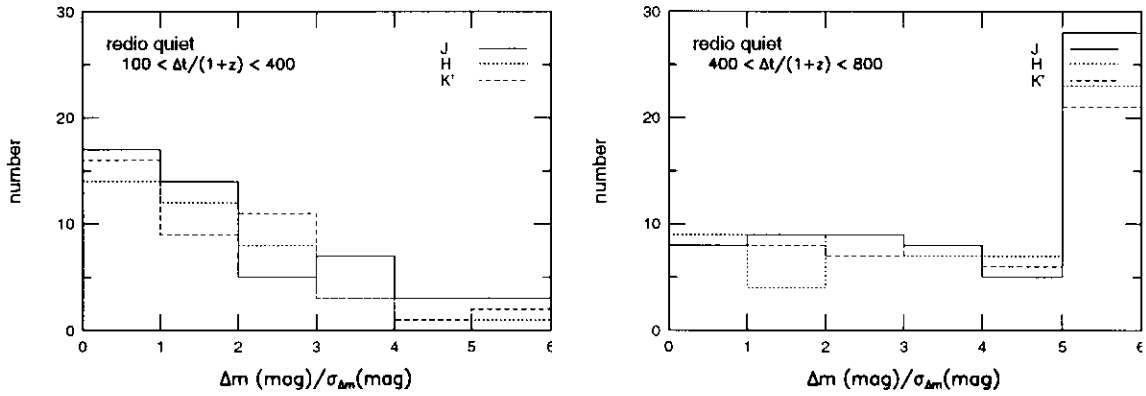

Figure B.15: Frequency distribution of probability of having varied Δm(mag)/$\sigma_{\Delta m}$(mag) for each radio quiet object at J,H and K' band. Left and right figure represents the sample with short interval of the observation (100days $< \Delta t/(1+z) <$400days) and with long interval of the observation (400days $< \Delta t/(1+z) <$800days). Only the data estimated with more than two reference objects and with accuracy higher than 0.1mag are plotted.

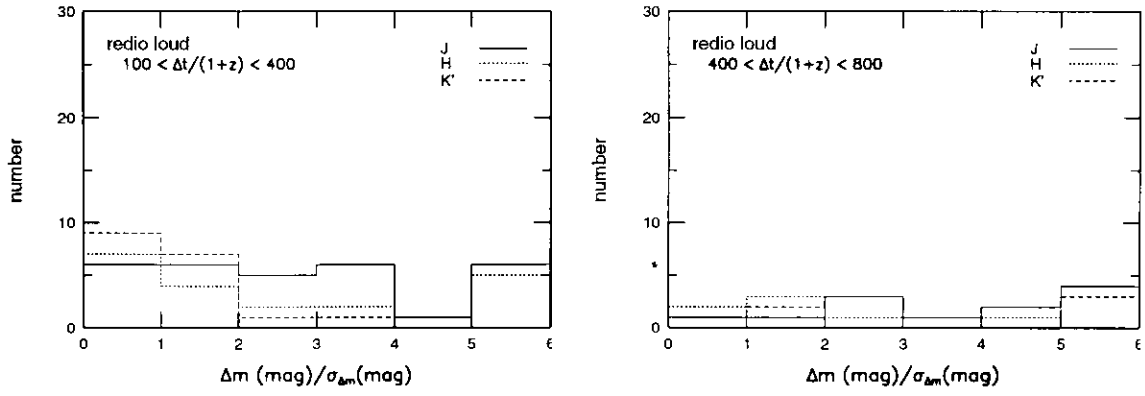

Figure B.16: Frequency distribution of probability of having varied Δm(mag)/$\sigma_{\Delta m}$(mag) for each radio loud object at J,H and K' band. Left and right figure represents the sample with short interval of the observation (100days $< \Delta t/(1+z) <$400days) and with long interval of the observation (400days $< \Delta t/(1+z) <$800days). Only the data estimated with more than two reference objects and with accuracy higher than 0.1mag are plotted.

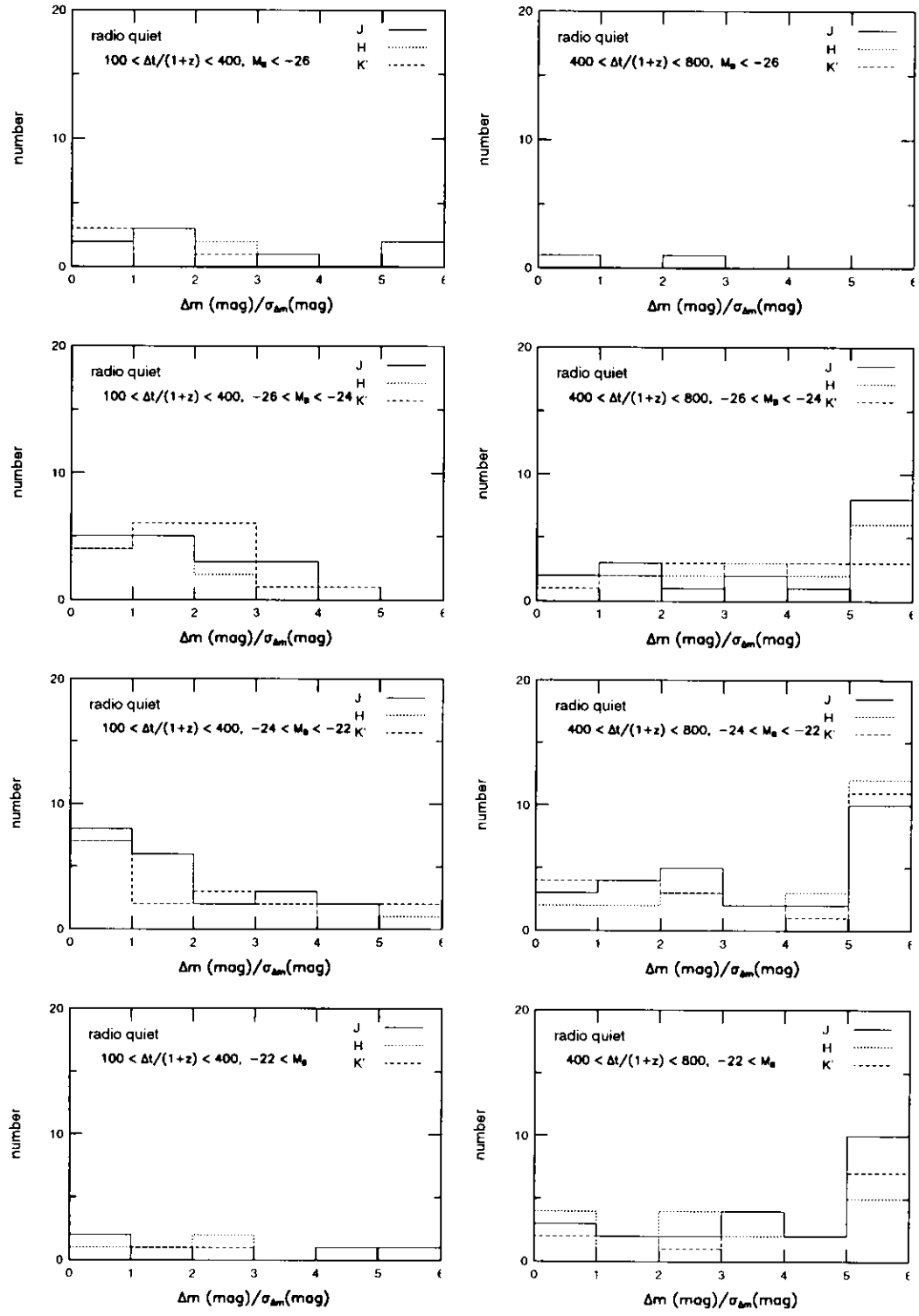

Figure B.17: Frequency distribution of Δm(mag)/$\sigma_{\Delta m}$(mag) for each radio quiet object at J,H and K' band. Left side figures represent the sample with short interval further divided by M_B. Right side figures are same but for long interval sample. Only the data estimated with more than two reference objects and with accuracy higher than 0.1mag are plotted.

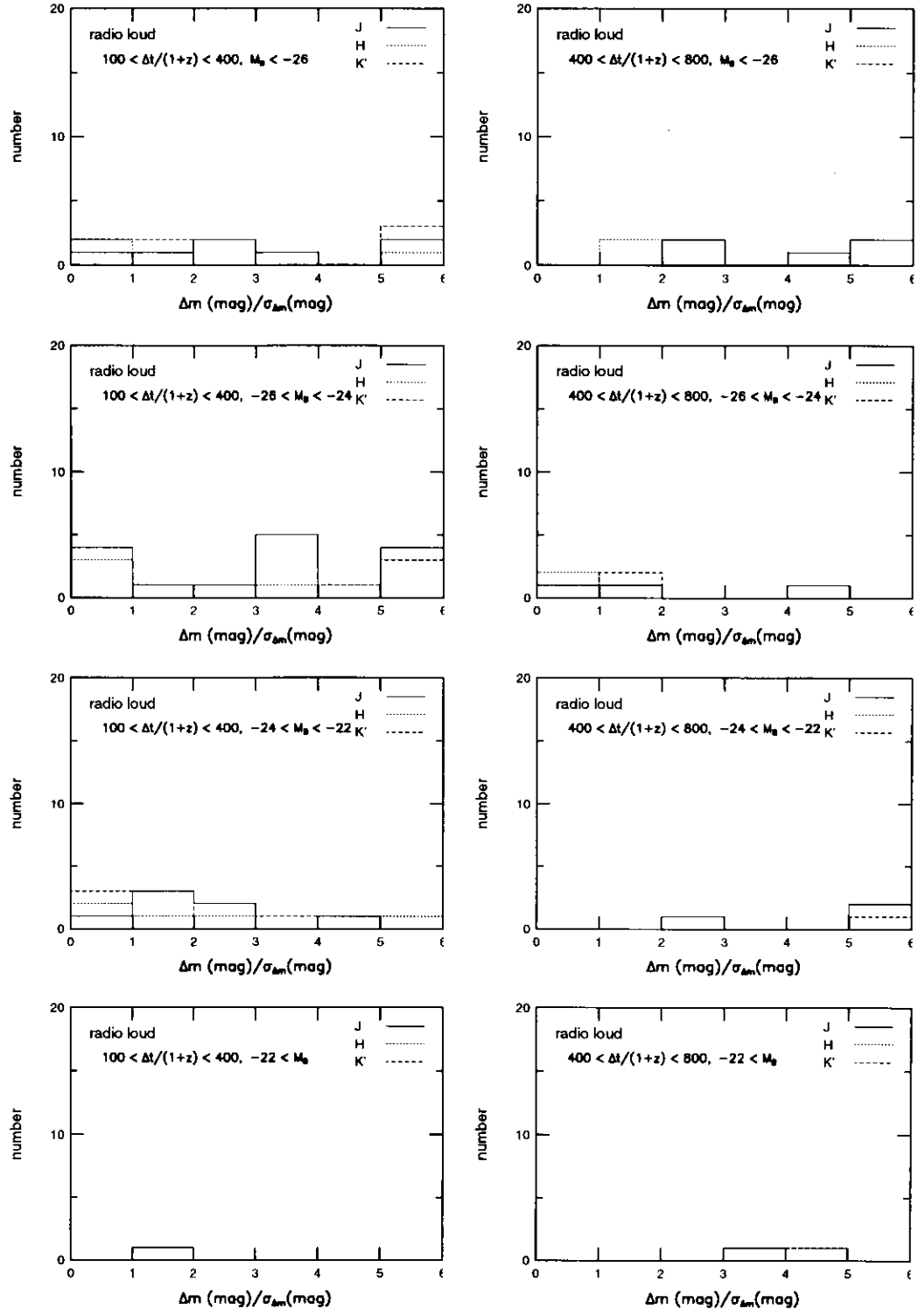

Figure B.18: Frequency distribution of Δm(mag)/$\sigma_{\Delta m}$(mag) for each radio loud object at J,H and K' band. Left side figures represent the sample with short interval further divided by M_B. Right side figures are same but for long interval sample. Only the data estimated with more than two reference objects and with accuracy higher than 0.1mag are plotted.

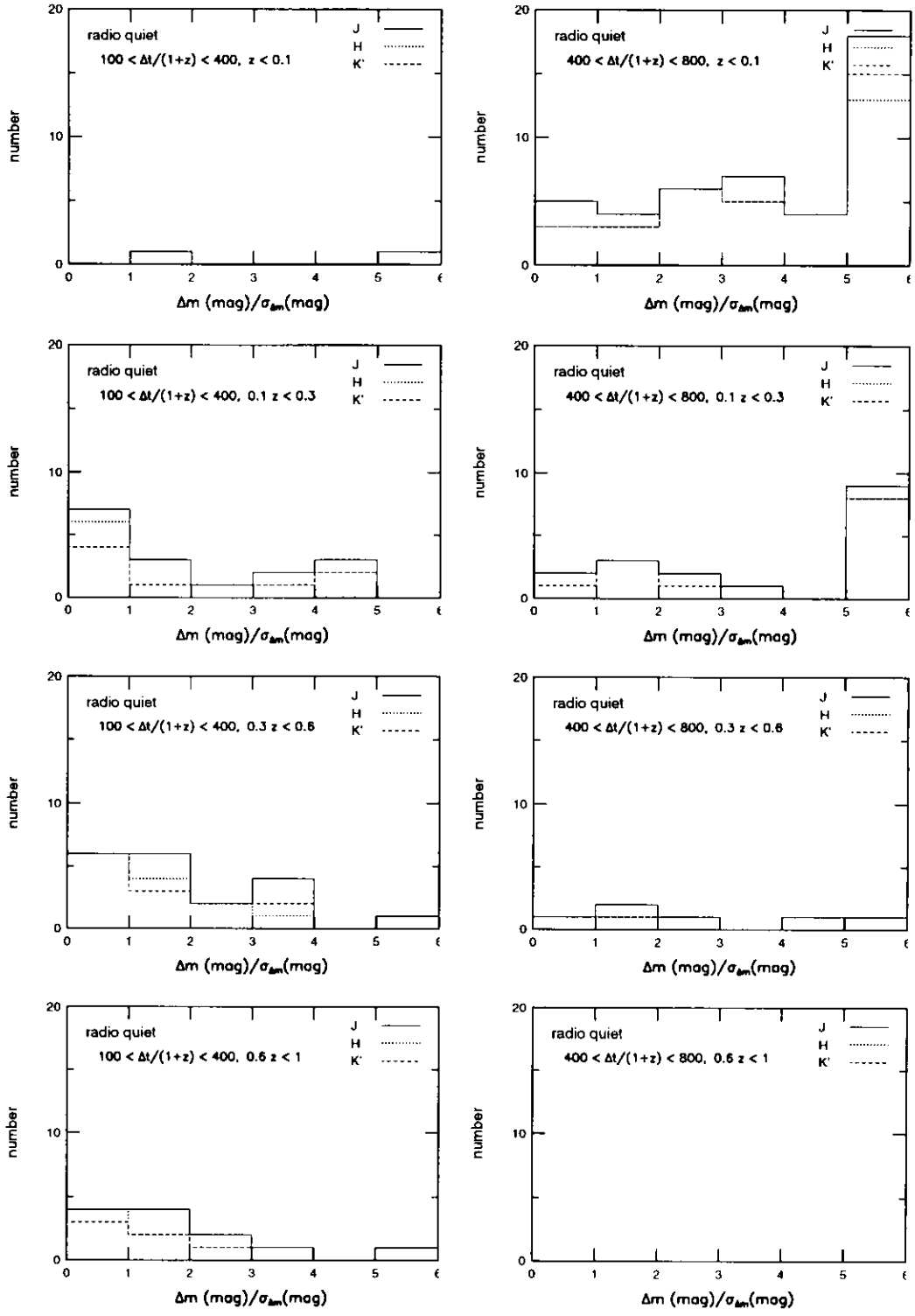

Figure B.19: Frequency distribution of Δm(mag)/$\sigma_{\Delta m}$(mag) for each radio quiet object at J,H and K' band. Left side figures represent the sample with short interval further divided by z. Right side figures are same but for long interval sample. Only the data estimated with more than two reference objects and with accuracy higher than 0.1mag are plotted.

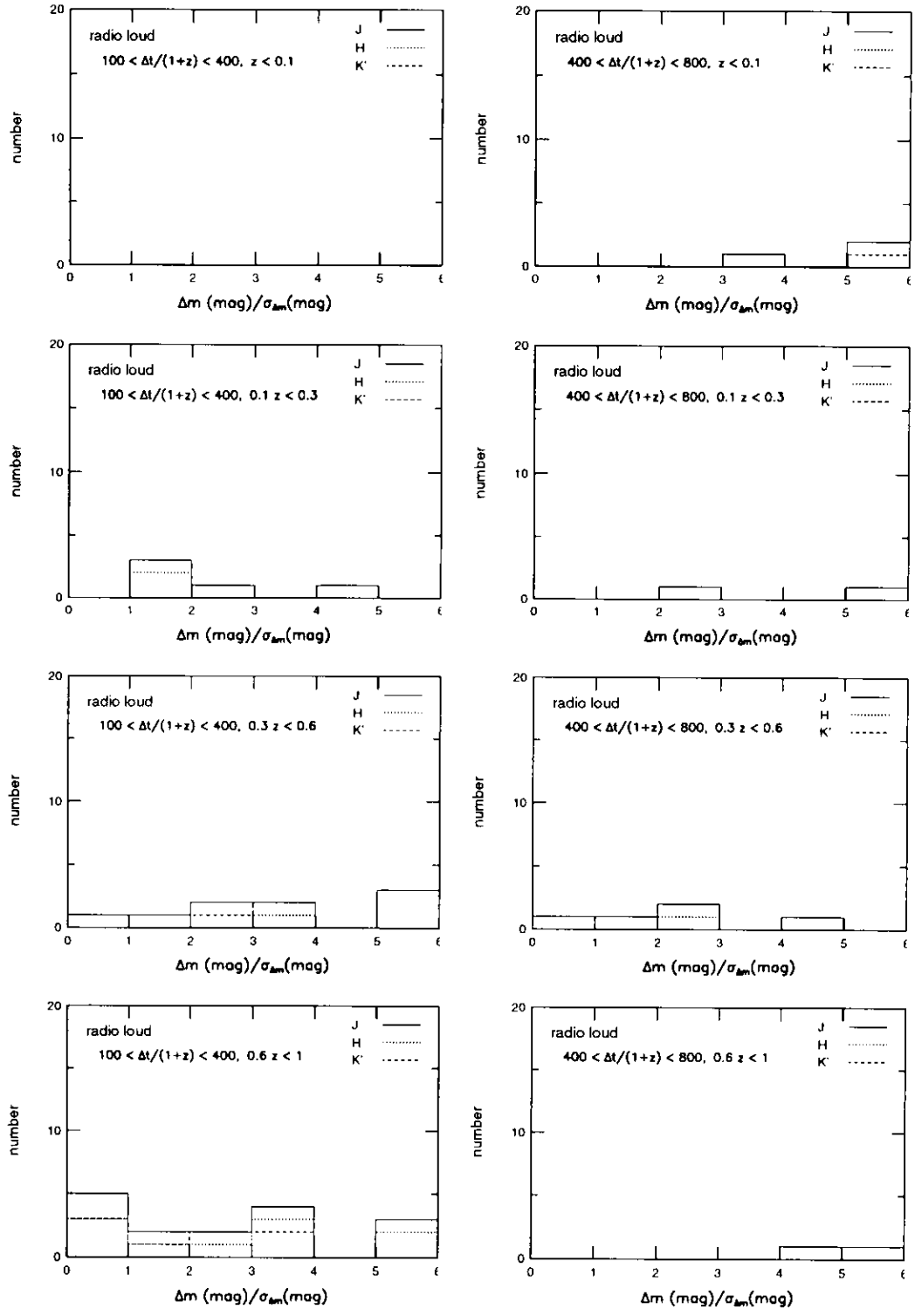

Figure B.20: Frequency distribution of Δm(mag)/$\sigma_{\Delta m}$(mag) for each radio loud object at J,H and K' band. Left side figures represent the sample with short interval further divided by z. Right side figures are same but for long interval sample. Only the data estimated with more than two reference objects and with accuracy higher than 0.1mag are plotted.

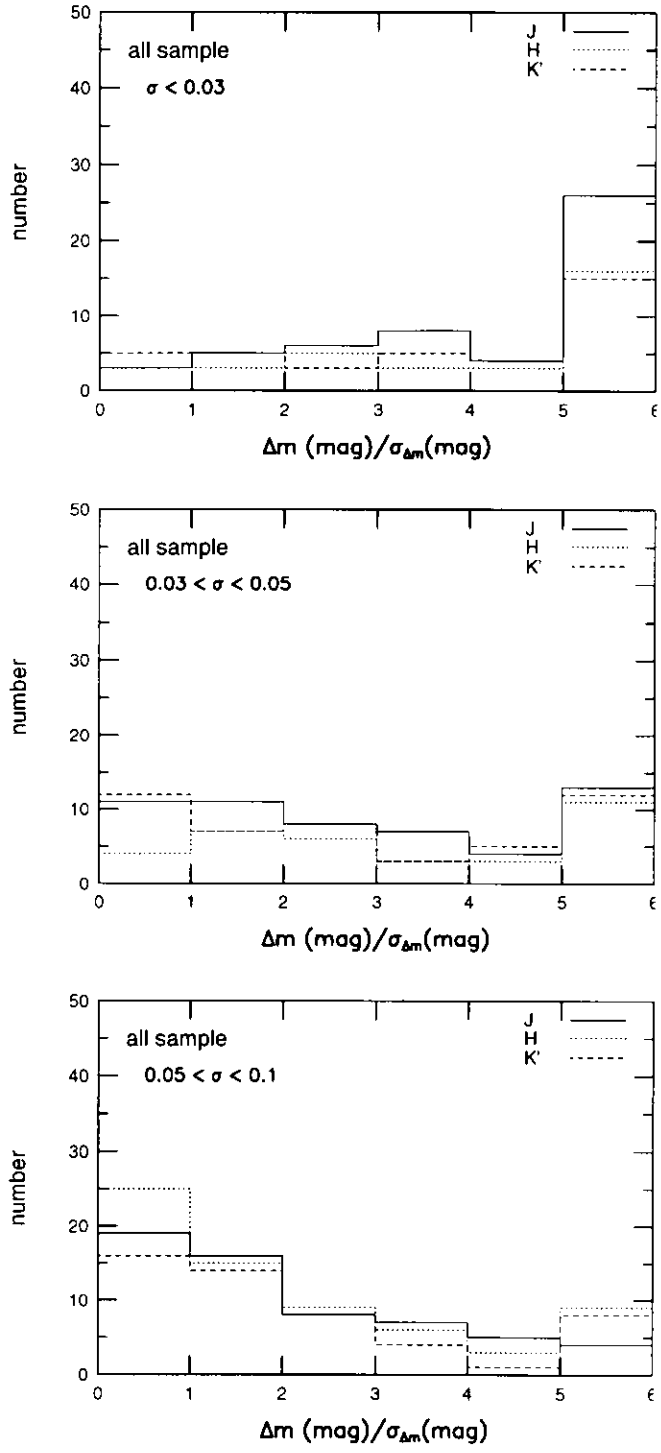

Figure B.21: Frequency distributions of the probability of having varied Δm(mag)/σ(mag) of each AGN in the subsample made by dividing all sample by the accuracy of variability determination. Top, middle and bottom figure represents the highest accuracy group with σ(mag)$<$ 0.03, intermediate accuracy group with 0.03$<$ σ(mag)$<$0.05 and the lowest accuracy group with 0.05$<$ σ(mag)$<$0.1. Only the data estimated with more than two reference objects and with accuracy higher than 0.1mag are plotted.

B.4 frequency distribution of variability

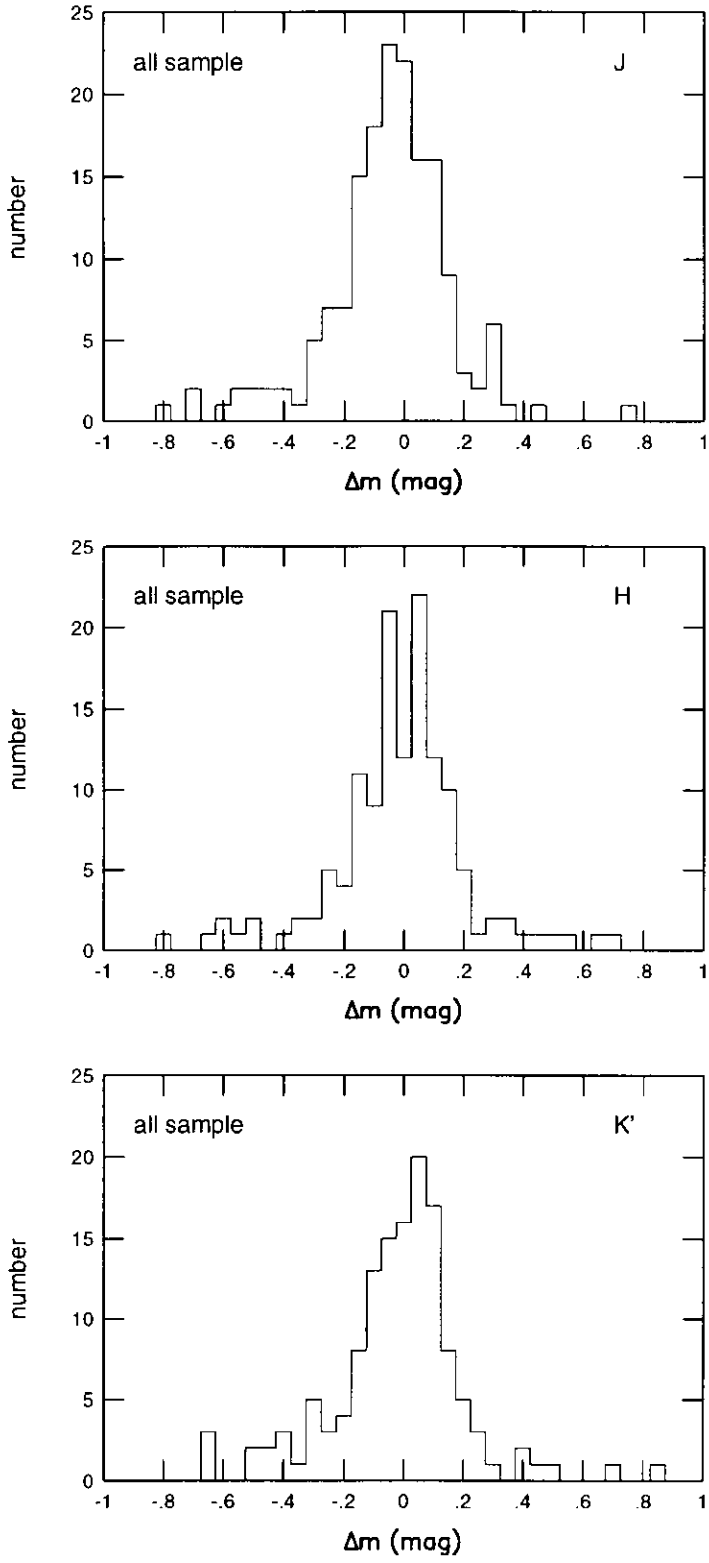

Figure B.22: Frequency distribution of the variability of the all sample at J,H and K' band. Only the data estimated with more than two reference objects and with accuracy higher than 0.1mag are plotted.

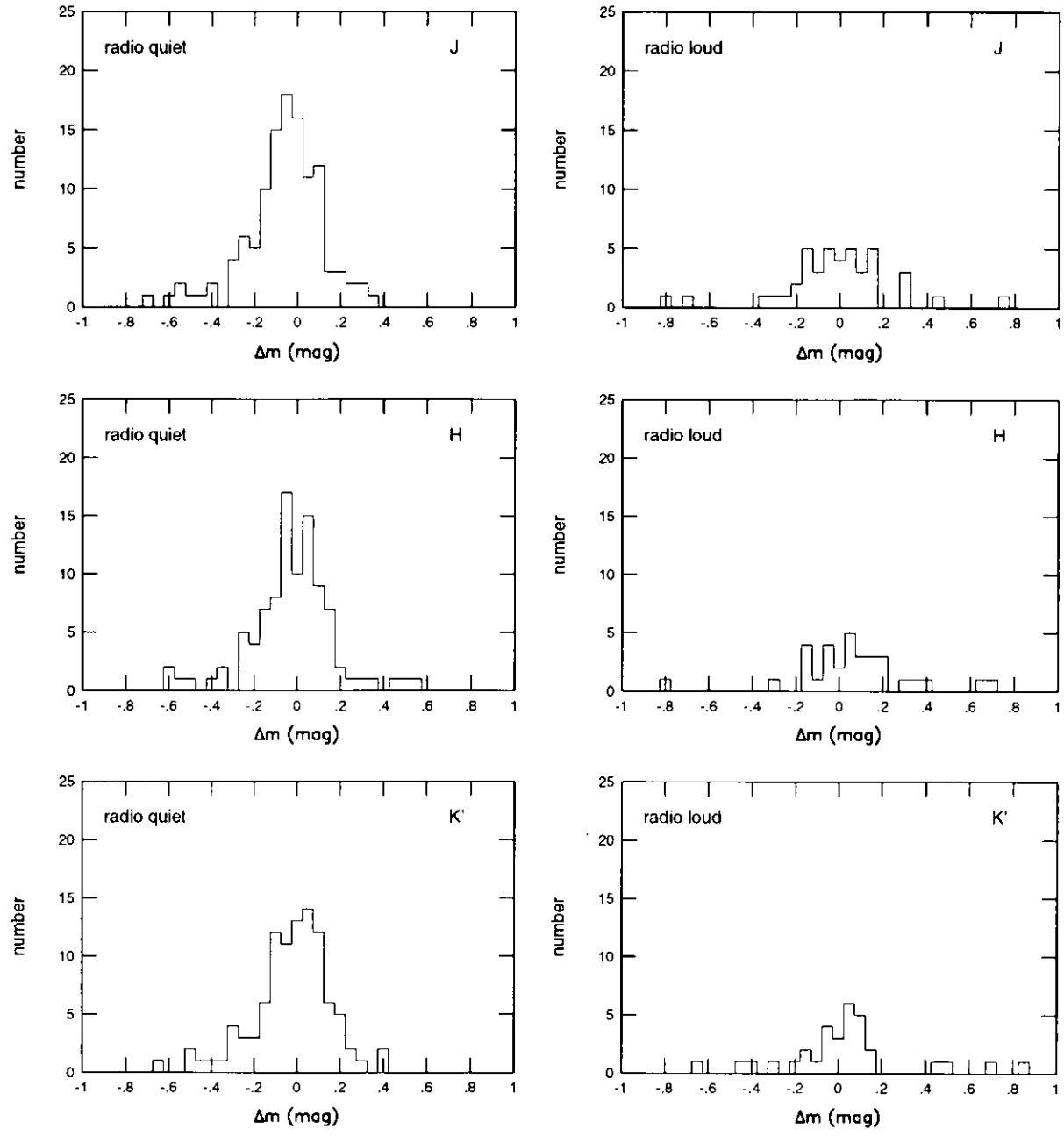

Figure B.23: Left side figures show frequency distribution of the variability of the radio quiet sample at J,H and K' band. Right side figures are same but for the radio loud sample. Only the data estimated with more than two reference objects and with accuracy higher than 0.1mag are plotted.

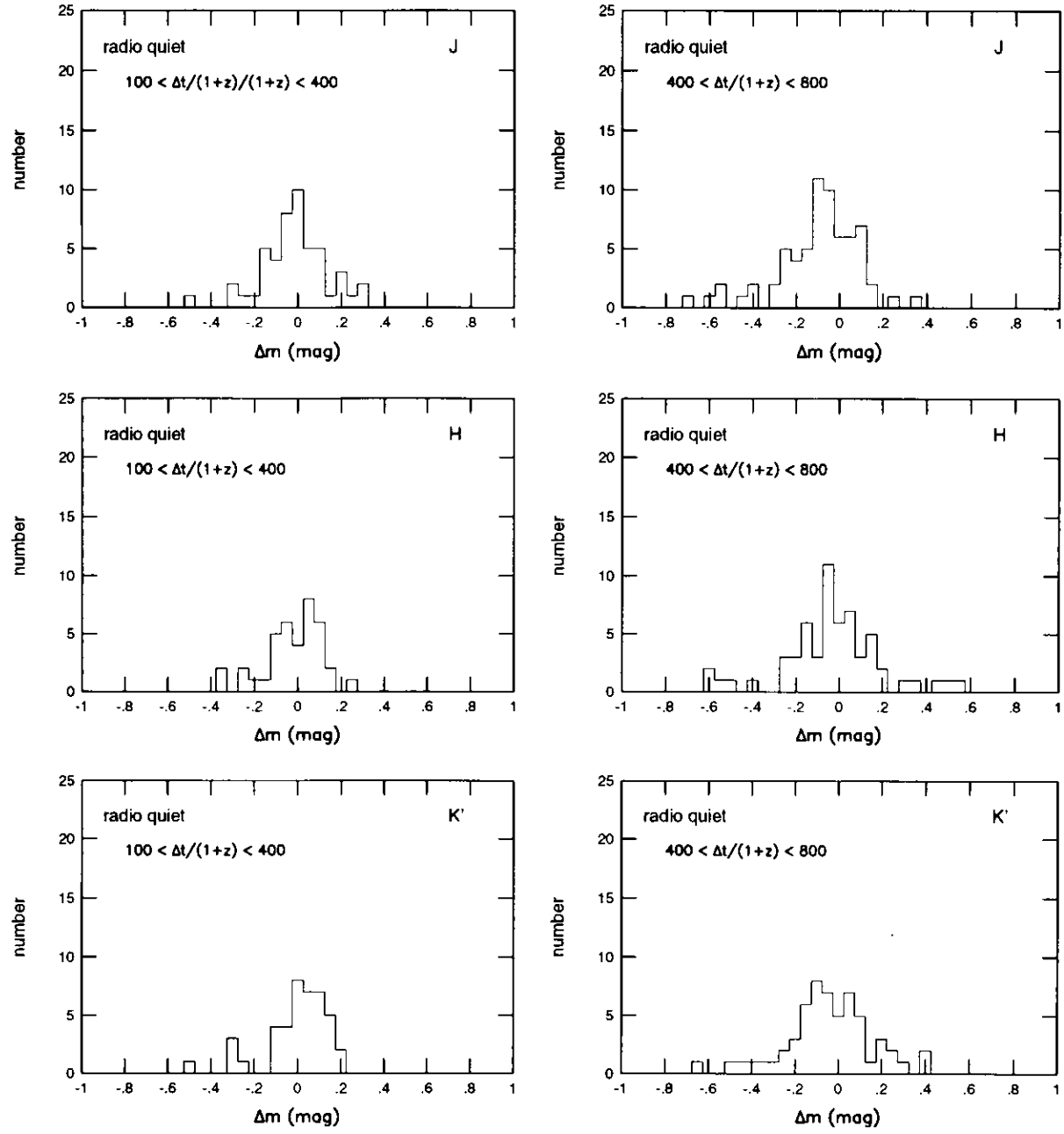

Figure B.24: Left side figures show frequency distribution of the variability of the radio quiet sample with short interval of the observation 100days $< \Delta t/(1+z) <$400days at J,H and K' band. Right side figures are same but for the sample with long interval of the observation 400days $< \Delta t/(1+z) <$800days. Only the data estimated with more than two reference objects and with accuracy higher than 0.1mag are plotted.

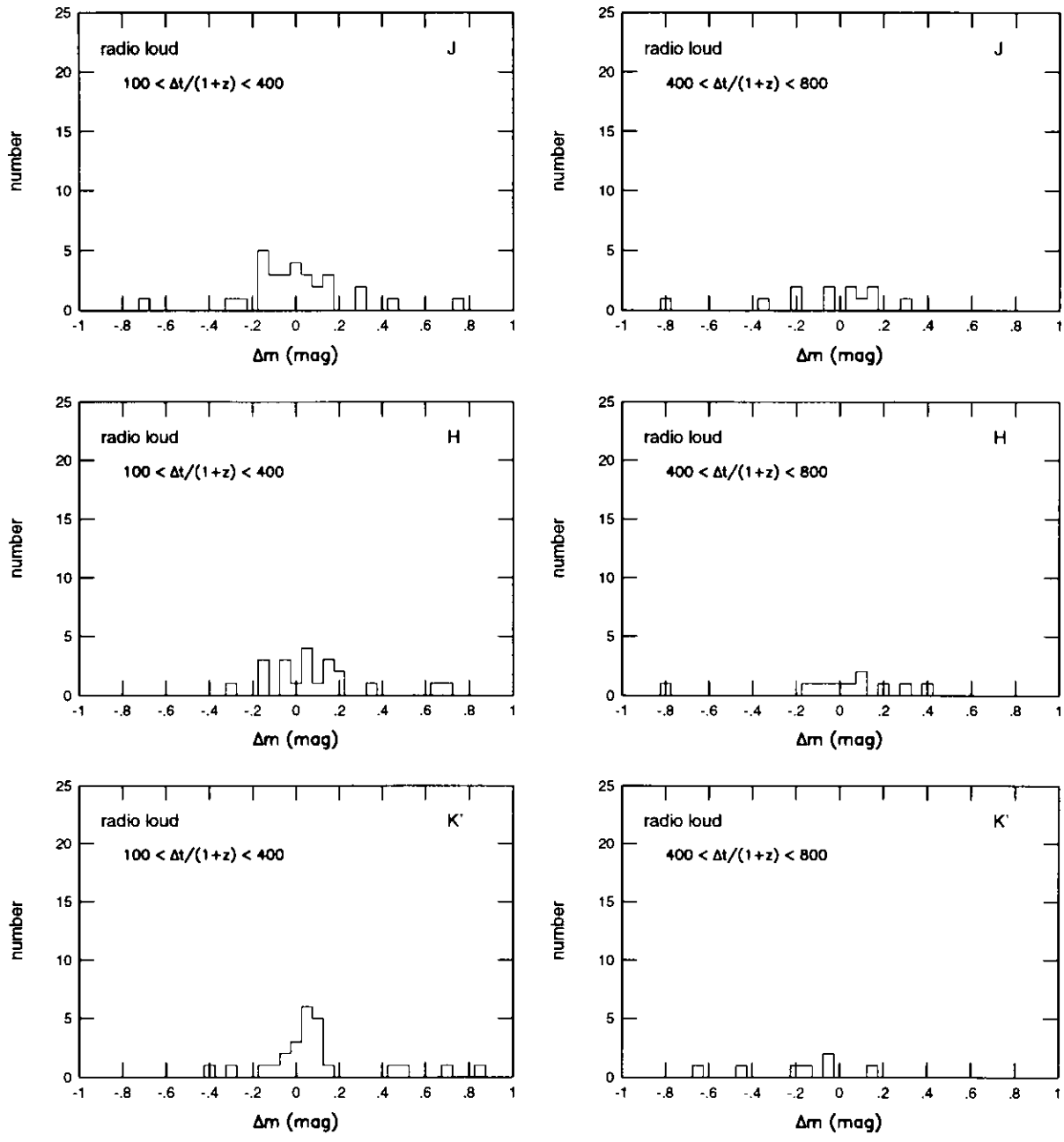

Figure B.25: Left side figures show frequency distribution of the variability of the radio loud sample with short interval of the observation 100days $< \Delta t/(1+z) <$400days at J,H and K' band. Right side figures are same but for the sample with long interval of the observation 400days $< \Delta t/(1+z) <$800days. Only the data estimated with more than two reference objects and with accuracy higher than 0.1mag are plotted.

B.5 correlation of variability of different band

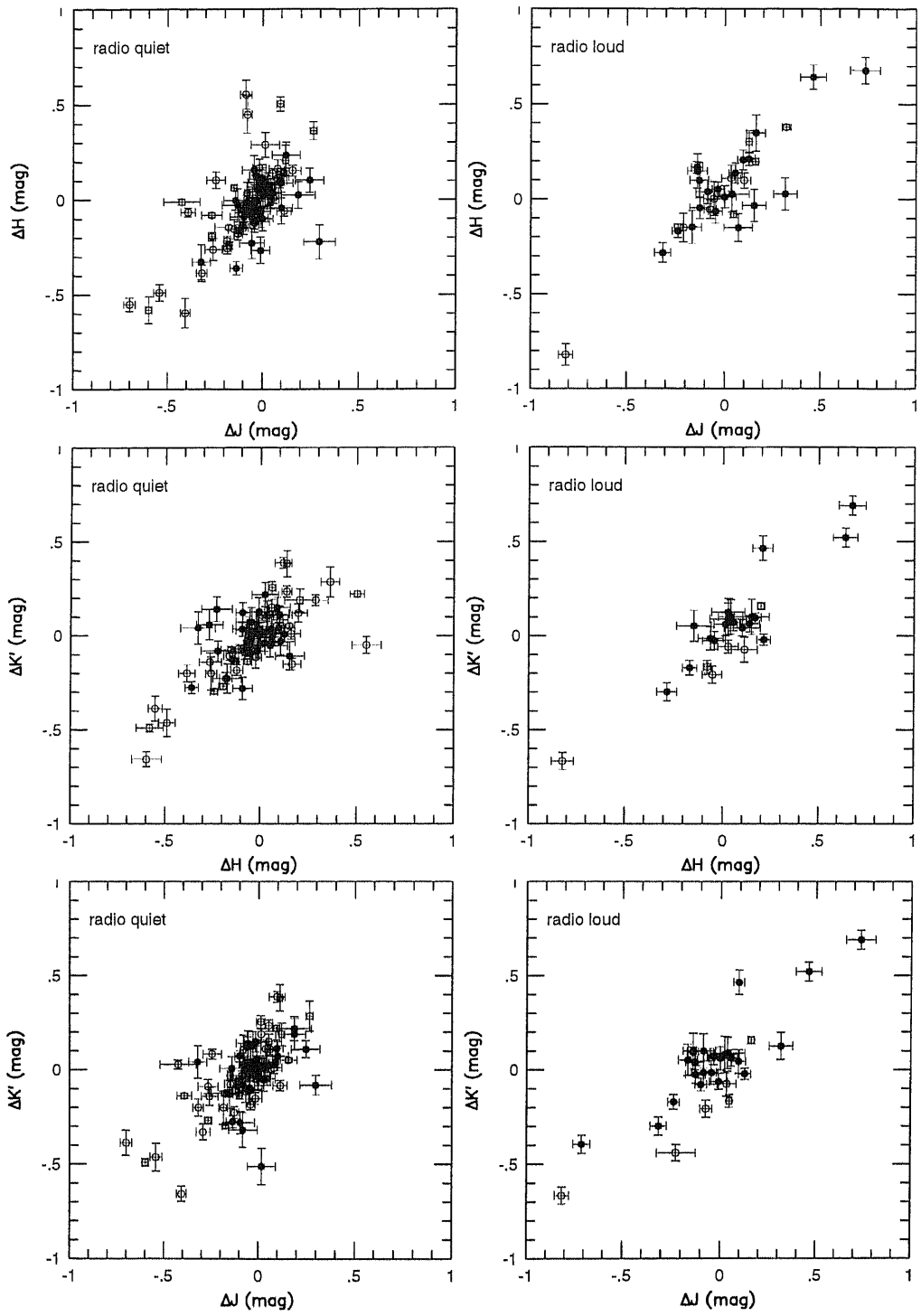

Figure B.26: Left side figures show the correlation of the variability of J and H, H and K', J and K' band for each radio quiet object. Filled circle represents the sample with short rest frame interval of the observation $100days < \Delta t < 400days$ and long. Open circle represents same but with long interval $400days < \Delta t < 800days$. Right side figures are same but for the radio loud sample. Only the data estimated with more than two reference objects and with accuracy higher than 0.1mag are plotted.

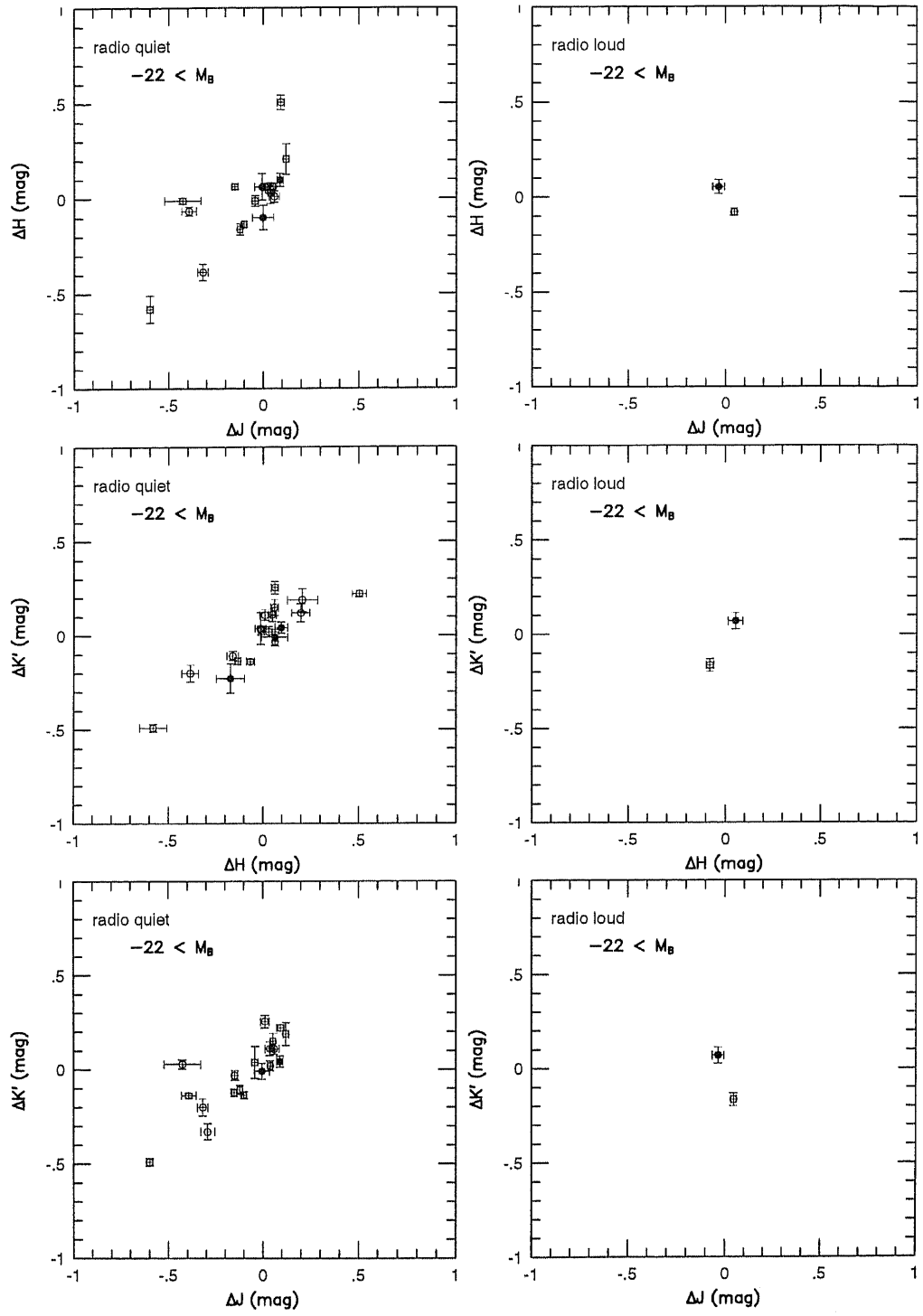

Figure B.27: Left side figures show the correlation of the variability of J and H, H and K', J and K' band for each radio quiet object with $-22 < M_B$. Filled circle represents the sample with short rest frame interval of the observation $100days < \Delta t < 400days$ and long. Open circle represents same but with long interval $400days < \Delta t < 800days$. Right side figures are same but for the radio loud sample. Only the data estimated with more than two reference objects and with accuracy higher than 0.1mag are plotted.

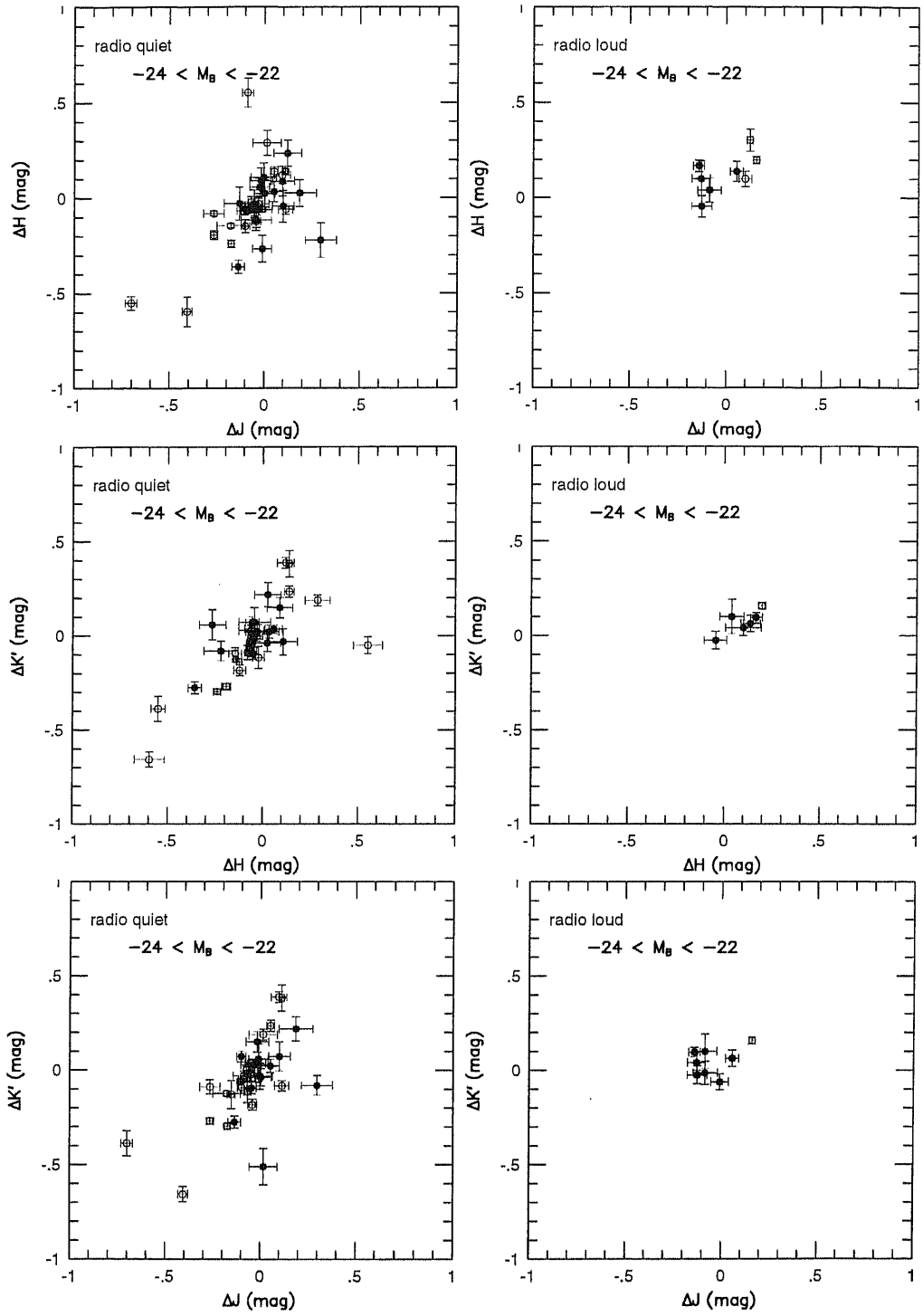

Figure B.28: Left side figures show the correlation of the variability of J and H, H and K', J and K' band for each radio quiet object with $-24 < M_B < -22$. Filled circle represents the sample with short rest frame interval of the observation $100 days < \Delta t < 400 days$ and long. Open circle represents same but with long interval $400 days < \Delta t < 800 days$. Right side figures are same but for the radio loud sample. Only the data estimated with more than two reference objects and with accuracy higher than 0.1mag are plotted.

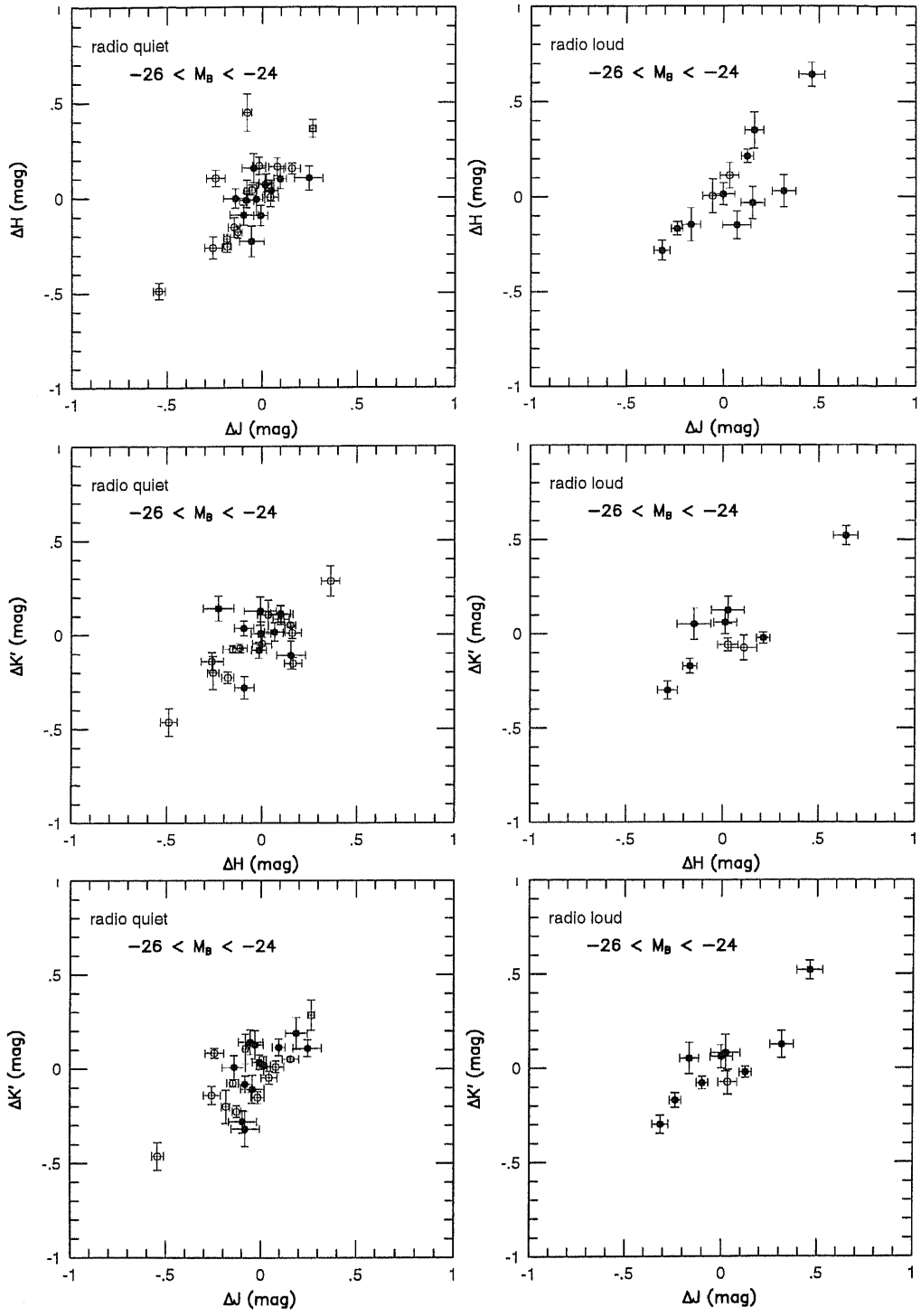

Figure B.29: Left side figures show the correlation of the variability of J and H, H and K', J and K' band for each radio quiet object with $-26 < M_B < -24$. Filled circle represents the sample with short rest frame interval of the observation $100days < \Delta t < 400days$ and long. Open circle represents same but with long interval $400days < \Delta t < 800days$. Right side figures are same but for the radio loud sample. Only the data estimated with more than two reference objects and with accuracy higher than 0.1mag are plotted.

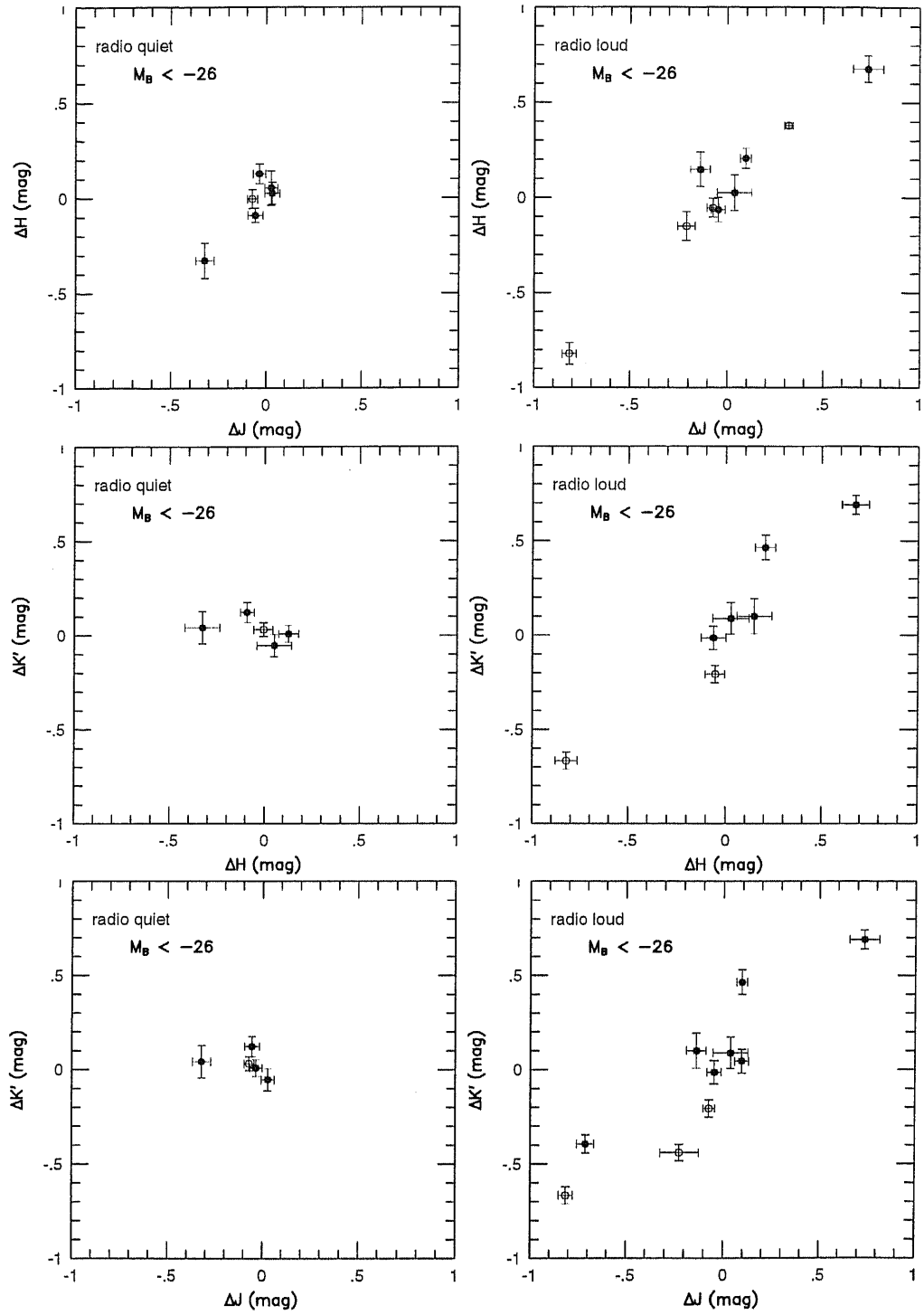

Figure B.30: Left side figures show the correlation of the variability of J and H, H and K', J and K' band for each radio quiet object with $M_B < -26$. Filled circle represents the sample with short rest frame interval of the observation $100days < \Delta t < 400days$ and long. Open circle represents same but with long interval $400days < \Delta t < 800days$. Right side figures are same but for the radio loud sample. Only the data estimated with more than two reference objects and with accuracy higher than 0.1mag are plotted.

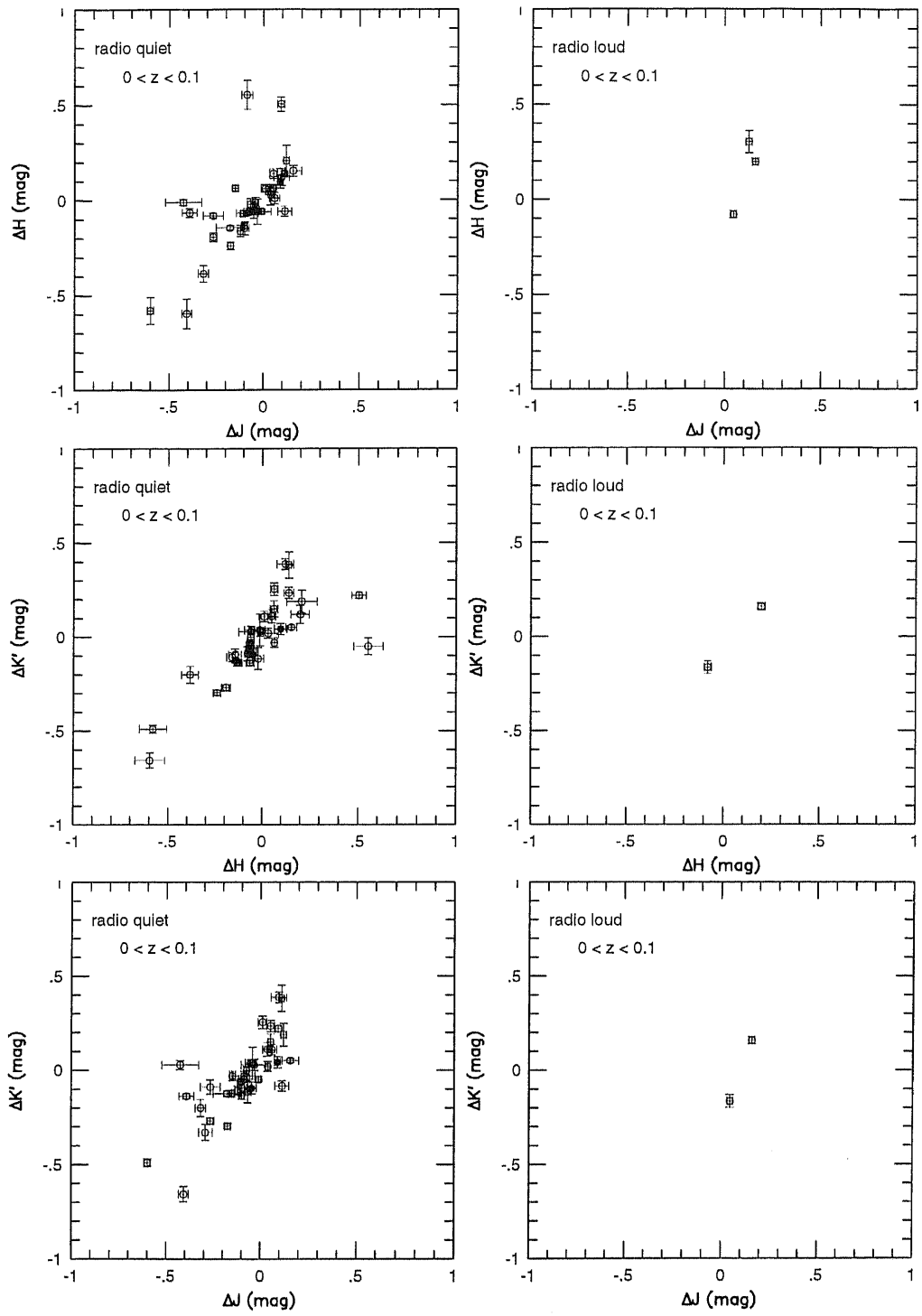

Figure B.31: Left side figures show the correlation of the variability of J and H, H and K', J and K' band for each radio quiet object with $0 < z < 0.1$. Filled circle represents the sample with short rest frame interval of the observation $100 days < \Delta t < 400 days$ and long. Open circle represents same but with long interval $400 days < \Delta t < 800 days$. Right side figures are same but for the radio loud sample.

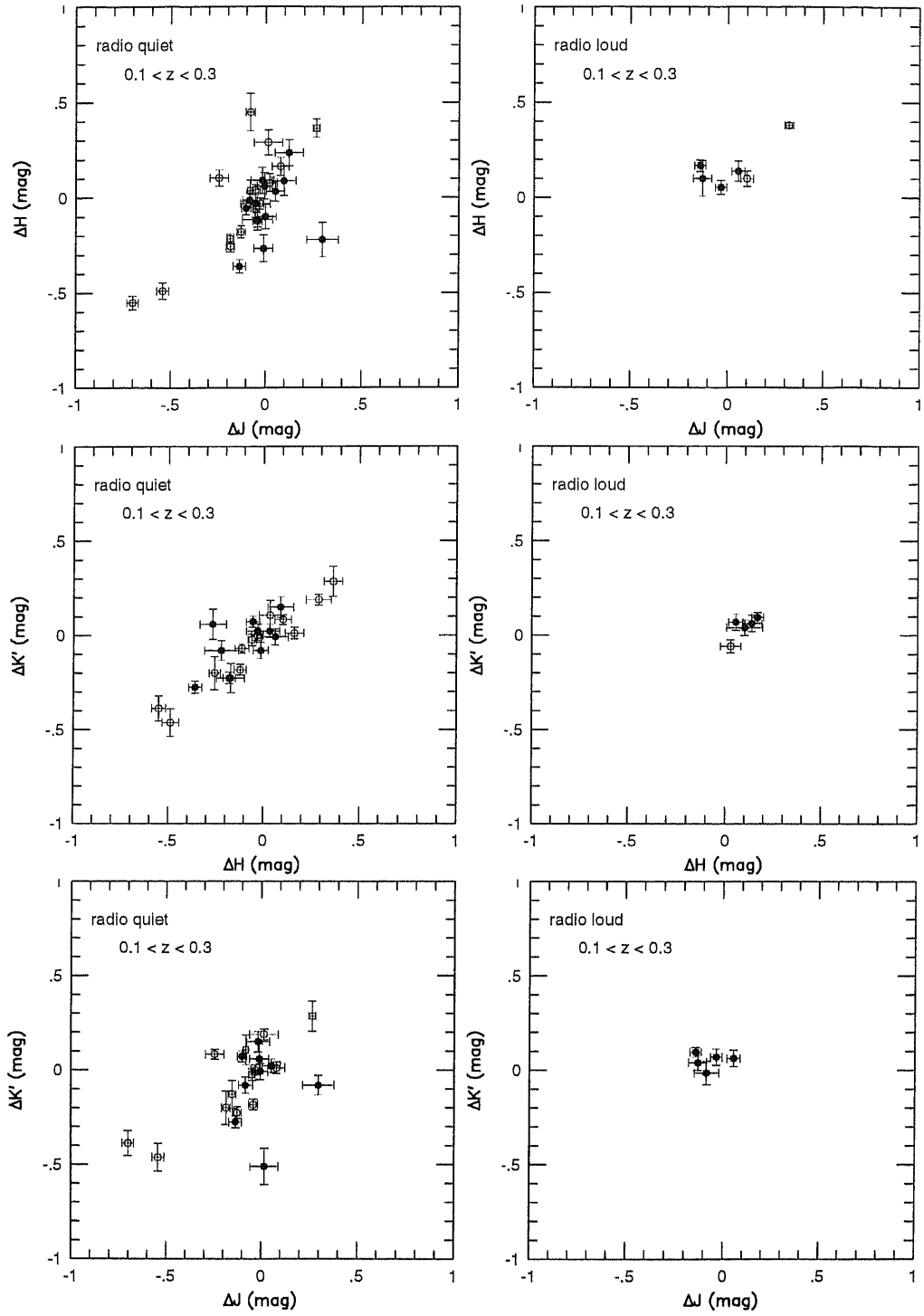

Figure B.32: Left side figures show the correlation of the variability of J and H, H and K', J and K' band for each radio quiet object with $0.1 < z < 0.3$. Filled circle represents the sample with short rest frame interval of the observation $100days < \Delta t < 400days$ and long. Open circle represents same but with long interval $400days < \Delta t < 800days$. Right side figures are same but for the radio loud sample. Only the data estimated with more than two reference objects and with accuracy higher than 0.1mag are plotted.

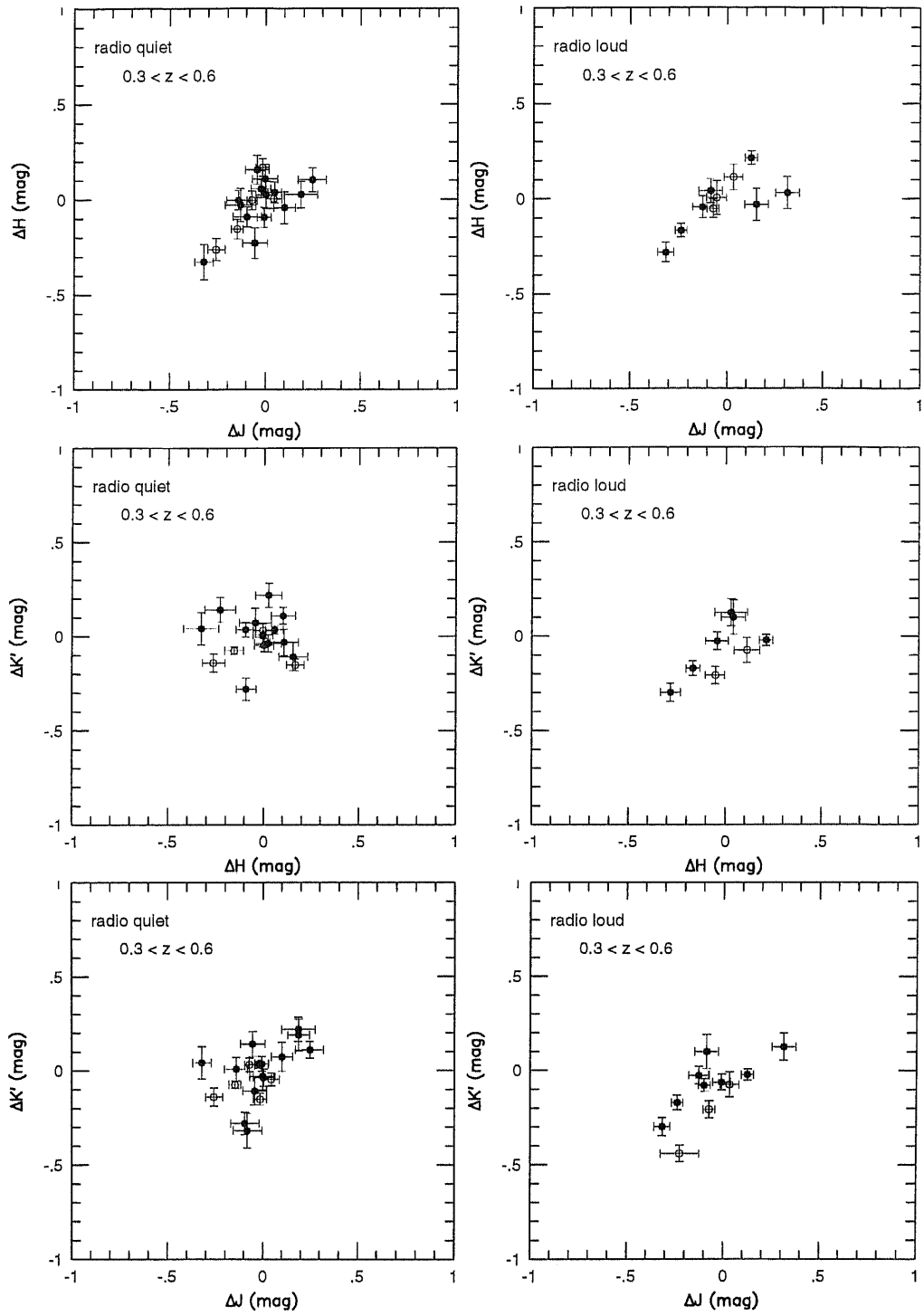

Figure B.33: Left side figures show the correlation of the variability of J and H, H and K', J and K' band for each radio quiet object with $0.3 < z < 0.6$. Filled circle represents the sample with short rest frame interval of the observation $100days < \Delta t < 400days$ and long. Open circle represents same but with long interval $400days < \Delta t < 800days$. Right side figures are same but for the radio loud sample. Only the data estimated with more than two reference objects and with accuracy higher than 0.1mag are plotted.

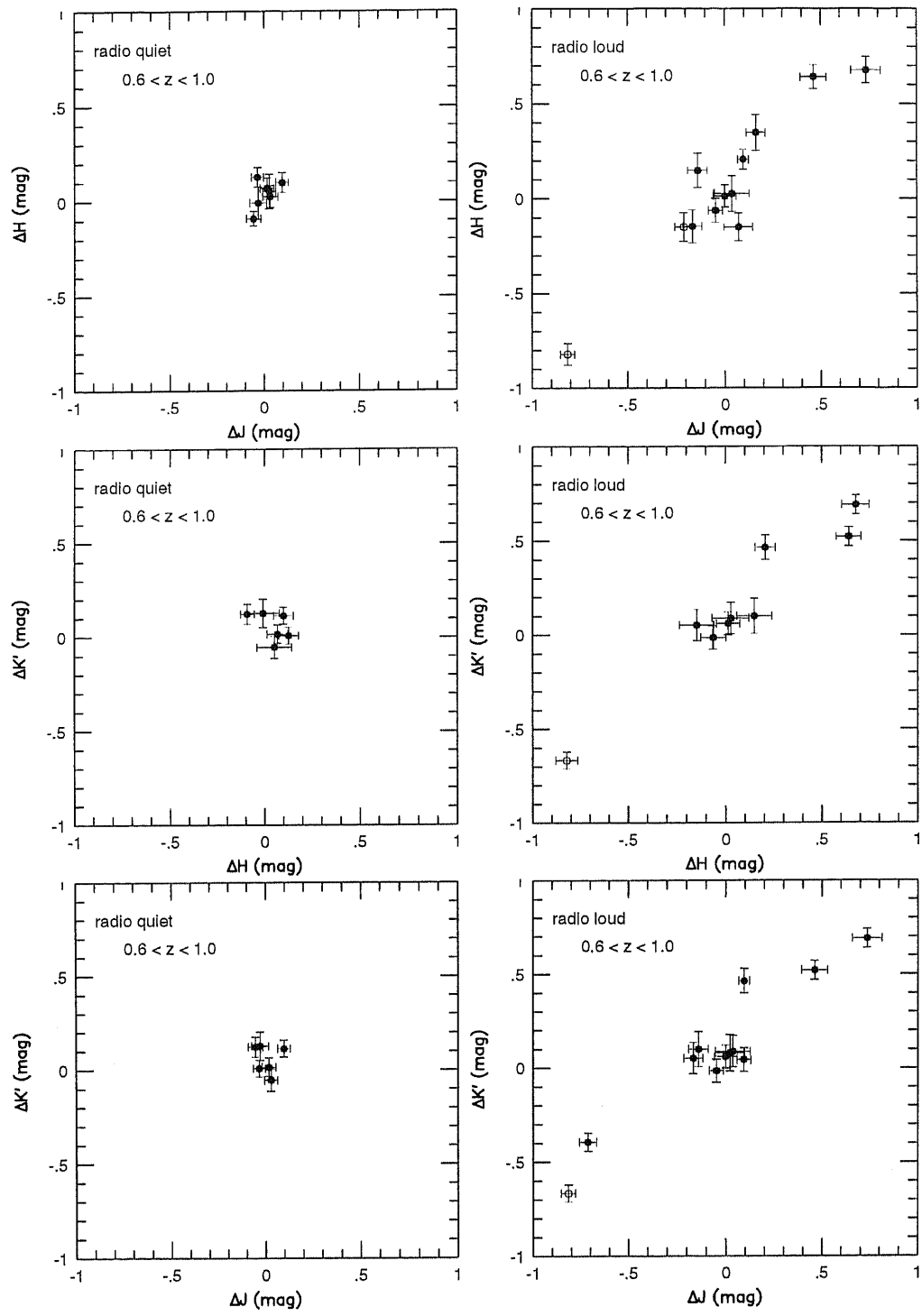

Figure B.34: Left side figures show the correlation of the variability of J and H, H and K', J and K' band for each radio quiet object with $0.6 < z < 1.0$. Filled circle represents the sample with short rest frame interval of the observation $100days < \Delta t < 400days$ and long. Open circle represents same but with long interval $400days < \Delta t < 800days$. Right side figures are same but for the radio loud sample. Only the data estimated with more than two reference objects and with accuracy higher than 0.1mag are plotted.

B.6 JHK' 2 color diagram

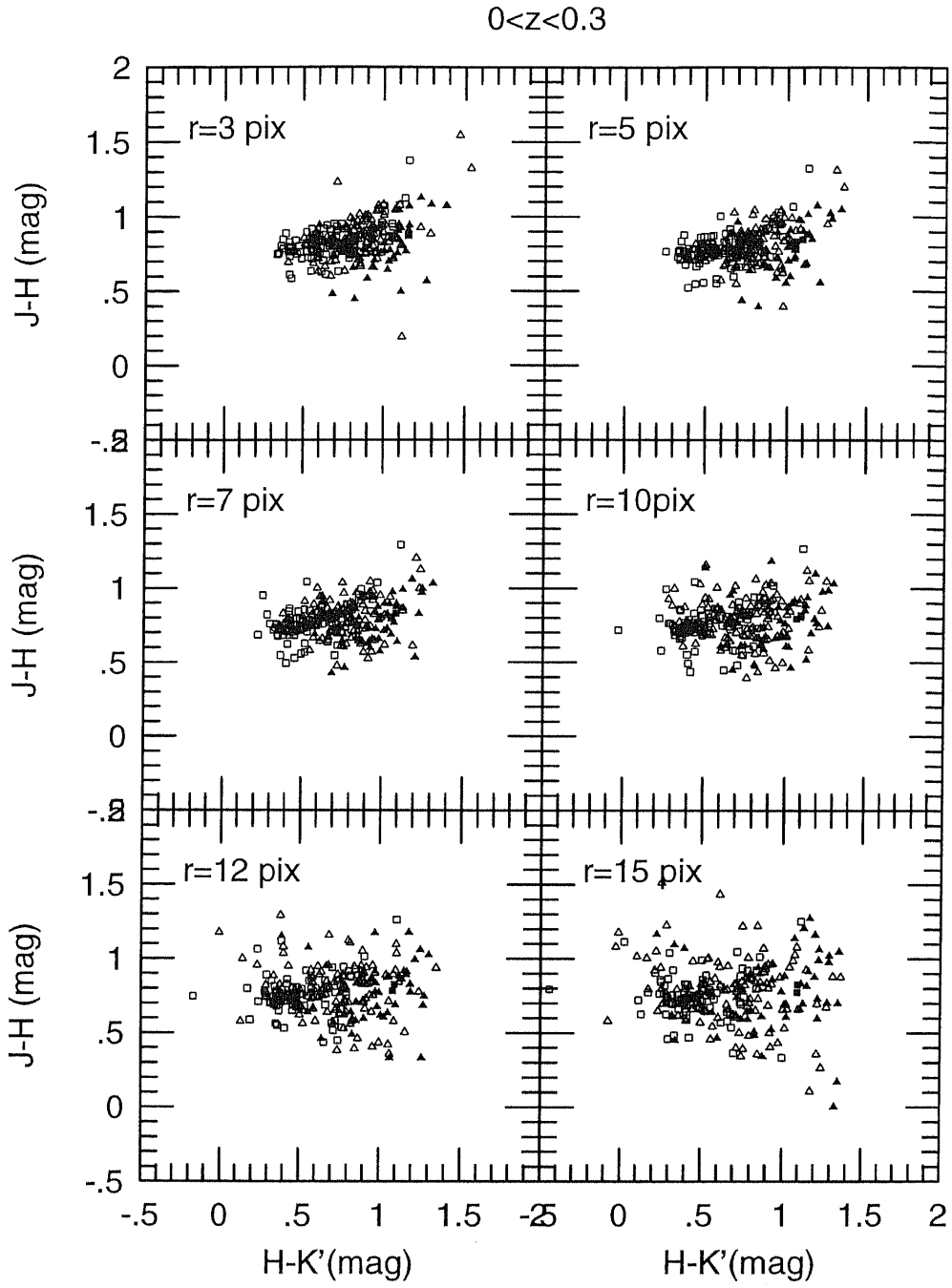

Figure B.35: JHK' tow color diagram of the objects in z<0.3 classified by their M_B. Only the data of which the accuracy is more than 0.2mag at 12 pixel apertuers are plotted. Open square and triangle represents M_B<-26 and -26<M_B<-24 objects, and filled triangle and square represents -24<M_B<-22 and -22<M_B, respectively.

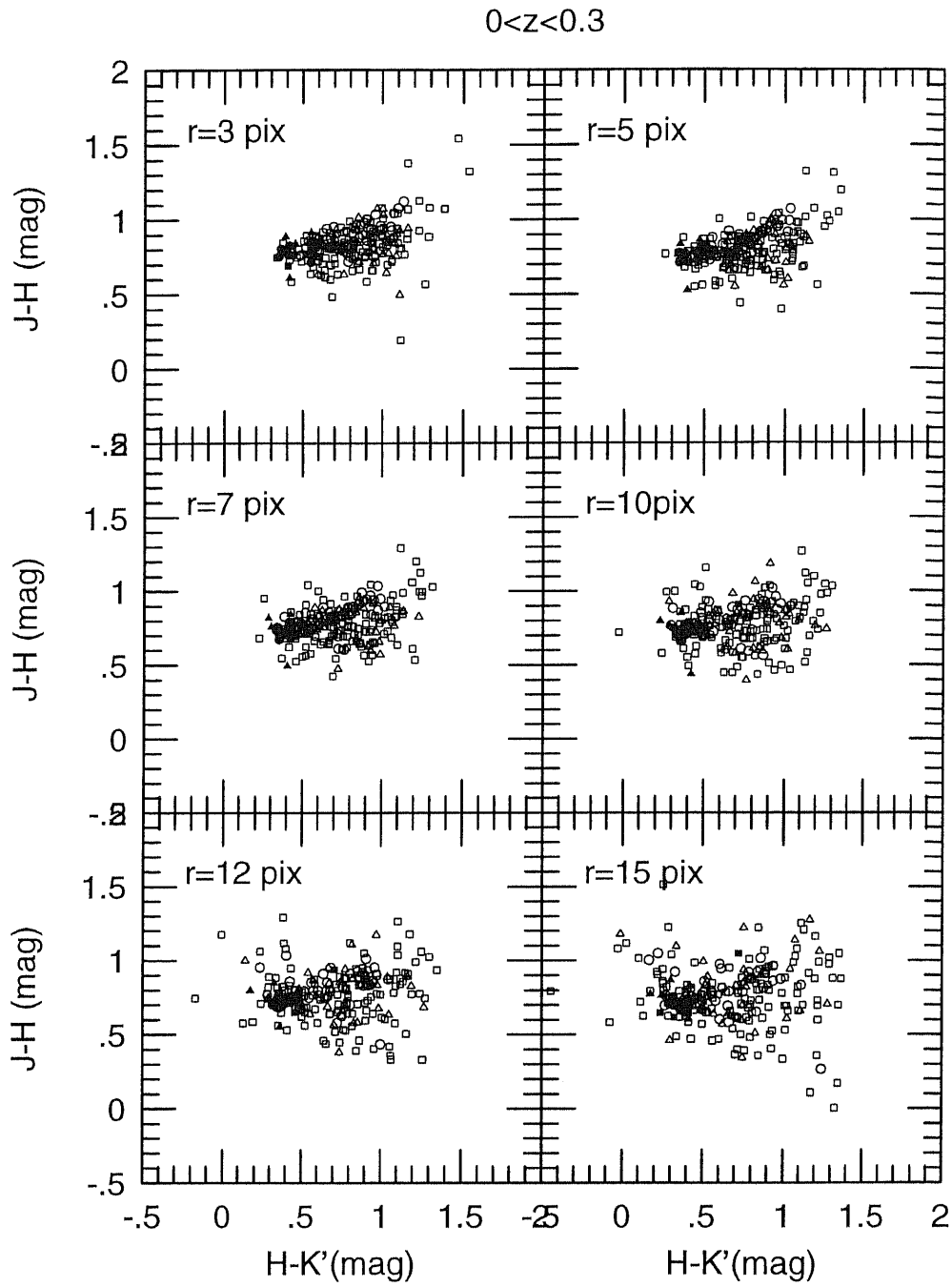

Figure B.36: JHK' tow color diagram of the objects in z<0.3 classified by their Seyfert type. Only the data of which the accuracy is more than 0.2mag at 12 pixel aperture are plotted. Open square, triangle and circle represents Seyfert 1, 1.2 and 1.5 objects, and filled circle, triangle and square represents Seyfert 1.8, 1.9 and 2, respectively.

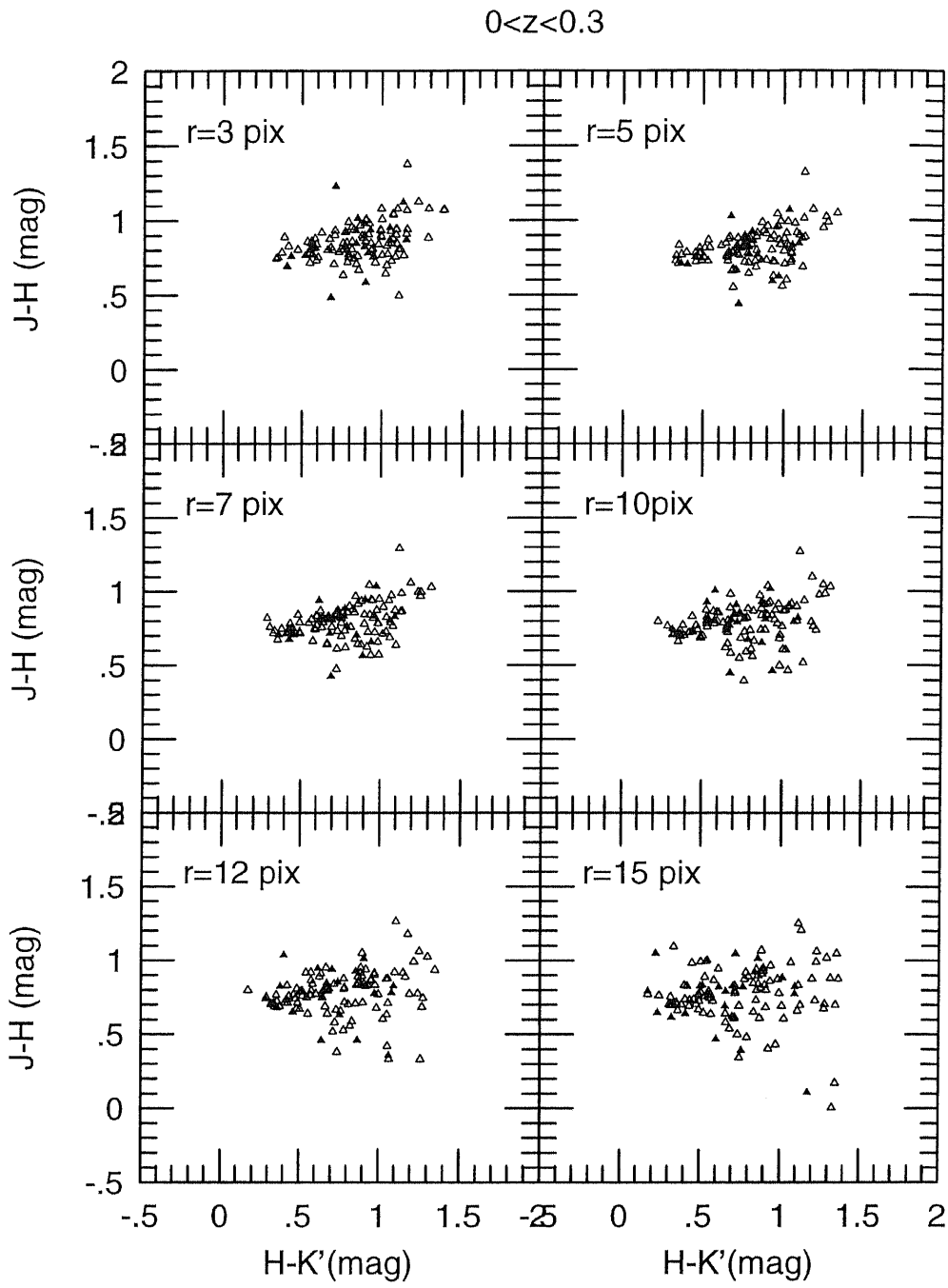

Figure B.37: JHK' tow color diagram of the objects in z<0.3 classified by their radio activity. Only the data of which the accuracy is more than 0.2mag at 12 pixel aperture are plotted. Open triangle represents objects with $f_{\nu 6cm}/f_{\nu V} < 10$, and filled triangle represents objects with $f_{\nu 6cm}/f_{\nu V} > 100$.

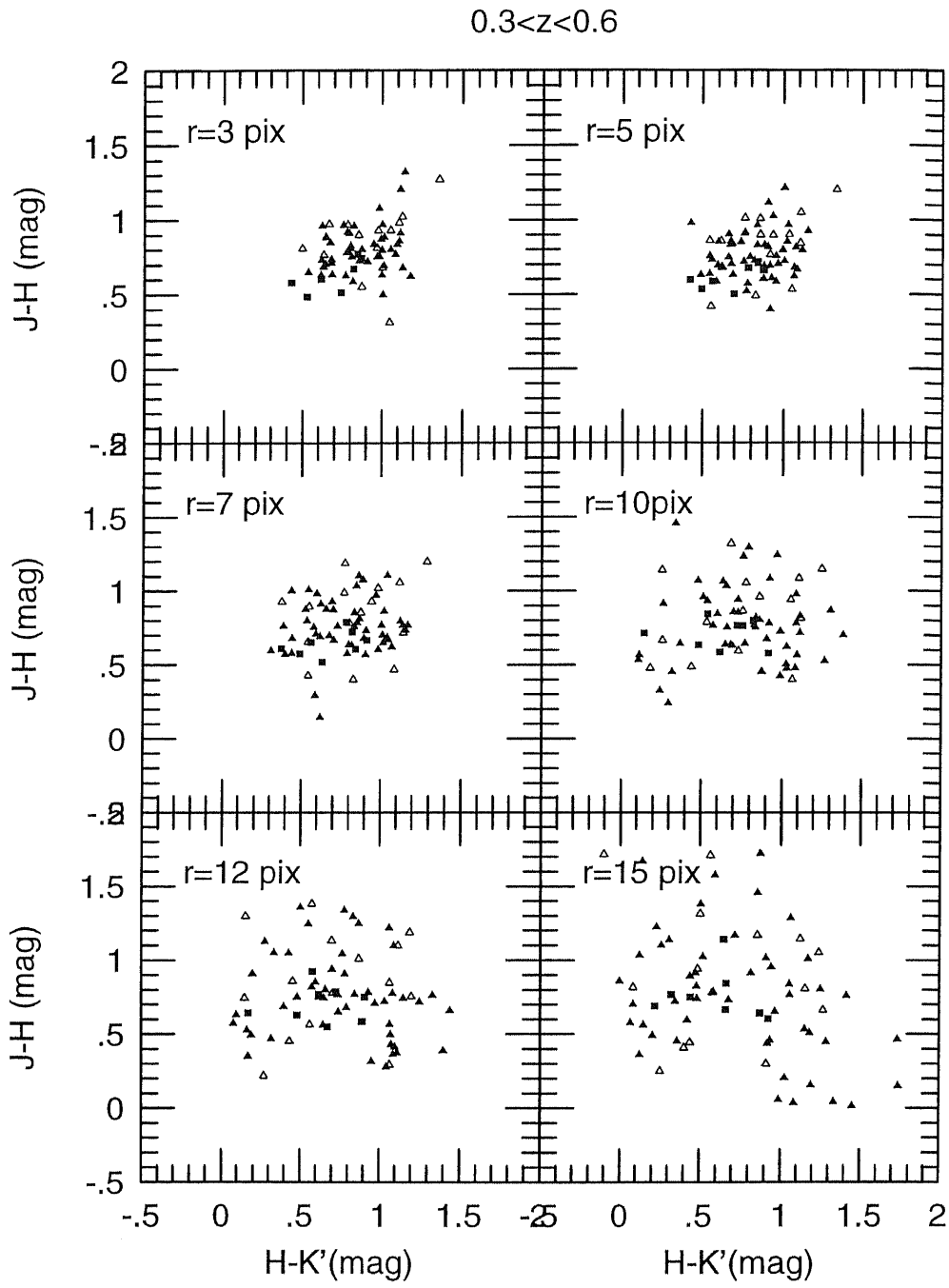

Figure B.38: JHK' tow color diagram of the objects in 0.3<z<0.6 classified by their M_B. Only the data of which the accuracy is more than 0.2mag at 12 pixel aperture are plotted. Open square and triangle represents M_B<-26 and -26<M_B<-24 objects,

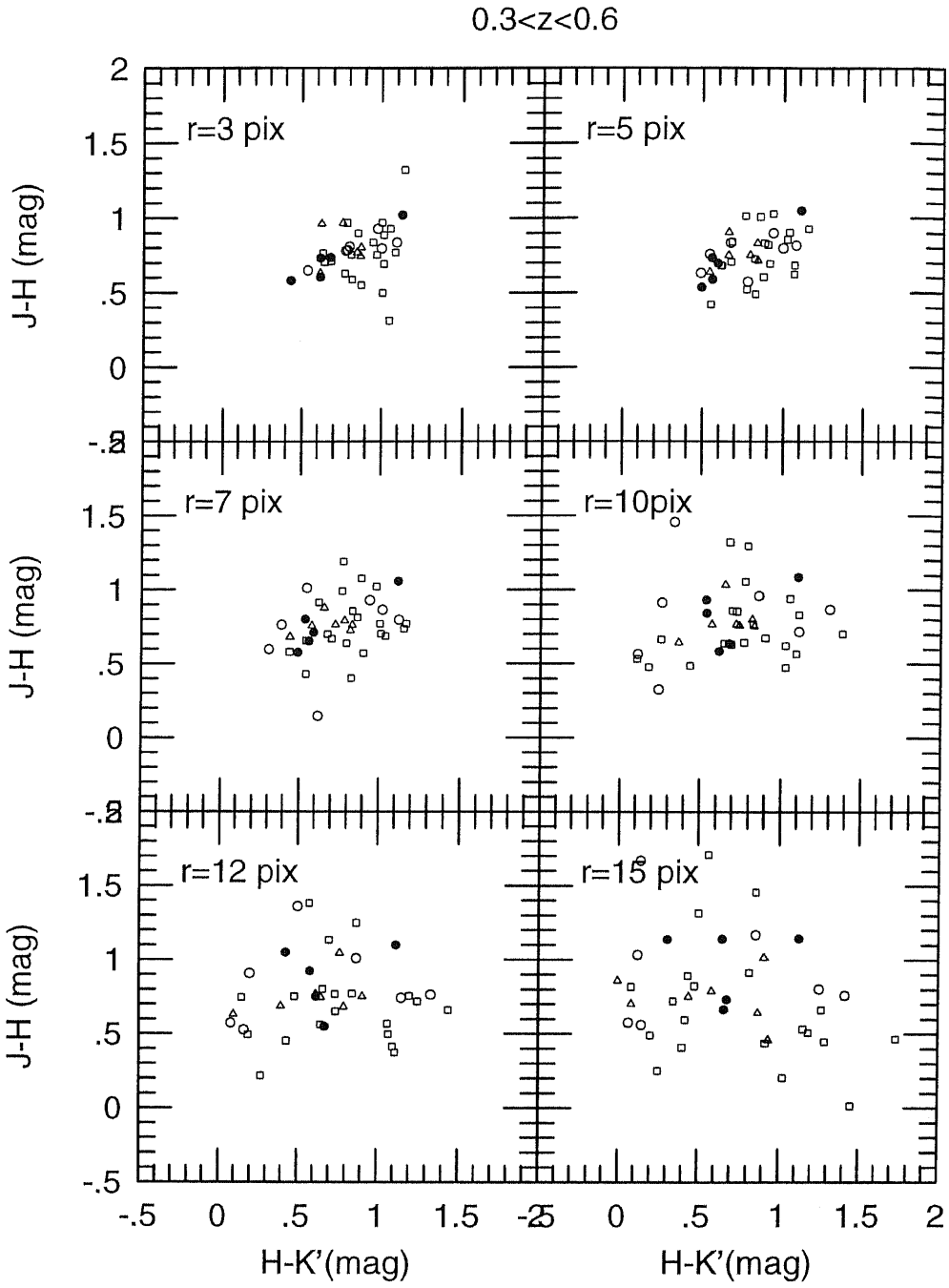

Figure B.39: JHK' tow color diagram of the objects in 0.3<z<0.6 classified by their Seyfert type. Only the data of which the accuracy is more than 0.2mag at 12 pixel aperture are plotted. Open square, triangle and circle represents Seyfert 1, 1.2 and 1.5 objects, and filled circle, triangle and square represents Seyfert 1.8, 1.9 and 2, respectively.

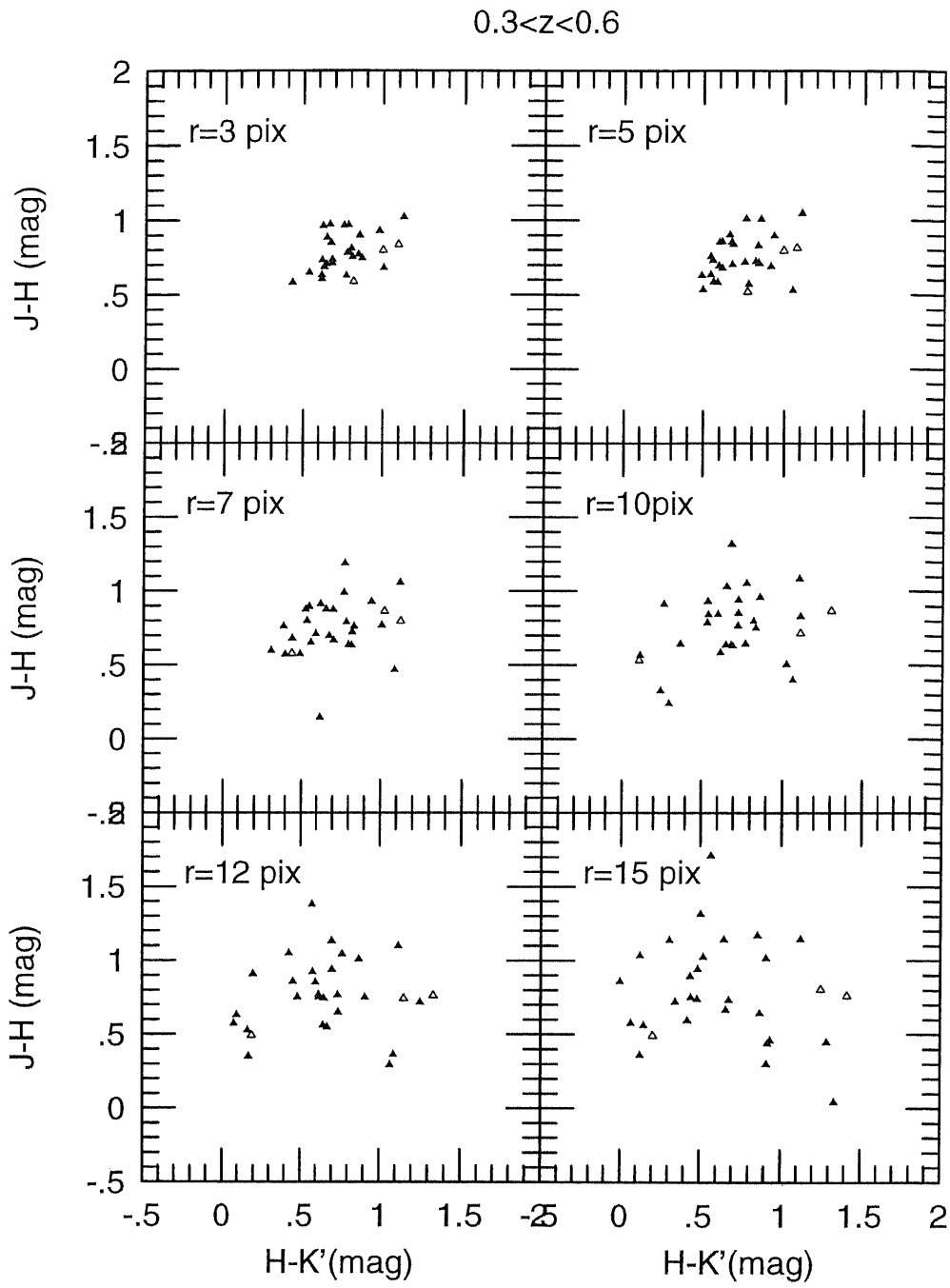

Figure B.40: JHK' tow color diagram of the objects in 0.3<z<0.6 classified by their radio activity. Only the data of which the accuracy is more than 0.2mag at 12 pixel aperture are plotted. Open triangle represents objects with $f_{\nu 6cm}/f_{\nu V} < 10$, and filled triangle represents objects with $f_{\nu 6cm}/f_{\nu V} > 100$.

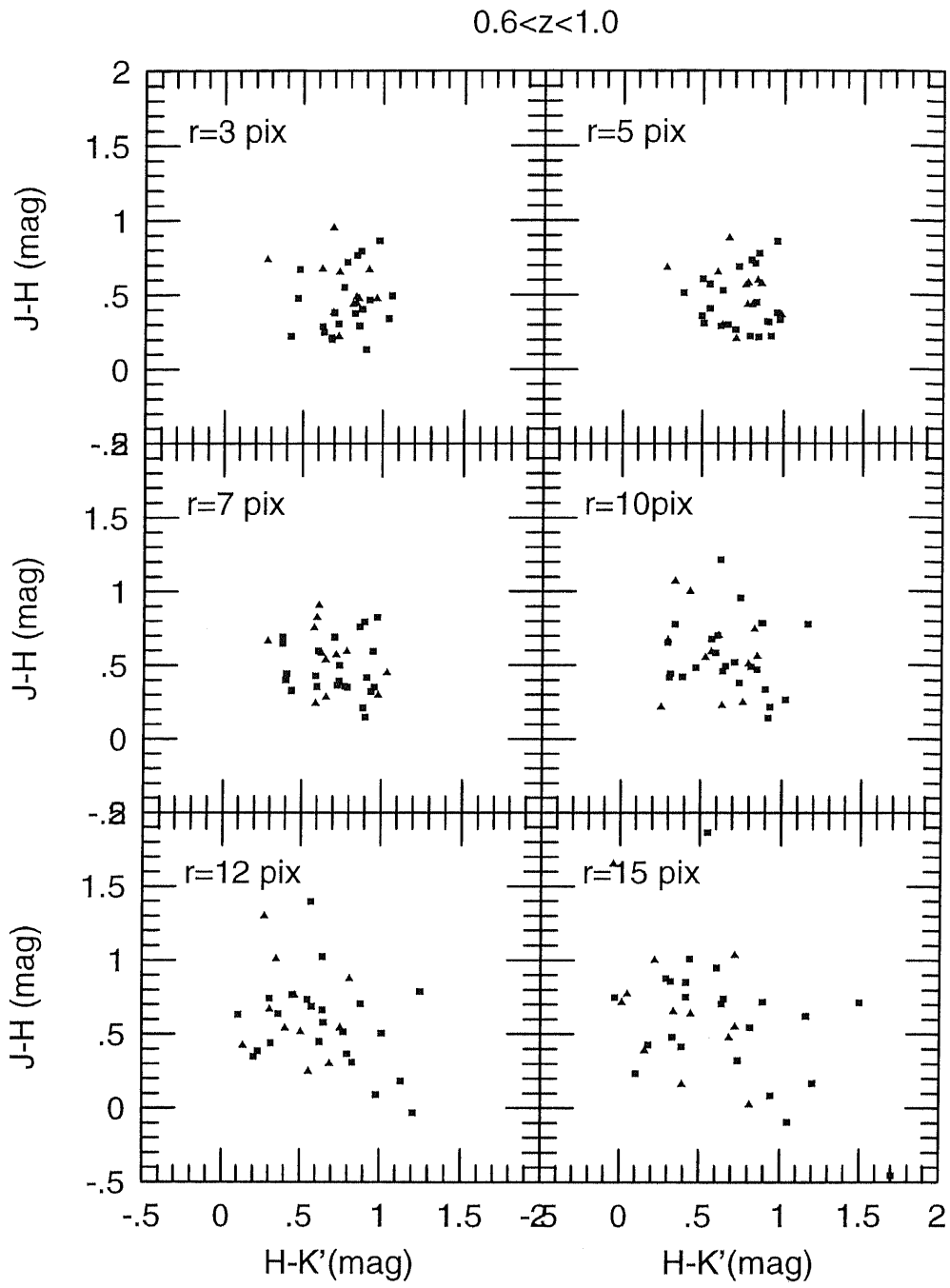

Figure B.41: JHK' tow color diagram of the objects in 0.6<z<1 classified by their M_B. Only the data of which the accuracy is more than 0.2mag at 12 pixel aperture are plotted. Open square and triangle represents M_B<-26 and -26<M_B<-24 objects,

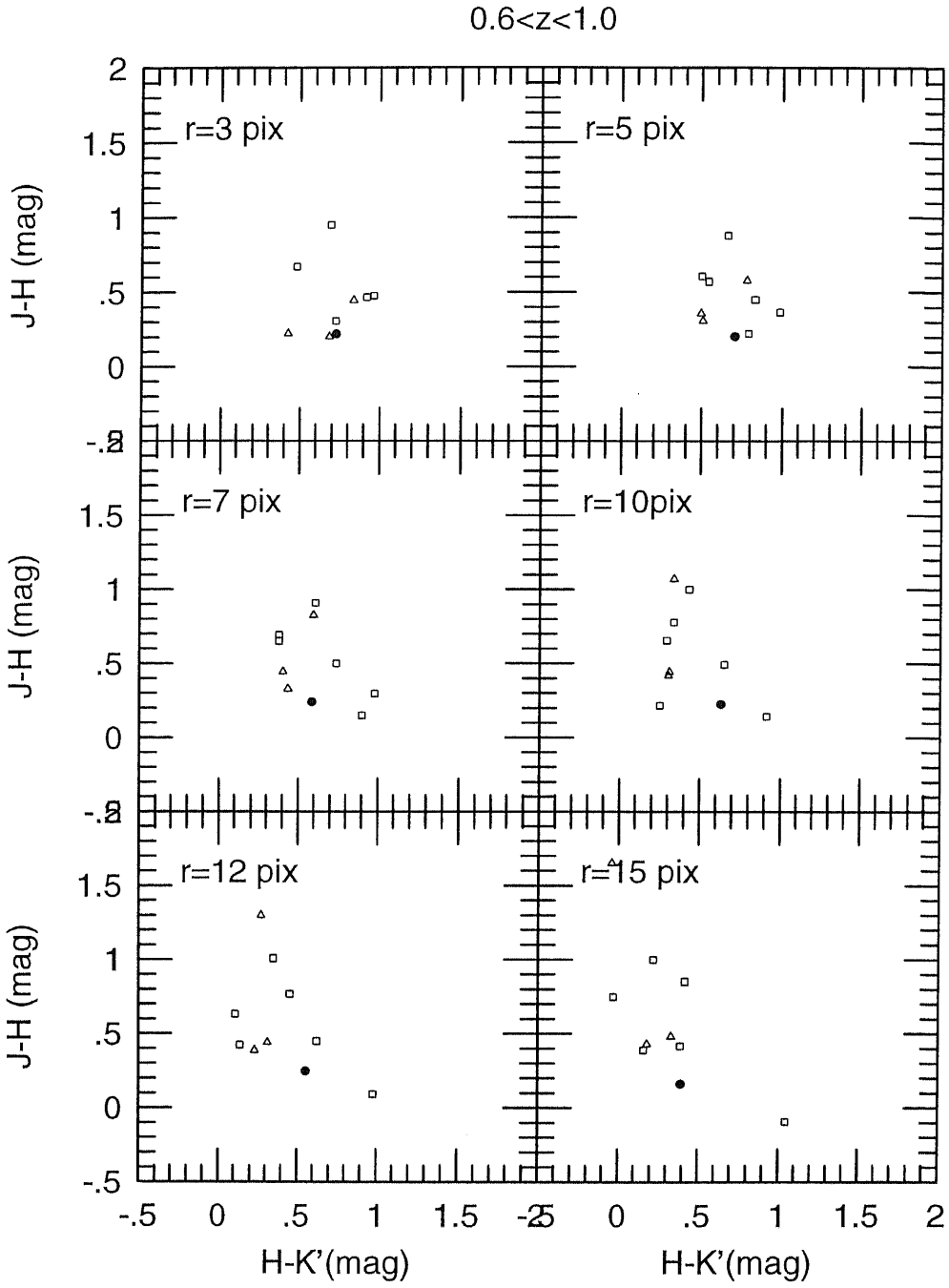

Figure B.42: JHK' tow color diagram of the objects in 0.6<z<1 classified by their Seyfert type. Only the data of which the accuracy is more than 0.2mag at 12 pixel aperture are plotted. Open square, triangle and circle represents Seyfert 1, 1.2 and 1.5 objects, and filled circle, triangle and square represents Seyfert 1.8, 1.9 and 2, respectively.

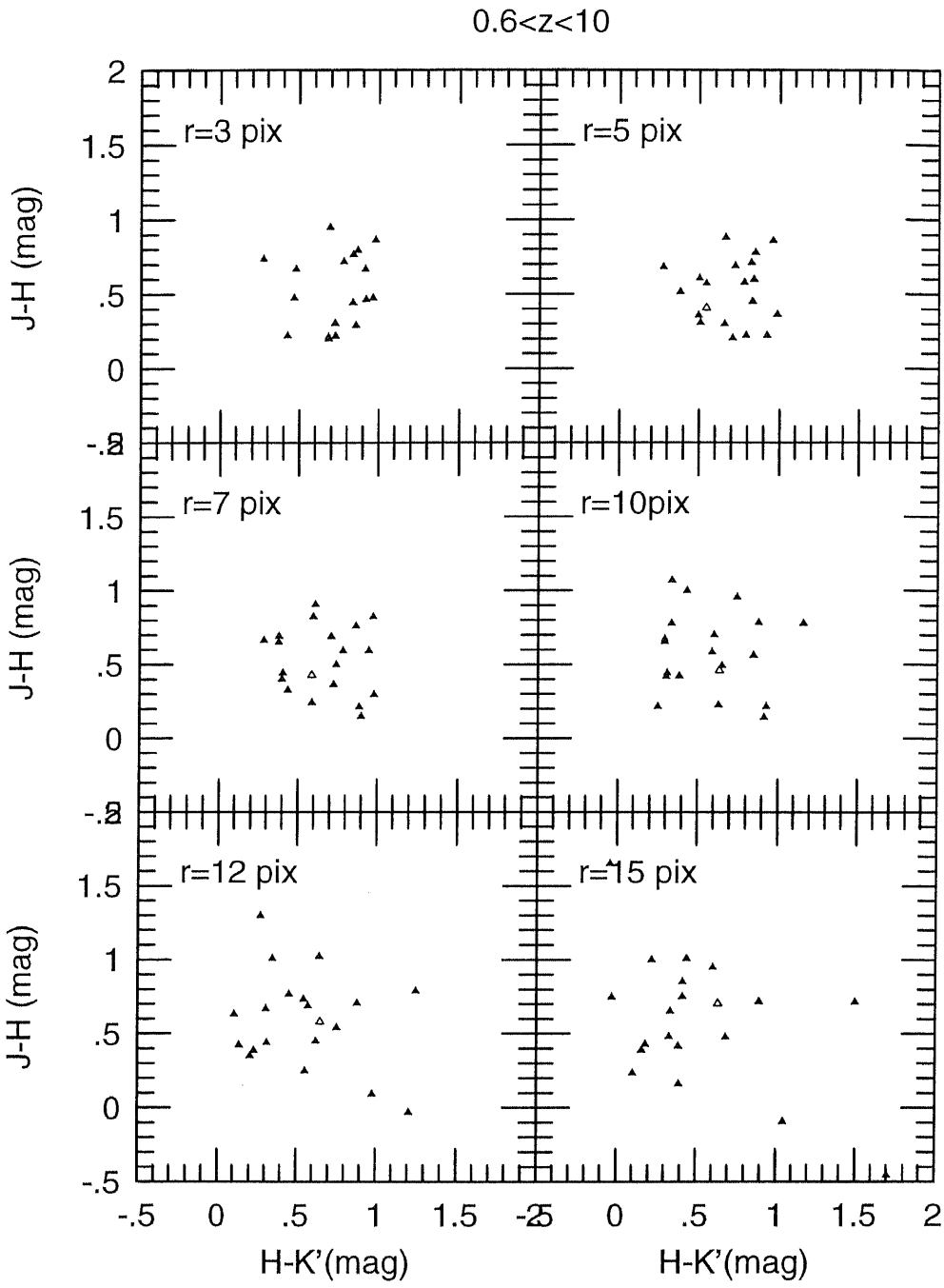

Figure B.43: JHK' tow color diagram of the objects in 0.6<z<1 classified by their radio activity. Only the data of which the accuracy is more than 0.2mag at 12 pixel aperture are plotted. Open triangle represents objects with $f_{\nu 6cm}/f_{\nu V} < 10$, and filled triangle represents objects with $f_{\nu 6cm}/f_{\nu V} > 100$.

Appendix C

estimation of the ensemble variability

In this section, it is shown how to estimate the variability and its error in this work from the data of which sample number and the accuracy are limited. The format of the data of the variability obtained by this work is like $(\Delta m_1, \sigma_1), (\Delta m_2, \sigma_2) ... (\Delta m_N, \sigma_N)$ for the sample of AGN_1,AGN_2 ... AGN_N. Here $\Delta m_i, \sigma_i$ represent the variability and the error of the i-th object. Hereafter the real variability of the i-th object is described as v_i, and the difference between v_i and m_i is as e_i. e_i can be regarded as random variable described by the normal distribution of which the average is 0 and the standard deviation is σ_i. based on the test considered in sec.3.3.4. i.e.

$$\Delta m_i = v_i + e_i, \quad < e_i >= 0, \quad < e_i^2 >= \sigma_i. \tag{C.1}$$

$<>$ represents the expectation. It is assumed that the real variability of the i-th object v_i is the random variable described by the normal distribution of which the average is 0 and the standard deviation is v_0, what is independent from i.

The dispersion of the ideal observation of which the errors of each data are 0 and the sample number is infinity is minded as next.

$$\lim_{N \to \infty} \left[\frac{\sum_i^N v_i^2}{N} \right] \tag{C.2}$$

Hereafter it is the aim to estimate the value of eq.(C.2) and the error from the observed data $(\Delta m_1, \sigma_1), (\Delta m_2, \sigma_2) ... (\Delta m_N, \sigma_N)$.

Considering the next relation

$$v_i^2 = \Delta m_i^2 - 2 v_i e_i - e_i^2, \tag{C.3}$$

Since expectation of the right hand side second term becomes 0 because of independence of v_i and e_i, the expectation of v_i^2 becomes as below.

$$< v_i^2 >= \Delta m_i^2 - \sigma_i^2 \tag{C.4}$$

The observed data is used for eq.(C.2), and the eq.(C.2) becomes

$$\lim_{N\to\infty}\left[\frac{\sum_i^N v_i^2}{N}\right] \sim \frac{\sum_i^N v_i^2}{N} \sim \frac{\sum_i^N \Delta m_i^2 - \sum_i^N \sigma_i^2}{N} \equiv \overline{v_0^2}. \tag{C.5}$$

where the first $\sim$ relate to the finite sample number and the second $\sim$ relate to the error of each data. The overline of $\overline{v_0^2}$ means to be the estimated value by such way.

As the next step, the error of eq.(C.5) is considered. at the first,the error caused by the estimation of ideal value available only by infinite times observation by the finite sample number is focused. It should be thought that $\sum_i^N (v_i/v_0)^2$ is the random variable described by χ^2 distribution with the freedom being of N, therefore the expectation being N and the dispersion being 2N, because $v_i/v_0, i = 1,2,3...N$ is the random variable described the normal distribution with the average being 0 and the standard deviation being 1. Therefore $\pm\sqrt{2v_0^4/N}$ is obtained as the error caused by the being finite of sample number.

Next, the error caused by the estimation of ideal value available only by infinite accuracy observation by the finite accuracy data is focused. the expectation of the difference between v_i^2 and $< v_i^2 >$ is calculated as

$$\begin{aligned} < (v_i^2 - < v_i^2 >)^2 > &= < (\Delta m_i^2 - 2e_i v_i - e_i^2 - \Delta m_i^2 + \sigma_i^2)^2 > & \text{(C.6)} \\ &= < 4e_i^2 v_i^2 + e_i^4 + \sigma_i^4 + 4e_i^3 v_i - 4e_i v_i \sigma_i^2 - 2e_i^2 \sigma_i^2 > & \text{(C.7)} \\ &= 4\sigma_i^2 < v_i^2 > + < e_i^4 > - \sigma_i^4, & \text{(C.8)} \end{aligned}$$

where the independence between v_i and e_i and eq.(C.1) is used. Using that $< e_i^4 >$ corresponds to $3\sigma_i^4$ and eq.(C.4), next equation is obtained.

$$\begin{aligned} < (v_i^2 - < v_i^2 >)^2 > &= 4\sigma_i^2 < v_i^2 > + 2\sigma_i^4 & \text{(C.9)} \\ &= 4\sigma_i^2 \Delta m_i^2 - 2\sigma_i^4. & \text{(C.10)} \end{aligned}$$

Therefore $\pm\sqrt{\sum_i^N (4\Delta m_i^2 \sigma_i^2 - 2\sigma_i^4)/N^2}$ is obtained as the error of eq.(C.5) caused by the non-zero error of each variability data.

Considering those error factor and using eq.(C.5), the estimated value of v_0^2 and its error are obtained.

$$\overline{v_0^2} = \frac{\sum_i^N \Delta m_i^2 - \sum_i^N \sigma_i^2}{N} \pm \sqrt{\frac{2v_0^4}{N} + \frac{\sum_i^N (4\Delta m_i^2 \sigma_i^2 - 2\sigma_i^4)}{N^2}} \quad \text{(C.11)}$$

$$\sim \frac{\sum_i^N \Delta m_i^2 - \sum_i^N \sigma_i^2}{N} \pm \sqrt{\frac{2(\sum_i^N \Delta m_i^2 - \sum_i^2 \sigma_i^2)^2}{N^3} + \frac{\sum_i^N (4\Delta m_i^2 \sigma_i^2 - 2\sigma_i^4)}{N^2}} \quad \text{(C.12)}$$

Finally, the estimated value of v_0 and its error are also obtained by usual propagation of errors as following.

$$\overline{v_0} = \sqrt{\frac{\sum_i^N \Delta m_i^2 - \sum_i^N \sigma_i^2}{N}} \quad \text{(C.13)}$$

$$\pm \frac{1}{2}\left[\frac{\sum_i^N \Delta m_i^2 - \sum_i^N \sigma_i^2}{N}\right]^{-1/2} \sqrt{\frac{2(\sum_i^N \Delta m_i^2 - \sum_i^2 \sigma_i^2)^2}{N^3} + \frac{\sum_i^N (4\Delta m_i^2 \sigma_i^2 - 2\sigma_i^4)}{N^2}} \quad \text{(C.14)}$$

Appendix D

statistic estimation and test

D.1 estimation of correlation coefficient and its confidence interval

When there are such format data of $(x_1, y_1), (x_2, y_2), (x_3, y_3)...(x_n, y_n)$, and the sample number is N, correlation coefficient is r, reliability is A, r is determined as below.

$$r = \frac{\sum_{i=1}^{n}(x_i - \overline{x})(y_i - \overline{y})}{\sqrt{\sum_{i=1}^{n}(x_i - \overline{x})^2(y_i - \overline{y})^2}}. \tag{D.1}$$

The confidence interval of r was estimated as following. Using $\alpha = 1 - A$, the percent point of the normal distribution where the upside probability equal to $\alpha/2$ is determined and described as $Z_{\alpha/2}$. Z transformation value is calculated by the Fisher's Z transformation.

$$Z_0 = f_{(r)} = \frac{1}{2}\ln\left(\frac{1+r}{1-r}\right). \tag{D.2}$$

Next, Z_U, Z_L are estimated by next form.

$$Z_U = Z_0 + \frac{Z_{\alpha/2}}{n-3}, \quad Z_L = Z_0 - \frac{Z_{\alpha/2}}{n-3}. \tag{D.3}$$

Then by the inverse of Fisher's transformation

$$r_U = f^{-1}_{(Z)} = \frac{\exp(2Z) - 1}{\exp(2Z) + 1} \tag{D.4}$$

the confidence interval of r is obtained, The upper side confidence interval r_U and the lower side confidence interval r_L are following.

$$r_U = f^{-1}_{(Z_U)}, \quad r_L = f^{-1}_{(Z_L)}. \tag{D.5}$$

D.2 equivalence test of correlation coefficients and the estimation of mother correlation coefficients

The data set of

$$\begin{aligned}
&(x_{1,1}, y_{1,1}), (x_{1,2}, y_{1,2}), (x_{1,3}, y_{1,3}) \ldots (x_{1,n_1}, y_{1,n_1}) \ldots (1) \\
&(x_{2,1}, y_{2,1}), (x_{2,2}, y_{2,2}), (x_{2,3}, y_{2,3}) \ldots (x_{2,n_2}, y_{2,n_2}) \ldots (2) \\
&\qquad\qquad \ldots \\
&(x_{N,1}, y_{N,1}), (x_{N,2}, y_{N,2}), (x_{N,3}, y_{N,3}) \ldots (x_{N,n_N}, y_{N,n_N}) \ldots (N)
\end{aligned}$$

are assumed. The correlation coefficients of group (1),(2)...(N) are calculated and described as $r_1, r_2 \ldots r_N$. To test the equivalence of mother correlation coefficients, the null hypothesis in which all mother correlation coefficients are equal to each other, and the alternative hypothesis in which all mother correlation coefficients aren't equal to each other are assumed. Using those hypothesis, the tow-sided test is done with confidence level of α. χ^2 is calculated from the Z transformation $Z_1, Z_2 \ldots Z_N$ of $r_1, r_2 \ldots r_N$.

$$\chi_0^2 = \sum_{i=1}^{N} (n_i - 3) Z_i^2 - \frac{\left(\sum_{i=1}^{N} (n_i - 3) Z_i\right)}{\sum_{i=1}^{N} (n_i - 3)}. \tag{D.6}$$

when χ^2 is the random variable described by χ^2 distribution, the confidence probability P is estimated.

$$P = Pr(\chi^2 \geq \chi_0^2). \tag{D.7}$$

If $P \geq \alpha$, the null hypothesis is accepted, where all mother correlation coefficients are equal to each other. If $P < \alpha$, the null hypothesis is rejected, where all mother correlation coefficients are not equal to each other.

If the null hypothesis is accepted in equivalence test, it is possible to estimate one mother correlation coefficient. At the first of the estimation, the weighted average Z_m is calculated from $Z_1, Z_2 \ldots Z_N$ as

$$Z_m = \frac{\sum_{i=1}^{N}(n_i - 3)Z_i}{\sum_{i=1}^{N}(n_i - 3)}. \tag{D.8}$$

Then $f_(^{-1}Zm)$ is obtained by the inverse of the Fisher's transformation as

$$r_0 = f_(^{-1}Zm) = \frac{\exp(2Z_m) - 1}{\exp(2Z_m) + 1}. \tag{D.9}$$

Appendix E

automatic reduction system for MAGNUM project

E.1 background

At the MAGNUM project, hundreds of AGN will be monitored automatically for more than some years at the wavelength from UV to infrared. So there are basic the features of the data analysis at the MAGNUM project as next.

- The amount of the data is very large.
- Similar process is repeated.

Those process is appropriate to be done by the computer automatically, and in fact, the atomization of the process is indispensable to treat such amount of data.

The differential photometry will be adopted to broad band images at from UV to infrared to detect the variability of AGN. Therefore essential of the data analysis process in the MAGNUM project is similar to the process of this work. As described following section, most of the data analyzing process is atomized in this work, what has the aim not only to analyze the data of this work more efficiently but also to check the feasibility of full automatic system planning for MAGNUM and to list up the problems.

In this section, the problems that was found as the result of developing atomization of this work, their solution and the conception of the full automated system for MAGNUM are discussed. Furthermore, the benchmark test of reduction the data obtained in one night was executed and the results are discussed.

E.2 the scope of automatic reduction

Fig.E.1 shows the flow from the data transfer to determining the cosmological parameters. In those process, the MAGNUM automatic reduction system(hearafter MAG-RED) execute the process until summarizing the magnitude table as text file. Main information written in the magnitude table

are the magnitude of AGN, reference stars and photometric standard if observed, the accuracy and reliability and FWHM of the objects. The property of the process until and after summarizing the magnitude table is different, therefore to atomize the former process is reasonable. There are some property as below in process until summarizing the magnitude table compared with the process after summarizing the magnitude table.

- deal the data set of each night serially.
- deal image data
- therefore the scale of the data is very large
- repeat similar process

Those features show that it is more easy than the later process and efficient to atomize the process until summarizing the magnitude.

E.3 feasibility of full automated reduction system

It is necessary to atomize the image reduction to realize the MAG-RED. The process that was not automated in this work are listed up and the solutions of the problem are discussed.

The automatic process sometimes is stopped by the error of the effect of the dust on the optics. However, this trouble is merely by the problem of the programming, therefore not discussed in this section. In such case, the process that isn't automated in image reduction of this work are next three.

- (1) selection of the frame to make each sky flat image.
- (2) identification of the abnormal frames and their rejection.
- (3) trying and error to combine frames when the position reference star is not found

About (1), the reduction script automatically made is adjusted for that all image is analyzed by the self sky flat image. Manual operation is not necessary if the default type of the script is available. However, some of the bad frame is identified from the observation log notebook, and it is impossible in this work to improve the script automatically to avoid those frames. At the MAGNUM project where the all observation log is remained as machine readable form, it is expected that completely automatic formation of the script will become possible using the log file of not only the telescope, camera but also cloud monitor and weather monitor.

About (2), there is possibility to identify the extremely abnormal frames to check the statistic of the frame with, for example, IRAF imstat task. The same treatment is also effective for frame

affected by the cosmic ray or airplane, however it may be possible to neglect the frames if the frequency of born is low. Identification of frames affected by stray light is difficult because of their faintness but important because such frames tend to born continuously and therefore couldn't be neglected. Though to reject the influence of the stray light is very hard, it is thought that some of them is able to be avoided comparing the sky flat image to other typical images. On the other hand, it is important to execute the error estimation including the effect of the stray lighten the differential photometry, what is done in this work. And then it becomes feasible to avoid the fatal fault conclusion by the stray light.

About (3), if the position reference star is not found automatically, detection parameter was varied by manual operation to detect the reference and combine the frames. However, this problem can be avoid on MAGNUM because only AGN that has some reference stars around itself will be selected referring the result of this work and other data. It is also important for accurate identification of the objects in the field that the telescope is maintained and the pointing and tracking is good condition.

As shown in sec.E.5, most of the process of the data reduction have already automated. Furthermore, it is thought to be possible at MAG-RED to atomize the process not automated in this work as the result of total effort for not only the reduction software system but also digital log file, hardware like telescope and camera and AGN selection adjusted for reduction. After all, it is concluded possible to realize full automated data reduction system at the development of MAG-RED.

E.4 conception of the MAGNUM reduction system(MAG-RED)

The MAGNUM reduction system(MAG-RED) is designed to have following features.

- full automatic running from the data expansion to summarizing the magnitude table. Following process not atomized in this work is atomized.
  - production of all scripts.
  - identification of abnormal frame.
  - identification of known objects.
- specialized system for the unique systems on MAGNUM
  - for hardwares like telescope, multi-color imaging photometer, dome flat system.
  - for machine readable observation log automatically produced
  - for the cloud monitor. Its output is used to judge the reliability of each data.

- adjust to IRAF V2.11 or more, C language, perl script
- detection of moved objects
- detection of new appeared objects
- ability to finish the reduction of the data obtained in one night in less than 24 hours(E.5).

E.5 benchmark test of automatic reduction in this work

Beaus hundreds of AGN will be monitored automatically by multicolor observation for more than some years in MAGNUM project, it is essential that the MAG-RED has ability to finish the reduction of the data obtained in one night in less than 24 hours. To obtain the rough estimation of the time, it was tested how long each process of the automatic reduction need the time by the atomized reduction in this work. The data obtained on February 12,1998 was used in this test. All process of the reduction was continuously executed automatically using the data where the part needed human's check had been done. The data was 1662 of 256×256 frames, that is the typical number of this work. The rest was done with workstation S4/5 m85 at the Astronomical Data Analysis Center of NAOJ. The starting and ending time of each subscript was written in log file automatically. TableE.1 shows the result of the benchmark test.

The typical manual process in this work needs 1∼1.5 hours in the reduction of the data obtained on one night. On the other hand, the automatic process needs 36 hours, for example, the case of tableE.1. The time of atomized process is depend on the amount of the data, operating speed of the workstation and the other user's job. Furthermore, result of this test doesn't include the time for the reduction of GCD image, because the observation in optical was not done in this work. However, the result of this test is useful as the rough information. The ratio of time for human operation to atomized process is 2.7∼4.0% in the case of tableE.1 where total automatic process needs 36 hours.

In the process shown in tableE.1, the longest time is used for the 2nd round of AGN image. It is the cause of this feature that the 2nd round of AGN frames include fitting and subtraction of the 50Hz noise for many frames. The 2nd round of the dome flat frame needs much more than the 1st round, and the process of the dark frames, photometric standard frames need also somewhat time. These tendency is originated by fitting and subtraction of the 50Hz noise because those process include the 50Hz noise subtraction though the frames aren't as many as AGN frames.

In the benchmark test of this section, more than 24 hours is required to complete the reduction of the data in one night. Furthermore, the amount of the data obtained at MAGNUM is larger than this work where the optical observation is done with the infrared observation simultaneously. However, those facts doesn't mean that it is impossible to complete the reduction in 24 hours because the workstation used here isn't the newest. We prepared SUN ULTRA30 for the data

reduction of the MAGNUM project that would be 10 times faster in the CPU speed and several times faster in disk access speed than S4/5 m85. Therefore it is thought possible to finish the data reduction of the data in one night in 24 hours without preparing multi-workstation system.

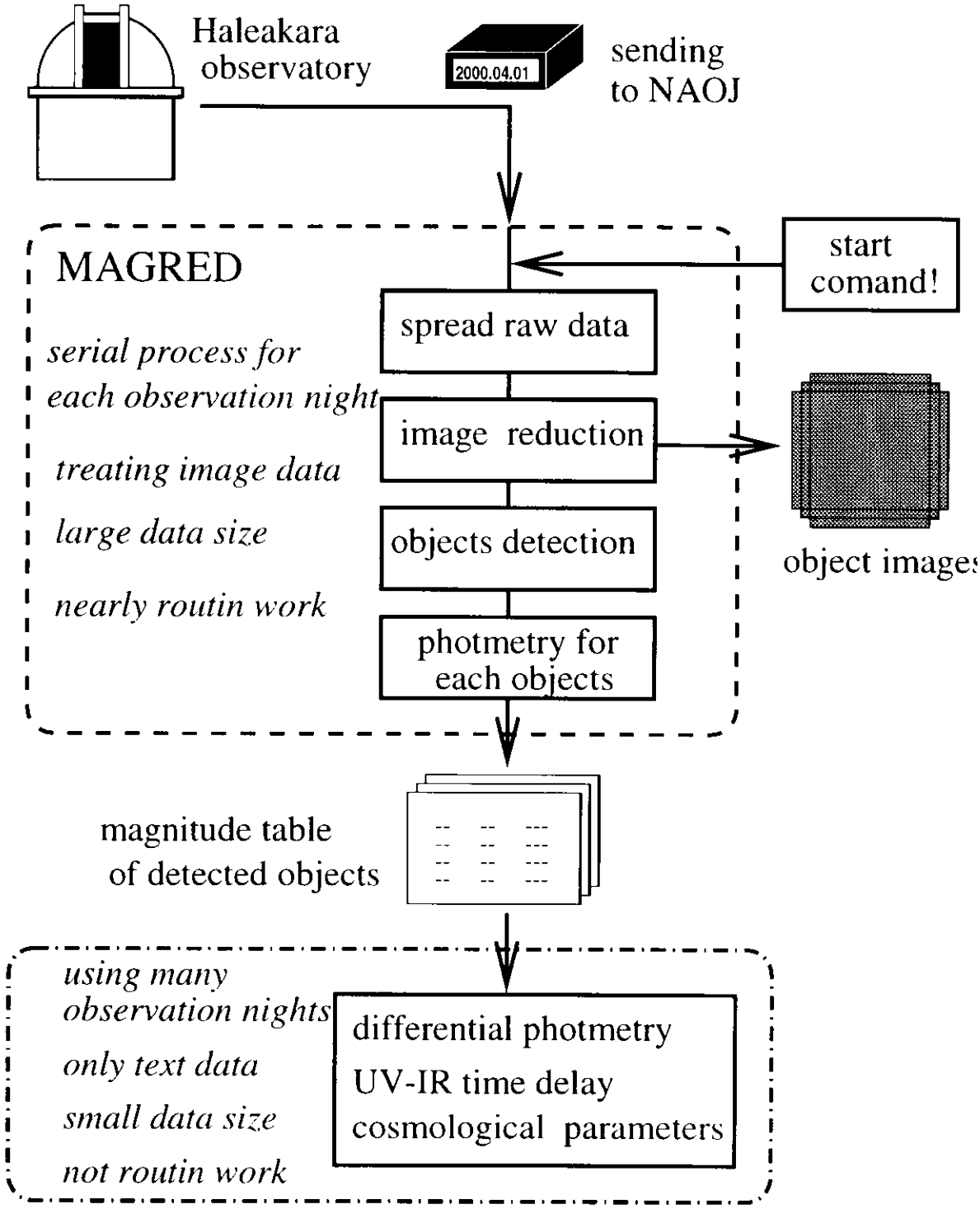

Figure E.1: Flow from the sending of the observed data to determine cosmological parameters in MAGNUM project. Media saved the data is sent by post to Advanced Technology Center of NAOJ. MAGRED is responsible for the process in the dashed line and execute those process completely automaticaly.

process	time(min)
dark frames	240
dome flat	
dome flat frames the 1st round	5
dome flat frames the 2nd round	60
AGN frames	
AGN frames the 1st round	180
AGN frames the 2nd round	1200
combination of AGN frame	
reference detection	90
apertuer reducing the 1st round	20
apertuer reducing the 2nd round	20
combining the frames	120
standard star frame	
image reduction	210
photometry of J band	7
photometry of H band	10
photometry of K' band	10
total	2172

Table E.1: The result of the benchmark test of the automized data reduction of this work. The data of 1998 Frburary 12 were used in this test. Using the data and scripts of which check by human' eye hab been done beforehand, the resuction in this test was executed without break. The requierd time for each process was examined to log the starting and ending time of the each subscript into a file automatically. Total of the time requiered for all automized process was $\sim$36 hours. The ratio of the requierd time for all manual process to total time was about 4% or less.